Structural and functional studies of bacterial mechanosensitive channels

Charles Cox

A thesis submitted to Cardiff University in accordance with the requirements for the degree of Philosophiae Doctor

September 2012

(submitted)

Cardiff University

School of Pharmacy and Pharmaceutical Sciences

Redwood Building

King Edward VII Avenue

Cathay, Cardiff, Wales

CF10 3NB, UK

Acknowledgments

Firstly I would like to thank my supervisors in equal measure, Prof Ken Wann and Prof Tony Campbell. I am indebted to them for all their guidance and scientific input over the last four years. A more perfect supervisor combination for my PhD I could not have wished to find. More than anything I am privileged to say that I completed a PhD under their tuition.

Many thanks also to Prof Boris Martinac for all his help and advice throughout my PhD. His kind offer to visit his lab in Sydney, Australia was a great adventure and an even greater opportunity. I will be forever grateful for his generosity and kindness.

I would like to thank all my lab colleagues who shared insightful comments, scientific hints and tips and shared many good and bad times with me over the last four years. They include; Dr Neil Henney, Dr Pablo Reviriego, Dr Dwaine Burley and Mr Zana Azeez. A special thanks goes to Dr Zhang Jin, whom for four years I relied upon heavily for advice and support.

I would also like to thank all the countless 4th year pharmacy project students and Erasmus students from various corners of the globe for creating a fun and vibrant place to work. In particular, a special thanks to Miss Cornelia Ziegler a German Erasmus student who I very much enjoyed working with.

Immense thanks also to the TOT, the greatest group of friends a man could wish for. A group of people who are more like family than friends and who have supported me, guided me and laughed at me whenever the situation called for it. In no particular order; Mr K Chapman-Weirsma, Mr R Crowlegroves, Mr O David, Mr S Everson, Mr A Howard, Mr L Lewis, Mr M Nicholas, Mr S Roberts, Mr R Tanner and Mr D Varsani.

And finally thanks to my family who have supported me and put up with me for four years, complaining, whining, pontificating and generally babbling on about things they neither know nor indeed wish to know.

Summary

Bacterial mechanosensitive (MS) channels represent the most primitive form of MS channels gating solely in response to changes in bilayer tension. The two main families of bacterial MS channels are MscS and MscL. In concert these channels are imperative to obviate the effects of toxic downshocks in external osmolarity. While osmoprotection is the best characterised physiological role for these channels the genetic diversity of this family hints at as yet undiscovered physiological functions. This thesis explores one such possibility, showing that MscS expression provides a selective advantage in the presence of cell wall attack with knockout *E. coli* strains of MscS having increased susceptibility to cell wall targeting antibiotics. This thesis also shows, using the Ca^{2+} sensitive photoprotein aequorin, that on gating these channels become not only a gateway for solute efflux but also a conduit for ion entry. In particular, influx of Ca^{2+} may represent a physiologically relevant signal but more importantly this finding may pave the way for a high-throughput screen for novel MS channel activators which would be of potential value as lead compounds for antibiotics. Furthermore, this thesis demonstrates that in the presence of divalent cations (Ca^{2+} & Ba^{2+}) MscS exhibits increased anion selectivity, rectification and eight distinct long-lived subconducting states at hyperpolarising membrane potentials. In an attempt to identify the structural basis of these subconducting states the first single residue MscS mutants that display altered anion selectivity are reported. This selectivity, in contrast to voltage-gated K^+, Na^+ and Ca^{2+} channels, is not determined by residues in the pore region but rather by charged residues in the cytoplasmic domain and is likely conserved throughout the MscS family.

List of abbreviations

$[Ca^{2+}]_i$	Intracellular calcium concentration
aa	Amino acid
ATP	Adenosine triphosphate
BCA	Bicinchoninic acid assay
BAC	Benzalkonium chloride
BK	Large conductance Ca^{2+}-activated K^+ channel
BSA	Bovine serum albumin
C	Closed
CD	Cytoplasmic domain
CLP	Cardiolipin
CPZ	Chlorpromazine
DDM	n-dodecyl maltoside
EDTA	Ethylenediaminetetraacetic acid
EGTA	Ethyleneglycoltetraacetic acid
EPR	Electron paramagnetic resonance
FO	Fully open state
FRET	Fluorescence resonance energy transfer
GOF	Gain of function
HEPES	4-(2-hydroxyethyl)-1-piperazineethanesulfonic acid
IPTG	Isopropyl β-D-1-thiogalactopyranoside
KO	Knockout
LA	Local anaesthetic
LB	Lysogeny broth

LJP	Liquid junction potential
LOF	Loss of function
LPC	Lysophosphatidylcholine
LPS	Lipopolysaccharide
M9	Minimal media used for bacterial culture
MIC	Minimum inhibitory concentration
MS	Mechanosensitive
MscK	MS channel dependent on periplasmic/external K^+
MscL	MS channel of large conductance
MscM	MS channel of mini conductance
MscS	MS channel of small conductance
NAG	N-acetyglucosamine
NAM	N-acetylmuramic acid
nt	Nucleotide
OD	Optical density
PBP	Penicillin binding protein
PBS	Phosphate buffered saline
PC	Phosphatidylcholine
PE	Phosphatidylethanolamine
PG	Phosphatidylglycerol
PolyP/PHB	Polyphosphate/polyhydroxybutyrate
P_t	Pressure threshold
SEM	Scanning electron microscopy
SC	Subconducting state
TEM	Transmission electron microscopy

TM	Transmembrane
TRP	Transient receptor potential channel
WT	Wild type

Publications relevant to this thesis

Peer-reviewed meeting abstracts

Cox, C. D., Campbell A. K. and Wann, K. T. (2010) Outward current through 'low' conductance non-mechanosensitive. *Biophys J,* 100(3): 278a

Cox, C. D., Campbell A. K. and Wann, K. T. (2011) A Mechanosensitive channel (MscS) with multiple conducting states shows stronger selectivity for anions in the presence of divalent cations. *Biophys J,* 102(3): 123a

Cox, C. D., Ziegler, C. S., Campbell, A. K., Wann, K. T. and Martinac, B. (2012) Ion selectivity of the mechanosensitive channel MscS is determined by charged residues within the cytoplasmic vestibulum. *Proc Aus Phys Soc*.

Cox, C. D., Ziegler, Campbell, A. K., Wann, K. T. and Martinac, B. (2013) Selectivity of the mechanosensitive channel MscS is determined by the cytoplasmic domain. *Biophys J*.

Publications

Petrov, E., Palanivelu, D., Constantine, M., Rohde, P. R., Cox, C. D., Minor, D. L. Jr., and Martinac, B. (2013) Functional characterization of the MscS-like mechanosensitive channel from *Silicibacter pomeroyi. Biophys J.*

Publications currently under review

Cox, C. D., Nomura, T., Ziegler, C. S., Campbell, A. K., Wann, K. T. and Martinac, B. (2013) Selectivity of the mechanosensitive channel MscS is determined by the cytoplasmic domain.

Contents

Chapter 1: General introduction

1 General Introduction

1.1 Ion channel background

Ion channels are integral membrane proteins which, to date; have been identified in all domains of life (archaea, bacteria and eukarya). Their role in higher organisms includes generation and propagation of action potentials in neurons, muscular contraction, neurotransmitter and hormone release and a plethora of other processes ranging from proliferation to fertilisation (Darszon *et al.,* 1999, Ashcroft, 2000, Jentsch *et al.,* 2004, Ashcroft 2006, Lehen'kyi *et al.,* 2011). Their functional roles in bacteria and archaea are, in the main, much less well understood. Despite this fact a large proportion of the information we now possess about ion channels comes from bacteria and archaea. In fact the Nobel Prize in Chemistry in 2003 was awarded jointly to Roderick Mackinnon "*for structural and mechanistic studies of ion channels*". This work included determination of the specific architecture of the K^+ channel selectivity filter and mode of K^+ ion conduction and was exclusively carried out using channels of bacterial origin (KscA from *Streptomyces lividans*) (Doyle *et al.,* 1998). Numerous scientists over recent years have pointed out how ironic it is that most of our knowledge about ion channels comes from bacteria where we have little to no idea what functional role(s) they play.

The utilisation of bacterial systems for the electrophysiological study of ion channels presents many advantages but also a number of problems. To appreciate these advantages and disadvantages we first need to have an

understanding of bacterial physiology and in particular the make-up of the bacterial cell wall.

1.2 Bacterial cell physiology

The following description centres round the physiology of *Escherichia coli* a motile, facultative anaerobe which is part of the *Enterobacteriaceae* family. This bacterium will be used throughout this thesis as a model system. It has a characteristic rod-shaped morphology and is usually ~2 µm in length and ~0.75 µm in width.

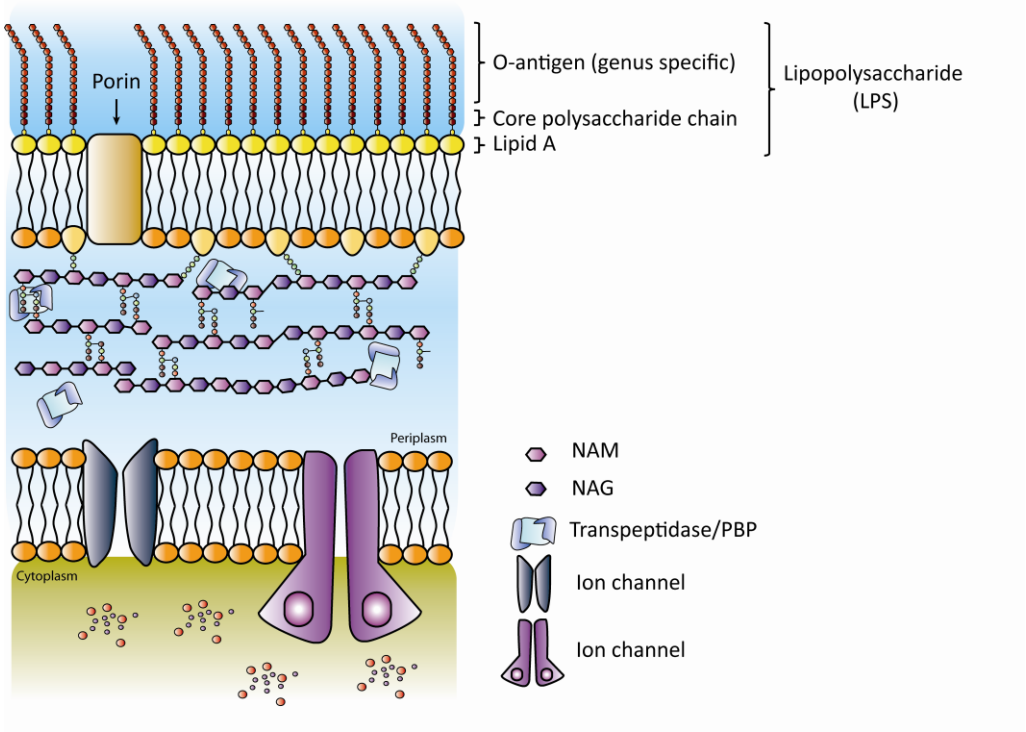

Figure 1.1 Illustration of the *E. coli* cell wall. The illustration shows the inner and outer membrane separated by a mesh work of peptidoglycan that affords the bacterial cell wall such strength.

This bacterium has long since been used as a model system in research due to the ease with which it can be grown and molecularly manipulated. It is

classified as a gram negative bacterium and as such contains both an outer and inner membrane separated by a mesh work of peptidoglycan as illustrated in Figure 1.1. Peptidoglycan consists of alternating residues of N-acetylmuramic acid (NAM) and N-acetylglucosamine (NAG)(Typas *et al.,* 2010, Typas *et al.,* 2012). These polysaccharide chains are then cross-linked via short peptides (3 - 5 amino acids in length) between NAM moieties, a process catalysed by transpeptidases or penicillin binding proteins (PBPs). It's this meshwork of peptidoglycan, anchored to the outer membrane through attachment to lipoproteins, which affords such strength to the bacterial cell wall. Incorporation of peptidoglycan and the consequent growth of the peptidoglycan sacculus is a dynamic process under strict control (Typas *et al.,* 2012). This tight control is imperative in order to maintain normal cellular morphology. Disruption of peptidoglycan synthesis and normal cell wall turnover is achieved by numerous antibiotics (i.e. β-lactams) and enzymes (lysozyme) resulting in a complex chain of events (Discussed further in chapter 6) that ultimately leads to lytic and/or non-lytic cell death (Kohanski *et al.* 2010).

The outer membrane is arguably more complex than the inner one. The lipids lining the inner leaflet are, in the main, 'regular' phospholipids but those facing the external environment are lipopolysaccharides (LPS) made up of the glycolipid lipid A, O antigen and a core polysaccharide component (Figure 1.1)(Delcour, 2009). The LPS constituent of the outer membrane acts as an endotoxin and is extremely antigenic generating a concerted immune

response. The negatively charged chains are stabilised by the binding of the divalent cations Ca^{2+} and Mg^{2+}.

The outer membrane is also peppered with proteins including braun lipoproteins (a centre for peptidoglycan attachment) and porins such as OmpC and OmpF (Basle *et al.,* 2004). Porins are trimeric proteins that span the entirety of the outer membrane and are important in allowing molecules and ions to pass through the outer membrane unhindered (Basle *et al.,* 2006, Delcour, 2009).

The focus in this thesis is the inner membrane which in *E. coli* is composed of three major phosphoplipids: Phosphatidylethanolamine (PE: 70–80%), Phosphatidylglycerol (PG: 20–25%), and cardiolipin (CL: 5–10%) (Icho and Raetz, 1983, Miyazaki *et al.,* 1985, Dowhan, 1997). The resting membrane potential (V_m) of *E. coli* has been estimated to be between -140 and -200 mV depending on which stage in the cell cycle the bacterium is at (Bot and Prodan, 2010). It is, in the main, this large V_m that drives ATP production via membrane bound H^+-ATPases (Dimroth *et al.,* 2000). This inner membrane is also littered with numerous channels and transporters and it's the channels in particular that are the main foci of this thesis. The next section explores arguably the best characterised channels that have been identified in *E. coli;* mechanosensitive (MS) channels.

1.3 *E. coli* mechanosensitive channels

Currently seven mechanosensitive channels have been identified in *E. coli*. The best characterised are MscL (**m**echano**s**ensitive **c**hannel of **l**arge conductance), MscS (**m**echano**s**ensitive **c**hannel of **s**mall conductance), MscK (**m**echano**s**ensitive **c**hannel – **k**allium) and MscM (**m**echano**s**ensitive **c**hannel of **m**ini conductance). In addition, recent evidence points towards the presence of an extra 3 MscS-like mechanosensitive channels in *E. coli* membranes (Edwards & Booth, 2011, Edwards *et al.,* 2012). The exact genetic origin of these channels is discussed in the following sections.

1.3.1 History

The first report of such channels in *E. coli* was in 1987 (Martinac, *et al.,* 1987). The report highlighted the presence of mechanosensitive channel activity in *E. coli* spheroplasts with a conductance of ~1 nS. The following sentence is present in the discussion:

"When NaCl replaced KCl, the pressure sensitivity and opening probability of the channels decreased" (*Martinac et al.,* 1987).

This is consistent with activity from both MscK and MscS. We now know that MscK is dependent on periplasmic potassium (≥ 10 mM) and that MscS has a higher pressure threshold of activation and inactivates. This likely explains the differences reported between NaCl and KCl (Discussed in more detail in 1.3.4 and 1.3.5).

Much of the early work relating to bacterial mechanosensitive channels courted controversy and it wasn't until the cloning of MscL that their existence was made totally irrefutable. In fact, a paper published in Science actually denounced the existence of any mechanosensitive channels inferring that all data was merely artifact; "This discrepancy suggests that single-channel mechanosensitivity is an artifact of patch recording"(Morris and Horn, 1991). A proposition which was later, partly through the cloning of MscL, seen to be totally false (Sukharev *et al.,* 1994).

1.3.2 Main physiological function of bacterial MS channels

Mechanosensitive channels in *E. coli* act as 'emergency release valves' gating in response to hypoosmotic down shock resulting in the release of osmotically active solutes and a corresponding diminution of cellular turgor in turn preventing cellular lysis (Levina *et al.,* 1999, reviewed in Booth *et al.,* 2007). On reduction of external osmolarity H_2O floods into the cell causing a rapid rise in cell turgor. Left unchecked this rise in cell turgor could potentially result in cellular lysis. As the cell turgor rises membrane tension increases which in turn can directly gate mechanosensitive channels. Channel gating then allows osmotically active solutes (K^+, betaine, proline and glutamate) to flood out of the cell relieving the built up pressure preventing cellular lysis (Levina *et al.,* 1999). While the exact mechanisms of osmoprotection are many and varied it is clear that on acute exposure to a hypoosmotic environment mechanosensitive channels have an imperative role to play.

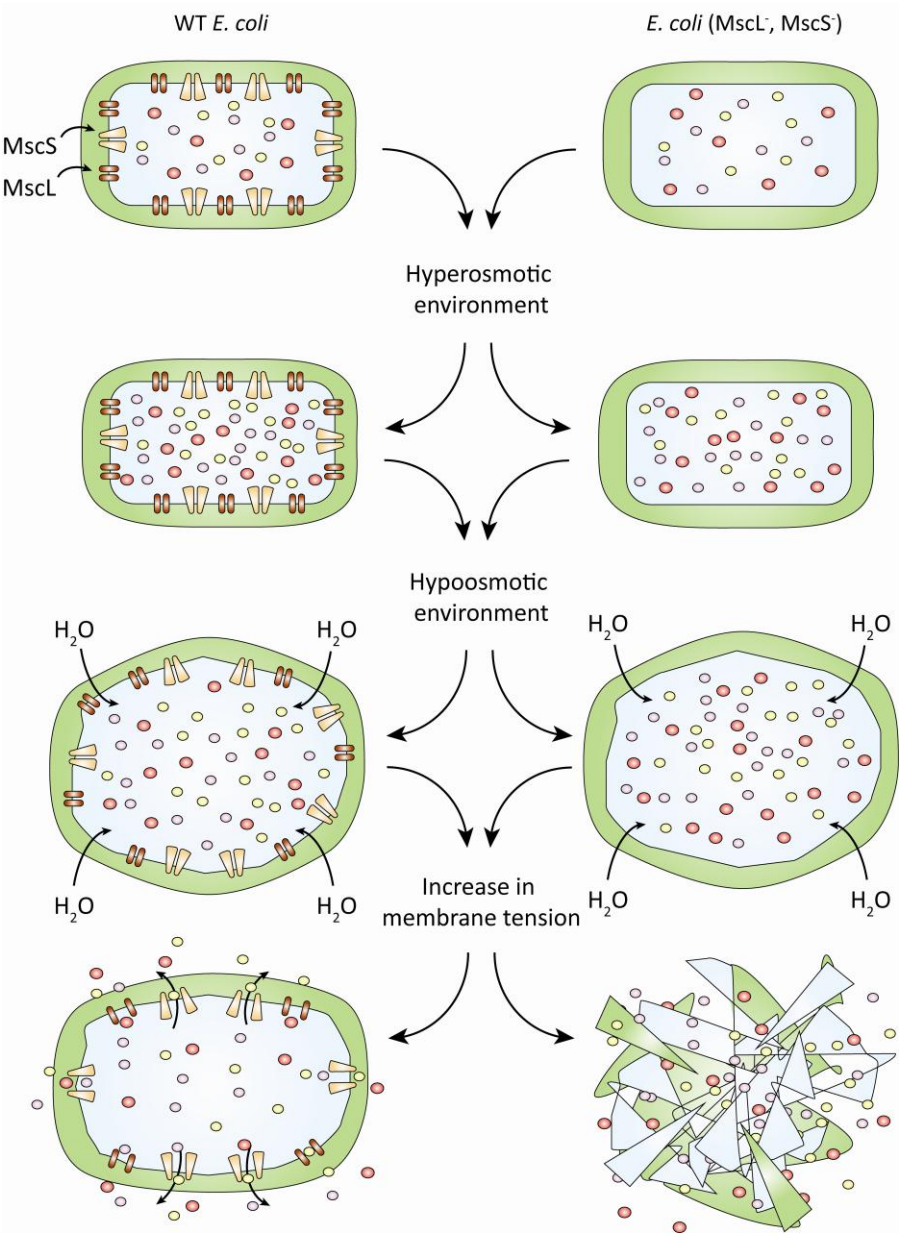

Figure 1.2 Illustration of the physiological role of bacterial MS channels. In response to a reduction in external osmolarity H_2O floods into bacterial cells (via bacterial aquaporins) resulting in swelling and a corresponding rise in cellular turgor and membrane tension. This rise in membrane tension gates MS channels relieving this pressure preventing cellular lysis (left panel). In the absence of MS channels this rise in membrane tension is left unchecked and results in cell lysis (right panel).

Initial investigation showed that single MS channel gene deletions give rise to no noticeable phenotype. However, double knockouts of *mscL* and *yggB,* the MscS gene, give rise to a clone highly susceptible to hypoosmotic shock

(Levina, *et al.,* 1999). This susceptibility can be ameliorated by the insertion and expression of *yggB* or *mscL* containing plasmids but not by *kefA,* the gene encoding MscK.

In addition, halophilic marine bacteria such as *Vibrio alginolyticus* (Nakamaru *et al.,* 1999) and *Salinispora tropica* (Bucarey *et al.,* 2012) which are usually susceptible to lysis in low osmolarity environments are also protected by the expression of MscL homologues. Furthermore the MscM-like activity of *ybdG* can also provide some protection to *E. coli* cells devoid of MscL and MscS against minor hypoosmotic shocks (~300 mOsm) but not larger shocks (> 500 mOsm) (Schumann *et al.,* 2010).

This role in osmoregulation is the main physiological role described for mechanosensitive channels but due to their ubiquitous nature and genetic diversity especially the seeming redundancy of certain channels (i.e. MscK) it seems likely that they serve other yet undiscovered roles. One of the aims of this thesis is to address this very point by testing the hypothesis that:

"Mechanosensitive channel expression provides a selective advantage to bacteria in the presence of cell wall attack mediated by antibiotics and enzymes"

Bacteria often come into contact with compounds which compromise the integrity of the cell wall. This includes antibiotics such as β-lactam antibiotics and enzymes such as lysozyme. While the mechanism of action of these compounds is complex they culminate in lytic and non-lytic forms of cell death

(Kohanski *et al.,* 2010). The reduction in cell wall integrity makes lysis of the inner membrane as a result of normal cellular turgor pressure more likely. This hypothesis suggests that as the cell wall integrity is compromised the tension in the inner membrane increases resulting in MS channel activation which works to ameliorate this rise in tension thus preventing lysis. If this hypothesis were correct then MS channel knockout strains would show increased susceptibility to cell wall targeted antibiotics and enzymes. This is fully discussed in *chapter 6*.

1.3.3 MscL: Structure and biophysical characteristics

MscL was the first bacterial MS channel to be cloned (Sukharev *et al.,* 1994) and is arguably the best characterised MS channel. It is a non-selective channel which exhibits a linear current voltage relationship and a unitary conductance of ~3 nS. The exact tension required to gate MscL is high and lies immediately below the lytic limit of the cell membrane (Sukharev *et al.,* 1999, Liu *et al.,* 2009). The *E. coli* MscL homologue is 136 amino acids in length and is likely arranged as a homopentamer (Folgering *et al.,* 2005) with each monomer consisting of two transmembrane helices termed TM1 and TM2 with both N and C-termini located on the cytoplasmic side. The C-termini are arranged in α-helical bundles which are a conserved feature of MscL homologues and are reported to stabilise the open state (Anishkin *et al.,* 2003).

The TM1 helix from MscL lines the pore of the channel and shows relatively high similarity with the pore-lining TM3 helix of MscS (Pivetti *et al.,* 2003). A

huge amount of information about this channel has been gleaned from the crystal structure of the *Mycobacterium tuberculosis* MscL homologue which was solved to 3.5 Å resolution (Chang *et al.,* 1998)(Figure 1.3). This structure is assigned as the closed state and again points towards a pentameric arrangement for MscL (Chang *et al.,* 1998). In contrast the structure of the *Staphalycoccus aureus* MscL homologue has also been published and illustrates a tetramer rather than a pentamer (Liu *et al.,* 2009). As pointed out by Liu *et al.,* 2009 it is not unprecedented that related multimeric proteins show different oligomeric structures between species. However, subsequent work has shown, through the use of numerous techniques, that the *Staphalycoccus aureus* MscL homologue is in fact a pentamer *in vivo* and that detergent solubilisation can affect the stochiometry of membrane proteins such as MscL (Dorwart *et al.,* 2010). This study confirms that the detergent used to solubilise MscL for the X-ray crystallographic work reported in Liu *et al.,* 2009 results in a tetrameric arrangement rather than a pentameric arrangement. There is no crystal structure available for the open conformation of MscL however there is a huge amount of information regarding the open state which has been gained using molecular dynamic simulations, fluorescence resonance energy transfer (FRET) in conjunction with confocal microscopy and electron paramagnetic resonance spectroscopy. The first model developed by Sukharev and Guy (Sukharev *et al.,* 2001) suggests gating requires only marginal TM1 rotation. Other work using EPR

spectroscopy adds to this and sheds further light on the gating mechanism of MscL (Perozo *et al.,* 2002).

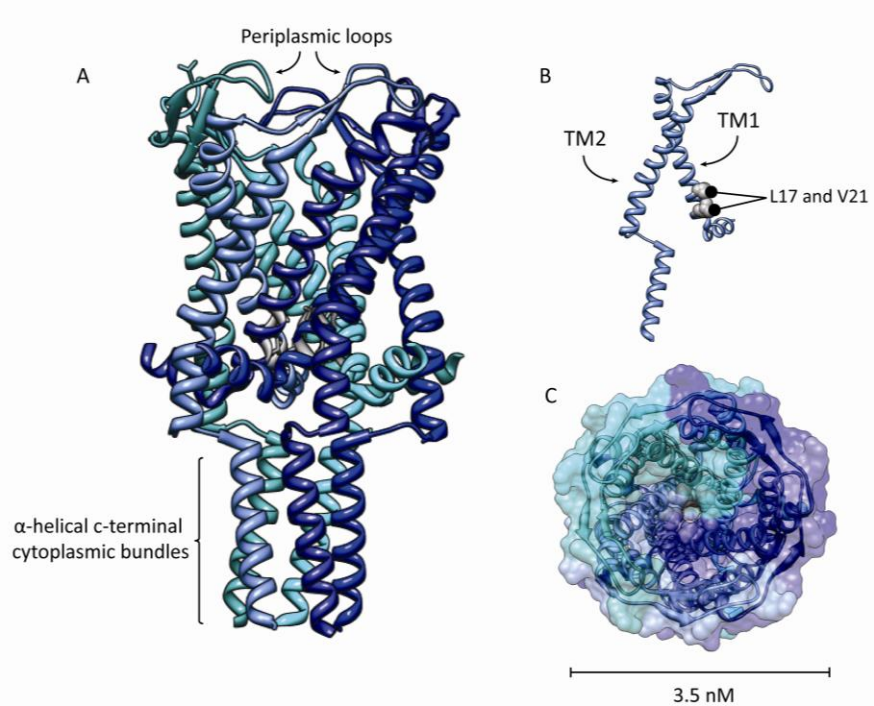

Figure 1.3 Structure of the MscL homologue from *M. tuberculosis.* (A) The structure as viewed laterally, visible are the periplasmic loops or rim. Interestingly loss of function mutants have been identified in this area for the *E. coli* MscL homologue (Yoshimura *et al.,* 2004). (B) Illustration of a monomer from the penatmeric MscL homologue from *M. tuberculosis* showing the two TM helices TM1 and TM2. TM1 lines the pore and the residues highlighted (L17 and V21) correspond to those found to be important for the hydrophobic constriction in *E. coli* MscL (L19 and V23). (C) Periplasmic view of the *M. tuberculosis* MscL homologue.

In this study there was a much larger rotation of TM1 (~110°). The gating cycle put forward by Perozo *et al.,* 2002 is characterised by large rearrangements of TM1 and TM2 and a massive change in channel area. Corry *et al.,* 2010 estimate a much smaller rotation in TM1 akin to that reported by Sukharev *et al.,* 2001 using *in silico* simulations and FRET confocal microscopy. All models involve the transition into at least one intermediate state and movement of a

constriction point near G26 (Iscla *et al.,* 2004). This hydrophobic constriction point also involves L19 and V23 (Ou *et al.,* 1998). One hypothesis in fact is that the change in hydrophobicity of residues lining one of the TM1 helices drives gating (Birkner *et al.,* 2012). This constriction at the cytoplasmic side immediately prior to the cytoplasmic α-helical bundles can be weakened by the introduction of hydrophilic residues at position G22 resulting in channels that gate at lower pressures and some which even exhibit spontaneous activity (i.e. G22E) (Yoshimura *et al.,* 1999). The gating mechanism has been described as iris-like with the resulting open pore estimated to be between 25 – 40 Å (Cruickshank *et al.,* 1997, Perozo *et al.,* 2002). Amazingly, efflux studies using fluorescence have shown that molecules up to the size of 6.5 kDa can move through the MscL open channel (van den Bogaart *et al.,* 2007).

In the case of bacterial mechanosensitive channels, force is directly passed from the lipid bilayer to channel. This is in part proven by the reconstitution of channels such as MscL into liposomes and the retention of pressure activated channel characteristics. This fact is further supported by the observation that amphipaths such as chlorpromazine (CPZ) and local anaesthethics (i.e. procaine) can reduce the pressure thresholds of activation and cause spontaneous activation of MS channels (Martinac *et al.,* 1990). In addition, lyophosphatidylcholine (LPC) also increases the open probability of MS channels by insertion into the lipid bilayer (Perozo *et al.,* 2002, Corry *et al.,* 2010, Grage *et al.,* 2011, Nomura *et al.,* 2012). Despite this understanding the exact interactions that mediate tension sensing are unknown. However some

important residues in this process have been recently identified by Iscla *et al.,* 2011.

1.3.4 MscS: Structure and biophysical characteristics

MscS is a homoheptameric protein with each monomer consisting of 286 amino acids. This 210 kDa protein, along with MscL, is imperative for *E. coli* survival in the event of hypoosmotic shock as previously discussed. MscS is encoded for by the *yggB* gene (Levina *et al.,* 1999) and is extremely widely studied a fact aided by the abundance of structural data available. The initial crystallographic structure of MscS (PDB: 1MXM)(Bass *et al.,* 2002) was refined to give (PDB: 2OAU)(Steinbacher *et al.,* 2007) a structure which was thought to illustrate MscS in the open state however since then the general consensus has become that this structure represents a non-conductive state with the pore area largely dehydrated (Anishkin and Sukharev, 2004, Sotomayor and Schulten, 2004). A number of years later the open structure was also published (PDB: 2VV5)(Wang *et al.,* 2008).

The basic structure of MscS consists of three transmembrane regions termed TM1-3 which are sat at ~30° to vertical and a large water filled cytoplasmic domain which comprises more than 60% of the whole protein (Bass *et al.,* 2002, Wang *et al.,* 2008)(Figure 1.4). TM1 and TM2 are involved in tension sensing and enable force to be transmitted to be pore lining TM3 helix which is split into two parts; TM3a and b. Simulation studies have shown that two leucine residues at positions 105 and 109 in TM3a are responsible for the formation of a ‘vapour lock’ that prevents hydration of the pore and thus ion

conduction (Anishkin and Sukharev, 2004, Sotomayor and Schulten, 2004). These residues are shown to protrude into the pore in the closed/non-conductive pore (PDB: 2OAU) and are largely removed from the ~16 Å pore in the open structure (PDB: 2VV5) (Figure 1.4 shows these residues in hot pink). In addition to this, a gain of function MscS mutant where L109 is substituted for a hydrophilic serine residue increases hydration of the pore and is extremely toxic when expressed in *E. coli* (Miller *et al.,* 2003a).

The TM3 helix then kinks around G113 and leads into TM3b which runs almost parallel with the bacterial inner membrane. The large cytoplasmic domain which follows is made of almost solely β-sheet. This structure is split into three distinct structural parts; the β-domain, αβ-domain and β-barrel (Bass *et al.,* 2002). Most interestingly of all, the cytoplasmic vestibule is perforated by 8 portals. Seven of these perforations line the lateral walls of the domain with the last being aligned coaxially with the transmembrane pore. The seven lateral portals are ~13 Å in diameter with the final pore being 8 Å in diameter. The cytoplasmic domain seems to be a dynamic structure that plays an active role in gating. It may also play a role in selectivity (Discussed fully in following paragraphs, also *see chapter 5*) (Gamini *et al.,* 2011). Evidence from electrophysiology and cysteine cross-linking suggests that the cytoplasmic domain volume changes significantly on gating (Miller *et al.,* 2003b, Grajkowski *et al.,* 2005). It may also impact on inactivation kinetics (Nomura *et al.,* 2008). These effects are likely brought about by an electrostatic

interaction between the TM1-TM2 linker and charged residues in the β-domain (Nomura *et al.,* 2008).

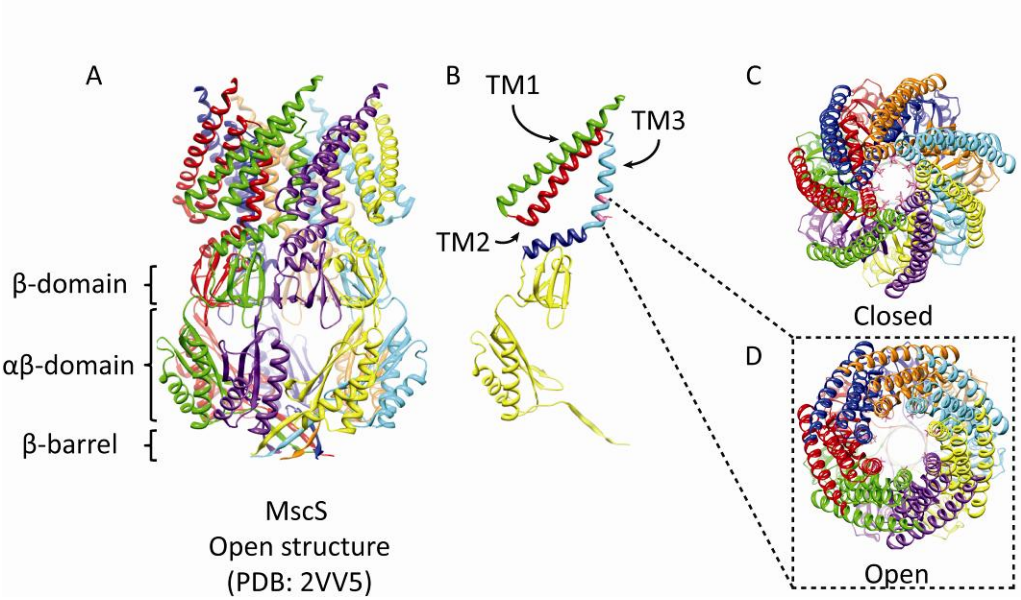

Figure 1.4 Basic structure of MscS. (A) Structure of MscS in the open state (PDB: 2VV5) with each of the seven monomers displayed as a different colour. (B) Structure of one monomer of MscS from the open structure illustrating the TM1, TM2 and TM3 which lines the pore (TM3 is split into TM3a *light blue* and TM3b *dark blue*). The two pink coloured residues are L105 and L109 which form a hydrophobic lock preventing ionic movement in the closed state as shown in (C). In the open state these leucine residues are withdrawn from the pore allowing hydration of the pore and thus forming a water-filled pathway for ions as shown in (D).

The mechanosensitivity of MscS is complex and involves multiple separate processes at the molecular level. Firstly tension needs to be transmitted from the bilayer to the TM1-TM2 region through this region and finally to the pore where a conformational change is required to gate the channel. Important residues for MscS mechanosensation include those identified by Nomura *et al.,* 2006 via asparagine scanning mutagenesis (including A34, I37, I48, A51, F68, L55, L85 and L86) (Figure 1.5).

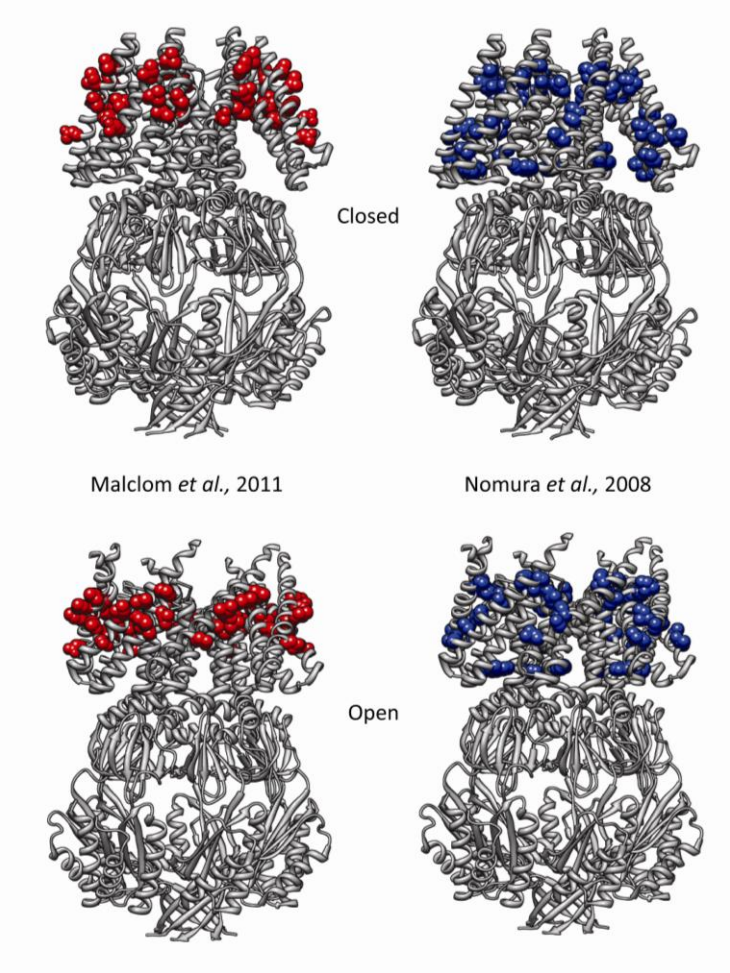

Figure 1.5 Mechanosensing residues in MscS. This diagram illustrates where in the open and closed structures of MscS the mechanosensing residues are situated. The red residues are those identified by Malcolm *et al.,* 2011 and are more lipid facing than those identified by Nomura *et al.,* 2006 (blue).

These residues are likely involved in gating i.e transmission of mechanical force but as described by Malcolm *et al.,* 2011 may not interact directly with the lipid environment. Malcolm *et al.,* also used site directed mutagenesis (mutations to alanine) and identified numerous residues which may interact with the lipid environment and thus constitute the 'actual tension sensors' (L35, I39, L42, I43, N50, I78 and L82) or at least regions which directly interact with the lipid membrane (Malcolm *et al.,* 2011). The tension then seems to be

transmitted from the TM3 facing F68, identified by Nomura *et al.,* 2006, of TM2 via interactions with L111 and L115 as serine mutations at any of these points greatly increases the pressure threshold for activation (Belyy *et al.,* 2010). These LOF mutants (F68S, L111S and L115S) also exhibit much stronger, faster inactivation than the WT channel (Belyy *et al.,* 2010).

MscS undergoes a reversible partial and total loss of sensitivity to pressure. These processes have been termed desensitisation (Maksaev and Haswell, 2011), adaptation (Koprowski *et al.,* 2011), inactivation (Akitake *et al.,* 2007, Belyy *et al.,* 2010) and a combination of both inactivation and desensitisation (Akitake *et al.,* 2007). Desensitisation and adaptation refer to a situation in which the channel requires a larger pressure stimulus to gate whereas inactivation refers to a process whereby the channel becomes completely refractory to pressure application (Akitake *et al.,* 2007). The data documenting inactivation is very compelling although the physiological relevance of MscS inactivation is debatable. The main question arises from:

"How would inactivation benefit a channel whose activation naturally dissipates the only relevant physiological stimuli?"

This refers specifically to the slow kinetics of MscS inactivation. In comparison to the physiological response to hypoosmotic downshock which is rapid on the low millisecond timescale inactivation takes much longer (Akitake *et al.,* 2007, Boer *et al.,* 2011). The suggestion is that the slow inactivation kinetics exhibited by MscS are there to prevent continual MscS activation in response to low level hypoosmotic shock aiding the recovery process (Boer *et al.,* 2011).

The slow time frame also ensures that some channels are still primed and ready should the cell then be subjected to a larger down shift in external osmolarity (Boer *et al.,* 2011). As a result it does seem that inactivation is relevant to the physiological function of MscS.

At the molecular level inactivation seems to be centred round the TM3 kink that occurs at G113. Replacement of G113 with an amino acid of higher helical propensity abolishes inactivation (Akitake *et al.,* 2007). This kink prevents the interaction documented above between F68 (TM2) and L111/L115 (TM3) resulting in a state totally refractory to pressure application. An important interaction also seems to be present, to allow the kink at G113, between the TM3b helix and cytoplasmic domain (Koprowski *et al.,* 2011). (For further discussion surrounding the molecular basis of MscS inactivation *see chapter 5*).

The MscS gating cycle involves the sliding of the tightly packed TM helices across each other. This is supported by the fact that bulky substitutions in the TM3 helix result in an increased pressure threshold for channel activation (G101A, G104A, A106L, G108A) and removal of bulkier side chains results in channels which gate at lower pressures (A106G) (Edwards *et al.,* 2005). The current gating model is one in which on application of pressure TM1 and TM2 move almost as one rigid paddle and rotate anti-clockwise. This rotation and slight downward incline in TM1 is transmitted to the TM3 helix which rotates substantially and straightens, around the kink at G113, moving out away from

the pore (Belyy *et al.,* 2010). This movement removes L105 and L109 from the pore allowing hydration of the pore and subsequent ion permeation (Vasquez *et al.,* 2008).

MscS exhibits a weak level of anionic selectivity with P_{Cl}/P_K values ranging from 1.2 – 3 (Martinac *et al.,* 1987, Li *et al.,* 2002, Sukharev, 2002, Sotomayor *et al.,* 2007, Edwards *et al.,* 2008). This weak level of selectivity is discussed in more detail in chapter 3. The structural basis of this low level selectivity is unknown but seems not to be inferred by residues in the pore lining helix as mutations in this region do not effect selectivity (Edwards *et al.*, 2008). Thus selectivity apparatus must be housed in the large cytoplasmic domain. It has been shown that the cytoplasmic domain fulfils a filter function (Gamini *et al.,* 2011). This structure is supposed to enable balanced efflux of osmolytes which the authors suggest minimises the likelihood of MscS activation affecting membrane potential which as mentioned previously is imperative for H^+-ATPase activity (Dimroth *et al.,* 2000).

The initial report of MscS activity suggested it was a voltage sensitive channel (Martinac *et al.,* 1987) however this seems not be the case. Data presented in Akitake *et al.,* 2005 shows that MscS activation is not affected by voltage but that inactivation is voltage-dependent. When Bass *et al.,* 2002 reported the first crystal structure of MscS they pointed towards three important charged residues that may be involved in voltage sensitivity; arginine 46, 74 and 88. It

is possible that these charged residues are important for voltage-dependent inactivation (Akitake *et al.,* 2005).

1.3.5 MscK: Structure and biophysical characteristics

MscK is encoded for by the gene *kefA* and was discovered during the search for the genetic identity of MscS channel conductance (Levina *et al.,* 1999). MscK is made up of 1120 amino acids which makes it the largest MscS paralogue found in *E. coli*. Previous work suggests that it has 11 TM domains as opposed to the three seen in MscS (Mclaggan *et al.,* 2002). The major extension in MscK is found in the N-terminal part with extra transmembrane domains and a large region (~400 amino acids) purported to sit in the periplasmic space (Mclaggan *et al.,* 2002). It is the C-terminal region that shows the highest identity with MscS including the large cytoplasmic vestibule (Levina *et al.,* 1999, Mclaggan *et al.,* 2002). To complement this a truncated version of MscK does infer protection to a double $MscS^-$ and $MscL^-$ mutant, illustrating just how closely related this C-terminal portion is to MscS (Miller *et al.,* 2003b)

MscK exhibits almost identical conductance (~1 nS) to MscS (Levina *et al.,* 1999), albeit slightly lower (Hurst *et al.,* 2009). However, despite this similarity in unitary conductance there are many features of its activity that distinguish it from MscS. Firstly MscK gates at markedly lower membrane tensions than MscS meaning that during electrophysiological inspection of *E. coli* spheroplasts the first channel to gate in most cases is MscK (Martinac *et al.,* 1987, Hurst *et al.,* 2009). In order for gating to be achieved MscK requires not

only membrane tension but also large periplasmic concentrations of K^+ (≥ 10 mM). This can be mimicked using NH_4^+, Rb^+ or Cs^+ but not Li^+ or Na^+ (Li *et al.,* 2002). Furthermore, while MscK was initially suggested to be a cation specific channel (Mclaggan *et al.,* 2002) work has subsequently shown that it exhibits very weak anion selectivity (P_{Cl}/P_K = ~1.2)(Li *et al.,* 2002), even weaker than MscS (P_{Cl}/P_K = 1.2 - 3)(Martinac *et al.,* 1987, Li *et al.,* 2002, Sotomayor *et al.,* 2007, Edwards *et al.,* 2008). While MscK does exhibit some rectification at negative pipette potentials it is much less marked than that demonstrated by MscS (Li *et al.,* 2002).

Physiologically it seems that MscK is not imperative for survival in acute hypoosmotic shock. Expression of the *kefA* gene alone cannot rescue a double MS channel knockout mutant from hypoosmotic shock nor does ablation of the *kefA* gene add to the susceptibility of a double knockout mutant to a hypoosmotic shock (Levina *et al.,* 1999). Instead MscK seems to play a role in osmotic adaptation (Mclaggan *et al.,* 2002). The reason for its potassium dependence and its structural basis is not at all understood and could well be linked to its primary function.

MscK does *NOT* display inactivation. The structural basis of this is purported to be the replacement of a glutamate residue at the residue aligned with G113 in MscS. The replacement of the glycine, which has low helical propensity, for a glutamate in MscK is proposed to prevent any kink in the pore-lining helix meaning that a tension insensitive configuration cannot be

reached. This is supported by the lack of inactivation in MscS G113D mutants (Akitake *et al.,* 2007)

1.3.6 MscM: Structure and biophysical characteristics

Relatively little is known about MscM in comparison to its higher conducting counterparts. In fact the genetic origin of this electrophysiological activity is still not completely known. Firstly a report in 2010 about a mutant product of the gene *ybdG* (V229A) was shown to have MscM-like activity with a unitary conductance of 350-400 pS (Schumann *et al.,* 2010). However, other openings in *ΔybdG* mutants which were identical to that attributed to *ybdG* were also observed suggesting another similar channel or channels were present. This resulted in the conclusion that *ybdG* gave rise to MscM-like activity but was not the sole component of the MscM channel activity that had been previously reported. This situation mirrors what was found on inspection of MscS activity i.e. the isolation of two separate genes with similar unitary conductance (*yggB* and *kefA*)(Levina *et al.,* 1999). More recently it has been suggested that MscM activity is encoded for by the gene *yjeP* (Edwards *et al.,* 2012). This report shows an increase in MscM activity (~300 pS) in the absence of all seven of the reported *E. coli* MS genes when a plasmid containing *yjeP* was expressed. The two other characterised MscS channel paralogues in *E. coli* are *ybiO* (~1 nS) and *ynaI* (~100 pS) (Edwards *et al.,* 2012).

While MscL and MscS are two of the most widely studied mechanosensitive channels MscM comparatively receives little research attention which is not without reason. While MscL and MscS are, in concert, imperative for *E. coli*

survival in response to a reduction in external osmolarity (~600 mOsm) MscM is not (Levina *et al.,* 1999). Schumann *et al.,* 2010 did however show a slight (~30 %) increase in survival rate of double knockout (*mscL* $^{-}$*, yggB*$^{-}$) *E. coli* mutants on mild (~300 mOsm) hypo-osmotic shock (Schumann *et al.,* 2010). Furthermore MscM exhibits a relatively small conductance of 100 - 400 pS and its expression is low with only around 5-10% of spheroplasts patched exhibiting MscM activity (Stokes *et al.,* 2003, Scumann *et al.,* 2010). There is also currently no crystal structure available for MscM and it exhibits low sequence homology with MscS despite being part of the MscS super family.

1.3.7 Bacterial MS channel expression and distribution

Expression of MS channels seems to be, at least in part, under the control of the stress sigma factor, RpoS (Stokes *et al.*, 2003). During the exponential phase of growth MS channel expression is limited, however on entry into stationary phase MS channel expression increases (Stokes *et al.,* 2003). This enables *E. coli* cells to better repel any toxic down shifts in environmental osmolarity. In addition, growth in hyperosmotic media increases MS channel expression through RpoS presumably in order that any reduction in external osmolarity can be dealt with effectively. In agreement with this is the observation that an *ΔrpoS* mutant is more susceptible to hypoosmotic downshock than WT *E. coli* cells (Stokes *et al.,* 2003).

There are various different reports for the exact number of MS channels expressed in WT *E. coli* cells and as mentioned above this number changes depending on where in its life cycle the bacterium finds its self and also the

media it's grown in. Electrophysiological estimation of channel numbers is complicated by the necessary procedure to make bacteria amenable to patching, i.e. giant spheroplast formation (discussed in section 1.5), and gives rise to highly variable estimates from 5 – 100 channels per cell for MscL and much higher for MscS (Stokes *et al.,* 2003, Bialecka-Fornal *et al.,* 2012). A radiolabelling study of MscL is in agreement with these estimates calculating around 50 MscL channels per cell at any one time in stationary phase *E. coli* cells (Hase *et al.,* 1997). However quantitative western blots and fluorescence microscopy measurements suggest that there may in fact be many more channels present than estimated from electrophysiological experiments (Bialecka-Fornal *et al.,* 2012). These experiments estimate there are between 300 – 1000 MscL channels per cell. This is a huge number of channels and activation of a large cohort of this number, considering the unitary conductance (~3 nS), would surely be extremely detrimental for the cell. This raises an interesting question about the activity of all these channels. Recent work suggests that MscL channels have an inherent ability to form clusters regardless of the membrane lipid composition (Grage *et al.,* 2011). This clustering said to be a result of "lipid mediated protein-protein interactions" seems not to be confined to MscL as clustering between MscS and MscL has also recently been shown (Nomura *et al.,* 2012). This process seems to influence the mechanosensitive properties of MscS resulting in an increased pressure threshold for activation (Nomura *et al.,* 2012). Taking into account all of this data there does seem to be a physiological role and relevance for

clustering of MS channels in bacteria, allowing large cohorts of channels to be present (> 100) but preventing all channels from opening in concert. This would mean physiologically that many channels are available to act in the face of hypoosmotic downshock but that clustering prevents all of the channels from opening at once.

Interestingly in addition to clustering it has also been shown, for both MscL and MscS, that cellular distribution is not uniform and is highest at the poles of the cell (Romantsov *et al.,* 2010, Grage *et al.,* 2011). In the case of MscS this is driven in part by the phospholipid cardiolipin. The exact physiological reason, if any, for this is to date unknown.

1.3.8 Bacterial MS channel homologues

MscL and MscS homologues are ubiquitously expressed throughout the three domains of life. Interestingly no homologous proteins have been identified in the human genome. The MscL family is not quite as large as the MscS family but homologues can still be found in fungi, archaea and both Gram-positive and Gram-negative bacteria (Pivetti *et al.,* 2003). This includes many pathogenic microbes such as *Mycobacterium tuberculosis*, *Staphylococcus aureus*, *Streptococcus pneumonia and Pseudomonas aeruginosa* (Chang *et al.,* 1998, Pivetti *et al.,* 2003, Liu *et al.,* 2009). The MscS superfamily is much larger and can be broadly divided into the smaller MscS-like proteins and larger MscK-like proteins. These proteins can be found in archaea (Kloda and Martinac, 2001), bacteria (Martinac *et al.,* 1987, Borngen *et al.,* 2010) plants (Gensen and Haswell, 2012), yeast and protists (Nakayama *et al.,* 2007). Again

many of these organisms are pathogenic including; *Vibrio cholera, Pseudomonas aeruginosa* and *Helicobacter pylori*. The ubiquitous expression of these proteins in many pathogenic microbes and the lack of any kind of human homologues makes these proteins attractive antibiotic targets. Their utility in this setting is discussed in the following section.

1.3.9 Bacterial MS channel utility

Bacterial MS channels are in essence large water-filled pores sensitive to mechanical stimuli. Gating of bacterial MS channels imposes a large metabolic strain on bacterial cells. In the case of MscL opening results in the loss of many precious intracellular solutes and likely impacts on membrane potential, the major driver for ATP synthesis (Dimroth *et al.,* 2000). While gating of MscS is proposed not to impact on membrane potential (Gamini *et al.,* 2011) it still results in the loss of many intracellular solutes such as K^+ that the bacterium spends large amounts of energy collecting from its environment. Taking into account their ubiquitous expression and lack of human homologues targeting MS channels seems like an attractive target for antibiotic development. Any compound that could cause continual MS channel activation would likely impair bacterial growth much in the same way that MS channel GOF mutants do when expressed in *E. coli,* examples being the MscL mutant G22E and the MscS mutant L109S (Yoshimura et al., 1999, Miller *et al.,* 2003b).

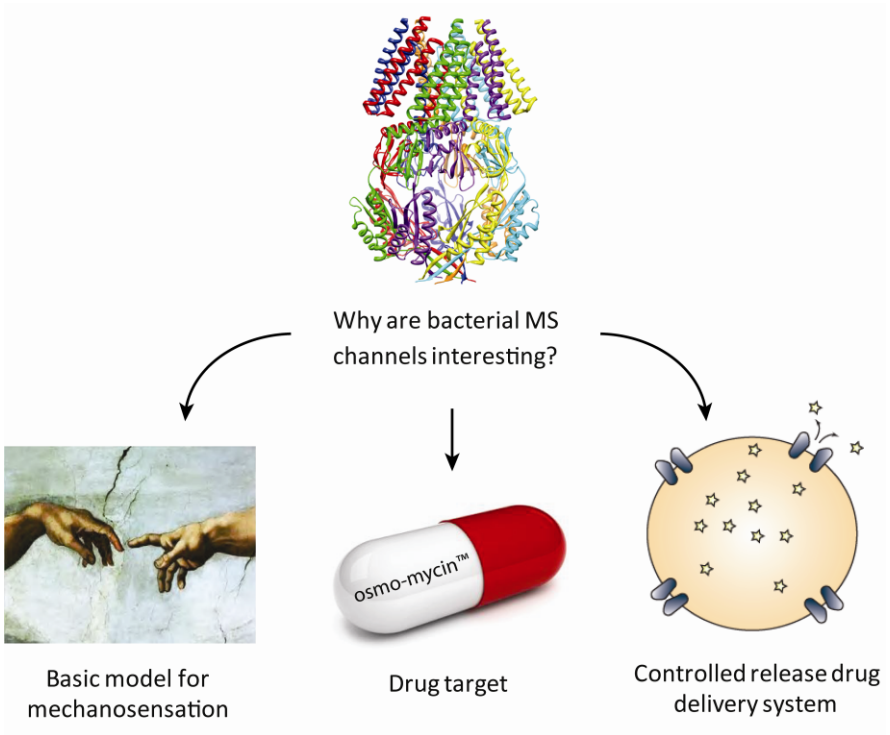

Figure 1.4 Interesting uses of bacterial MS channels. MS channels can be used as basic models for mechanosensing. They also represent a novel antibiotic target and can be utilised in sustained release drug delivery systems.

Some antimicrobials may already work in this fashion for example parabens, which are widely used preservatives, are known to activate MS channels and this may in part account for their antimicrobial activity (Nguyen *et al.,* 2005). In addition to this, gating of a large pore like MscL which has the ability to allow molecules up to and including the size of insulin (≤ 6.5 kDa) through may also be beneficial in aiding entry of other antimicrobials that require access to the bacterial intracellular compartment such as tetracyclines (i.e. oxytetracycline) or macrolides (i.e. erythromycin) (van den Bogaart *et al.,* 2007). The fact that MscL can allow large molecules to pass through has also been looked at from the point of view of sustained drug delivery systems and nano-devices (Kocer *et al.,* 2005, Kocer *et al.,* 2006, Yang and Blount, 2011).

Incorporation of MscL into liposomes containing drug molecules enables sustained or prolonged release and protection of the drug molecule from the harsh conditions in the stomach. The issue then becomes what stimuli to use to gate the channel to allow drug efflux? One idea has been to modify the channel so it gates in response to changes in pH (Kocer *et al.,* 2006). Another idea would be to use a spontaneously active MscL mutant such as G22E (Yoshimura *et al.,* 1999, Petrov *et al.,* 2011).

So far the discussion has centred round solute efflux however the fact that these channels have pores with such wide diameters (MscL ~40 Å, MscS ~16 Å) raises the question can ions or solutes permeate into the cell when they are open and not just out?

1.4 Ca^{2+} regulation bacteria

Ca^{2+} is a universal signalling messenger and regulator in eukaryotic systems. It plays a central role in muscle contraction, exocytosis of neurotransmitters and hence nerve conduction, fertilisation, proliferation and many other processes (Campbell, 1983). However microbiologists have found it more difficult to pinpoint specific roles for Ca^{2+} in bacteria. The first major indicator of an important role for Ca^{2+} in bacteria came from the observation that bacteria, like eukaryotes, keep intracellular Ca^{2+} very low (≤ 300 nM)(Gangola and Rosen, 1987, Knight *et al.,* 1991, Watkins *et al.,* 1995, Tisa and Adler, 1995). In addition to keeping Ca^{2+} low in the cytosol evidence also points to differential regulation in the periplasm (Jones *et al.,* 2002). In fact, Jones *et al.,* 2002 demonstrate using periplasm-targeted expression of the photoprotein

aequorin that Ca^{2+} was at least three fold higher in the periplasm than the external environment (Jones *et al.,* 2002). From this we can suggest that the periplasm may act as a calcium store/sink with its own distinct Ca^{2+} regulation mechanisms. In order to keep Ca^{2+} this low in the face of µM or mM periplasmic or external Ca^{2+} there must be mechanisms present that can remove Ca^{2+} from the cytoplasm. These ATP driven transporters or exchangers however are yet to be identified. Two candidate genes include *chaA* a putative Ca^{2+}-H^{+} exchanger and *yrbG* a putative Ca^{2+}-Na^{+} exchanger although neither seemed to affect Ca^{2+} efflux under the experimental conditions used in Naseem *et al.,* 2009. This is despite the fact that pH and monovalent cations are known to regulate intracellular Ca^{2+} in *E. coli* (Naseem *et al.,* 2008). The only gene which was shown to definitively impair Ca^{2+} efflux was *atpD* which forms part of the F_OF_1 ATPase (Naseem *et al.,* 2009) leading to the assumption that Ca^{2+} efflux is ATP dependent.

Just as little is known about Ca^{2+} influx mechanisms in bacteria. Much interest surrounded the discovery of a non-proteinaceous channel made from polyhydroxybutyrate and polyphosphate that showed selectivity for divalent cations (~100 pS) however activity of this channel *in vivo* or a physiological role have not been forthcoming (Das *et al.,* 1997). Despite information lacking about specific Ca^{2+} transport systems the number of bacterial proteins that interact with Ca^{2+} has grown (Zhou *et al.,* 2006). So too has the number of Ca^{2+}-dependent physiological processes in bacteria. One of the first physiological processes associated with Ca^{2+} in live bacteria was chemotaxis

(Tisa and Adler, 1992). Other processes affected include cell division, differentiation, sporulation and gene transcription with over 100 genes being influenced by Ca^{2+} levels (Naseem *et al.,* 2009)(Reviewed in Norris *et al.,* 1996, Dominguez, 2004). In summary although little is known about specific Ca^{2+} transport mechanisms it seems clear that Ca^{2+} is an important regulator and signalling agent in bacteria.

The following section discusses how, if at all, bacterial MS channels may affect intracellular Ca^{2+}.

1.4.1 Bacterial Mechanosensitive channels in Ca^{2+} regulation

While MscL has been implicated in Ca^{2+} movement in the cyanobacterium *Synechocystis* it seems unlikely that *E. coli* MscL or any MS channel plays an integral role in Ca^{2+} regulation in bacteria (Nazarenko *et al.,* 2003). In fact it has been shown that Ca^{2+} efflux is unaffected by single knockouts of *E. coli* MscL, MscS and MscK (Naseem *et al.,* 2009). This is unsurprising as under normal conditions MS channels will be tightly closed to prevent any unwanted ionic movement that would impact on bacterial ionic homeostasis. However, in the event that an MS channel opens, which in the case of MscS, MscK and MscM is well below the lytic limit of bacterial cells, it becomes not only a pathway for osmolyte efflux but also potentially a conduit for ion influx. This is particularly relevant for Ca^{2+} as not only the concentration but also the membrane potential will drive Ca^{2+} influx. The question then becomes can a counter current of ions, especially Ca^{2+} due to the large electrochemical gradient, enter the cell against ion efflux? And under what conditions can this

occur? It would also thus be interesting to speculate that such a movement however small may then provide a signal affecting gene expression or protein function. This thesis aims to look at the Ca^{2+} permeability of MS channels and also to see whether Ca^{2+} permeates through MS channels *in vivo* using the Ca^{2+} sensitive photoprotein aequorin (For further information about aequorin *see chapter 3*).

1.5 Introduction to methods

Bacteria are themselves not amenable to patch-clamp analysis. Both their size and cell wall precludes the possibility of achieving a giga seal. So in order to study bacterial MS channels electrophysiologically and look at Ca^{2+} permeability one of two techniques will be used. Either channels will be expressed and purified then reconstituted in liposomes prior to patching or bacterial cells will be exposed to a protocol that results in the formation of giant spheroplasts. Both have advantages and draw backs and both have been used extensively to study this family of channels in particular MscL and MscS. The first technique used to study these channels was giant spheroplast formation (Martinac *et al.,* 1987). This utilises the β-lactam antibiotic cephalexin to form elongated filamentous bacteria termed 'snakes' and the enzyme lysozyme that cleaves the peptidoglycan rich cell wall. On clipping of peptidoglycan bonds the bacteria swell as they lose cell wall integrity and eventually all of the outer membrane and cell wall are stripped away leaving a 'nude' inner membrane and an object amenable to patch-clamp called a giant spheroplast. This thesis aims to employ both of these methods to look into

whether Ca^{2+} permeates through MS channels and how, if at all, the biophysical characteristics of these channels are affected in the presence of Ca^{2+} and other divalent cations (i.e. Ba^{2+}).

1.6 Thesis hypotheses and aims

The overarching aim of this thesis is to definitively show Ca^{2+} permeation via bacterial MS channels. This includes investigating whether MS channel biophysical characteristics and behaviour are affected by divalent cations such as Ca^{2+}. In addition, the Ca^{2+} sensitive photoprotein will be used to probe any potential Ca^{2+} movement *in vivo* via MS channels. And finally on top of these biophysical questions this thesis aims to test whether MS channels have a physiological role during periods of cell wall stress for example as a result of antibiotic exposure. The specific aims are as follows:

- Definitively show Ca^{2+} permeation through mechanosensitive channels.
- Investigate MS channel behaviour in the presence of Ca^{2+} and other divalent cations.
- Determine whether Ca^{2+} can permeate through MS channels *in vivo* using the Ca^{2+} sensitive photoprotein aequorin.
- Test the hypothesis that MS channel expression provides a selective advantage to *E. coli* in the presence of cell wall targeting antibiotics and enzymes.

Chapter 2: Materials and methods

2 Materials and Methods

2.1 Reagents

All reagents were analytical grade and purchased from Sigma Aldrich unless otherwise stated.

2.2 Bacterial strains

The genotypic details of strains used within this thesis are shown in the following tables (Table 2.1 & Table 2.2).

Strain	Genotype details	Reference
FRAG-1	F$^-$, *lacZ82*(Am), λ$^-$, *rha-4*, *thi-1*, *gal-33*	(Epstein and Kim, 1971)
MJF453	FRAG-1, *ΔmscL::cm*, *ΔkefA::kan*	(Levina *et al.*, 1999)
MJF465	FRAG-1, *ΔkefA::kan, ΔmscL::cm, ΔyggB*	(Levina *et al.*, 1999)

Table 2.1. Genotypic details of multiple MS channel knockouts and their corresponding parent strain.

Strain	Genotype details
BW25113	*Δ(araD-araB)567, ΔlacZ4787(::rrnB-3), λ$^-$, rph-1, Δ(rhaD-rhaB)568, hsdR514*
ΔyggB	BW25113, *ΔyggB::kan*
ΔmscL	BW25113, *ΔmscL::kan*
ΔkefA	BW25113, *ΔkefA::kan*

Table 2.2. Genotypic details of single MS channel knockouts from the Keio collection and their corresponding parent strain.

Cm – Chloramphenicol **Kan** – Kanamycin (Tocris)

2.3 Bacterial culture

All *E. coli* strains were cultured with agitation at 37 °C in Lysogeny Broth (LB) media (1 % Tryptone (w/v); 0.5 % Yeast extract (w/v), 0.5 % NaCl (w/v)). Bacterial culture ingredients (Tryptone & yeast extract) were purchased from Oxoid via Fisher Scientific.

2.4 Bacterial transformation

2.4.1 Production of competent cells

Competent cells were generated using the following protocol. One single colony was selected and grown overnight in LB medium at 37 °C at 100 x g. The following day 300 µl of overnight culture was added to 15ml of LB in a 100 ml flask and grown to an OD_{600} = 0.4. The cells were then left on ice for 5 minutes. The cells were then centrifuged at 2700 x g for 5 minutes at 4 °C. The supernatant was discarded and the pellet resuspended on ice in 3.75 ml of ice cold 0.1 M $MgCl_2$. The resulting solution was then centrifuged at 2100 x g for 10 minutes at 4 °C. The bacterial pellet was then resuspended on ice in 750 µl of ice cold 0.1 M $CaCl_2$. An additional 6.75 ml of ice cold 0.1 M $CaCl_2$ was then added and left on ice for 30 minutes. The cells were then centrigued at 2100 x g for 10 minutes at 4 °C once again. The resulting pellet was resuspended in 50 µl of 0.085 M $CaCl_2$ in 15% glycerol and frozen on dry ice and stored at -80 °C.

2.4.2 Transformation

Competent cells were removed from -80 °C and put on ice. 50 µl of cells were added to a chilled 0.5 ml Eppendorf tube using chilled pipette tips. 2 µl of plasmid was added to the cells and then tubes were placed on ice for 20

minutes. Following this cells were heat shocked at exactly 42°C for 50 seconds and returned to ice for a further 2 minutes. To this mixture 450 µl of SOC (Super optimal broth with catabolite repression) medium was added and the resultant mixture was incubated for 1.5 hours at 37 °C and 100 x g. Then using a sterile spreader, 50 µl was spread onto LB agar plates containing the relevant antibiotic. Inverted plates were incubated over night and then stored in the fridge at 4 °C wrapped in parafilm.

2.4.3 Plasmid Isolation and Purification

This procedure was undertaken in accordance with the protocol set out by Qiagen using the QIAprep Spin Maxiprep Kit (Qiagen). The same procedure was used for all plasmids used in this thesis [Pmmb66EH-Aequorin (plasmid map available in chapter 3) , pQE60_LacI_MscS, pQE60_LacI_MscS_E187R, pQE60_LacI_MscS_E227A and pQE60_LacI_MscL (basic plasmid map shown in section 2.6.1)]. Individual colonies were inoculated into 10 ml of LB containing 100 µg.ml^{-1} of carbenicillin or kanamycin (depending on plasmid) and grown overnight at 37 °C and 100 x g. Bacterial cells were then harvested by centrifugation at 2500 x g for 15 minutes. The supernatant was removed and the pellet fully re-suspended in 10 ml of buffer P1 (50 mM Tris-HCl, pH 8.0; 10 mM EDTA; 100 µg/ml RNase). The resultant mixture was lysed with 10ml of buffer P2 (0.2 M NaOH; 1% SDS) by gentle mixing and incubated at room temperature for 5 minutes. 10 ml of chilled buffer P3 (3 M KAc, pH 5.5) was gently mixed in and incubated on ice for 20 minutes. The resultant mixture is centrifuged at 15500 x g for 30 minutes at 4°C. The supernatant is removed

and centrifuged again at 20000 x g for 15 minutes at 4 °C. A Qiagen-tip is then equilibrated via the addition of 10 ml of buffer QBT (750 mM NaCl; 50 mM MOPS, pH 7.0; 15% isopropanol (v/v); 0.15% Triton® X-100 (v/v)). The supernatant was then removed from the centrifuge and added to the Qiagen-tip and allowed to enter the resin by gravity flow. After full elution of the supernatant, 2 x 30 ml of buffer QC (1 M NaCl; 50 mM MOPS, pH 7.0; 15% isopropanol (v/v)) was added and again allowed to move through the tip via gravity flow. The DNA was then eluted using 15 ml of buffer QF (1.25 M NaCl; 50 mM Tris-HCl, pH 8.5; 15% isopropanol (v/v)) and collected in a 50 ml propylene centrifuge tube.

The next step was precipitation of the DNA. This was achieved via the addition of 10.5 ml of isopropanol. Once mixed the solution was centrifuged at 13000 x g for 30 minutes at 4 °C. The supernatant was decanted and the pellet washed with 5 ml of room temperature 70 % ethanol and centrifuged again at 13000 x g for 10 minutes. The supernatant was then carefully decanted and the pellet was air-dried for 5 - 10 minutes. The resulting DNA sample was resuspended in 200 µl of buffer TE (10 mM Tris-HCl, pH 8.0; 1 mM EDTA) and stored at -20 °C.

2.5 Formation of giant *E. coli* spheroplasts

A single colony of *E. coli* was inoculated into 10 ml of LB broth containing the antibiotic corresponding to the relevant resistance gene in the inserted plasmid (if present) and grown overnight at 37 °C in an orbital shaker at 100 x g. The next morning 100 µl of cells were transferred into 10 ml of LB broth

and grown to mid log phase OD_{600} = 0.4. At this point 3 ml of the broth was added to 27 ml of LB broth in a 250 ml flask and 180 µl of cephalexin (10 $mg.ml^{-1}$) was added to obtain a final concentration of 60 $\mu g.ml^{-1}$. The bacteria were then incubated for a period of between 2 - 3 hours at 37 °C and 100 x g in order to form filaments between 50 - 100 µm in length. After incubation 1 ml of the solution was transferred to an Eppendorf tube and centrifuged for 1 min at 1200 x g. The supernatant was then removed and replaced with 500 µl of 0.8 M sucrose, the pellet was NOT resuspended and was incubated at room temperature for 1 minute. The supernatant was removed and discarded and the pellet resuspended with 500 µl of 0.8 M sucrose. The following solutions were then added to the plasmolysed cells in a stepwise manner:

(i) 150 µl of 125 mM Tris-HCL, pH 8 KOH

(ii) 120 µl of 5 $mg.ml^{-1}$ Lysozyme (chicken egg white)

(iii) 30 µl of 5 $mg.ml^{-1}$ DNase 1

(iv) 75 µl of 250 mM EDTA, pH 8 KOH

Subsequently the cells were incubated at room temperature for between 5 - 10 minutes. A 5 µl sample was taken to monitor the process via phase contrast microscopy. Finally the stop solution (10 mM $MgCl_2$; 10 mM TRIS-HCl, pH 8; 800 mM Sucrose) was added and the final mixture incubated on ice for 4 minutes. Spheroplasts were either used for immediate electrophysiological study or stored at -20 °C. Spheroplasts were stable at -20

°C for up to 2 months with no difference in channel activity or seal formation observed over this period as previously reported (Martinac *et al.*, 1987).

2.6 Reconstitution of bacterial MS channels into Liposomes

2.6.1 Protein expression and purification

The M15 *E. coli* expression strain was transformed with separate pQE60-LacI vectors (plasmid map shown below) containing the relevant full-length coding sequence for MscL and MscS donated by Prof Boris Martinac's lab. Each protein had a 6x-His tag to aid in purification. This pQE60-MscS plasmid was used to carry out site directed mutagenesis (For further information see chapter 5).

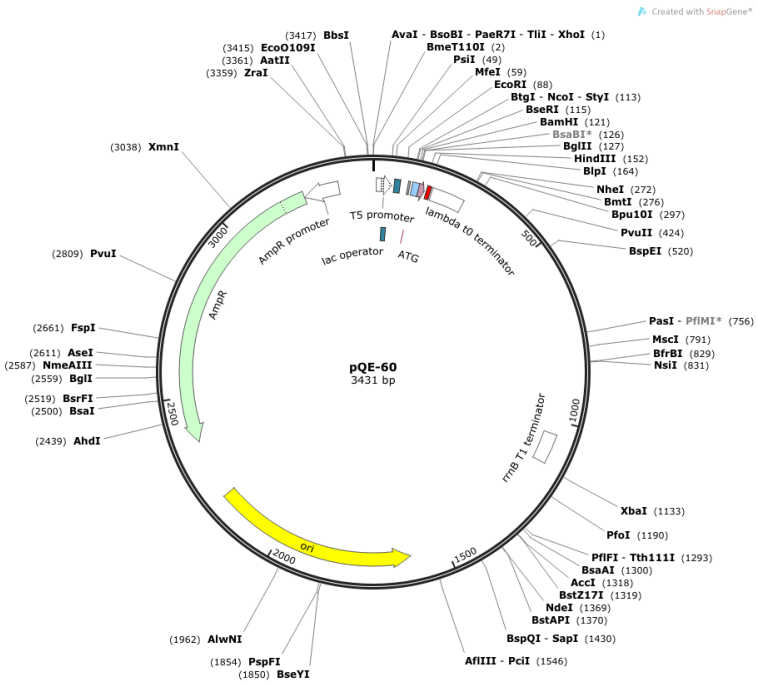

One single colony of transformed M15 *E. coli* (expression strain) was inoculated into 10 ml LB with 100 µg.ml^{-1} ampicillin and grown overnight at 37 °C and 100 x g. The next morning the overnight culture was added to 1 L of

fresh LB containing 100 µg.ml^{-1} ampicillin and incubated at 37 °C and 50 x g in an orbital shaker. The culture was grown to an OD of ~1 which took approximately three hours. The culture was then removed from the incubator and left at room temperature for 15 minutes while the incubator was set to 25 °C. To induce expression of the channels the culture was then supplemented with IPTG to a final concentration of 0.8 mM and glycerol to final concentration of 0.4%. This resulting culture was incubated at 25 °C for four hours at 50 x g. The cells were pelleted at 8900 x g for 10 minutes at 4 °C in a Beckman optima centrifuge (Beckman Coulter) and the supernatant discarded. The pellets were gently resuspended in phosphate buffered saline (PBS) pH 7.5 supplemented with 1 mM phenylmethanesulfonyl fluoride (PMSF), a generic protease inhibitor, using a fine tipped paint brush. The resulting cell suspension was supplemented with 100 µM DNase and disrupted using a Thermo electron FA-078AE French press (Thermo electron Corp.). The resulting sample was then stored at -20 °C until the following day. The samples were thawed the next morning using tepid tap water and the resulting suspension was pelleted at 8900 x g for 22 minutes. This step is to pellet unbroken cells and inclusion bodies leaving membrane-protein complexes in the supernatant. Next the membrane-protein complexes were pelleted in an Optima LE Beckman Coulter ultracentrifuge (Beckman Coulter) at 22500 x g for 170 minutes at 4 °C. The pellet was then resuspended in 5ml solubilisation buffer consisting of PBS pH 7.5 containing 10% glycerol, 1 mM PMSF and 10 mM n-dodecyl maltoside (DDM) and then topped up to 50 ml

and placed on a rocker at 4 °C overnight. The next morning the sample was centrifuged at 19000 x g for 15 minutes at 4 °C. The supernatant was then mixed with Talon metal affinity resin (Clontech)(2 ml per 1 L supernatant) for 3 hours at 4 °C on a rocker. The talon metal affinity resin is highly selective for his-tagged proteins. In this thesis 6x-His tags were used for WT-MscS, MscS mutant channels and WT-MscL. The incubated resin was then poured into PD-10 desalting column (Amersham) and allowed to settle prior to removal of the bottom cap. The column was washed through first with 20 ml of PBS pH 7.5, supplemented with 1 mM DDM and 10 % glycerol, and then with 20 ml of PBS pH 6 supplemented with 1 mM DDM, 10 % glycerol and 5 mM imidazole. During this stage proteins not of interest are run through the column. Elution of the target channel protein was carried out using 5ml of PBS pH 6 supplemented 1 mm DDM, 10 % glycerol and 500 mM imidazole. The imidazole has higher affinity for the resin than the his-tagged channel protein and thus drives the protein from the column. The solution was then concentrated to around 1 ml using a 100 kDa Ultra-15 centrifugal filter device (Millipore). This was carried out using a bench top centrifuge at 1100 x g and 4 °C for 15 minutes. The final concentrated protein solution was kept at 4 °C prior to use. The wild type MscS used in this thesis was donated by the Martinac laboratory.

2.6.2 Protein quantification

The Bicinchoninic acid (BCA) assay kit (Sigma) was used to quantify the amount of purified MscS protein in each sample. The standard protein used in

this protocol was bovine serum albumin (BSA)(stock solution 10 $mg.ml^{-1}$). Dilution of this stock solution was carried out to give concentrations of 8, 4, 2, 1, 0.5, 0.25 and 0.125 $\mu g.ml^{-1}$. The solutions were placed in a 96 well plate in triplicate (10 µl). In addition 5 µl of the MscS protein sample was also placed into the same 96 well plate in triplicate. One part BCA protein assay reagent B (Copper II Sulphate pentahydrate 4 % solution) was added to 50 parts BCA protein assay reagent A (Bicinchoninic acid solution, pH 11.25) and 200 µl of the resulting mixture was added to each well of the 96 well plate. The plate was covered with aluminium foil and placed in a shallow water bath at 37 °C for 30 minutes. The absorbance at 540 nm was then measured using an microtitre (MT) plate reader. The corresponding absorbance of each concentration of BSA solution was then used to construct a standard curve and the equation of the line was used to calculate the concentration of protein in each MscS protein sample.

2.6.3 Protein incorporation into liposomes and liposome formation

Liposomes were formed by the dehydration-rehydration method (Hase *et al.*, 1995). Soyabean azolectin was chosen as the lipid vehicle for channel reconstitution as MS channels have been extensively studied in this system and it is comparatively cheap. Azolectin is comprised of Phosphatidylcholine (PC: ~33%), phosphatidylethanolamine (PE: ~33%) and Phosphatidylinositol (PI: ~33%). While the lipid composition of azolectin is not identical to that of the bacterial inner membrane (see chapter 3), this is not a huge problem in

this study as the parameters being studied are largely lipid composition independent.

A 20 ml glass test tube was washed thoroughly with double distilled water and dried using continuous nitrogen flow and 20 mg of azolectin added. The azolectin was then suspended in around 1 ml of chloroform. After full dissolution the chloroform was blown off gently using a slow nitrogen flow while rotating the glass test tube, resulting in an even coating of azolectin on the bottom of the tube. The azolectin was dissolved in 2ml of dehydration-rehydration (DR) buffer (200 mM KCl, 5 mM HEPES 5; pH 7.4, KOH). The azolectin DR buffer mix was then vortexed using a rotamixer mixer-vortex (HTZ) and placed in a Branson 200 bath sonicator (Emerson Industrial Automation) for 30 minutes. The resulting semi-transparent emulsion was added, in 200 µl aliquots, to 15 ml plastic tubes. The relevant amount of protein was added and diluted to 3 ml using DR buffer. The resulting mixture was incubated in a cold room at 2 – 8 °C for one hour. After this approximately 25 g of SM-2 adsorbent Biobeads (Bio-Rad) were added to each plastic tube and incubated again in a cold room at 2 – 8 °C this time for three hours. The Biobeads enable the removal of detergent, in this case DDM, which can damage the protein and have other deleterious effects during electrophysiological experimentation. Following this incubation the samples were centrifuged in an Optima LE Beckman Coulter ultracentrifuge (Beckman Coulter) at 22500 x g for 40 minutes at 4 °C. The pellet was then resuspended in 30 µl of supernatant and blotted onto a clean glass coverslip. The coverslips

were placed into a glass dessicator and left for at least six hours but usually overnight. The next morning samples were rehydrated with 20 µl of DR buffer and left for at least 2 hours before patching.

2.7 Electrophysiology

2.7.1 Electrophysiological equipment

The electrophysiological experiments undertaken in this thesis were carried out in both Cardiff University, Cardiff, UK and The Victor Chang Cardiac Research Institute, Sydney, Australia.

Cardiff: An I-V converter amplifying headstage (Axon instruments) mounted on a three dimensional hydraulic micromanipulator (Narashige) was connected to a silver chloride recording wire. Negative pressure applied via a syringe to activate MS channels was monitored via a piezoelectric pressure transducer (Thermosense) linked to Dempster WinEDR software. An OX722 oscilloscope (ITT Instruments) was used to visualise electrical activity with signals amplified by an Axopatch 1D amplifier (Axon instruments). Signals were also filtered by a four pole Bessel filter and subsequently digitised by a 12-bit AD converter (Axon Instruments) and sampled at 5 – 20 kHz. Recording electrodes were pulled from borosilicate glass capillaries (Harvard apparatus), with an inside diameter of 0.86 mm, using a DMZ-Universal puller (Zeitz-Instruments GmbH). The resulting microelectrodes typically had resistances ranging from 2 – 7 MΩ when filled with KCl recording solutions. Single channel analysis was done using WinEDR software (Strathclyde University).

SYDNEY: Borosilicate glass microelectrodes were formed from borosilicate glass capillaries (Drummond Scientific Co.,) using a Flaming/Brown pipette puller (P-87, Sutter Instruments Co.,). The resulting microelectrodes typically had resistances ranging from 2 – 7 MΩ when filled with KCl recording solutions. MS channel activity subsequent to negative pressure application monitored via a piezoelectric pressure transducer (Omega Engineering) was recorded using an Axon 1D patch-clamp amplifier (Axon Instruments) at a sampling rate of 10 kHz and filtered at 5 kHz. Single channel analysis was done using pCLAMP10 software (Axon Instruments).

2.7.2 Patch-clamp method: Spheroplasts

A solution of spheroplasts was thawed prior to patching with 1 µl then being added to 500 µl of recording solution inside a recording chamber. The recording chamber was then transferred to the stage of a Nikon inverted microscope (Nikon). The spheroplasts were inspected at 400x magnification to identify large enough specimens for patching. A recording electrode was backfilled with a suitable solution and placed over the silver chloride recording wire and screwed into place. On insertion of the electrode tip into the recording solution a large amount of positive pressure (~100 mmHg) was applied to prevent debris (from lysed spheroplasts) occluding the electrode tip. Also any junction potential that formed was negated manually using the DC offset on the amplifier. The recording electrode tip was then advanced towards the spheroplasts once the electrode tip was close enough to the spheroplast and before the positive pressure resulted in any movement of the

spheroplast the positive pressure was removed. The electrode tip was then moved towards the membrane of the spheroplast and a mild negative pressure was applied (~20 mmHg). In order for a seal to form prolonged periods (up to 45 minutes) of mild negative pressure were required. In addition, a holding potential of around + 30 mV also seemed to aid seal formation. Giga ohm seal formation took between 5 and 50 minutes.

2.7.3 Patch-clamp method: Liposomes

An aliquot of the liposome preparation (1 µl) was added to 500 µl of bathing solution in the recording chamber. The resulting unilamellar blisters that formed on the bottom of the recording chamber were used to record channels in the excised inside-out configuration at room temperature.

2.8 Measuring bacterial growth using a Microtitre plate reader.

One single colony of *E. coli* was inoculated into 10 ml of LB broth and grown overnight at 37 °C and 100 x g. A 96 well plate was then covered with a plastic coating and air holes were made for each corresponding well using a sterilised needle tip. The coating was then removed and 190 µl LB was placed in each well. Subsequently test compounds were added to a triplicate of wells including the addition of vehicle controls. Each well had 2 µl of test compound added resulting in a 100 fold dilution to the concentration of interest. Once this had been completed, 10 µl of cells were added to the relevant wells and the plastic coating was replaced. As a result each well had exactly the same volume. The Beer-Lambert law states that the absorbance is proportional to

the path length as shown below which is the reason for keeping the volumes the same.

$$A=\varepsilon bc$$

A - absorbance / light scattering

ε - molar absorptivity.

b - path length of the sample.

c - concentration of the compound in solution.

The Microtitre plate was then placed into the reader and the optical density at 590 nm (OD_{590}, which is proportional to cell number) was measured and recorded by the Microtitre plate reader software. The following program cycle was used;

1. 10 seconds shaking at 37 °C and 100 x g
2. OD reading at 590 nm.
3. 15 minutes incubation at 37 °C without agitation.

The protocol above is repeated up to a maximum of 33 times per run and bacterial growth was measured over periods of between 4 and 24 hours. After completion, data was transferred to Microsoft Excel 2007 and Graphpad Prism for statistical analysis.

Generation times of the bacterial strains were also calculated by first plotting OD_{590} (y-axis) against time (x-axis) and taking points within the linear portion

(i.e. log phase) of the resulting graph. The Log absorbance$_{590}$ of those points was then plotted against time resulting in a linear plot. The generation time was then calculated via the following equation;

$$G = \frac{\ln 2}{m}$$

Where G is generation time and m is the slope of the line generated by plotting log absorbance$_{590}$ (y-axis) against time (h) (x-axis).

2.9 Statistical analysis

Data are presented within this thesis as means ± SEM unless otherwise stated, with the number of replicates n indicated in respective figure legends. Statistical significance was determined using either one-way ANOVA or student T-test with statistical significance assumed with p-values < 0.05. Post-hoc tests were used in combination with one-way ANOVA in order to determine statistically significant differences between specific groups, the post-hoc tests employed were either Bonferroni's (group size < 4) or Tukey's (groups size > 4).

Chapter 3: Divalent cation permeation through bacterial MS channels

3 Divalent cation permeation through bacterial MS channels

3.1 Introduction

Since the first report of bacterial MS channels in 1987 (Martinac *et al.*, 1987) almost every publication and report of their activity has been undertaken in the presence of fairly large concentrations of divalent cations (Mg^{2+} and Ca^{2+})(Akitake *et al.*, 2007, Edwards *et al.*, 2008, Martinac *et al.*, 1987, Sukharev, 2002). For example the first report of MS channel activity (Martinac *et al.*, 1987) was carried out in the presence of 90 mM $MgCl_2$ and 10 mM $CaCl_2$. The main reason suggested for this is to stabilise the 'nude' membrane of giant *E. coli* spheroplasts, enabling the formation of a giga seal. However, despite these relatively high levels of divalent cations no reports are available of MS channel activity in the presence of divalent cations alone and no information is available regarding *in vivo* divalent cation movement through MS channels. This chapter aims to address this by recording MS channels in the presence of divalent cations alone and to investigate whether MS channels permeate Ca^{2+} *in vivo*.

When we look at the relative pore sizes of MscL (~25 - 40 Å) (Perozo *et al.*, 2002, Cruickshank *et al.*, 1997) and MscS (~13 Å) (Wang *et al.*, 2008) it seems improbable that divalent cations would not permeate. In various solutions of slightly differing divalent ionic composition reports show no difference in the open probability or pressure sensitivity of MscL or MscS but differences are seen in the unitary conductance of these channels. This in all likelihood is

related to the differing bulk conductivities of the test solutions (Martinac *et al.*, 1987, Sukharev, 2002, Edwards *et al.*, 2005). From this we can suggest that divalent cations permeate through both MscS and MscL but this by itself is not definitive evidence. For example permeability ratios in MscS for Cl^- against Ca^{2+} or Ba^{2+} have never been determined experimentally. The lack of ion selectivity and large pore diameter means that MscL would almost certainly allow Ca^{2+} to permeate (Sukharev *et al.*, 1993).

The situation is slightly different for MscK as ionic composition dramatically affects its activity. Without the presence of external K^+ (≥ 10 mM K^+) even in the presence of applied pressure the channel does not open (Li *et al.*, 2002). So while its pore size is purported to be similar to MscS, and when open would likely conduct divalent cations, studying MscK in the presence of divalent cations alone is not possible (Li *et al.*, 2002). With respect to the products of *ybdG*, *ybiO, yjeP* and *ynaI* which are recently reported *E. coli* MS channels (Edwards and Booth, 2011, Edwards *et al.*, 2012, Schumann *et al.*, 2010) we have no real structural information and no idea as to whether they would be permeable to Ca^{2+}. As a result this chapter will look for any form of mechanosensitive channel activity in native *E. coli* membranes in the presence of Ca^{2+}.

In addition to investigating divalent cation permeation work in this chapter aims to look at whether MS channel behaviour changes in the presence of

divalent cations alone, and whether divalent cations could play a regulatory role for any of the MS channels. For example one mechanosensitive channel parameter that may be affected by the presence of divalent cations is selectivity. MscL shows absolutely no ionic preference. MscK exhibits extremely weak anionic preference with a reversal potential in a three-fold KCl gradient that very slightly (~2 mV) approaches the reversal potential of Cl^- (Li *et al.*, 2002). So in the case of MscK and MscL, selectivity is unlikely to be affected as little to none is exhibited by these respective channels. MscS on the other hand displays weak but noticeable anion selectivity. The reported values for P_{Cl}/P_K are shown in Table 3.1 and range from 1.2 - 3. Initially it seems as though there is little correlation between the concentration of divalent cations in the recording solutions, or the pH given the reported P_{Cl}/P_K values. However, on closer inspection the P_{Cl}/P_K values, with the exception of that reported in Sotomayor *et al.,* 2007, seem to increase as the concentration of divalent cations increase.

E_{rev} pipette potential (mV)	**P_{Cl}/P_K**	**Bath solution (mM)**	**Pipette solution (mM)**	**$MgCl_2$ / $CaCl_2$ (mM)**	**pH**	**System**	**Ref.**
- 2.2	1.2	KCl 300	KCl 100	90 / 10	6	Spheroplasts	Sotomayor *et al.,* 2007
- 5	1.5	KCl 300	KCl 100	40 / n/a	6	Liposomes	(Sukharev, 2002)
- 8	2.7	KCl 400	KCl 200	40 / 10	7.2	Spheroplasts	(Martinac *et al.*, 1987)
- 9.5	2.1	KCl 600	KCl 200	90 / 10	7.1	Spheroplasts	(Edwards *et al.*, 2008)
- 12	3.0	KCl 600	KCl 200	90 /10	6	Spheroplasts	Li *et al.,* 1999

Table 3.1 Summary of published literature on MscS selectivity.

The question thus arises do divalent cations impact on the selectivity of MscS? The putative structural basis of MscS selectivity is further discussed in chapter 5 but this chapter will investigate the difference in anion-monovalent cation and anion-divalent cation permeability ratios of MscS.

Another parameter that could be affected by the presence of divalent cations is rectification. Noticeable rectification is seen in MscS but not MscL or MscK. MscS rectifies such that its conductance at positive pipette potentials (corresponding to hyperpolarising potentials) is larger than that at negative pipette potentials (depolarising potentials)(Li *et al.*, 2002, Martinac *et al.*, 1987, Sukharev, 2002).

The current paradigm suggests that electrostatic interactions are responsible for this rectification in particular residues such as K166, but this is yet to be definitively proven (Sukharev, 2002, Sotomayor *et al.*, 2006). The possibility thus remains that ionic interactions with these MscS residues could result in changes in the degree of rectification.

While *in vitro* experiments aimed at teasing out the effects of divalent cations on mechanosensitive channels are interesting a major question that exists is whether MS channels are permeable to Ca^{2+} *in vivo,* and if so, under what conditions?

3.1.1 Ca^{2+} movement via MS channels *in vivo.*

The question of Ca^{2+} movement arises due to fact that:

(a) There is a high concentration gradient (low µM – mM) for Ca^{2+} movement into the cell.

(b) There is a large membrane potential driving Ca^{2+} entry (~- 150 mV).

(c) MscL, MscS and MscK have large open pore diameters with the ability to accommodate multiple ions.

However under 'normal' conditions MS channels will be tightly closed to prevent any cytoplasmic leakage or Ca^{2+} movement. In this chapter MS channel modulators such as chlorpromazine (CPZ) and the local anaesthetic procaine, in addition to a reduction in external osmolarity are used to investigate this question (Martinac *et al.*, 1990). The central tenet is the addition of MS channel activators, or a reduction in external osmolarity will cause MS channel activation. During the opening of MS channels they become not only a mechanism for the efflux of intracellular osmolytes but also a conduit for Ca^{2+} influx because of this large driving electrochemical gradient for Ca^{2+} entry. In this scenario Ca^{2+} would essentially have to 'swim against the tide' of K^{+}, glutamate and other intracellular osmolytes being jettisoned. However if Ca^{2+} were to move in this manner, then it throws open the door to Ca^{2+} as a signal to initiate downstream effects such as gene transcription. Previous work suggests a rise in intracellular Ca^{2+} does not directly affect the transcription of MS channel genes (Naseem *et al.,* 2009), but it may affect other genes such as RpoS which have demonstrable importance in MS

channel expression. As discussed in the general introduction Ca^{2+} does influence the transcription of numerous bacterial genes (> 100)(Naseem *et al.*, 2009). Whether this counter current of Ca^{2+} would be possible, or cause any noticeable depolarisation, is unknown but what we can estimate is that only around an extra 500 ions would be needed to increase the intracellular Ca^{2+} concentration from 100 nM to 1 µM. So only brief channel open times would be required to provide enough Ca^{2+} to produce an intracellular Ca^{2+} transient. In order to monitor these potential changes in intracellular Ca^{2+} which may be produced by MS channel activators, or reductions in external osmolarity, the calcium sensitive photoprotein aequorin was utilised.

3.1.2 Aequorin

The photoprotein Aequroin was isolated from the luminous jellyfish *Aequorea victoria* (Shimomura *et al.,* 1963). It consists of a 189 amino acid apo-protein and the imidazolopyrazine prosthetic group coelenterazine (Campbell *et al.*, 1994). Aequorin contains three EF-hand domains where Ca^{2+} binding can occur, two of high affinity and one of lower affinity (Toma *et al.*, 2005). The binding of Ca^{2+} to these domains results in a conformational change which permits, with the use of O_2, conversion of coelenterazine to coelenteramide and the emission of CO_2 and the subsequent release of light in the blue spectrum (469 nm). Aequorin has been used for many years as a sensitive probe for intracellular free Ca^{2+}. This is not only of value for eukaryotes but also for bacteria (Jones *et al.*, 2002, Naseem *et al.*, 2007, Naseem *et al.*, 2008).

In this chapter aequorin is utilised to see whether Ca^{2+} can permeate through MS channels *in vivo* as described above. The advantages of using aequorin are that it has a high signal to noise ratio, it can be used over a wide Ca^{2+} range (100 nM to 100 µM) and it possesses high calcium selectivity.

3.1.3 Chapter aims

The overarching aim of this chapter is to show definitively divalent cation permeation through MS channels and to investigate how divalent cations affect MS channel behaviour with particular respect to MscS. The specific aims of this chapter are as follows:

- To set up protocols for the electrophysiological study of bacterial ion channels in native membranes and azolectin liposomes.
- To identify whether any channel activity can be seen in *E. coli* spheroplast membranes in symmetrical 100 mM $CaCl_2$ and $BaCl_2$.
- To determine whether divalent cations like Ca^{2+} and Ba^{2+} pass through MS channels.
- To characterise MS channel behaviour in the presence of $CaCl_2$ and $BaCl_2$.
- To determine whether Ca^{2+} permeates MS channels *in vivo* using the calcium sensitive photoprotein aequorin.

3.2 Methods

3.2.1 Electron Microscopy

3.2.1.1 Fixation

All samples were fixed *in situ* (i.e. directly in culture) with 25% v/v glutaraldehyde solution giving a final volume of 2.5% v/v glutaraldehyde. Bacterial cultures were fixed at 37 °C for 2hrs.

3.2.1.2 Scanning Electron Microscopy (SEM)

All samples were harvested by filtration onto Millipore filters (5.5 mm diameter, 0.45 µm pore size) prior to processing for SEM observation. Firstly the sample was washed with double distilled water for 5 minutes then washed numerous times with ethanol in order to dehydrate the sample (60% ethanol for 15 minutes then 70% ethanol for 15 minutes then 90% ethanol for 15 minutes and finally 100% ethanol for 60 minutes). Finally the sample was immersed in Hexamethyldisilazane for three 15 minute long washes. The samples were then air dried and stuck to an aluminium stub for SEM observation using double-sided tape. The sample was then sputter coated with gold for 2.5 minutes and observed in a JEOL 840A scanning electron microscope (JEOL Ltd) operating at 10 kV. False colour SEM images were then created in Photoshop Elements 9 (Adobe Systems Inc).

3.2.1.3 Transmission Electron Microscopy (TEM)

E. coli cells were harvested from culture media by centrifugation at 1500 x g for 5 minutes at room temperature while *E. coli* spheroplasts were harvested in a similar manner at 100 x g for 4 minutes at room temperature. The resulting pellets were resuspended in 4% agarose w/v (in ddH_2O)(Fisher),

allowed to solidify, and cut into small pieces roughly 1 mm^3. The resulting pieces were placed in distilled water for 5 minutes and then processed for EM in the acrylic resin LR White. The sample was then dehydrated in a similar manner to the SEM sample with numerous washes with ethanol. Firstly samples were washed with the following solutions for the corresponding amount of time:

- 50% ethanol for 15 minutes
- 70% ethanol for 15 minutes
- 90% ethanol for 15 minutes
- 100% ethanol for 60 minutes
- 1:1 LR White:100% ethanol for 30 minutes
- 1:0 LR White Three x 30 minutes
- 1:0 LR White overnight

The agarose pieces were then put into pre-cooled LR White (0°C), which had been dispensed into gelatine capsules (size '0'). Subsequent polymerisation was achieved by the cold catalytic method at 0°C for 24hr. After 24 hours the capsules were transferred into a 50 °C oven for 2 hours. After this 2 hour period the gelatine capsules were removed and the resin block was stored at room temperature. Ultra-thin sections were cut on a LKB III Ultramicrotome (LKB) and stained firstly with 4% uranyl acetate for 5 minutes followed by

Millonig's lead acetate for 30 seconds. Sections were observed using an FEI CM12 transmission electron microscope (Philips) operating at 80 kV with images recorded on an SIS MegaView III CCD digital camera.

3.2.2 Intracellular Ca^{2+} measurements

3.2.2.1 Bacterial transformation

FRAG-1 and MJF465 *E. coli* were cultured, made competent and transformed with the pMMB66EH plasmid [AmpR] as described in chapter 2.

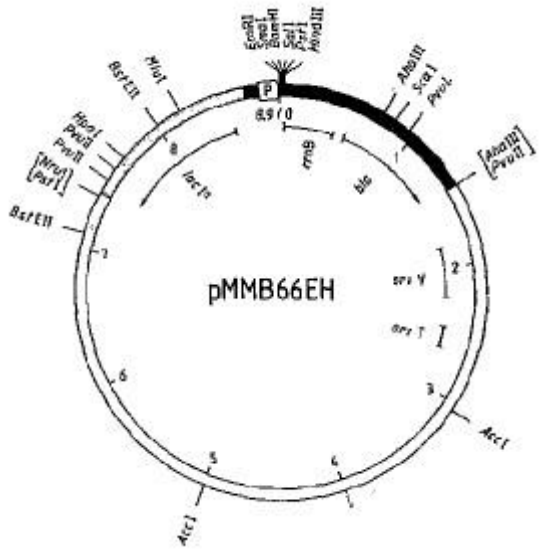

Previously it has been shown that apoaequorin is free inside *E. coli* cells when expressed in this plasmid and not taken up into inclusion bodies. Expression is controlled by a LacZ promoter and the addition of IPTG.

3.2.2.3 Expression of apoaequorin and reconstitution of functional aequorin

A single colony of transformed cells (FRAG-1 and MJF465) was inoculated into 10ml of LB broth containing 100 $\mu g.ml^{-1}$ ampicillin and grown overnight in an orbital shaker at 37 °C at 100 x g. The following day 1 ml of the overnight culture was transferred into a 250 ml flask containing 24 ml of fresh LB media

and grown up to an OD_{600} of ~0.25. Then IPTG was added to the flask at a final concentration of 1 mM and the cells were incubated for two hours in the orbital shaker at 37 °C at 100 x g. The resulting cells were centrifuged at 1400 x g for 5 minutes and the resulting pellet was washed three times with buffer AK (in mM: 125 NaCl, 1 $MgCl_2$, 3 KCl, HEPES 25; pH 7.4). This enables the removal of any excess Ca^{2+}. After this process the pellet was resuspended in buffer AK containing a final concentration of 5 µM coelenterazine and left in the dark for one hour. The cells were again centrifuged at 1400 x g and washed three times with buffer A this time to wash away excess coelenterazine. The bacteria were then stored at 4 °C prior to measurements of $[Ca^{2+}]_i$.

3.2.2.4 $[Ca^{2+}]_i$ measurements using a homebuilt luminometer

Equipment

The luminometer used in this thesis was designed in Cardiff (Campbell, 1988). The housing chamber consisted of a brass cylinder which rotated enabling the accommodation of LP3 plastic test tubes (Fisher). The PMT (Thorn EMI) was connected to an adjustable high voltage supply and cooled to -22.5 °C using FACT50 air-cooled thermoelectric housing (Thorn EMI) to reduce thermal noise. Test solutions were injected through a port housed directly above the sampling chamber. Due to multiple additions during each experiment there were light leaks which resulted from swapping syringes. These values were removed during data analysis.

3.2.2.5 $[Ca^{2+}]_i$ measurements procedure

Initially 50 µl of transformed bacterial cells were added to 450 µl of buffer AK. Counts were then measured for 60 seconds. These counts relate to basal intracellular calcium levels. Following this 500 µl of buffer AK supplemented with 2 mM $CaCl_2$ was added, resulting in a final experimental concentration of 1 mM external Ca^{2+}. The counts were then recorded for a further 120 seconds before the addition of either test compounds plus 1 mM $CaCl_2$ or control buffer AK with supplemented 1 mM $CaCl_2$ for comparison. The subsequent counts were recorded for 300 seconds and then buffer AK, supplemented with 40% NP40 (nonylphenoxypolyethoxylethanol), which is a detergent and was added to lyse all bacterial cells. The counts after NP40 addition were recorded for a further 300 seconds. The NP40 allows the release of unconsumed aequorin which enables the counts to be directly converted to intracellular Ca^{2+} levels. The conversion of light emission to calcium concentration was carried out using the following equation:

	Range of pCa
$pCa = 0.403 (-\log k) + 4.872$	8.5 – 4.5

The equation above is only valid in the range of pCa indicated and is documented in (Badminton *et al.*, 1996). In its basic form Ca^{2+} binding to aequorin and corresponding light emission follows a power law with a doubling of Ca^{2+} concentration giving a five-fold increase in light emission. In

order that the above equation can be solved, the following two points need to be addressed:

- calibration of aequorin in solutions of known Ca^{2+} concentration
- light output is corrected for aequorin consumption.

The second point is achieved by converting the emission of light to a rate constant (k^{-1}). The rate constant is calculated by dividing the number of counts by the remaining counts. This method allows the measurement of intracellular calcium between the ranges of 100 nM and 100 µM (Campbell, 1988).

3.2.3 Conductivity measurements

The bulk conductivities of recording solutions were measured using a Hanna 8633 conductivity meter (Hanna Instruments). Measurements were taken in triplicate and carried out as per the manufacturers protocol at room temperature (~22 °C). The conductivity meter probe was inserted into a tube containing around 35 ml of the appropriate solution ensuring the probe measuring holes were covered. The conductivity meter then measured the temperature which was subsequently adjusted manually on the meter. The conductivity meter then gave a conductivity reading in mS.cm to one decimal place. The probe was washed with room temperature double distilled water between solution readings.

3.2.4 Liposome reconstitution

Purified MscS protein was reconstituted in azolectin liposomes as described in chapter 2. In this chapter MscS was reconstituted at a protein to lipid ratio of 1:10000. Dehydrated liposomes were stored at 4 °C in a glass desiccator until required for use.

3.2.5 Electrophysiology

The electrophysiology set up was as described in chapter 2. The resistance of microelectrodes for patch clamping spheroplasts was between 4 – 7 MΩ and for liposomes was between 2 – 5 MΩ. All recordings were carried out in the excised inside-out configuration. In order to excise liposomes the microelectrode was gently moved away from the unilamellar blisters resulting in rupture of the liposome and an inside out patch being formed. In spheroplasts excised patches were more difficult to form. One of two methods were used to form excised patches. The first was to rapidly remove the spheroplast from the bathing solution and return it to the bath during which time the spheroplast would burst resulting in an excised inside-out patch. The second method was to apply shear pressure to the microelectrode by flicking the coarse manipulator to move the recording electrode which in turn 'threw' the spheroplast off the pipette. The pressure was then manually applied using a syringe, monitored using a pressure transducer and recorded using WinEDR software (Strathclyde University).

3.2.5.1 Electrophysiological recording solutions

All monovalent ionic solutions contained 40 mM $MgCl_2$ and 5 mM HEPES (pH 7.4 adjusted with NaOH). All divalent ionic solutions contained 5 mM HEPES (pH 7.4 adjusted with NaOH). Final concentrations of Na^+ after pH adjustment did not exceed 1.1 mM. For giant *E. coli* spheroplasts the bath solutions contained 300 mM sorbitol to prevent rupture.

3.2.5.2 Liquid junction potentials (LJP)

LJPs are potentials set up between the boundaries of two solutions of differing compositions. In the following chapter during the measurements of reversal potentials in differing solutions some large junction potentials were created. In order to correct corresponding reversal potentials the magnitude of said LJPs were estimated using JPCalc software (Barry, 1994). The measured reversal potential was then adjusted accordingly.

3.2.5.4 Calculating anion-cation permeability ratios

The anion-cation permeability ratios of MscS were calculated in this chapter using the following versions of the Goldman-Hodgkin-Katz equation.

Eq 3.1

Eq 3.2

Where X is a monovalent cation and Y is a divalent cation. The other terms are; R - the universal gas constant = 8.314 J K^{-1} mol^{-1}, F – the Faraday constant = 9.648 533 99(24)×10^4 C mol^{-1} and T is the temperature in Kelvin (295 K).

3.2.6 Hypoosmotic shock assay

One single colony of FRAG-1 and MJF465 *E. coli* was inoculated into 10 ml Hyperosmotic media (containing in mM: 60 Na_2PO_4, 5 K_2HPO_4, 7 Citric acid, 7.5 $(NH_4)_2SO_4$, 0.003 thiamine, 0.8 $MgSO_4 \cdot 7H_2O$ & 0.005$(NH_4)_2SO_4 \cdot FeSO_4 \cdot 6H_2O$; pH7) supplemented with 0.2 % glucose and 500 mM NaCl and grown overnight at 37 °C and 100 x g. The overnight cultures were then grown to an OD_{600} of 0.2 in fresh hyperosmotic media supplemented with 0.4 % glucose and 500 mM NaCl. Both strains were then diluted 1:20 into hyperosmotic (+ 500 mM NaCl) and hypoosmotic (- NaCl) media. The bacteria were then exposed to the relevant conditions for a period of either 5 or 30 minutes. Subsequent to this serial dilution of 1:10 in identical media was undertaken in triplicate and a 75 µl sample was plated out onto agar plates. After overnight incubation at 37 °C colonies were enumerated and the percentage cell survival was calculated. This was done by comparing the number of colonies present on agar plates from each strain not exposed to shock with the agar plates from solutions containing strains exposed to hypoosmotic shock.

3.3 Results

3.3.1 Spheroplast formation

Giant *E. coli* spheroplasts amenable to patch clamping were successfully generated from the following *E. coli* strains (for comprehensive genotypic details see chapter 2):

- BW25113 (Keio collection parent strain)
- Keio clone knockout mutants (Δ*mscL*, Δ*yggB,* Δ*kefA*)
- FRAG-1 (MJF parent strain)
- MJF465 (Δ*mscL*, Δ*yggB,* Δ*kefA*)

No measurable or noticeable morphological differences, at any stage of the spheroplast formation process, were observed between strains. All *E. coli* strains were around 2 µm in length and 0.5 - 0.75 µm in width. After treatment of log phase cells with cephalexin (60 $\mu g.ml^{-1}$) elongated cells or 'snakes' 25 – 100 µm in length were produced. Treatment of *E. coli* snakes made from log phase cells with Lysozyme/EDTA resulted in the formation of giant *E. coli* spheroplasts with diameters up to 15 µm. Using *E. coli* 'snakes' left over night at 4 °C resulted in a very low subsequent yield of giant *E. coli*

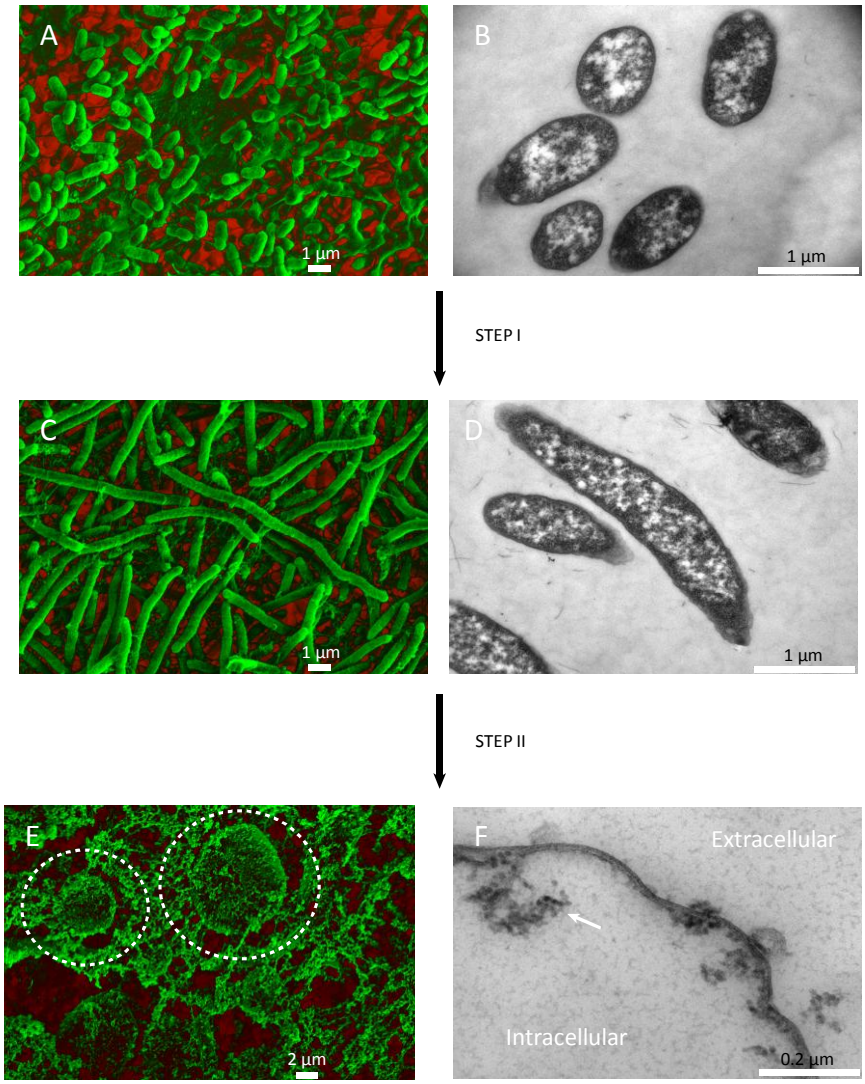

Figure 3.1. Spheroplast formation process. (A) False colour SEM image of FRAG-1 *E. coli* (B) TEM image of FRAG-1 *E. coli* (C) False colour SEM image of *E. coli* 'snakes' formed as a result of treatment with cephalexin (60 µg.ml^{-1}) (D) TEM image of *E. coli* 'snakes' formed as a result of treatment with cephalexin (60 µg.ml^{-1}) (E) False colour SEM image of *E. coli* spheroplasts (F) TEM image of *E. coli* spheroplasts with the arrow indicating a small amount of 'round debris' associated with the 'nude' inner membrane.

spheroplasts (< 10 %). The giant *E. coli* spheroplast population produced was heterogeneous with the majority measuring up to 10 µm in diameter and a small percentage (~10%) larger than 10 µm in diameter. There was roughly a 50:50 split of dark phase bright spheroplasts and light grey almost translucent spheroplasts.

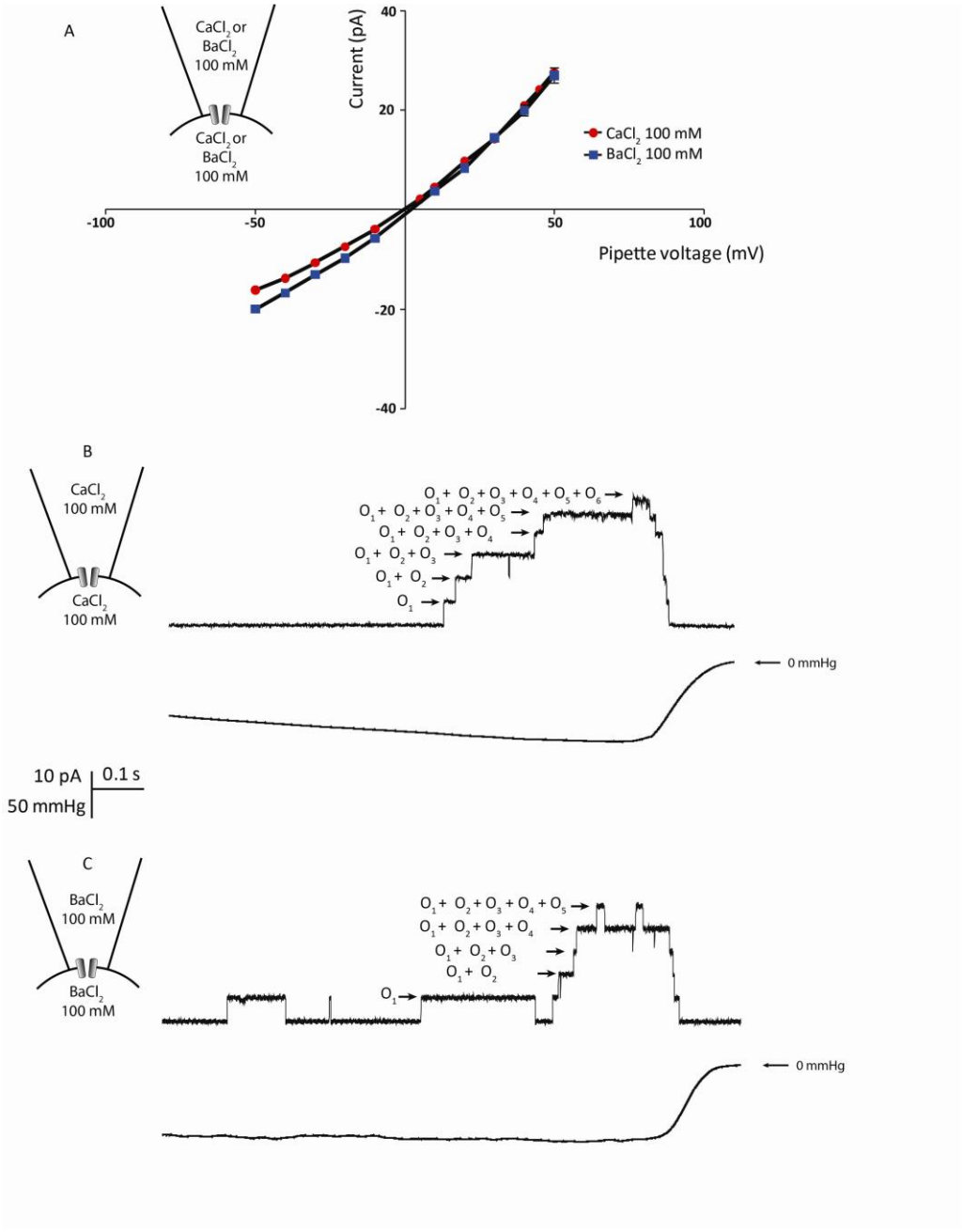

Figure 3.2 Mechanosensitive channel activity in excised inside-out patches of BW25113 *E. coli* spheroplasts. (A) Current-voltage plot for a mechanosensitive channel in symmetrical 100 mM $BaCl_2$ (n=4) or 100 mM $CaCl_2$ (n=3), both contained HEPES 5 mM, pH 7.4. Error bars represent SEM. Raw records illustrating activity of mechanosensitive channels at + 30 mV pipette potential in (B) symmetrical 100 mM $CaCl_2$ and (C) symmetrical 100 mM $BaCl_2$ with corresponding pressure traces shown beneath.

Samples from the three morphological stages of spheroplast formation were fixed with 2.5 % glutaraldehyde and visualised using scanning electron

microscopy (SEM) and transmission electron microscopy (TEM) (Figure 3.1). Interestingly the spheroplasts viewed under SEM seem to have multiple perforations in their membranes (Figure 3.1E). In addition, a large amount of debris is evident likely to be remnants of the outer membrane. The TEM image in Figure 3.1F displays the 'nude' inner *E. coli* membrane and some 'round debris' associated with the intracellular side of the membrane.

3.3.2 Patching giant *E. coli* spheroplasts

Patching giant *E. coli* spheroplasts was technically challenging and time consuming with giga ohm seals taking up to 45 minutes to form in a large percentage of cases (~70%). It seemed as though dark spheroplasts which appeared phase bright were more amenable to patching (i.e. seals formed quicker) than light grey translucent ones. Despite this fact no difference was observed between MS channel activities in dark spheroplasts as opposed to light grey translucent ones. The patch stability seemed to be a function of time taken for the seal to be formed. The longer it took for seals to form the longer lasting and more stable the patches were. Although this was only an observation and was not quantified in anyway.

3.3.2.1 Mechanosensitive channels in giant *E. coli* spheroplasts

Initial experiments were carried out using symmetrical 100 mM $CaCl_2$. The only difference in solutions was the addition of 300 mM sorbitol to the bathing solution to prevent rupture of spheroplasts due to osmotic pressure.

On initial inspection one type of mechanosensitive channel activity was identified in the presence of symmetrical 100 mM $CaCl_2$. On the manual application of negative pressure via a syringe a single population of channels opened. The number of channels that opened in each patch ranged from 2 channels to 10 channels. As shown in Figure 3.2B immediately on removal of negative pressure the channels closed.

From the I-V plot shown in Figure 3.2 it is evident that this channel rectifies such that its conductance is larger at positive pipette potentials than negative pipette potentials. At positive pipette potentials the conductance of this channel in symmetrical 100 mM $CaCl_2$ was 545 ± 26 pS (r^2 = 0.99) (n = 3). At negative pipette potentials its conductance was 330 ± 19 pS (r^2 = 0.98) (n = 3). Thus the conductance at positive pipette potentials was some 1.65 times higher. This is taking into account only the linear portions of the I-V plot at both negative and positive potentials respectively.

In addition to symmetrical $CaCl_2$, similar activity was seen in symmetrical 100 mM $BaCl_2$ (Figure 3.2C). In 100 mM $BaCl_2$ the conductance at positive potentials was 559 ± 22 pS (r^2 = 0.98) (n = 4) and at negative potentials was 363 ± 14 pS (r^2 = 0.98) (n = 4). The same rectification noted in the presence of $CaCl_2$ was seen in the presence of $BaCl_2$. In the case of $BaCl_2$ the conductance at positive potentials was 1.54 times higher.

3.3.2.2 Pressure threshold

As shown in Figure 3.3 the pressure threshold (P_t) to activate this channel was unaffected by voltage over a range of + 50 to - 50 mV pipette potential. In the

presence of $CaCl_2$ the average P_t was 123.8 ± 22.9 mmHg (n = 4). The P_t in the presence of symmetrical $BaCl_2$ was 128.7 ± 20.5 mmHg (n = 4) and was also unaffected by voltage. There was no statistically significant difference between the P_t of this channel in symmetrical $CaCl_2$ and $BaCl_2$.

A

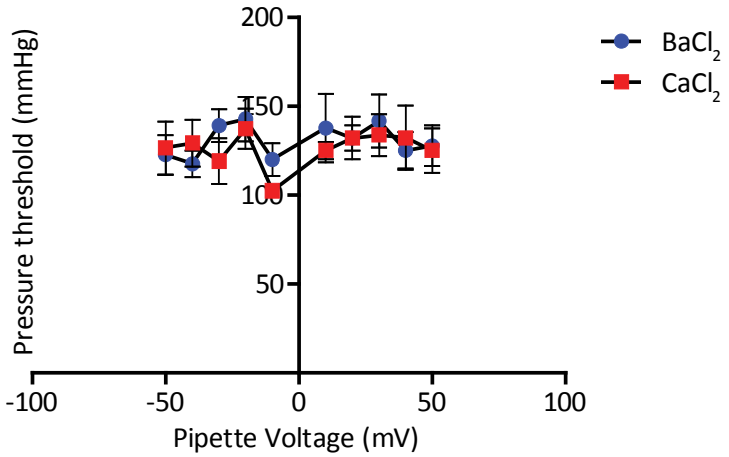

B

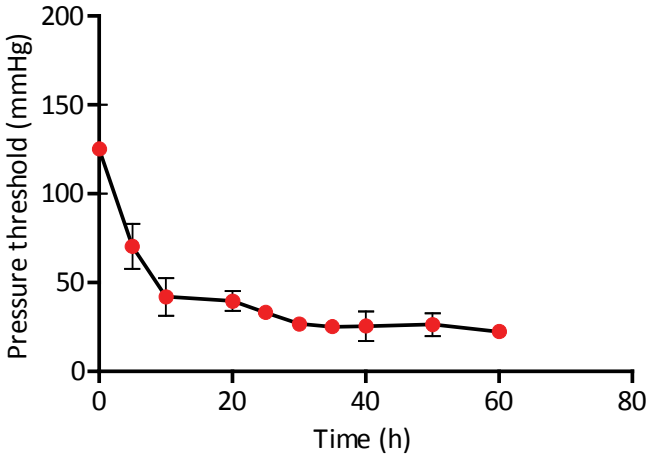

Figure 3.3 Pressure threshold of activation of a mechanosensitive channel in the presence of $BaCl_2$ and $CaCl_2$ in E. coli spheroplast membranes. (A) Pressure threshold of activation of the mechanosensitive channel in excised inside-out patches measured in mmHg at different pipette voltages in the presence of symmetrical 100mM $BaCl_2$ and $CaCl_2$. Errors bars represent ± SEM. (B) Pressure threshold against time at a constant pipette voltage of + 30 mV. Each point is made up of an intra-patch average of at least 6 openings averaged over n patches. In the case of the 60

minute (n = 1). Errors bars represent ± SEM in some cases the error bar is smaller than the plotted point.

Interestingly the pressure threshold of this channel reduced over time. The initial pressure threshold as previously mentioned was 123.8 ± 22.9 mmHg (n=4). The initial drop over the first 10 minutes was quite noticeable and rapid. By the 10 minute mark the P_t had dropped to 48.9 ± 10.5 mmHg (n = 4). After 20 minutes the pressure threshold had dropped to an average value of 39.5 ± 5.6 mmHg (n=4). The P_t then only reduced very slowly over the next 40 minutes. Only one patch managed to survive to the 60 minute time point. At this point the threshold had reduced to 22.3 mmHg. Over this period there was no noticeable change in open channel characteristics.

3.3.3 A 'novel' channel?

In addition to this mechanosensitive channel activity, another channel was identified in symmetrical $CaCl_2$. This channel was seen infrequently (3/17 patches) and required substantial depolarising steps (~65 mV) to gate. Once open, the channel stayed in the open state only for brief periods with the patch returning to a quiescent state after around 5 seconds. The channel conductance in symmetrical 100 mM $CaCl_2$ was 89 ± 14 pS (R^2 = 0.797). The spheroplast membranes were very unstable at or above + 65 mV pipette voltage and as a result the data became difficult to analyse (i.e. low signal to noise ratio). Figure 3.4A shows a segment of raw record documenting this 'novel' activity.

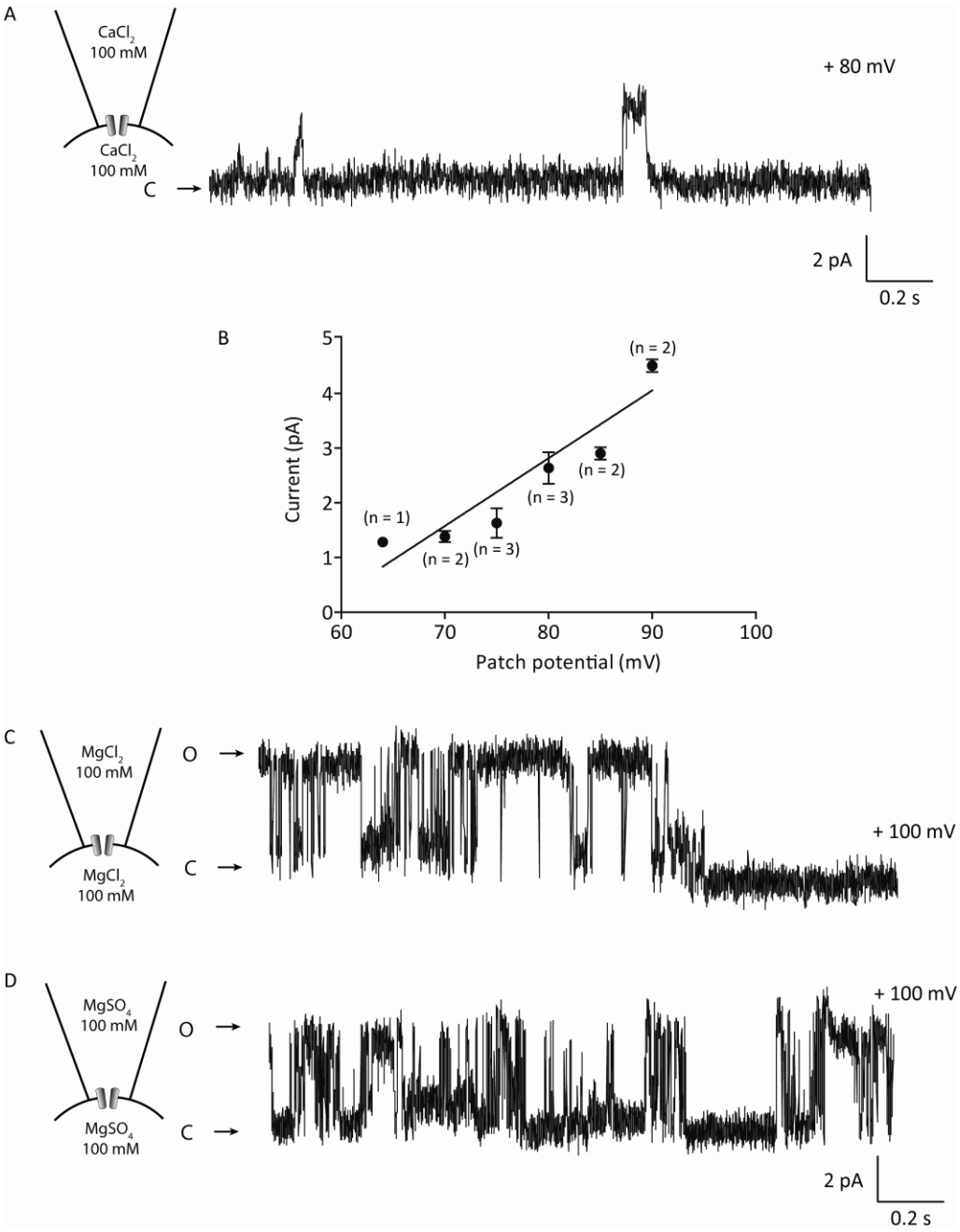

Figure 3.4 'Novel' channel activity identified in *E. coli* spheroplast membranes. (A) Raw record illustrating 'novel' channel activity in the presence of symmetrical 100 mM $CaCl_2$ after a + 80 mV step in membrane voltage. (B) Current-voltage plot constructed from 'novel' channel activity in the presence of symmetrical 100 mM $CaCl_2$ fitted with a linear regression line (R^2 = 0.797) yielding a single channel conductance of 89 ± 14 pS. (C) Raw record illustrating 'novel' channel activity in the presence of symmetrical 100 mM $MgCl_2$ after a + 100 mV step in membrane voltage. (D) Raw record illustrating 'novel' channel activity in the presence of symmetrical 100 mM $MgSO_4$ after a + 100 mV step in membrane voltage.

To try to determine whether this activity was due to a cation permeable channel or Cl^- permeant channel, recording solutions containing $MgCl_2$ and $MgSO_4$ were used. The reason $CaSO_4$ was not used was due to problems with pH buffering and ionic dissociation. Similar activity as that documented above was identified in the presence of symmetrical 100 mM $MgCl_2$ and $MgSO_4$ (2/7 and 2/9 patches respectively)(Figure 3.4C & D). Insufficient analysable records were obtained to construct an I-V plot although the amplitude of openings at + 100 mV patch potential were in keeping with what was seen in symmetrical $CaCl_2$ (at + 90 mV patch potential the current amplitude was 4.5 ± 0.2 pA). At + 100 mV patch potential in $MgSO_4$ the opening amplitude was ~4.7 pA and in symmetrical 100 mM $MgCl_2$ it was ~5.2 pA (Figure 3.4C & D). Due to the low signal to noise ratio and the relative small prevalence of this channel no further characterisation was attempted.

3.3.4 Molecular identification of MS channel seen in symmetrical $CaCl_2$ and $BaCl_2$

The next aim was to decipher what the mechanosensitive channel activity seen in spheroplasts membranes in symmetrical $CaCl_2$ and $BaCl_2$ was due to. The small conductance in comparison to MscL and the inability of MscK to open in the absence of periplasmic/external K^+ meant that the most likely candidate channel was MscS. So to test this purified MscS protein was incorporated in azolectin liposomes and patched in the presence of symmetrical $CaCl_2$ and $BaCl_2$.

3.3.4.1 Liposome formation

The process by which unilamellar liposomes form is complex and is to a large extent unknown (Akashi *et al.*, 1996). In the presence of 100 mM $CaCl_2$ and $BaCl_2$ it was difficult to form unilamellar blisters (shown in upper inset of Figure 3.5). In general the unilamellar blisters that did form were much smaller in size than those formed in the presence of 200 mM KCl (the standard solution used when patching mechanosensitive channels in azolectin liposomes (Sukharev, 2002)). These blisters tended not to be larger than 10 μm in size, whereas in standard solutions they could be up to 30 μm in diameter. In addition the relative density of these blisters was also reduced in comparison to the standard bathing solution. On multiple occasions only one or two unilamellar blisters could be identified in the recording chamber around 20 - 30 minutes after addition.

3.3.4.2 MscS reconstituted in liposomes

In the presence of symmetrical 100 mM $BaCl_2$ and $CaCl_2$ the conductance of MscS at positive pipette potentials was 555 ± 24 pS (n = 12) and 547 ± 35 pS (n = 4) and at negative pipette potentials was 354 ± 17 pS (n = 12) and 337 ± 32 pS (n = 4) respectively. Channel activity in $CaCl_2$ and $BaCl_2$ was indistinguishable as shown in Figure 3.5. If we then compare the mechanosensitive activity seen in spheroplast membranes with that of MscS reconstituted in liposomes we see they are identical (Figure 3.6).

Interestingly MscS rectifies in exactly the same direction in liposomes as in spheroplast membranes i.e. the conductance at negative pipette potentials

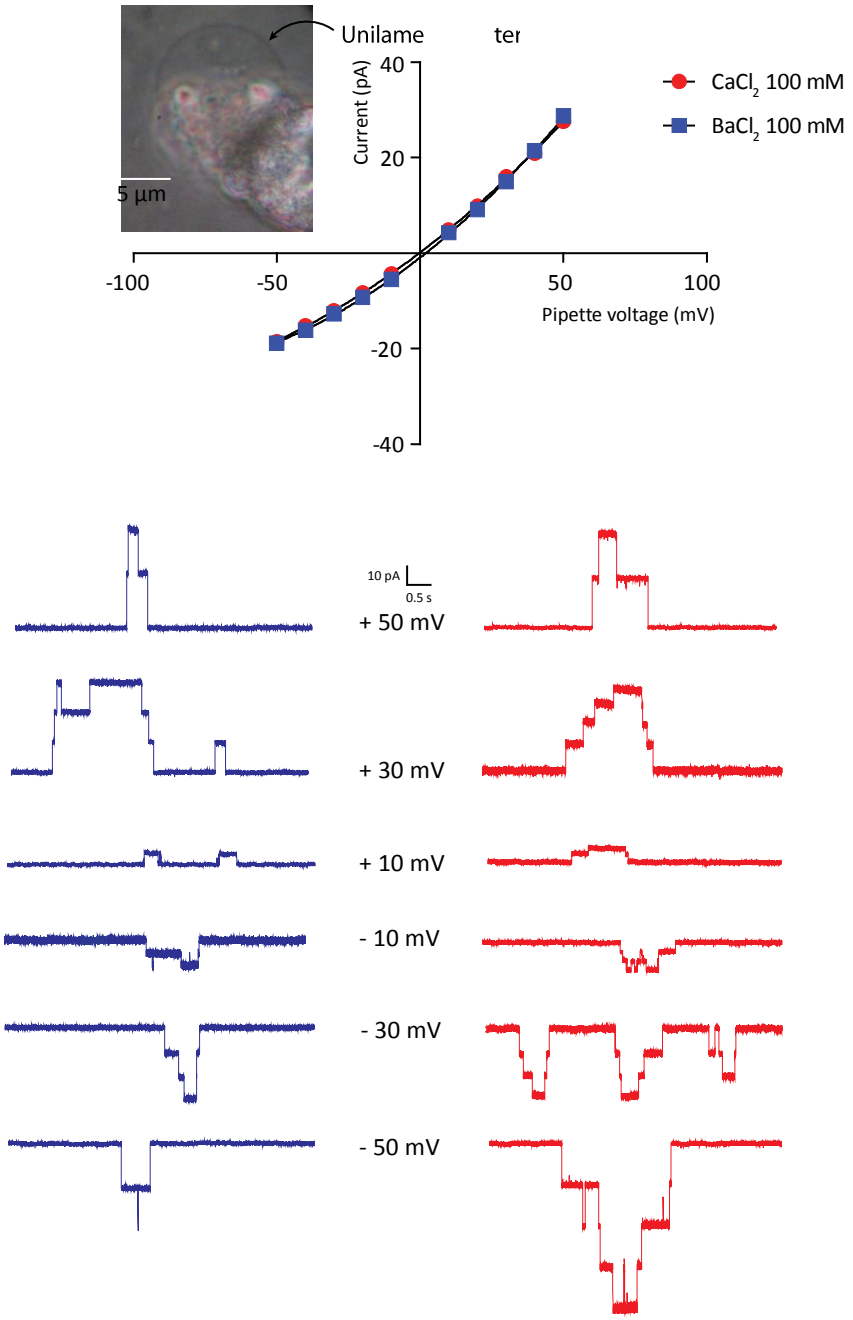

Figure 3.5 Comparsion of MscS activity reconstituted in azolectin liposomes in symmetrical $CaCl_2$ and $BaCl_2$. Top panel is an I-V plot illustrating the current voltage relationship in the presence of symmetrical 100 mM $CaCl_2$ (red) and $BaCl_2$ (Blue). The inset shows a phase contrast microscopy image of a liposomal blister patched during these experiments at x400 magnification. The lower panel shows raw records of channel activity in the symmetrical $CaCl_2$ (red) and $BaCl_2$ (blue) at various pipette potentials.

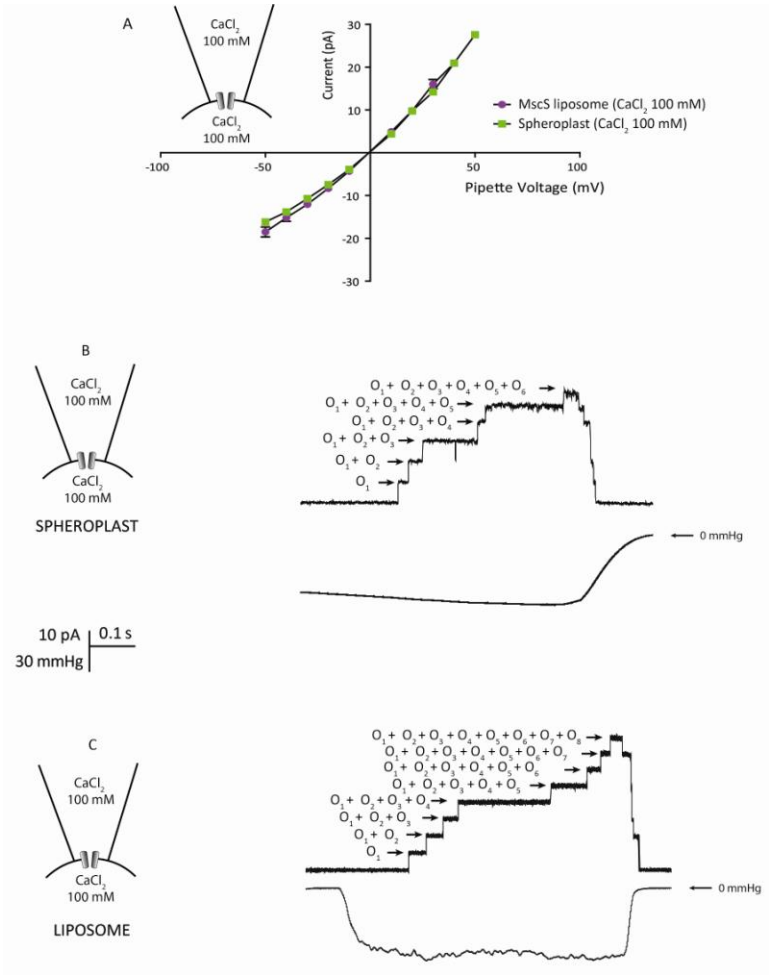

Figure 3.6 Comparison of mechanosensitive channel activity observed in symmetrical $CaCl_2$ 100 mM in excised inside-out patches from BW25113 *E. coli* spheroplasts and MscS reconstituted in azolectin liposomes (1:10000). (A) Current voltage plot of MscS activity in azolectin liposomes (n=4) against mechanosensitive channel activity observed in BW25113 *E. coli* spheroplasts (n=2) recorded in symmetrical $CaCl_2$ 100 mM, HEPES 5 mM, pH 7.4. (B) Raw record of MscS activity in azolectin liposomes in $CaCl_2$ 100 mM, HEPES 5 mM, pH 7.4 at + 30 mV patch potential. (C) Raw record of mechanosensitive channel activity in BW25113 *E. coli* spheroplasts in $CaCl_2$ 100 mM, HEPES 5 mM, pH 7.4 at + 30 mV pipette potential.

(depolarising potentials) is smaller than at positive pipette potentials (hyperpolarising potentials). In addition to this, there seems to be a greater degree of rectification in the presence of $BaCl_2$ and $CaCl_2$ in comparison to the standard solution containing KCl (a comparison with $BaCl_2$ is shown in Figure

3.7). The conductance ratio (i.e. conductance at positive pipette potentials over the conductance at negative pipette potentials) in the presence of symmetrical 100 mM $BaCl_2$ being 1.57 while in 200 mM KCl it was 1.35. In fact when the $BaCl_2$ concentration was increased to 200 mM the conductance ratio increased to 1.75 [g_+ : 1110 ± 72 pS (n = 3), g_- : 634 ± 72 pS (n = 3)]. The conductance of MscS at positive pipette potentials in the presence of symmetrical 200 mM $BaCl_2$ exceeded that seen in the standard KCl solution [g_+ : 1078 ± 30 pS (n = 7)]. When the bulk conductivities of solutions were measured it was found that the lower conductance of MscS in the presence of $CaCl_2$ and $BaCl_2$ could be explained simply by the lower bulk conductivity (15 and 17 mS.cm respectively) in comparison to the standard KCl solution (24 mS.cm). The conductance of MscS at positive potentials increases with increasing bulk conductivities of recording solutions although the relationship seems not to be totally linear when we compare divalent and monovalent cations (Figure 3.7B).

The activity of MscS in the presence of equimolar alkali metal chlorides is shown in Figure 3.7C. This shows that the largest conductance at positive pipette potentials is seen in KCl. Whereas MscS shows the lowest conductance at positive pipette potentials in the presence of LiCl, which also

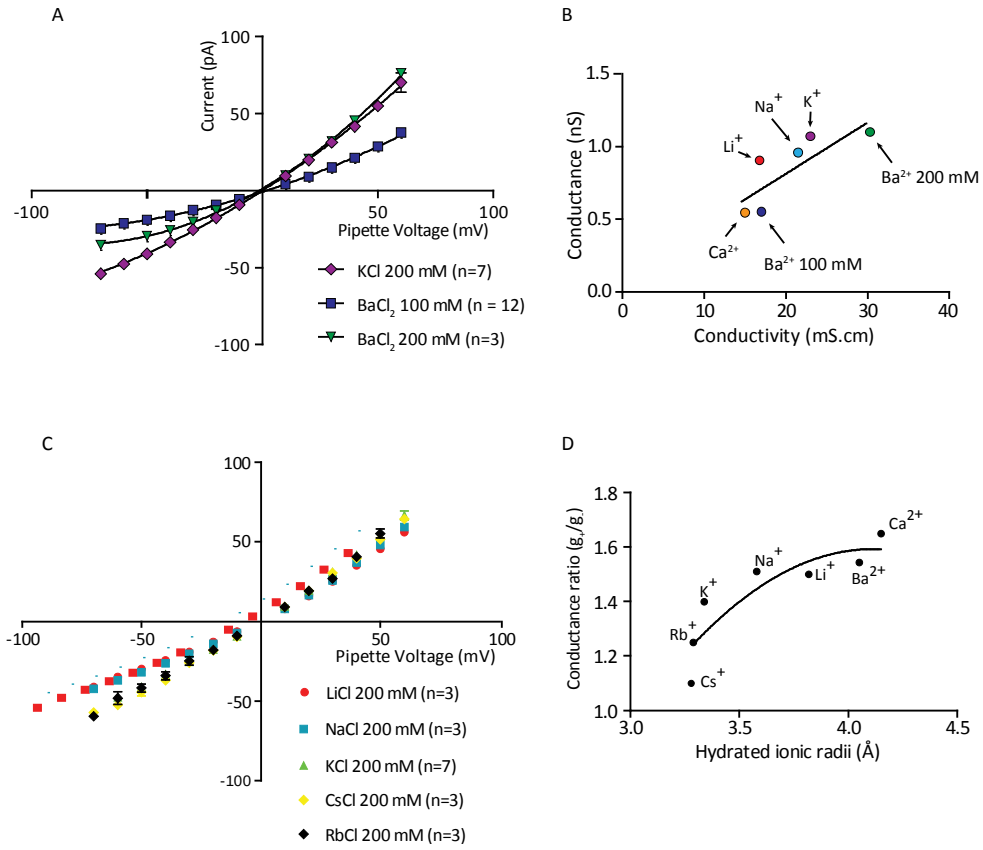

Figure 3.7 MscS rectification and conductance in the presence of different monovalent and divalent cations. (A) Current-voltage plot for MscS in the presence of symmetrical KCl 200 mM, $BaCl_2$ 100 mM and $BaCl_2$ 200 mM, HEPES 5 mM pH 7.4. There is a larger degree of rectification at negative pipette potentials in the presence of Ba^{2+} than when K^+ is the major permeant cation. (B) Conductance at positive pipette potentials against bulk solution conductivity, fitted with a linear regression line (R^2 = 0.644), to illustrate how MscS conductance increases with increasing bulk solution conductivity. (C) Current voltage plots for MscS in the presence of equimolar alkali metal chlorides. An increase in rectification is seen at negative pipette potentials as the hydrated ionic radii of the major permeant cation is increased (See table 1.1 for full details). (D) Conductance ratio of MscS plotted against the hydrated ionic radii of the major permeant cation. This shows how the rectification increases with increasing hydrated ionic radii.

Solution	Conductance at positive	Conductance at negative	Conductance ratio
LiCl	905 ± 18	605 ± 19	1.50
NaCl	960 ± 36	635 ± 15	1.51
KCl	1078 ± 30	799 ± 21	1.35
RbCl	1029 ± 61	822 ± 69	1.25
CsCl	1033 ± 48	894 ± 50	1.15

Table 3.2 Conductance of MscS in the presence of symmetrical alkali metal chlorides. The corresponding conductance ratio, as an indicator of rectification, is also shown.

along with NaCl shows the largest degree of rectification (g_+/g_- : 1.50 & 1.51 respectively). If we compare the hydrated ionic radii of the major permeant cation with the degree of rectification we can see that as the hydrated ionic radii increases so too does the degree of rectification (Figure 3.7D).

3.3.4.3 MscS subconducting states

During experimentation it was noticed that MscS exhibited a number subconducting states (Figure 3.8A & B). These have previously been reported however in the presence of symmetrical 100 mM $CaCl_2$ and $BaCl_2$ they are very long lived. These subconducting states are explored further in chapter 4 of this thesis.

3.3.4.4 Anion-cation permeability ratios

As previously mentioned, MscS exhibits weak anion selectivity with reported P_{Cl}/P_K values ranging from 1.2 – 3. The exact information pertaining to the reported P_{Cl}/P_K values are set out in Table 3.1 and 3.3. Firstly the P_{Cl}/P_K was calculated by measuring the reversal potential in a three-fold KCl gradient of 200 mM to 600 mM. In this case with 600 mM KCl in the bath it was extremely

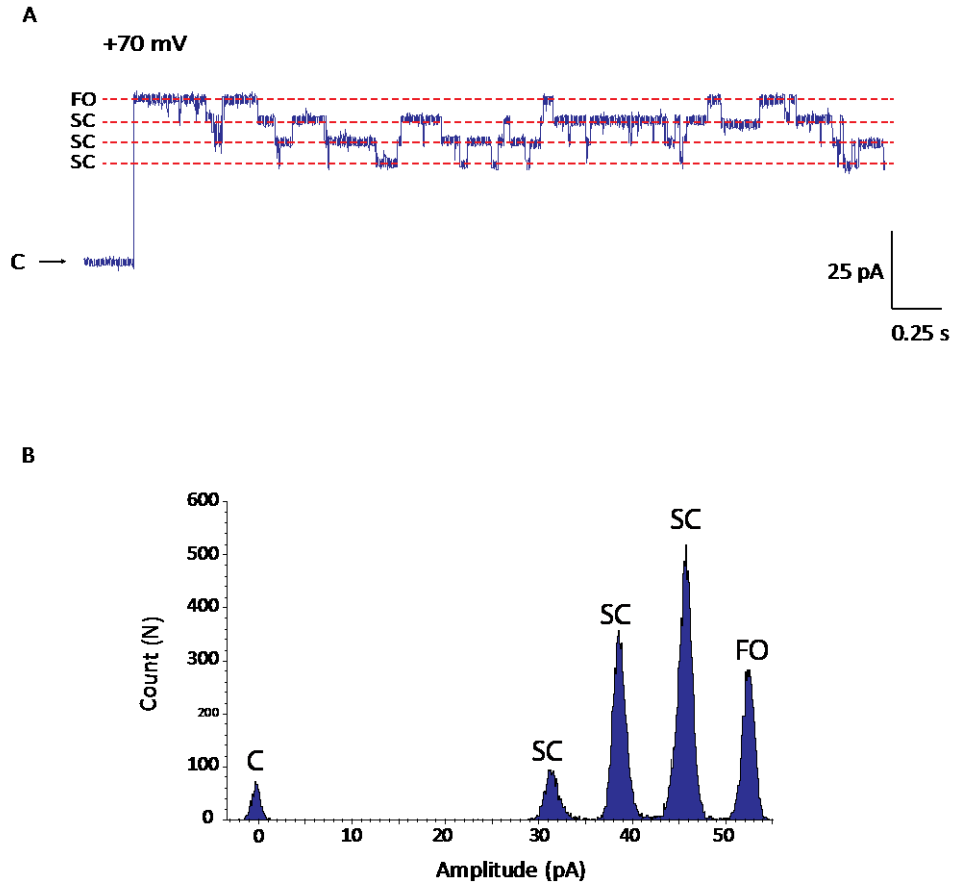

Figure 3.8. Subconducting states in MscS in the presence of symmetrical $BaCl_2$. (A) Raw record of MscS activity reconstituted in azolectin liposomes at + 70 mV pipette potential in inside-out patches under symmetrical conditions ($BaCl_2$ 100 mM, HEPES 5 mM, pH 7.4). The record shows 3 long lived subconductance states. (B) All points distribution of current histogram from raw record depicted in (A) illustrating the presence of 3 subconducting states [C: Closed, FO: Fully open, SC: Subconductance state].

difficult to form unilamellar blisters, so the gradient was reversed as shown in the inset in Figure 3.9. This resulted in a reversal potential of + 12.22 ± 1.07 mV (n = 4). The liquid junction potential (LJP) in this scenario was -0.4 mV as calculated using JPCalc (Barry, 1994) giving a corrected reversal potential of + 11.82 ± 1.07 mV. Using the Goldman-Hodgkin-Katz (GHK) equation this gives a P_{Cl}/P_K = 2.7. The same was carried out for $BaCl_2$. In this case 200 mM $BaCl_2$ was placed in the recording electrode and 50 mM $BaCl_2$ in the bathing solution.

Due to the low mobility of Ba^{2+} ions in comparison to Cl^- ions this results in a large LJP of -11.1 mV. The resulting corrected reversal potential being +16.08 ± 0.87 mV (n = 3). Again using a modified version of the GHK equation (see materials and methods section chapter 3) the P_{Cl}/P_{Ba} was calculated using the corrected reversal potential and was 3.9, a much higher value than that of P_{Cl}/P_K.

E_{rev} pipette potential (mV)	**P_{Cl}/P_K**	**Bath solution (mM)**	**Pipette solution (mM)**	**$MgCl_2$ / $CaCl_2$ (mM)**	**pH**	**System**	**Ref.**
- 2.2	1.2	KCl 300	KCl 100	90 / 10	6	Spheroplasts	Sotomayor *et al.,* 2007
- 5	1.5	KCl 300	KCl 100	40 / n/a	6	Liposomes	(Sukharev, 2002)
- 8	2.7	KCl 400	KCl 200	40 / 10	7.2	Spheroplasts	(Martinac *et al.*, 1987)
- 9.5	2.1	KCl 600	KCl 200	90 / 10	7.1	Spheroplasts	(Edwards *et al.*, 2008)
+ 11.8	**2.7**	**KCl 200**	**KCl 600**	**40 / n/a**	**7.4**	**Liposomes**	**This thesis**
- 12	3.0	KCl 600	KCl 200	90 /10	6	Spheroplasts	Li *et al.,* 1999

Table 3.3. Reported relative permeabilites of MscS and corresponding experimental conditions including the value reported in this thesis.

The P_{Cl}/P_{Ca} was also calculated as 3.7 from a corresponding corrected reversal potential of + 15.41 ± 1.05 mV (n = 4). Interestingly increasing the anion size using $Ca(NO_3)_2$ increased the anion-cation permeability ratio markedly. The P_{NO3}/P_{Ca} was calculated as 24.4 from a corresponding corrected reversal potential of + 30.4 mV ± 2.35 (n = 5).

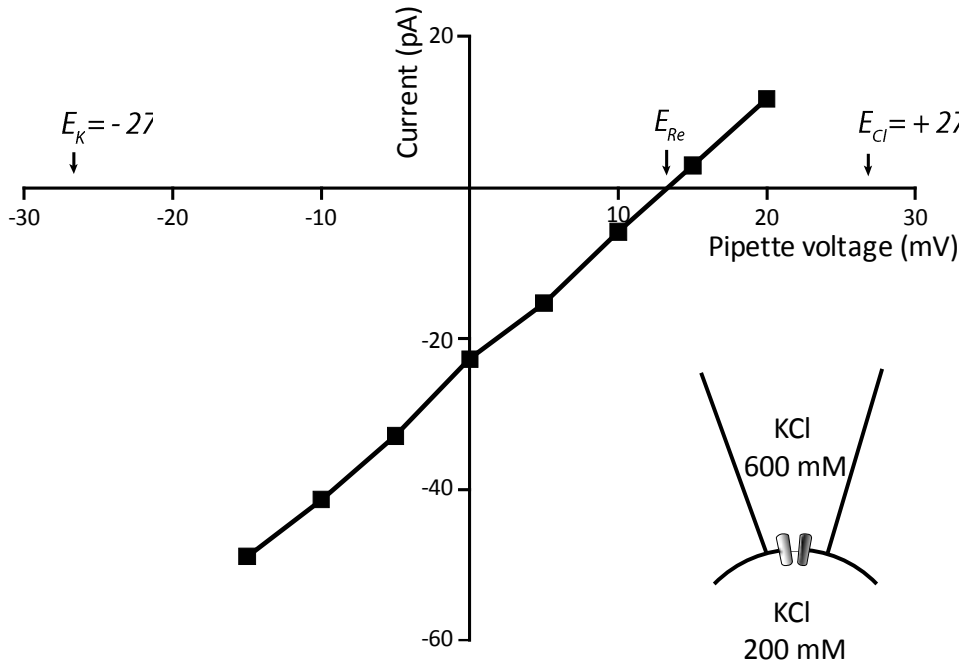

Figure 3.9. Reversal potential of MscS in asymmetric KCl. Representative current-voltage plot of MscS in the presence of assymetrical KCl 600 mM pipette/200 mM bath (right inset). The mean reversal potential was calculated from the mean of four determinations (+ 12.22 ± 1.07 mV). The calculated reversal potentials for K^+ and Cl^- are indicated on the x-axis for clarity as the equivalent pipette voltage.

Up to this point it is *patently* clear that both Ba^{2+} and Ca^{2+} permeate MscS from the anion-cation permeability ratios calculated in this chapter. In addition to this, MscS exhibits differing selectivity and rectification behaviour in the presence of these divalent cations alone in comparison to monovalent cations. The next section of this chapter aims to investigate whether Ca^{2+} permeation via MS channels occurs *in vivo.*

3.3.5 Ca^{2+} movement via MS channels *in vivo*

In order to investigate Ca^{2+} movement *in vivo* the triple knockout *E. coli* strain MJF465 was used (Levina *et al.*, 1999). In order to confirm the absence of MS channel (MscL, MscS and MscK) functionality in this strain an hypoosmotic shock assay was carried out, and spheroplasts of both FRAG-1 and MJF465 strains were patched (Figure 3.10).

The hypoosmotic assay resulted in a much lower survival rate in MJF465 against FRAG-1 *E. coli* at both 5 and 30 minute exposure periods. The survival rate of MJF465 after a 5 minute hypoosmotic shock exposure was 62 ± 3.1 % (n = 3) and was reduced even further down to 4.7 ± 2.6 % after a 30 minute exposure (n=3). This illustrates the inability of MJF465 to deal with large reductions in external osmolarity, a phenotype directly related to the absence of MscL and MscS expression (Levina *et al.*, 1999). Although there is a reduction in survival rate in the FRAG-1 strain between the 5 minute (98 ± 8.9 %: n = 3) and 30 (74 ± 1.4 %: n = 3) minute exposure periods, this difference was not as large as shown for the MJF465 strain. In addition to this, mechanosensitive channel activity characteristic of MscS and MscL was identified in FRAG-1 *E. coli* membranes whereas no evidence of MS channel activity was seen in MJF465 membranes from 7 patches. Subsequently FRAG-1 and MJF465 (Triple knockout) *E. coli* strains were transformed with an aequorin containing plasmid [pMMB66EH (AmpR)](Naseem *et al.*, 2007)).

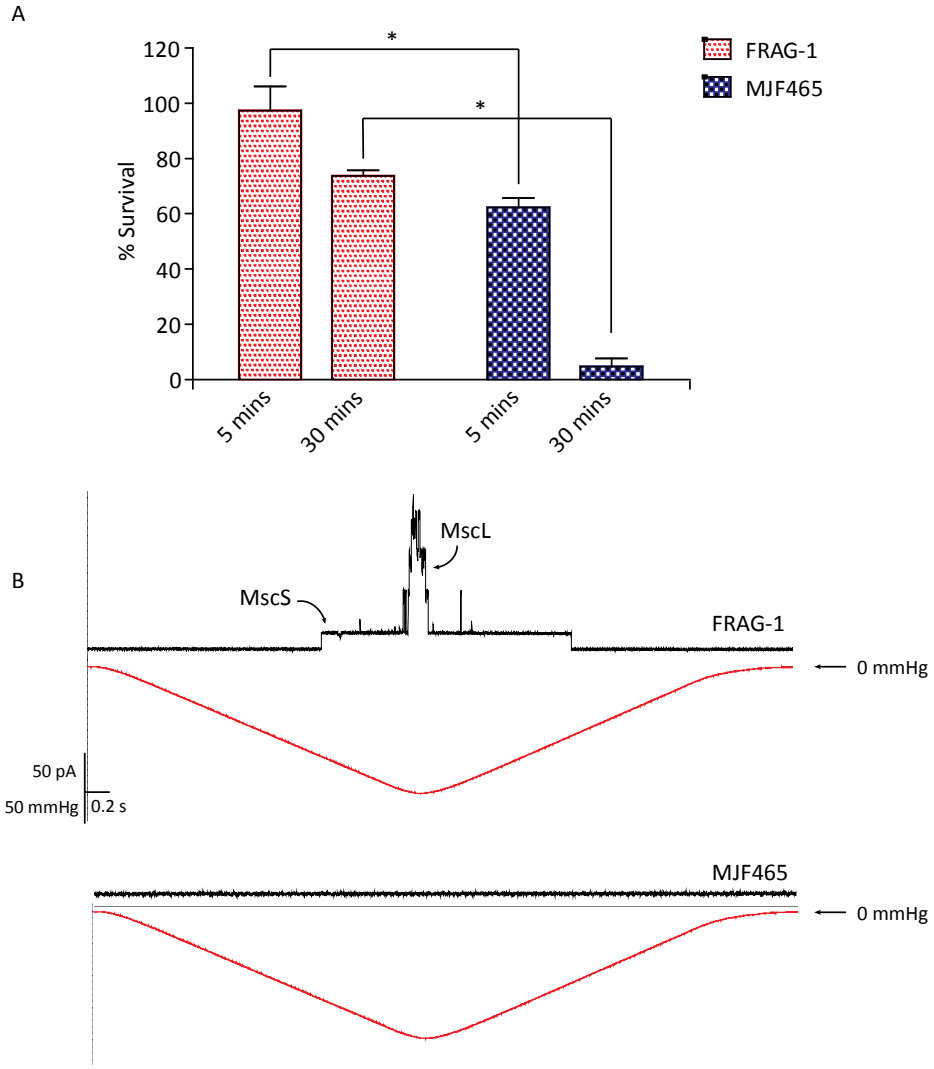

Figure 3.10. Confirming the lack of mechanosensitive channel activity in MJF465 triple knockout *E. coli* cells. (A) Histogram illustrating the percentage survival of FRAG-1 and MJF465 *E. coli* strains after 5 and 30 minute exposure to a ~1000 mOsm downshock (n = 3). (B) Upper panel shows a representative trace of mechanosensitive channel activity in FRAG-1 spheroplast membranes. Lower inset shows trace of mechanosensitive channel activity in MJF465 spheroplast membranes. No mechanosensitive channel activity was seen up to a pressure of 350 mmHg in 7 patches. * represents statistical significance determined by one-way ANOVA using Bonferroni's post-hoc test ($p < 0.05$).

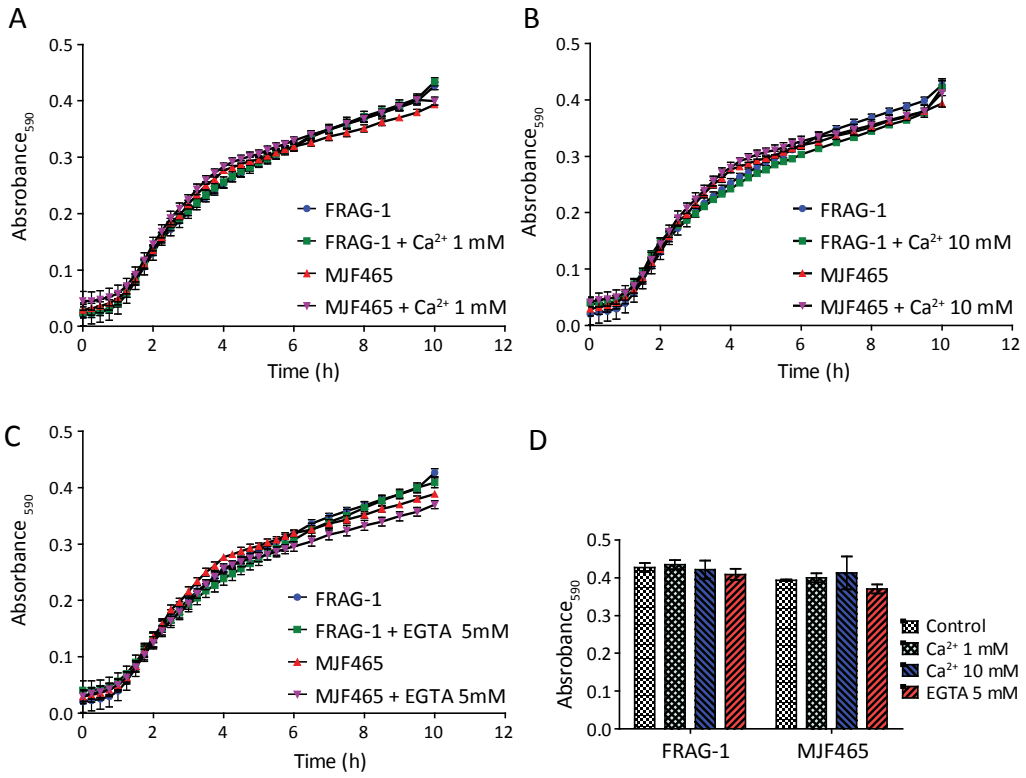

E

	Generation time (min)			
	Control	Ca^{2+} 1 mM	Ca^{2+} 10 mM	EGTA 5 mM
FRAG-1	38 ± 3.5	37 ± 6.3	38 ± 5.2	47 ± 9.6
MJF465	41 ± 4.9	44 ± 6.4	45 ± 7.3	45 ± 5.8

Figure 3.11. Growth of FRAG-1 and MJF465 (Triple KO) in different Ca^{2+} conditions. Growth of FRAG-1 and MJF465 (Triple KO) over a 10 hour period in LB media supplemented with (A) $CaCl_2$ 1 mM (B) $CaCl_2$ 10 mM and (C) EGTA 5 mM (pH 7.4, KOH). Error bars represent ± SD (n = 3). (D) Histogram illustrating the absorbance at 590 nm at the end of the 10 hour period between the two strains (FRAG-1 and MJF465) in the four experimental Ca^{2+} conditions. Error bars represent ± SD (n = 3). (E) Table of calculated generation times for both strains (FRAG-1 and MJF465) in each of the four Ca^{2+} conditions in minutes ± SD (n = 3).

Initially experiments were carried to see if Ca^{2+} handling was modified in the triple knock out. This was examined firstly by growing the FRAG-1 strain and the triple knockout in the presence of 1 mM Ca^{2+}, 10 mM Ca^{2+} (as chloride salt) and 5 mM EGTA. The generation times were very similar for each strain in each condition (Figure 3.11). However, the MJF465 grew consistently slower, albeit marginally, than the FRAG-1 strain with consistently lower

absorbencies at 10 hours [FRAG-1 control 0.427 ± 0.012 (n = 3) vs MJF465 control 0.393 ± 0.009 (n = 3)] and a slightly longer, yet not statistically significant, generation time [FRAG-1 control generation time in minutes 38 ± 3.5 (n = 3) vs MJF465 control generation time in minutes 41 ± 4.9 (n = 3)] (Figure 3.11). Furthermore there was a trend towards the generation time increasing in the presence of EGTA for both strains which was larger in magnitude for the FRAG-1 strain (Figure 3.11). The lag and log phase seemed consistent in length (~45 minutes and ~1 hour 30 minutes respectively) for both strains over all of the conditions tested.

The intracellular calcium concentration ($[Ca^{2+}]_i$) was measured of transformed FRAG-1 and MJF465 strains. The basal levels of $[Ca^{2+}]_i$ for FRAG-1 and MJF465 were not significantly different, and were measured as 0.41 ± 0.03 µM (n = 6) and 0.39 ± 0.02 µM (n = 6) respectively. After the addition of 2 mM Ca^{2+}, resulting in an extracellular Ca^{2+} concentration of 1 mM, the $[Ca^{2+}]_i$ rose slowly to a peak concentration of 1.50 ± 0.15 µM (n = 6) and 1.38 ± 0.25 µM (n = 6) respectively (Fig 3.12). There was no statistically significant difference between the two strains with respect to the basal levels of $[Ca^{2+}]_i$, the peak $[Ca^{2+}]_i$ after the addition of 2 mM Ca^{2+} or the rate at which the $[Ca^{2+}]_i$ rose.

The addition of 1 mM procaine had no effect on $[Ca^{2+}]_i$ in the FRAG-1 strain (n = 3) . However the addition of chlorpromazine (CPZ) caused a large rise in $[Ca^{2+}]_i$. This $[Ca^{2+}]_i$ rise was significantly higher in the FRAG-1 strain rising to 3.72 ± 0.11 µM (n = 3) while in MJF465 the $[Ca^{2+}]_i$ only rose to 2.81 ± 0.24 µM

µM (n = 3). Interestingly the rise in $[Ca^{2+}]_i$ caused by CPZ is relatively slow taking at least 2 minutes to reach the peak concentration.

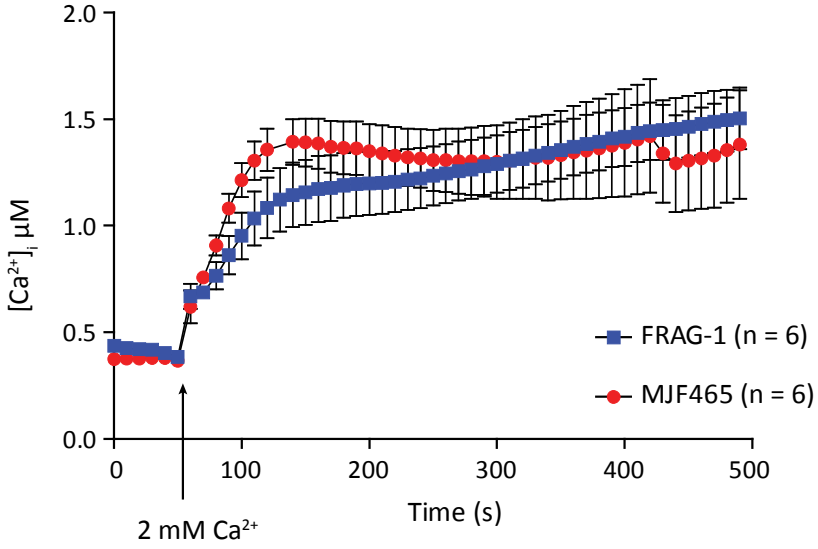

Figure 3.12 Comparison of $[Ca^{2+}]_i$ between FRAG-1 and MJF465 strains on the addition of 2 mM Ca^{2+}. (A) illustration of $[Ca^{2+}]_i$ over time for both strains after the addition of 2 mM Ca^{2+} after 60 seconds which results in a final extracellular Ca^{2+} concentration of 1 mM.

The addition of 1 mM procaine had no effect on $[Ca^{2+}]_i$ in the FRAG-1 strain (n = 1) (Figure 3.13A). However the addition of chlorpromazine (CPZ) caused a large, slow rise in $[Ca^{2+}]_i$. This $[Ca^{2+}]_i$ rise was significantly higher in the FRAG-1 strain rising to 3.72 ± 0.11 µM (n = 3) while in MJF465 the $[Ca^{2+}]_i$ only rose to 2.81 ± 0.24 µM µM (n = 3). Interestingly the rise in $[Ca^{2+}]_i$ caused by CPZ was relatively slow taking at least 200 seconds to reach the peak concentration (Figure 3.13B).

A reduction in external osmolarity resulted in a large rise in $[Ca^{2+}]_i$ in the FRAG-1 strain up to a peak of 9.39 µM ± 1.12 µM (n = 3) and a lesser rise to a maximum of 4.65 ± 0.11 µM (n = 3) in MJF465. These Ca^{2+} transients took ~20

seconds to peak and $[Ca^{2+}]_i$ returned to baseline after ~100 seconds (Figure 3.14.

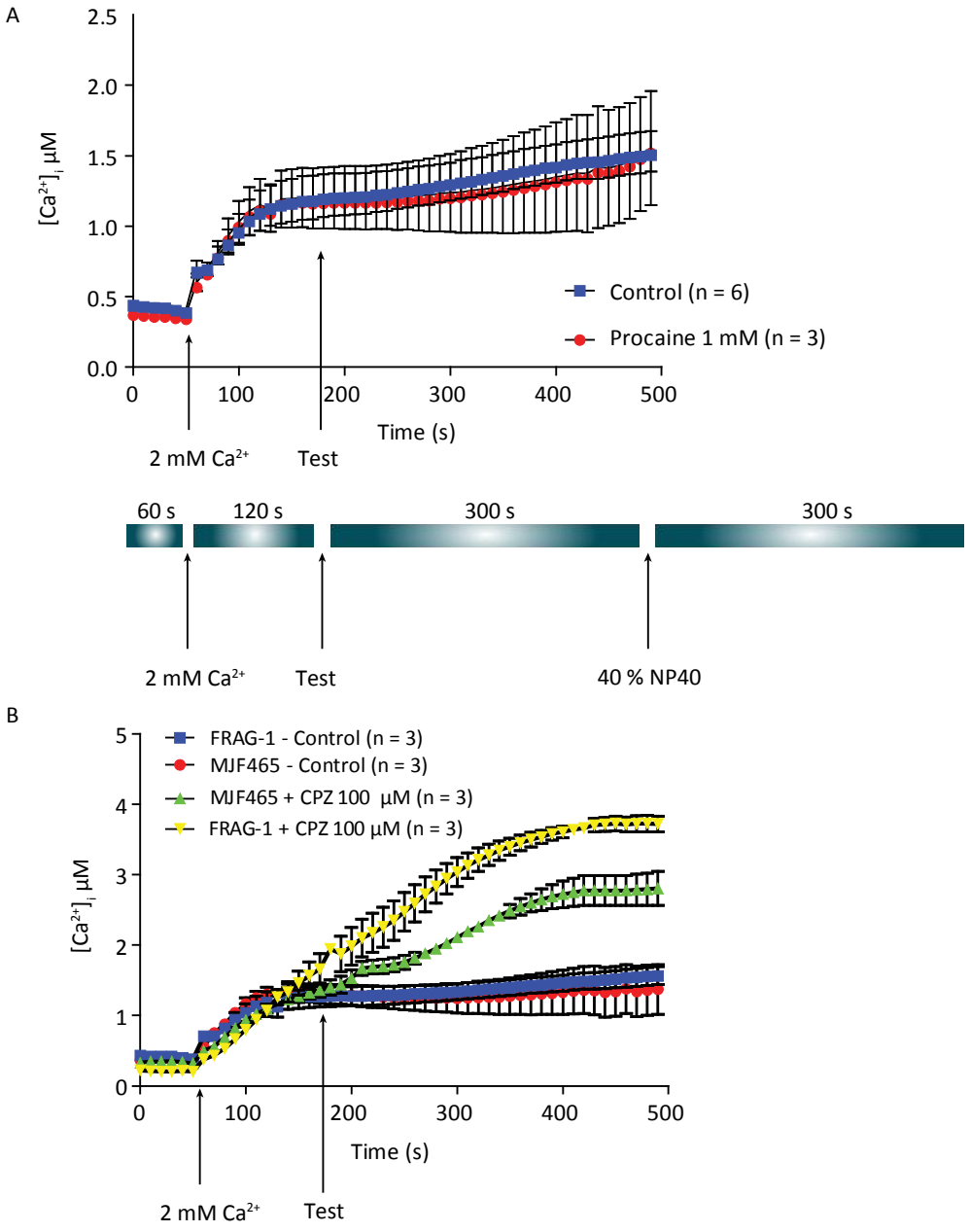

Figure 3.13 Effect of two known mechanosensitive channel modulators on $[Ca^{2+}]_i$. (A) The effect of procaine 1 mM on the $[Ca^{2+}]_i$ of FRAG-1. The experimental protocol is shown below for clarity. The NP40 is used to lyse bacteria and release all remaining unconsumed aequorin and is not shown in these figures. (B) The effect of CPZ 100 µM on the $[Ca^{2+}]_i$ of FRAG-1 and MJF465. The $[Ca^{2+}]_i$ rises slowly and reaches a larger peak in FRAG-1.

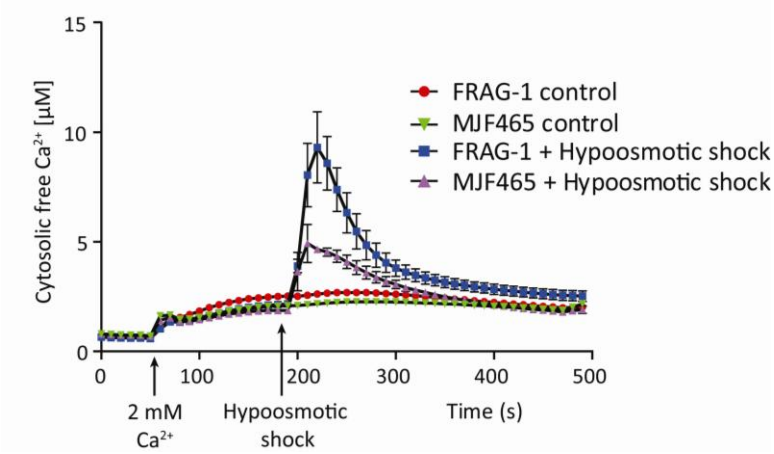

Figure 3.14 Effect of reducing external osmolarity (~ 350 mOsm downshock) on $[Ca^{2+}]_i$ in FRAG-1 and MJF465 strains. The rise in $[Ca^{2+}]_i$ in the MJF465 strain is roughly half that of the WT FRAG-1 strain (n = 3).

3.4 Discussion

From the SEM images generated it seems as though the giant *E. coli* spheroplasts used in this chapter have multiple membrane perforations. Whether this is an artifact of the image, or of the addition of glutaraldehyde fixation, or sample treatment protocol is unknown. If this were the case it would have implications for the utility of spheroplasts as a model system for the electrophysiological study of ion channels. This could be investigated further using dextran uptake assays looking at the integrity of the spheroplast membranes.

Initial patch clamp experimentation in giant *E. coli* spheroplasts in symmetrical $CaCl_2$ revealed activity of a mechanosensitive channel with a conductance at positive pipette potentials of 547 ± 35 pS (n = 4). The channel pressure threshold was unaffected by voltage and followed a time dependent reduction. This relationship of time with reduction in pressure threshold could

be caused by a phenomenon termed “patch creep”(Suchyna *et al.*, 2009). This phenomenon is reported to be driven by both voltage dependent and independent mechanisms and has recently been suggested as the basis for a similar effect seen in MscS and MscL reconstituted in liposomes (Nomura *et al.*, 2012). The basis for this being that over time the patch creeps up the microelectrode increasing the radius of curvature of the patch. As the gating of the channel is dictated in simple terms by the law of Laplace, as this radius increases, so too does the resting tension in the membrane. This means that a lower amount of applied pressure (suction) is subsequently required to increase membrane tension to a point where MS channels open.

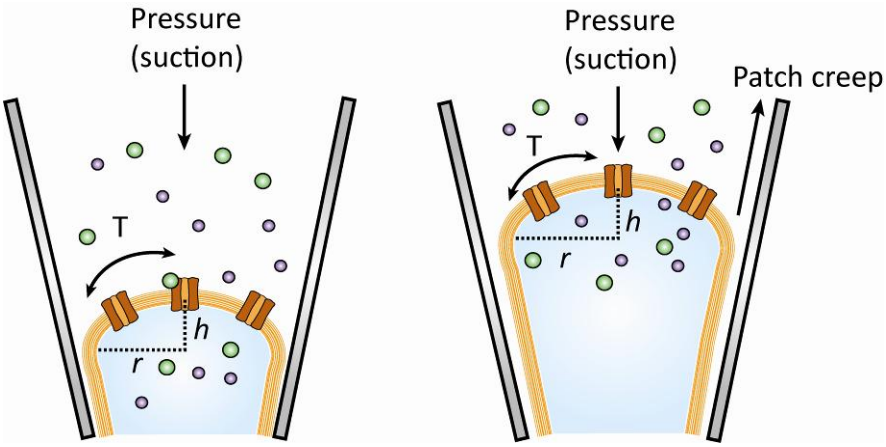

Figure 6.14 Illustration of ‘patch creep’. The pressure required to gate MS channels can be related to the tension in the membrane using Laplace’s Law: $T = R_c*P/2$ where T is the tension in the membrane, R_c is the patch curvature as calculated by patch radius r and height of patch dome h and P is the applied pressure via suction. Thus the amount of pressure required to increase membrane tension to a point where MS channels gate is directly related to patch geometry. It has been proposed that patches via voltage dependent and independent mechanisms can creep up microelectrodes. As the patch creeps up the microelectrode the radius r increases resulting in a lower pressure to open the channels which could explain the time dependent effect reported in this chapter (This figure is adapted from (Suchyna *et al.*, 2009).

The exact genetic origin of this channel seen in symmetrical $CaCl_2$ was to begin with unknown. The channel conductance was much smaller than previously reported for MscL (~3 nS) (Sukharev *et al.*, 1993) in addition this channel exhibited a non-linear I-V relationship which also pointed towards this channel *NOT* being MscL (Sukharev *et al.*, 1993, Hase *et al.*, 1995). The channel was also unlikely to be MscM as the conductance was larger than that reported for MscM (0.1 - 0.4 nS) (Schumann *et al.*, 2010). The conductance in symmetrical 100 mM $CaCl_2$ was smaller than the reported values for that of MscS and MscK (~1 nS) but the I-V plot does show rectification at negative pipette potentials as seen with MscS. MscK activity is dependent on extracellular K^+ so the most likely origin for this mechanosensitive channel activity was MscS.

The proposition that this initial channel activity was due to MscS was confirmed by incorporating purified MscS protein into 100% soybean azolectin liposomes. The activity seen in reconstituted liposomes was almost identical with respect to both rectification at negative pipette potentials and conductance in symmetrical $CaCl_2$ and $BaCl_2$ and the.

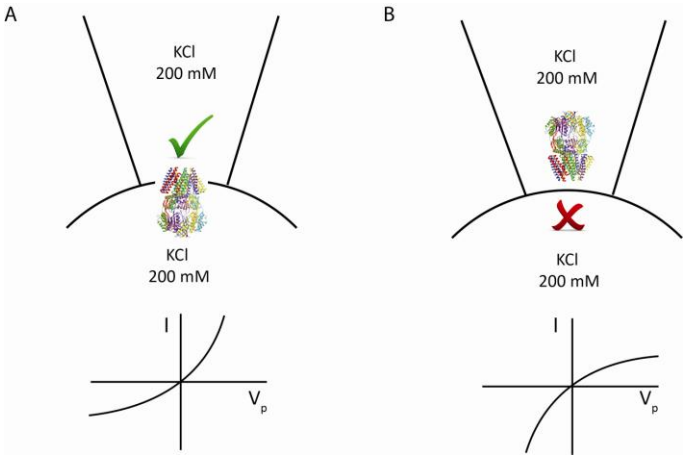

Figure 3.15. Cartoon illustration representing MscS incorporation into liposomal membranes. (A) Illustration of the how MscS is likely to be incorporated with a corresponding representative current voltage plot showing the rectification seen at negative pipette potentials as seen in liposomes and spheroplasts. (B) Illustration of unlikely mechanism of incorporation with putative current voltage shown, the opposite from what is seen in both spheroplasts and liposomes. (NB: more pronounced rectification than that exhibited by MscS is illustrated for clarity.)

The fact that the rectification seen in spheroplasts and liposomes is identical, i.e. that the conductance at positive pipette potentials is higher than at negative pipette potentials, is very interesting and has been noted before (Sukharev, 2002). From this we can suggest that the channel is incorporated into the membranes in the same orientation, in a non-random manner. To date there is little evidence to unequivocally show that this is the case for MscS, although some recently published work shows very similar results to those set out in this chapter i.e. the same rectification as noted in spheroplasts is seen in all the recordings of MscS reconstituted in liposomes (Nomura *et al.*, 2012). There is currently no explanation for this effect. One other possible explanation for this is that channels can be incorporated both ways but only those incorporated the 'right way up' are able to open due to the mechanical stress induced during patch-clamp experiments.

In addition to this mechanosensitive activity a 'novel' channel activity of ~90 pS was identified (3/17 patches). This activity could be due the putative non-proteinaceous polyphosphate polyhydroxybutyrate (PolyP/PHB) channel demonstrated by Reusch and co-workers (Das *et al.*, 1997). While these documented PolyP/PHB channels have a conductance of ~100 pS in symmetrical 200 mM $CaCl_2$ and do not require substantial depolarising steps to gate as seen with the documented 'novel' channel activity set out in this chapter (Das *et al.*, 1997). The fact that similar activity is seen in symmetrical 100 mM $MgCl_2$ and $MgSO_4$ goes some way to show this activity is not due to Cl^- movement and the PolyP/PHB channels do permeate Mg^{2+}, another reason why this channel could represent a PolyP/PHB channel. The lack of mechanosensitivity displayed by this channel means it is unlikely to be due to the YbdG, YbiO, YnaI or YjeP. Due to the instability of giant *E. coli* spheroplasts at high potentials it was difficult to accrue sufficient data to fully characterise the biophysical nature of this channel activity.

The behaviour of MscS in Ba^{2+} and Ca^{2+} is markedly different from that seen in solutions whose major permeant cation is monovalent. These differences involve a reduction in conductance, an increase in rectification, an increase in anion-cation permeability ratio and an increase in the presence of subconducting states. The multiple subconducting states seen at positive pipette potentials (equivalent to hyperpolarised membrane potentials) are extremely interesting. The literature contains numerous reports regarding the propensity of MscS to reside in subconducting states (Shapovalov and Lester,

2004, Sotomayor *et al,* 2007 Edwards *et al.,* 2008). However in the presence of 100 mM $CaCl_2$ and $BaCl_2$ these forays into subconducting states seem to be much longer lived. The following chapter aims to fully dissect these subconducting states and to investigate to what extent they are affected by divalent cations.

In the presence of symmetrical 100 mM $CaCl_2$ and $BaCl_2$ the conductance of MscS is lower compared with standard solutions used to monitor the activity of MscS (Martinac *et al.*, 1987, Petrov *et al.*, 2011). This is in the main due to a reduction of bulk conductivity between these solutions, but not solely. If we look at the conductance of MscS in symmetrical 200 mM LiCl which had a measured bulk conductivity of 16.8 mS.cm we see that the conductance at positive potentials was much higher than that of symmetrical 100 mM $CaCl_2$ and $BaCl_2$ despite their bulk conductivities being 15.0 and 17.1 mS.cm respectively. This suggests bulk conductivity is not the only factor influencing the change in conductance. This chapter also shows that the anion-cation permeability ratios in MscS of divalent and monovalent cations are markedly different (P_{Cl}/P_K = 2.7, P_{Cl}/P_{Ba} = 3.9, P_{Cl}/P_{Ca} = 3.7). From the anion-cation permeability ratios quoted between 7 and 8 Cl^- ions permeate through MscS for every 2 Ca^{2+} or Ba^{2+} ions.

One explanation for this occurrence is that the anion-cation permeability is directly affected by the hydrated ionic size of the counter-ion a similar story as to what is seen in the glycine receptor (Sugiharto *et al.*, 2008). An idea that

is further supported by the large permeability ratio calculated for NO^{3-} and Ca^{2+} (P_{NO3}/P_{Ca} = 24.4). This change in anion-cation permeability could be caused by cations binding to a site either within the pore of the channel or somewhere within the cytoplasmic vestibule that could impact on the permeability of anions. This idea and the structural basis for it are discussed in chapter 5 of this thesis.

To investigate whether Ca^{2+} moved via MS channels *in vivo* the triple KO strain MJF465 ($MscL^-$, $MscS^-$ and $MscK^-$) was used (Levina *et al.*, 1999). Both an hypoosmotic shock assay and patch clamping confirmed the lack of functionality of MS channels in the MJF465 strain. The reduction of survival rate of MJF465 down to 4.7 ± 2.6 % after a 30 minute exposure shows the lack of ability of the cell to respond to acute reductions in external osmolarity (Levina *et al.*, 1999). The fact that the survival rate did not reduce to 0 % is something which other studies have identified and this case is likely due to either MscM expression or expression of one of three other MS channels (Edwards and Booth, 2011, Schumann *et al.*, 2010, Edwards *et al.*, 2012).

Before measurements of $[Ca^{2+}]_i$ were taken the ability to grow in different Ca^{2+} conditions was assessed for both the WT parent strain FRAG-1 and MJF465 triple KO strain. There was no difference in the growth of FRAG-1 *E.coli* and the triple KO in the three Ca^{2+} conditions a result which supports what has been previously reported. Free Ca^{2+} in LB media has previously been estimated as 50 µM with a total Ca^{2+} content of 150 µM (Jones *et al.*, 2002).

Even assuming a concentration of free Ca^{2+} equal to 150 µM means that 5 mM of EGTA would theoretically reduce free Ca^{2+} down to low nanomolar levels (~10 nM) which from these experiments seems not to be detrimental to growth.

Both strains demonstrate a rise in intracellular Ca^{2+} as measured by aequorin chemiluminescence as a result of the addition of 2 mM Ca^{2+} to a Ca^{2+} free medium. The rise and rate of rise are comparable for both. Reducing the external osmolarity from ~1050 mOsm to ~700 mOsm caused a much larger rise in intracellular Ca^{2+} in the FRAG-1 strain than in the MJF465 strain. From this data the suggestion can be made that on opening MS channels *do* become a conduit for Ca^{2+} entry i.e. the reduction in external osmolarity gates MS channels allowing Ca^{2+} to flood in down its electrochemical gradient. However there are numerous questions surrounding this result. Firstly why there is still a peak in intracellular Ca^{2+} in MJF465? This could be due to a portion of cells lysing although Levina *et al.,* 1999 show that a shock of 0.2 M NaCl (~400 mOsm) doesn't affect survival of either FRAG-1 or MJF465 and hence shouldn't cause lysis. This precludes the possibility that the rise in the signal is due to aequorin being liberated from cells much akin to what happens on the addition of the detergent NP40. However this does *NOT* mean that MscS and MscL are not activated under these conditions as Levina *et al.,* 1999 also show that there is substantial K^+ efflux in FRAG-1 with a downshock of 0.2 M NaCl (~400 mOsm) and that MS channel knockouts retain a larger amount of their cytoplasmic K^+ pool under the same conditions. This aside

what could potentially be mediating this rise in $[Ca^{2+}]_i$ in the MJF465 strain? The MJF465 strain is not devoid of MscM nor of three other putative MS channels (Edwards and Booth, 2011, Edwards *et al.*, 2012). These channels could account for this rise in Ca^{2+} although alone are not sufficient to prevent cellular lysis in the face of a large enough hypoosmotic shock (Schumann *et al.*, 2010, Levina *et al.*, 1999).

In addition to external osmolarity causing a rise in $[Ca^{2+}]_i$ it was also identified that the phenothiazine anti-psychotic CPZ, a known MS channel activator, did cause a significant rise in $[Ca^{2+}]_i$ up to 3.72 ± 0.11 µM in the FRAG-1 strain. This rise was significantly larger than the rise seen in MJF465 (~ 50 %). In contrast the other known MS channel activator procaine (1 mM) did not cause a rise in $[Ca^{2+}]_i$ (Martinac *et al.*, 1990). Procaine is much more hydrophilic than CPZ and does not have any effect on *E. coli* growth up to a concentration of 50 mM (Tisa *et al.*, 2000). The fact that procaine is not antimicrobial like the lipophilic local anaesthetic (LA) tetracaine and does not cause a rise in $[Ca^{2+}]_i$ could possibly be linked to the fact that it does not partition as well into the membrane. As shown in Martinac *et al.,* 1990 the more lipophilic the LA, the more potent its activation of MS channels. In the case of procaine it may not be able to get to the inner membrane at sufficient quantity to cause MS channel activation. In addition Martinac *et al.,* 1990 showed that the effect of these amphipaths takes numerous minutes to occur (~20 minutes). As a result procaine may actually have an effect on $[Ca^{2+}]_i$ but over the time period of these particular experiments it was not detected.

Taking into account the effects of CPZ and a reduction in external osmolarity on $[Ca^{2+}]_i$ there does seem to be Ca^{2+} movement via MS channels *in vivo* under these conditions. Which channel the Ca^{2+} is moving through and whether this Ca^{2+} movement is physiologically relevant is at present unknown.

3.5 Conclusions and future work

The data contained within this chapter definitively shows that divalent cations permeate MscS *in vitro* and that both Ca^{2+} and Ba^{2+} affect the biophysical behaviour of MscS. From the findings documented here the suggestion can also be made that gating of MS channels may in fact allow Ca^{2+} influx under certain conditions *in vivo*. The data contained within this chapter also raise many interesting questions to be pursued, for example;

- SEM of *E. coli* spheroplasts seem to indicate numerous membrane perforations in spheroplasts around 10 μm in diameter. Do larger spheroplasts > 10 μm in size lack membrane integrity? This could be investigated using dextran uptake assays with dextrans of varying size.
- Is the reduction in P_t over time a result of patch creep? If so is this effect on P_t affected by voltage, pH, membrane lipid composition and or ionic composition? Patch fluorimetry could be used to visualise the patch concomitantly to taking P_t measurements to see if the spheroplast membrane does indeed move further up the patch pipette during experimentation. Although to a certain extent this has now been reported (Nomura *et al.*, 2012).

- Is this ~90 pS channel reported in this chapter really a “novel” channel. Further work could aim at extensive biophysical analysis and investigation of pharmacology.
- How many subconducting states does MscS exhibit? What is the structural basis of these subconducting states?
- Probably most exciting of all is the possibility of a Ca^{2+} counter current on opening of MS channels *in vivo* and whether this current could be a physiologically relevant signal? This could be further probed using other MS channel activators such as lysophosphatidylcholine (LPC)(Grage *et al.,* 2011, Nomura *et al.,* 2012, Birkener *et al.,* 2012) and using the Δ7 strain documented by Edwards and Booth, 2011.

Chapter 4: Characterisation of MscS subconducting states

4 Characterisation of MscS subconducting states

4.1 Introduction

The most straightforward model for an ion channel is one in which the channel can occupy just two states, the open state and the closed state. However on detailed analysis of many ion channels, including MscS, it becomes evident that the actual picture is much more complex than this i.e. the channel is able to conduct at numerous levels or substates. These substates have a lower conductance than that of the main open state.

The first problem encountered when looking at subconducting states is what actually constitutes a substate. How do we know that the state seen is indeed a substate? Firstly the substates seen should directly connect with other conducting levels including the main state. Secondly these substates must only be seen in the presence of the main open state. The fundamental principle being to test the hypothesis that; “The signal is the superposition of several independently gated channels, each with only two conducting states”(Fox, 1987, Laver and Gage, 1997). This is because identification of current amplitudes identical to those of putative subconducting states in the absence of the main open state indicates a number of discrete channels rather than a subconducting state.

4.1.1 The structural basis of subconducting states

There are four possible structural explanations for the occurrence of subconducting states, as discussed in Laver & Gage 1997, which are;

(i) different conformations of one pore as in the case of alamethicin channels (***Unipore hypothesis***)(Sansom, 1993a, Sansom 1993b).

(ii) the opening of distinct ion permeating pathways within the same protein as seen with porin channels (***Multipore hypothesis***). Incidentally the monomeric ion conducting pathways of these porins can also exhibit subconducting levels to confuse matters even further (Basle *et al.*, 2004).

(iii) the strongly coupled gating of covalently linked channel multimers as seen in the nicotinic acetylcholine receptor.

(iv) the weakly coupled gating of channels whereby ionic movement through one channel impacts on that of another.

4.1.2 The unipore hypothesis

This hypothesis states that subconducting states arise from altered conformations or electrostatic properties of a single channel pore. The pore may be formed by one single protein or be a multimer comprised of several monomers. This hypothesis purports that the subconducting states arise due to differential recruitment or movement of channel residues or monomers (Fox, 1987, Laver and Gage, 1997).

The strength of this hypothesis is based upon substate observations which cannot easily be explained using the multipore approach. A continuum or non-discrete distribution of subconductance states for example is not easily explained using a multipore model. An example of such a distribution is seen in the Zn^{2+}-induced substates of cardiac Na_v channels treated with

batrachatoxin (Schild *et al.*, 1991). In this particular case the ratio of conductance between the main state and substates varies with voltage. The BK channel also exhibits non-discrete subconductance states (Stockbridge *et al.*, 1991).

4.1.3 The multipore hypothesis

The multipore hypothesis states that discrete conducting levels are created by distinct ionic pathways. This is demonstrated usually by the occurrence of multiple equally spaced subconducting states for example in the trimeric porins (Basle *et al.*, 2004). In these cases each ion permeating pathway is separate and each usually has a distinct gate. As mentioned these subconducting states can then also have their own subconducting states brought about by the mechanisms described above.

4.1.4 Unipore or multipore?

The multitude and variety of ion channels and subconducting states observed means it is quite possible that for any channel both are equally as valid i.e. both hypotheses may initially be possible before experimental evaluation.

4.1.5 MscS subconductance states

There are a number of reports of subconducting behaviour in MscS (Akitake *et al.*, 2005, Shapovalov and Lester, 2004, Sotomayor *et al.*, 2007). The suggestion is that subconducting states are more prevalent at negative pipette potentials the reason for which is unknown. The literature notes that subconducting states do arise at positive pipette potentials but very little information is given (Sotomayor *et al.,* 2007).

The current paradigm for MscS substates is a unipore hypothesis. Akitake *et al.,* 2005 suggest that the MscS substates arise from differential recruitment of MscS monomers. This differential recruitment or dyssynchrony of inactivation results in corresponding changes in pore diameter and thus in conductance. This 'dash pot' mechanism of channel gating results in the corresponding changes in the pore size which gives rise to the substates observed. From this hypothesis we could suggest that this would result in a maximum of 7 conducting states. No concerted effort has been made thus far in the literature to investigate the number of MscS substates. Although Shapovalov and Lester, 2004, do encounter one predominant state at 2/3 of unitary conductance.

4.1.6 The physiological relevance of subconducting states

There are many reports of subconducting states in various channels however these reports simply point towards them as biophysical phenomenon rather than physiologically relevant. It is hard to envisage when such a biophysical phenomenon could become physiologically relevant. So currently the utility of studying and reporting subconductance states is limited to the potential structural information they can provide.

4.1.7 Aims

The main aim of this chapter is to explore the MscS subconductance states initially documented in chapter 3 at high positive pipette potentials. This will be achieved by incorporating purified MscS protein into azolectin liposomes

and patching channels in an excised inside-out configuration. This chapter will investigate;

- How many substates are exhibited by MscS?
- How the substates vary in the presence of differing major permeant cations. With particular reference to differences between monovalent and divalent cations.
- How the substates are affected by voltage.

4.2 Materials and Methods

4.2.1 Electrophysiology

The electrophysiology set up was again as described in chapter 2. The resistance of microelectrodes for patch clamping liposomes in standard KCl solutions was ~ 5 MΩ. In this chapter slightly higher resistance electrodes were used in order to reduce the area of each patch which in turn reduced the number of channels per patch. The sampling rate used throughout was 10 kHz.

4.2.2 Protein purification and liposome formation

Purified MscS protein, as described in chapter 2, was reconstituted in 100 % azolectin liposomes also as described in chapter 2. In this chapter MscS was reconstituted at a protein to lipid ratio of 1:20000. This higher ratio was to reduce the number of channels in each patch. This ratio gave a minimum of 1 and maximum 12 channels per patch. Dehydrated liposomes were stored at 4 °C in a glass desiccator until required for use for no longer than 7 days.

4.2.3 Electrophysiological recording solutions

All monovalent ionic solutions contained 40 mM $MgCl_2$ and 5 mM HEPES (pH 7.4 adjusted with NaOH). All divalent ionic solutions contained 5 mM HEPES (pH 7.4 adjusted with NaOH). Final concentrations of Na^+ after pH adjustment did not exceed 1.2 mM.

4.2.4 Statistical methods

The all points distribution of current amplitude histograms from raw records of MscS channel activity were fitted with Gaussian curves, the means from which were taken as the fully open channel current or subconductance level current. This was achieved using Clampfit 10.0.

4.3 Results

4.3.1 MscS substates in different ionic conditions

As mentioned in the previous chapter and discussed in the introduction to this chapter MscS exhibits subconducting states in both liposomes and spheroplasts. Forays into these subconducting states at positive pipette potentials when MscS is incorporated into azolectin liposomes in the presence of symmetrical 200 mM NaCl and KCl are infrequent and short lived (Figure 4.1).

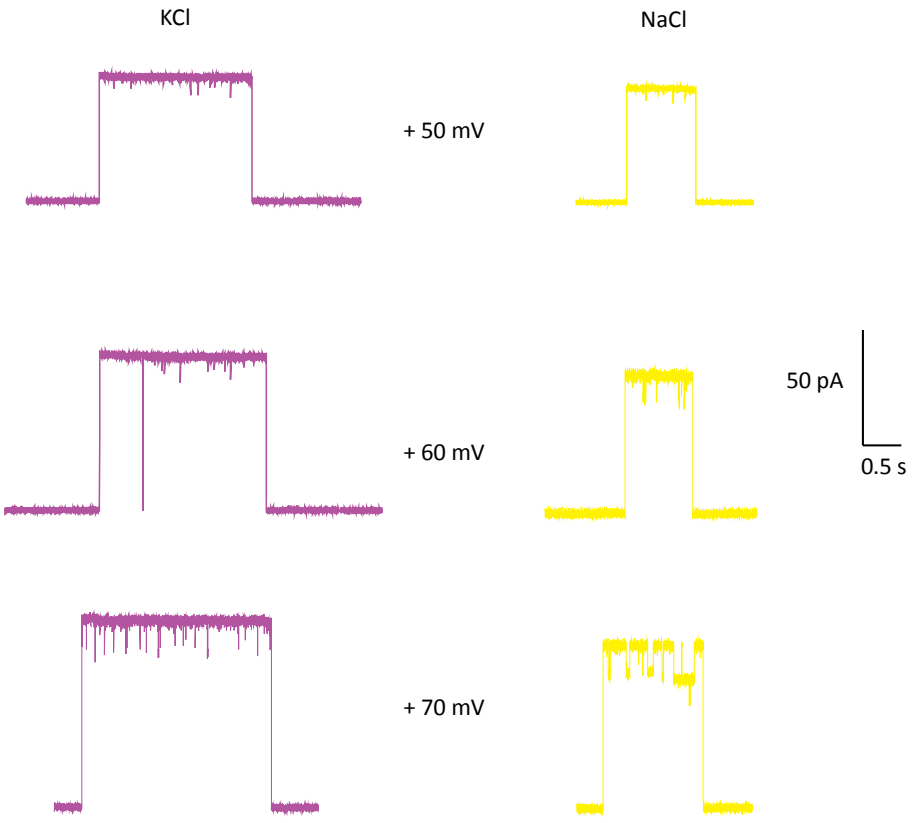

Figure 4.1 MscS activity in symmetrical 200 mM KCl (left panel: purple) and 200 mM NaCl (right panel: yellow). Raw records of MscS activity reconstituted in azolectin liposomes at the pipette voltage shown in the centre. The subconducting states become more noticeable at and above + 70 mV.

The subconducting states that arise begin to be seen more frequently when the pipette voltage exceeds + 70 mV (Figure 4.1). The subconducting states

are more distinct at positive pipette potentials at and above + 70 mV pipette potential than at equivalent negative pipette potentials where openings become very flickery and transitions between substates become very rapid (Figure 4.2). This is similar to what has been previously reported (Akitake *et al.,* 2005, Maksaev and Haswell, 2011). The difference in current amplitude between positive and negative pipette potentials is due to the rectification exhibited by MscS (*see chapter 3*).

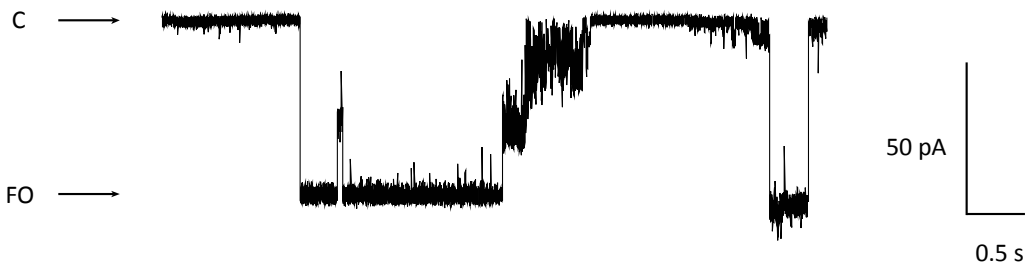

Figure 4.2 Example of MscS subconducting behaviour at -70 mV pipette potential in the presence of 200 mM KCl. Example of a raw record illustrating characteristic flicker MscS behaviour at negative pipette potentials equivalent to depolarising membrane potentials.

Over a 5 second time period at + 70 mV pipette potential in the presence of either symmetrical 200 mM NaCl or KCl MscS exhibited a maximum of 3 subconducting states, the average number being 2.17 ± 0.31 (n = 5) and 1.50 ± 0.28 (n = 5) respectively (Figure 4.3A). At this pipette voltage MscS spent 75.76 ± 4.17 % (n = 4) and 87.93 ± 2.72 % (n = 5) of the time respectively in the fully open state measured over a 5 second time frame (Figure 4.3B).

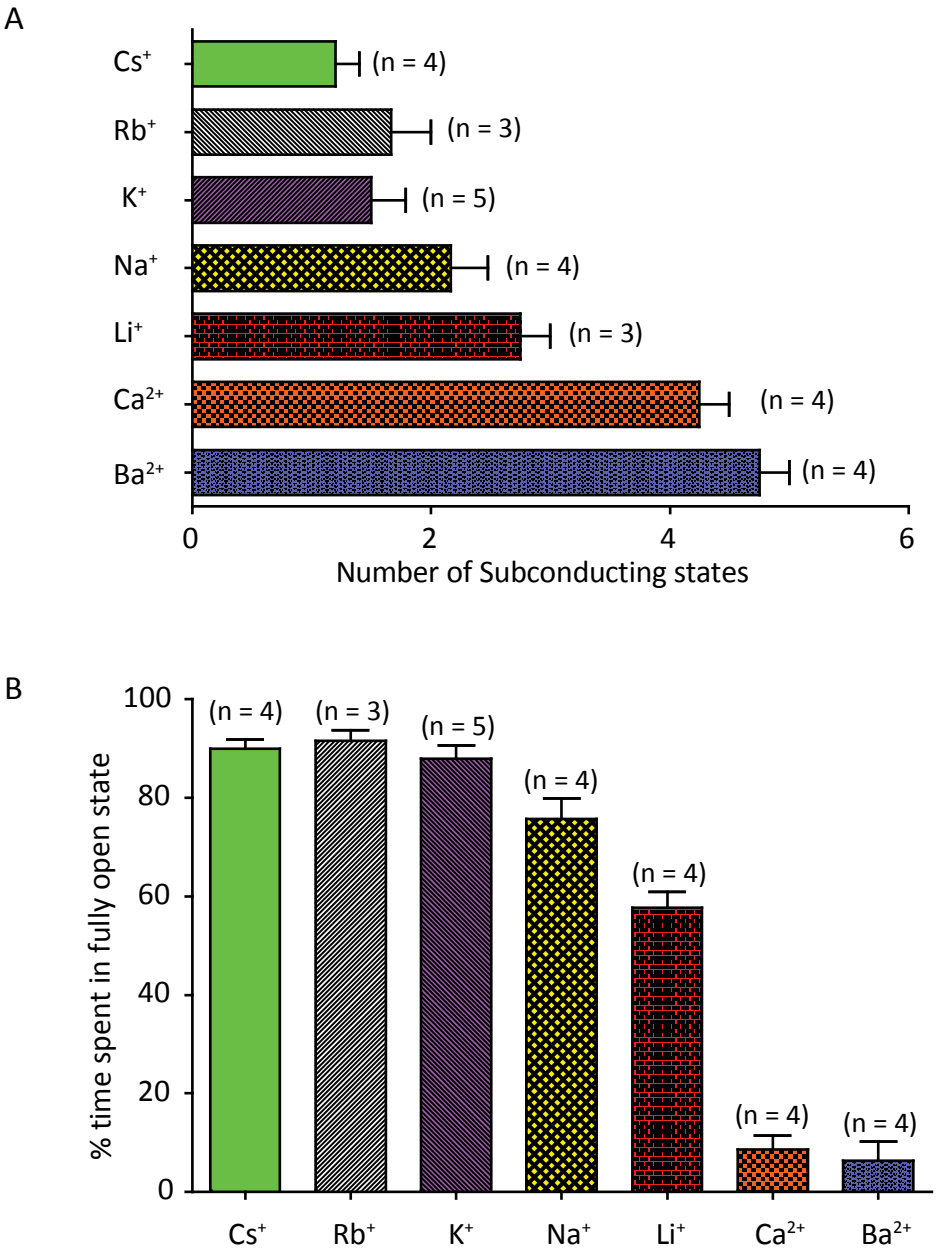

Figure 4.3 The affect of ionic conditions on MscS subconducting states. (A) Histogram representing the average number of subconducting states seen at + 70 mV pipette potential with each major permeant cation. (B) Histogram representing the average percentage of time MscS spent in the fully open state in the presence of each major permeant cation over a 5 second period. The results represent means ± SD.

The number of subconducting states exhibited by MscS was lowest in symmetrical 200 mM CsCl [1.20 ± 0.20 (n = 4)] and highest in symmetrical 100

mM $CaCl_2$ [4.25 ± 1.25 (n = 4)] and $BaCl_2$ [4.75 ± 1.25 (n = 4)] (Figure 4.3A). The number of subconducting states seen at + 70 mV in the different ionic conditions showed the following order: Cs < K < Rb < Na < Li < Ca < Ba (Figure 4.3A & Table 4.1).

Solution	No. of subconducting states	% time spent in fully open state
Cs^+	1.20 ± 0.20 (n = 4)	89.9 ± 1.91 (n = 4)
Rb^+	1.67 ± 0.33 (n = 3)	91.57 ± 2.17 (n = 3)
K^+	1.50 ± 0.28 (n = 5)	87.93 ± 2.74 (n = 5)
Na^+	2.17 ± 0.31 (n = 4)	75.76 ± 4.17 (n = 4)
Li^+	2.62 ± 0.22 (n = 3)	57.65 ± 3.22 (n = 4)
Ca^{2+}	4.25 ± 1.25 (n = 4)	8.63 ± 2.87 (n = 4)
Ba^{2+}	4.75 ± 1.25 (n = 4)	6.38 ± 3.88 (n = 4)

Table 4.1 Effect of major permeant cations on MscS subconducting states. This table documents the number of subconducting states and time spent in the fully open state as shown in figure 4.3A & B respectively.

In addition to the number of subconducting states changing in different ionic conditions the time spent in the subconducting states also changed (Figure 4.3B). Representative traces are shown in Figure 4.4. A particularly marked difference is seen between subconducting states when divalent cations are the major permeant cation as opposed to monovalent cations. In the presence of symmetrical 100 mM $CaCl_2$ and $BaCl_2$ numerous long lived subconducting states can be seen at +70 mV pipette potential. For example in the presence of symmetrical 200 CsCl, MscS spent 89.93 ± 1.91 % (n = 4) of

the time in the fully open state over a 5 second period under constant pressure application. In the presence of symmetrical 100 mM $CaCl_2$ and $BaCl_2$ MscS spent 8.63 ± 2.87 % (n = 4) and 6.38 ± 3.88 (n = 4) of the time respectively in the fully open state. Interesting in the presence of symmetrical LiCl the number of subconducting states observed at + 70 mV was higher than that in CsCl and KCl but not as high as in $CaCl_2$ and $BaCl_2$. Furthermore the time spent in the open state in the presence of LiCl [57.65 ± 3.22 % (n = 5)] was reduced in comparison to CsCl [89.93 ± 1.91 % (n = 4)] and KCl [87.93 ± 2.72 % (n = 5)]. In addition to this no examples of closed state to subconducting state transitions were observed throughout all experimentations under all conditions.

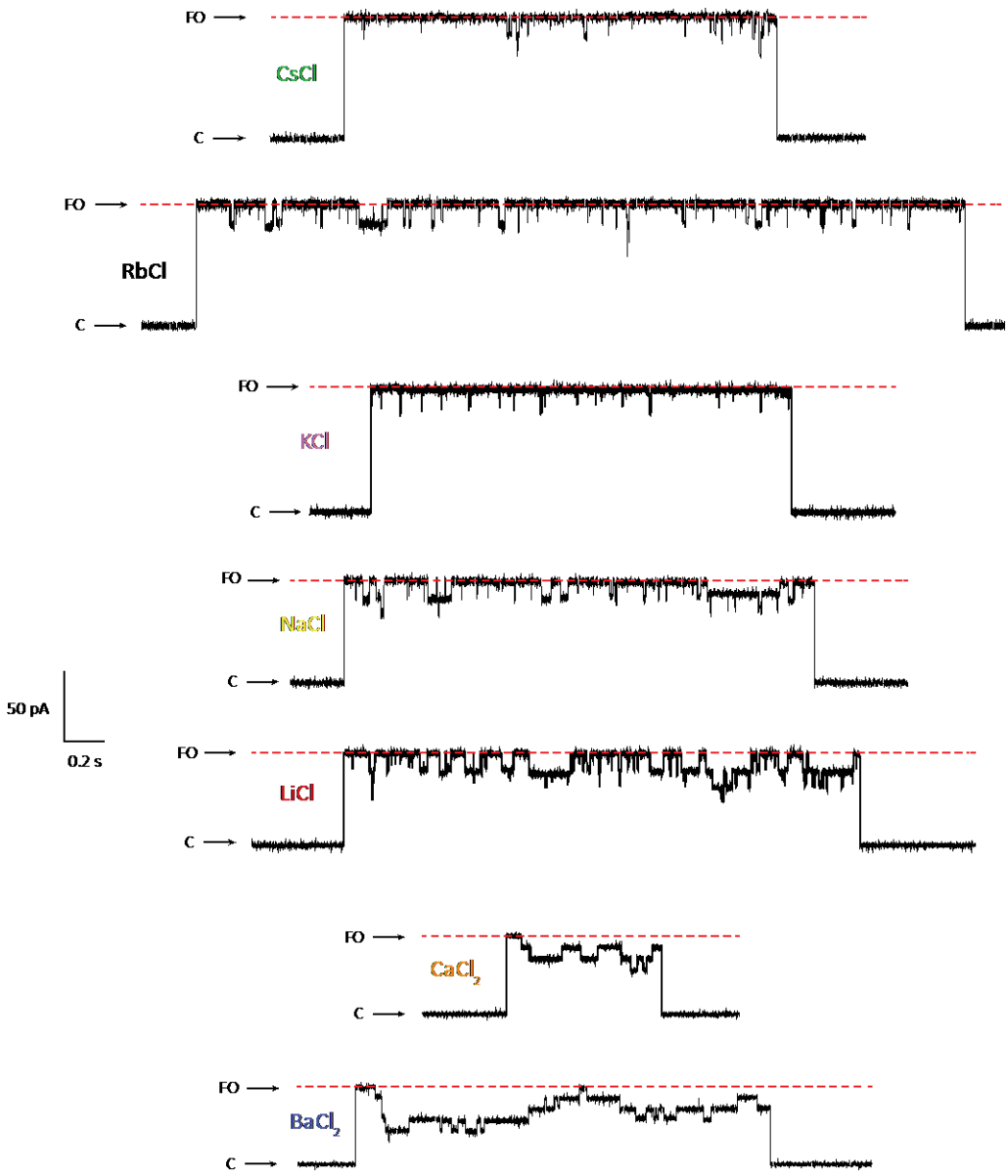

Figure 4.4 Raw records of MscS in different ionic conditions at + 70 mV pipette potential. Either symmetrical 200 mM XCl or symmetrical 100 mM YCl_2 where X is a monovalent cation and Y is a divalent cation.

4.3.2 MscS subconducting states in the presence of $CaCl_2$ and $BaCl_2$

In the presence of symmetrical 100 mM $CaCl_2$ as previously mentioned MscS exhibits numerous subconducting states that are long lived. These subconducting states were only seen in the presence of the fully open state with no closed to subconducting state transitions identified. Interestingly as

the pipette voltage increased so too did the number of subconducting states (Figure 4.5). The number increased up to a maximum number of 7 subconducting states or a total number of 8 conducting states if we include the fully open state. These 8 distinct conducting states are seen at and above +80 mV pipette potential. In addition, only 8 conducting states are seen up to +140 mV pipette potential (no experiments were carried out above this potential due to liposomal patch instability). The 8 conducting states are approximately equally spaced at around 10-14 % of unitary conductance (Figure 4.5). Identical behaviour is observed in the presence of symmetrical $BaCl_2$ (Figure 4.6).

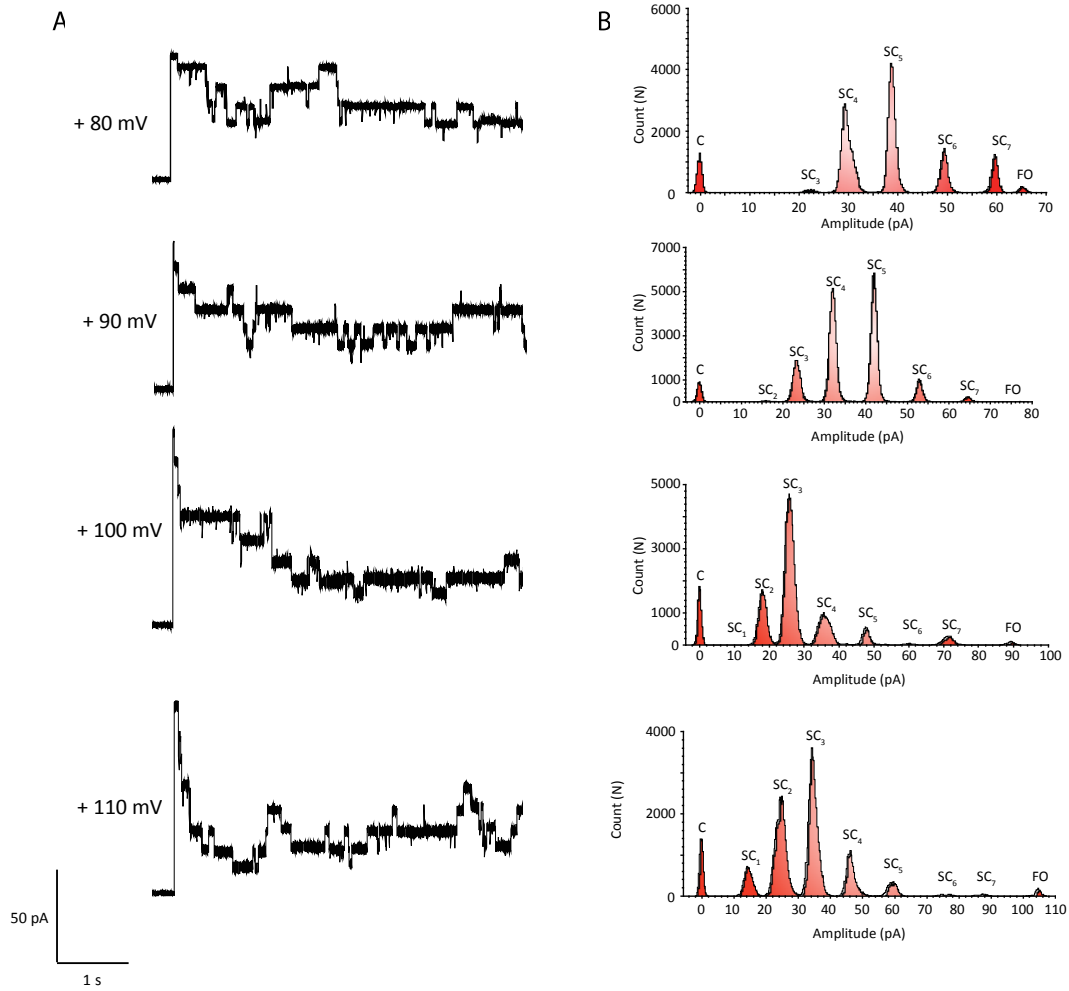

C

% Unitary conductance	80 mV	90 mV	100 mV	110 mV
SC7	89.3 ±3.9 (n=3)	85.5 ±2.1 (n=3)	82.9 ±2.7 (n=3)	83.3 ±0.4 (n=3)
SC6	75.0 ±0.7 (n=3)	67.8 ±4.2 (n=3)	69.1 ±1.6 (n=3)	71.8 ±2.5 (n=3)
SC5	61.8 ±3.3 (n=3)	51.7 ±2.4 (n=3)	55.2 ±1.5 (n=3)	58.7 ±1.5 (n=3)
SC4	47.7 ±3.0 (n=3)	41.0 ±1.7 (n=3)	42.8 ±1.0 (n=3)	47.9 ±1.2 (n=3)
SC3	35.7 ±5.2 (n=2)	30.5 ±0.6 (n=3)	31.5 ±2.2 (n=3)	36.6 ±4.9 (n=2)
SC2	26.5 n/a (n=1)	21.4 ±1.1 (n=3)	22.3 ±2.0 (n=3)	25.5 ±3.8 (n=3)
SC1	13.5 n/a (n=1)	14.0 ±1.0 (n=3)	14.6 ±2.1 (n=3)	15.3 ±3.1 (n=3)

Figure 4.5 MscS subconducting states in the presence of symmetrical 100 mM $CaCl_2$. (A) Raw records of MscS activity reconstituted in azolectin liposomes at + 80, 90, 100 and 110 mV pipette potential in inside-out patches under symmetrical conditions ($CaCl_2$ 100 mM, HEPES 5 mM, pH 7.4). (B) Distribution of current histograms from raw records depicted in (A) illustrating the rise in the number of subconducting states with increasing pipette voltage to a maximum of 8 conducting states as seen with $BaCl_2$. (C) Table illustrating mean percentage of unitary conductance of each subconducting state at four different voltages (80 - 110 mV) ± standard deviation. [C – closed, FO - Fully open, SC – Subconducting state].

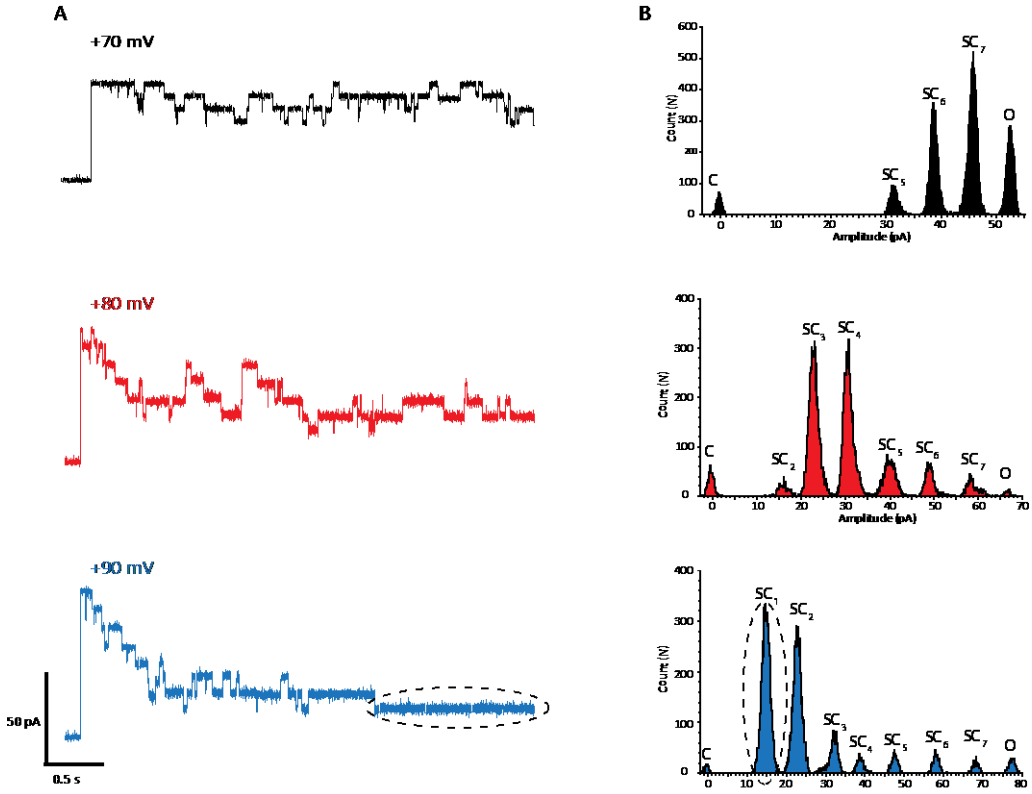

Figure. 4.6 Subconducting states in MscS in the presence of symmetrical 100 mM Ba^{2+}. (A) Raw records of MscS channel activity reconstituted in azolectin liposomes at + 70, 80 and 90 mV pipette potential in inside-out patches under symmetrical conditions ($BaCl_2$ 100 mM, HEPES 5 mM, pH 7.4). Numerous long-lived subconducting states were observed. (B) Distribution of current histograms from raw records depicted in (A) illustrating a rise in the number of subconducting states with increasing pipette voltage to a maximum of 8 conducting states similar to what is seen with Ca^{2+}. The dashed lines represent the lowest subconducting state SC1.

4.3.3 Effect of voltage on subconducting states

As described in the previous section an increase in pipette voltage resulted in an increase in the maximum number of subconducting states seen in all solutions. This was the case in all solutions not just in those whose major permeant cation was divalent. This is illustrated for symmetrical $BaCl_2$ and $CaCl_2$ in Figures 4.5, 4.6 and data are plotted in Figure 4.7. As a result of this, the time MscS spent in the fully open state decreased as the pipette voltage

increased. The relative magnitude of the subconducting states expressed as percentage of unitary conductance however was not affected by the pipette voltage as illustrated in Figure 4.8 (data in symmetrical $CaCl_2$).

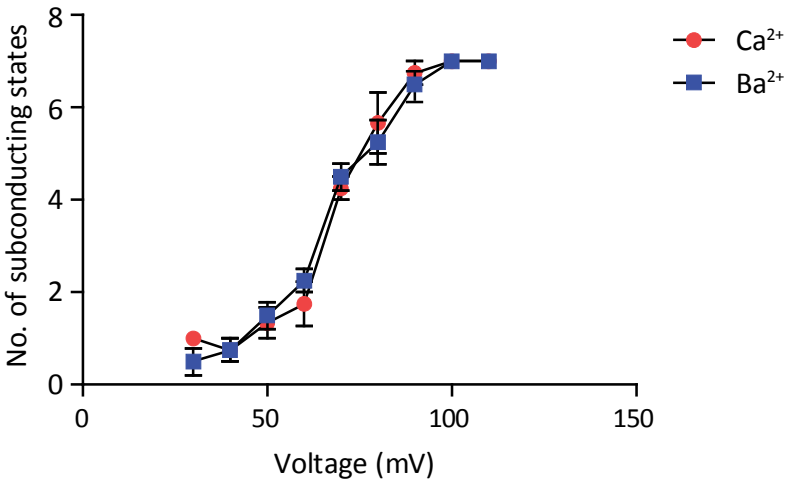

Figure 4.7 Illustration of how pipette voltage affects the number of subconducting states exhibited by MscS in symmetrical 100 mM $CaCl_2$ and $BaCl_2$.

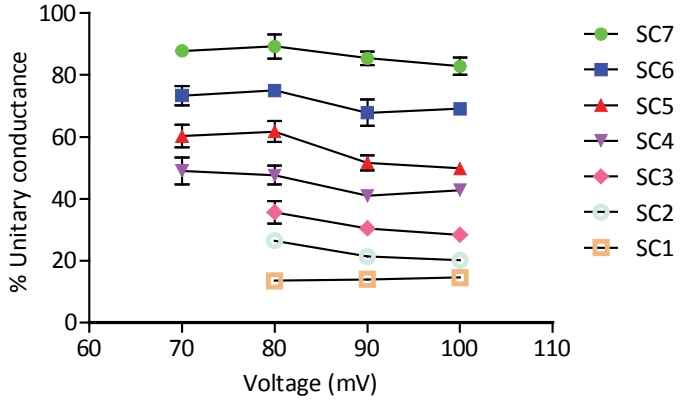

Figure 4.8 Illustration of how the magnitude of MscS subconducting states (SC), presented as percentage of unitary conductance, is affected by pipette voltage in symmetrical 100 mM $CaCl_2$.

The magnitude of the subconducting states presented as percentage of unitary conductance also does not differ significantly in the presence of different major permeant cations. This is shown in tables 4.2 and 4.3. One thing that is very noticeable is, as the voltage rises beyond + 90 mV in the

presence of symmetrical 100 mM $CaCl_2$ and $BaCl_2$, MscS continues to fluctuate

Figure 4.9 Illustration of MscS activity after pressure removal. Raw record illustrating MscS activity in an excised inside-out patch in symmetrical 100 mM $CaCl_2$. After the pressure is removed MscS continues to fluctuate between lower subconducting levels, in this particular case not closing until the applied pipette voltage was removed.

between subconductance states long after pressure has been removed (Figure 4.9). In certain cases the channel would continue fluctuating between conducting states many minutes (> 5 mins) after pressure had been removed. In these cases the only way to cause full closure was to remove the applied potential.

	$CaCl_2$		$BaCl_2$		$MgCl_2$	
	% UC		% UC		% UC	
	+ 90 mV	+ 100 mV	+ 90 mV	+ 100 mV	+ 90 mV	+ 100 mV
SC7	85.5 (n= 3)	82.9 (n= 3)	87.7 (n= 3)	87.4(n= 3)	85.0 (n = 1)	85.88 (n= 2)
SC6	67.8 (n= 3)	69.1 (n= 3)	74.5 (n= 3)	74.4 (n= 3)	66.7 (n = 1)	68.14 (n= 2)
SC5	51.7 (n= 3)	55.2 (n= 3)	60.8 (n= 3)	60.8 (n= 3)	53.5 (n = 1)	54.04 (n= 2)
SC4	41.0 (n= 3)	42.8 (n= 3)	48.9 (n= 3)	49.5 (n= 3)	45.4 (n = 1)	40.73 (n= 2)
SC3	30.5 (n= 3)	31.5 (n= 3)	38.4 (n= 3)	37.0 (n= 3)	33.3 (n = 1)	30.28 (n= 2)
SC2	21.4 (n= 3)	22.3 (n= 3)	28.1 (n= 3)	27.0 (n= 3)	22.8 (n = 1)	22.10 (n= 2)
SC1	14.0 (n= 3)	14.6 (n= 3)	18.2 (n= 3)	17.2 (n= 3)	-	15.78 (n= 2)

Table 4.2 Percentage of unitary conductance (UC) of subconducting states (SC1-7) in the presence of three different divalent cations (symmetrical 100 mM) at +90 mV and +100 mV pipette potential.

	NaCl	KCl	RbCl
	% UC	% UC	% UC
	+ 100 mV	+ 100 mV	+ 100 mV
SC7	80.31 (n = 1)	84.80 (n = 2)	82.94 (n = 4)
SC6	65.14 (n = 1)	67.14 (n = 2)	68.26 (n=4)
SC5	51.90 (n = 1)	54.95 (n = 2)	53.93 (n = 4)
SC4	47.21 (n = 1)	42.57 (n = 2)	41.58 (n = 3)
SC3	35.70 (n = 1)	33.20 (n = 2)	-
SC2	24.62 (n = 1)	-	-
SC1	-	-	-

Table 4.3 Percentage of unitary conductance (UC) of subconducting states (SC1-7) in the presence of three different monovalent cations (symmetrical 200 mM) at +100 mV pipette potential.

4.3.4 An alternative structural mechanism for subconducting states in MscS

As mentioned the current proposed structural mechanism for the presence of MscS subconducting is one in which asynchronous recruitment/inactivation of the 7 MscS monomers brings about a change in the MscS channel pore diameter with corresponding changes in unitary conductance (Akitake *et al.*, 2005). Using this structural hypothesis it is not immediately obvious how to account for the 8 equally spaced conducting states observed in this thesis. I suggest an alternative explanation which involves intermittent occlusion of the cytoplasmic vestibular portals. Taking into consideration the 7 lateral vestibular portals and the pore aligned coaxially to the transmembrane pore this would thus account for the 8 conducting states described in this chapter. Figure 4.10 provides an illustration of how structurally MscS (with each monomer as a different colour) could exhibit 8 conducting states.

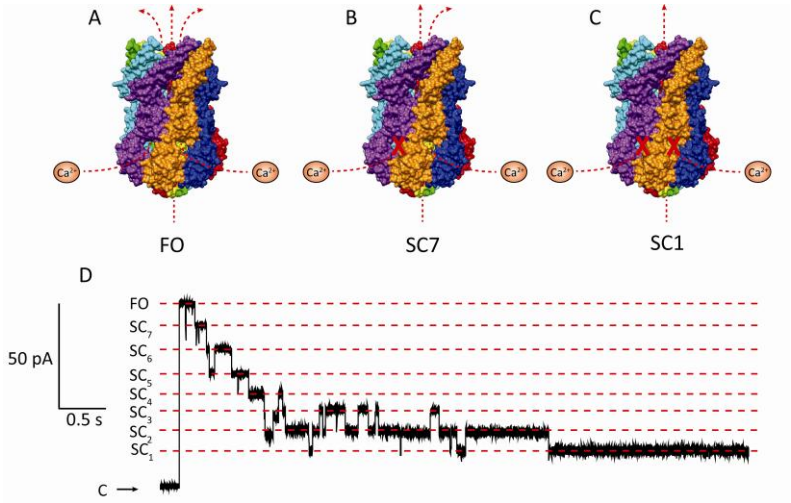

Figure 4.10 Illustration of MscS subconducting states. Illustrations showing how three of the purported 8 conducting states of MscS arise. (A) In the fully open state ion transit occurs through all 8 cytoplasmic perforations. (B) SC7 arising from the occlusion of one of the lateral vestibular portals and (C) SC1 arising from simultaneous occlusion of all 7 lateral vestibular portals leaving only the opening perforating the floor of the cytoplasmic domain to conduct ions. (D) Raw record of MscS activity clearly showing the 8 conducting levels at + 90 mV pipette potential in symmetrical 100 mM $CaCl_2$. (FO: Fully open, SC: Subconductance state, C: Closed).

4.3.5 Estimating pore diameter of the smallest subconductance state (SC1)

If the hypothesis regarding vestibular portal occlusion were correct then the lowest subconducting state would be a result of ion permeation via the pore aligned coaxially to the transmembrane pore alone. In order to estimate whether the smallest subconducting state (SC1) was indeed due to permeation via the pore aligned coaxially with the transmembrane pore a modified Hille's equation was utilised:

where , the bulk resistivity of the solutions, was measured as 0.58 and 0.66 $\Omega.cm^{-1}$ for $BaCl_2$ and $CaCl_2$, respectively. The conductance in $BaCl_2$ and $CaCl_2$ was estimated from the slope of an I-V plot constructed from current amplitudes of the smallest subconducting states at four potentials (242 ± 63 pS and 250 ± 83 pS respectively) (Figure 4.11).

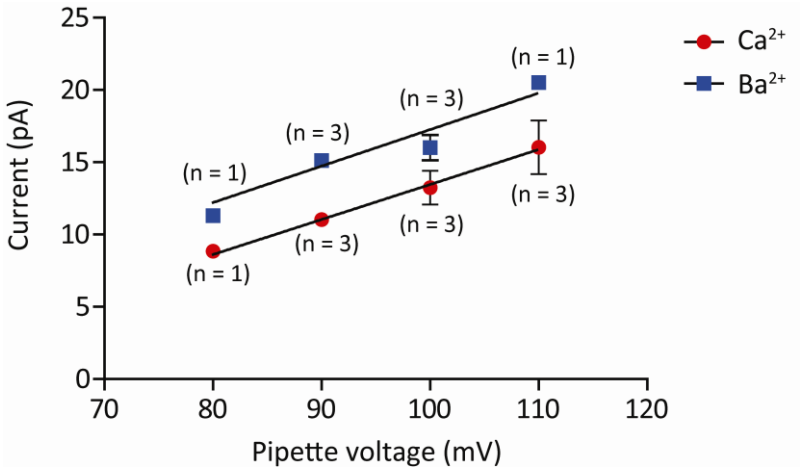

Figure 4.11 Current-voltage plot for the lowest subconducting state SC1 of MscS in the presence of symmetrical 100 mM $CaCl_2$ and $BaCl_2$. The current voltage relationships shown are fitted with linear regression lines and give conductances of 242 ± 63 pS in $CaCl_2$ (r^2 = 0.651) and 250 ± 83 pS in $BaCl_2$ (r^2 = 0.785).

In this case we estimated which represents bilayer thickness was estimated to be 35 Å (Cruickshank *et al.*, 1997) which resulted in an estimated in $CaCl_2$ of 9.2 Å and in $BaCl_2$ of 9.4 Å. Whereas the diameter of the vestibular portals is ~13 Å, the diameter of the pore aligned coaxially with the transmembrane pore is ~8 Å. Consequently, this indicates that the lowest subconducting state may originate from permeation via the pore aligned coaxially with the transmembrane pore alone. This data fits with the

suggestion that the other subconducting states may arise as a result of lateral vestibular portal occlusion.

4.4 Discussion

This chapter aimed to investigate the subconducting states exhibited by MscS at positive pipette potentials (documented in chapter 3). The subconductance states viewed in liposomes were much more distinct at high positive pipette potentials (> +70 mV) than at negative potentials. Above – 40 mV pipette potential openings become very flickery with numerous transitions difficult to delineate (Akitake *et al.*, 2005, Sotomayor *et al.*, 2007). This is in agreement with previous reports (Akitake *et al.*, 2005) which suggest in spheroplasts from -30 mV to +80 mV pipette potential very few examples of subconducting behaviour are seen. In addition to this the fact that substates identified became more evident and visible around +70 mV pipette potential is hence also in agreement with published data (Akitake *et al.*, 2005). There have been very few previous reports about subconductance states at positive pipette potentials (Sotomayor *et al.,* 2007). Current work in spheroplasts has only identified one subconducting state (Shapovalov and Lester, 2004) which is 2/3 of unitary conductance.

The number of subconducting states exhibited here at positive pipette potentials was higher in the presence of divalent cations (Ca^{2+} & Ba^{2+}) than monovalent cations (Cs^{+}, Rb^{+}, K^{+}, Na^{+} and Li^{+}). In a similar pattern to rectification (see chapter 3) the number of subconducting states increased with hydrated ionic radii. This resulted in a reduction in the time MscS spent

in the fully open state which in both Ba^{2+} and Ca^{2+} was less than 10% over a five second period immediately following activation.

As pipette voltage increased, so too did the number of subconducting states exhibited. This increased to a maximum of 8 conducting states at and above +80 mV pipette potential in Ca^{2+} and Ba^{2+}. This number of conducting states was not exceeded up to a maximum experimental pipette voltage of +140 mV. In addition to this, the subconductance states were equally spaced with each being around 10 – 14 % of unitary conductance, which was unaffected by voltage.

The current paradigm suggested for subconducting states in MscS cannot easily explain 8 conducting states. As a result a novel structural explanation for these subconducting states was proposed. The cytoplasmic domain of MscS is perforated by 8 openings. These openings include 7 lateral vestibular portals (~13 Å) and one opening aligned coaxially to the transmembrane pore (~8 Å) (Wang *et al.*, 2008). The suggestion is that sequential occlusion of these lateral vestibular portals gives rise to these subconducting states. In the event of all 7 of the lateral vestibular portals becoming occluded, this leaves the pore perforating the floor of the cytoplasmic domain to continue to conduct ions. This provides a simple explanation of the 8 conducting states observed. To try to provide evidence for such a hypothesis an attempt was made to estimate the pore diameter that would give rise to an opening of equivalent current amplitude to that of the lowest subconducting state termed SC1. If

this hypothesis regarding vestibular portal occlusion were correct, then the pore diameter calculated should match that of the opening on the floor of the cytoplasmic domain. The calculated pore diameters in Ca^{2+} and Ba^{2+} were 9.2 Å and 9.4 Å. This is close to the diameter of the pore aligned coaxially to the transmembrane and while this estimation is not exact this does give some credence to this hypothesis.

It has been suggested for K^{+} ions that occlusion of the lateral vestibular portals is unlikely or would be short lived (Gamini *et al.*, 2011). This might reflect the short lived subconducting states seen in this chapter. As the pipette voltage increases so too do the number of subconducting states seen which may well be a result of the increased ion transit. However in addition to suggesting portal occlusion is 'unlikely' Gamini *et al.,* 2011 also suggest that in their simulations the pore aligned coaxially to the transmembrane pore is largely unhydrated and unable to conduct ions. This final point does not fit with this hypothesis but it has not been proven experimentally. However some support for this hypothesis can be found in Gamini *et al.,* 2011.

If vestibular portal occlusion does give rise to these states, the question then becomes what structural determinants would allow for vestibular portal occlusion? And furthermore why do the lateral vestibular portals become occluded but not the narrower pore aligned coaxially with the transmembrane pore? The next chapter aims to look at the structure of MscS and 6 electrophysiological homologues in search of insights into these

questions. In addition it will look for structural determinants of ion selectivity within these homologues to provide further hints towards the structural basis of MscS selectivity which was also investigated in chapter 3.

The most interesting point about these subconducting states is that they are likely to occur in a physiological setting. The resting membrane potential of *E . coli* varies depending on where in the cell cycle the bacterium is, but is around – 150 mV (Bot and Prodan, 2010). The substates documented in this chapter are seen at +70 mV pipette potential and above, which equates to membrane potentials of -70 mV and above. If these subconducting states were to occur it would greatly reduce the conductance of MscS. This may be a protective mechanism of regulation preventing both the excessive efflux of internal osmolytes but also, as eluded to in chapter 3, the excessive influx of Ca^{2+}. Along with the pressure sensitivity and inactivation this could add another intricate layer to the regulation of this highly tuned channel.

4.5 Conclusions and future work

The work contained within this chapter illustrates that in the presence of divalent cations (Ca^{2+} and Ba^{2+}) alone MscS exhibits numerous equally spaced, long-lived subconducting states at positive pipette potentials. The maximum number of subconducting states identified was 7 which is not easily explained using the current paradigm (Akitake *et al.*, 2005). Therefore a new structural explanation was proposed for these substates based on the intermittent occlusion of the seven lateral vestibular portals of MscS. Thus the lowest subconducting state would be due to ionic permeation through the pore

aligned coaxially to the transmembrane pore. In addition the work in this chapter also raises numerous questions that need to be addressed:

- Does MscS exhibit these 8 conducting states in native *E. coli* membranes? This could be addressed by patching MscS in the presence of $CaCl_2$ or $BaCl_2$ in giant *E. coli* spheroplasts. If so, do these subconducting states have a physiological role in reducing internal osmolyte efflux and/or Ca^{2+} influx?
- Does the membrane composition affect MscS subconducting states? The possibility remains that the effect of Ca^{2+} and Ba^{2+} on the electrophysiological behaviour of MscS is mediated by effects on the membrane. This could be investigated by modifying the lipid composition of the liposomes MscS is reconstituted in and seeing whether MscS subconducting activity is altered.
- Are the MscS subconducting states due to vestibular portal occlusion? This could be tested by changing the charge distribution around the vestibular portals and investigating whether these mutant MscS channels display different subconducting behaviour.

Chapter 5: Structural comparison of six electrophysiologically characterised MscS homologues

5 Structural comparison of six electrophysiologically characterised MscS homologues

5.1 Introduction

The previous two chapters have examined the effects of divalent cations on MscS behaviour. In particular investigating differences in anion-cation permeability and subconducting states. MscS is a homoheptameric ~210 kDa protein with a vast array of homologues currently identified in protists (Nakayama *et al.*, 2007), bacteria (Martinac *et al.*, 1987), archaea (Kloda and Martinac, 2001) and plants (Haswell and Meyerowitz, 2006). This chapter aims to interrogate the structure of 6 electrophysiologically characterised MscS homologues paying particular attention to potential discriminators of selectivity or cation binding sites with a view to creating single residue MscS mutants that can shed light on the structural basis of the subconducting states seen and/or the channels' anion selectivity. The structural similarity between these MscS homologues and previous description of their biophysical properties means it is useful to make comparisons between these homologues. The main aim is to identify sites particularly in the cytoplasmic domain which could be involved in ionic interactions. These interactions may bring about the 7 distinct subconducting states identified in chapter 4, give some insight into the slight anion selectivity observed with MscS and also the increase in anion selectivity seen in the presence of divalent cations such as Ca^{2+} and Ba^{2+}.

The 6 electrophysiologically characterised homologues that will be looked at are; MscK from *E. coli,* MscCG from *Corynebacterium glutamicum*, MSC1 from *Chlamydomonas reinharditii*, MscSP from *Silicibacter pomeroyi* and MscMJ and MscMJLR from *Methanococcus jannaschii*. As previously discussed two crystal structures of MscS are available, thus from an amalgamation of protein sequence and electrophysiological data we can begin to look at structural determinants of biophysical behaviour. The following is an introduction to the homologues discussed in this chapter.

5.1.1 MscK

A number of bacteria possess MS channel paralogues a case in point being *E. coli* which has 6 electrophysiologically characterised MscS-like proteins (Edwards and Booth, 2011, Edwards *et al.*, 2012). One of these paralogues is MscK which is fully discussed in the general introduction. A particularly important point to note is that MscK is very slightly anion selective even in comparison to MscS.

5.1.2 MscCG

MscCG is a mechanosensitive channel found in *Corynebacterium glutamicum*. It plays an essential role in osmoprotection and its involvement in the jettisoning of intracellular glutamate is utilised commercially in the global production of glutamate (Nakamaru *et al.*, 2007). MscCG has a similar conductance to MscM of around ~400 pS (symmetrical KCl 200 mM, $MgCl_2$ 40 mM, HEPES 5 mM, pH 7.4) and exhibits weak cation selectivity (P_K/P_{Cl} = ~3)(Borngen *et al.*, 2010). Similarly to MscS this channels exhibits rectification

where the unitary conductance at positive potentials is markedly larger (roughly 3 times) than at negative pipette potentials. MscCG is interesting per se for a number of reasons particularly structurally. It possesses 4 putative transmembrane segments one of which is purported to be at the C terminal tail following its cytoplasmic domain (Borngen *et al.*, 2010).

5.1.3 MSC1

The MSC1 channel was isolated from the protist *Chlamydomonas reinharditii*. It has been shown to be a mechanosensitive channel with a conductance of 400 pS (symmetrical KCl 200 mM, $MgCl_2$ 40 mM HEPES 5 mM pH 7.4) and displays a higher anion-cation permeability ratio than MscS (P_{Cl}/P_K = ~5). This channel is expressed in the chloroplasts and cytoplasm and seems to have a role in chloroplast organisation, as knocking it out results in abnormal chlorophyll distribution (Nakayama *et al.*, 2007).

5.1.4 MscMJ and MscMJLR

Methanococcus jannaschii is a mesophilic coccoid methanogen which to date has two electrophysiologically characterised MS channels: MscMJ (*Methanococcus jannaschii*) and MscMJLR (*Methanococcus jannaschii* large and rectifying)(Kloda and Martinac, 2001). They are both cation selective (P_K/P_{Cl} = ~5 & ~6, respectively) mechanosensitive channels. MscMJ has a conductance in the region of 270 pS whereas MscMJLR has a much larger conductance (2.2 nS)(Kloda and Martinac, 2001). As the name suggests, MscMJLR displays marked rectification whereas MscMJ does not.

5.1.5 MscSP

There are no publications currently relating to the MscS homologue MscSP isolated from the sulphur degrading marine bacterium *Silicabacter pomeroyi*. Information regarding the biophysical activity of this channel is from personal communication with Prof B Martinac (Petrov *et al.,* unpublished). This channel gates in response to increasing membrane tension with a conductance that rectifies such that its conductance at positive potentials is 1/3 greater than at negative pipette potentials. MscSP has a smaller conductance than MscS (~20 % less) but exhibits similarly weak anion selectivity (PCl/PK = ~1.4). There are no data to suggest whether this channel can protect cells against an hypoosmotic shock.

5.1.6 Chapter hypothesis and aims

This chapter aims to identify putative regions that could be involved in selectivity and/or subconductance state generation, and then to test this using site directed mutagenesis. Firstly, to identify these potential regions, sequence alignment of MscS with six electrophysiological characterised MscS homologues with vastly different selectivity profiles will be carried out. Once residues for mutations have been identified, channel proteins will be expressed, purified and reconstituted in azolectin liposomes for electrophysiological characterisation. The specific aims are as follows:

- Align the full length MscS sequence with other MscS homologues.

- Align the MscS TM3 region and cytoplasmic domain with putative regions of the six channels described in the introduction using pairwise alignment.

- Identify any difference between the channels that could be important for describing their biophysical behaviour, in particular their selectivity.

- Identify regions in the cytoplasmic domains that could bind ions through electrostatic interactions.

- Create, purify and reconstitute MscS mutants in 100 % azolectin liposomes for electrophysiological characterisation.

5.2 Methods

5.2.1 Protein Sequence alignment

Multiple sequence alignment of MscS-like proteins was carried out using Clustal W (Thompson *et al.*, 1994) freely available software:

http://www.ebi.ac.uk/Tools/msa/clustalw2/

Pairwise alignments were carried out using the Needleman-Wunsch algorithm subsequent to multiple sequence alignment to decipher levels of sequence identity and similarity of full length proteins and specific protein regions (cytoplasmic domain and pore-forming helix). Sequence identity is defined as the percentage of residues in an aligned sequence that are identical. Sequence similarity is defined as the percentage of residues in an aligned sequence that have similar properties as set out by the algorithm.

5.2.2 Molecular modelling

Homology models of channels in this chapter were created using the SWISS-model server (Arnold *et al.*, 2006). They were created using both the open structure (PDB: 2VV5) and closed/intermediate structure of MscS (PDB: 2OAU).

http://swissmodel.expasy.org/

5.2.3 Computation of putative Transmembrane spanning segments

Putative membrane spanning regions were determined using the membrane protein identification without explicit use of hydropathy profiles and alignments (Minnou) software (Cao *et al.*, 2006).

5.2.4 Hydropathy plots

Hydropathy plots for MSC1, MscS, MscK, MscCG, MscMJLR and MscMJ were calculated using laser gene software with a window size of 19 using the Kyte-Doolittle scale. Peaks above + 1.6 indicate the possibility of a transmembrane spanning region.

5.2.5 Site directed mutagenesis

Site directed mutagenesis was carried out on the MscS gene (*yggB*) housed in a LacI containing pQE-60 vector using the Quick-change II mutagenesis kit (Stratagene). The associated protocol available online was used with some minor amendments as follows.

The mutagenic primers were designed using the following website:

https://www.genomics.agilent.com/CollectionSubpage.aspx?PageType=Tool&SubPageType=ToolQCPD&PageID=15

Primers were ordered from Sigma all had GC content above 40% (E187R - 53 %; E227A – 61 %), the particulars are shown below:

Mutant	Sequence	Length (nt)
E187R	5′- cgagccagttcgccgtacagatttattattggcgtggcg - 3′	40
E227A	5′- ctgtgcgcctgaacgcacttggtgcatcgtc - 3′	31

*Foward primers shown but an identical set of reverse primers were also used.

The two test reactions were formed by adding 5 µl of MscS encoding pQE-60 plasmid to 5 µl of 10x reaction buffer. To one of the test reactions 150 ng of both the forward and reverse primers for the E187R mutant were added and to the other test reaction 150 ng of the forward and reverse primers for the

E277A mutant were added. To both of the reactions 1 µl of dNTPs were also added and then both were topped up to 50 µl using ddH_20.

To all reactions 1.5 µl of PfuUltra high fidelity DNA polymerase (2.5 U. μl^{-1}) was then added. All reactions were then placed on a heating block using the following cycle:

Step	No.of Cycles	Temperature (°C)	Time (seconds)
Denaturing	1	95	30
Annealing	16	95	30
		55	60
		68	360

Once the Thermocycler (Thermoscientific) had finished the samples were placed on ice for 2 minutes. The temperature had to be reduced low enough not to denature the Dpn1 restriction enzyme. Once this had occurred 1 µl of Dpn1 (10 $U.\mu l^{-1}$) was added to each reaction. This enzyme breaks down the parent methylated template DNA. The Dpn1 was mixed with each reaction gently and incubated in an incubator at 37 °C for one hour. Subsequently 2 µl of the final reaction was added to 100 µl of super-competent XL-1 blue *E. coli* cells. The XL-1 blue cells were then transformed with mutant DNA in identical fashion to that documented in the material and methods section of this thesis (i.e. using heat shock). The transformed cells were then plated onto LB-agar plates containing 100 $\mu g.\mu l^{-1}$ ampicillin and 1 mM IPTG. They were incubated

at 37 °C over night. Minipreps of each plasmid (See *materials and methods chapter 2*) were done in order to send samples for sequencing. All sequencing was carried out by the Garvin Institute, Sydney, New South Wales, Australia. Sequencing results were visualised using the DNAstar Lasergene suite.

5.2.6 Protein purification and incorporation in liposomes

The mutants were expressed and purified as set out in the materials and methods section of this thesis. Again the dehydration-rehydration method was used to incorporate the purified channels into azolectin liposomes. The electrophysiology set up was exactly as set out in chapter 2.

5.2.7 SDS-page gel

To 4 µl of protein sample 2.5 µ l of Nupage LDS sample buffer (Invitrogen) was added and deionised water was then added to 10 µl. This sample was subsequently heated at 70 °C for 10 minutes using a UNO-thermoblock (Biometra). After placement of a Novex NuPAGE Bis-Tris 10% gel (Invitrogen) into an X-cell sure-lock mini-cell rig (Invitrogen) the upper and outer chambers were filled with NuPAGE MES buffer (Invitrogen). Subsequently 12 µl of each sample was loaded onto the gel along with 15 µl Novex Sharp Pre-stained standard (Invitrogen). The gel was then set to run for 45 minutes at 150 - 200 V. Images of stained gels were taken using a digital camera.

5.3 Results

5.3.1 Full length proteins

As previously reported by Pivetti *et al.,* 2003 the MscS family is broadly divided into two categories of smaller proteins (such as MscS circa 300 amino

acids) and larger proteins (such as MscK circa 900 amino acids)(Figure 5.1). These differences are made up from inserts and/or deletions in either the cytoplasmic domain or transmembrane regions. For example MscK has 11 putative TM helices whereas MscS has only 3 (Pivetti *et al.*, 2003, McLaggan *et al.*, 2002)(Figure 5.1). In this chapter most of the 6 electrophysiologically characterised MscS homologues described belong to the former. They are relatively small in size ranging from 268 – 533 amino acids long with 3 – 5 putative transmembrane regions as determined using hydropathy plots and the Minnou transmembrane predictor programme. Allied to this, the sequence similarity with each of these homologues is higher with MscS (30.4 – 70.8 %) than MscK (12.8 - 23 %)(Figure 1.2).

The transmembrane regions are highlighted in Figure 5.1 with horizontal grey boxes labelled with the corresponding TM region. In the hydropathy plots shown in Figure 5.1 using the Kyte-Doolittle scale a peak of above + 1.6 signifies sufficient hydrophobicity, with a window size of 19 (the window size being the number of amino acid residues looked at), to indicate a TM region. Incidentally the peak circled in red (+1.94) in Figure 5.1 is related to the transmembrane domain of MscCG which comes after the cytoplasmic domain and may play an extra role in tension sensing/glutamate selectivity. This is a point which makes MscCG structurally unique.

MSC1 the protist MscS homologue also has an interesting feature. The hydropathy plot shows a large N-terminal region (~120 aa's) that does not

form any TM helices. It is this N-terminal region that is removed in Nakayama *et al.,* 2007 in order to gain channel functionality. These authors surmise that this is a signal sequence requiring cleavage before the channel can become functional. This is the only channel in this chapter with such a sequence. They also suggest there may be a helical structure in this region which the hydropathy plot in Figure 5.1 does not corroborate as there are no peaks above +1.6 in this region.

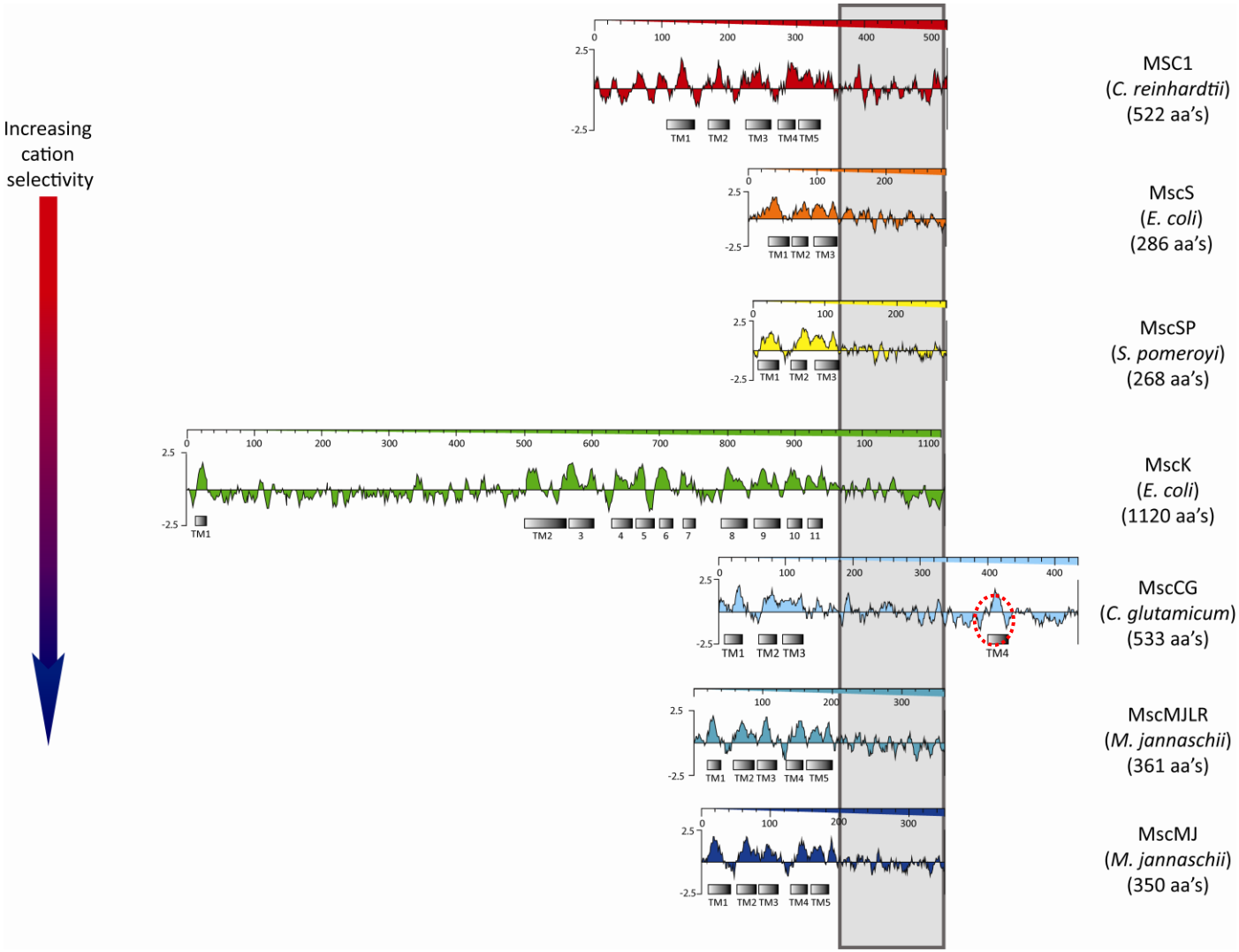

Figure 5.1 Hydropathy plots of MscS and 6 electrophysiologically characerised MscS homologues. Channels are arranged with the most anion selective (MSC1) at the top and most cation selective at the bottom (MscMJ)(Kyte-Doolittle scale). Grey shaded area illustrates the conserved cytoplasmic domain of all seven homologues. In the case of MscCG the cytoplasmic domain extends markedly outside the shaded area. Putative transmembrane regions are also shown for comparison by grey bars as deciphered from hydropathy plots and the online TM segment predictor Minnou.

Full length
% Identity

	MSC1	MscS	MscSP	MscK	MscCG	MscMJLR	MscMJ
MSC1	-	10.9	8.6	6.6	6.5	12.9	11.0
MscS	32.2	-	35.4	6.2	10.1	20.1	19.4
MscSP	28.1	70.8	-	5.4	9.2	18.5	20.3
MscK	23.0	17.2	16.2	-	4.6	6.6	6.1
MscCG	29.4	30.4	29.2	12.8	-	8.8	8.1
MscMJLR	41.6	51.1	50.3	19.6	25.7	-	40.7
MscMJ	38.4	52.8	49.1	18.1	29.2	75.6	-

% Similarity

Cytoplasmic domain
% Identity

	MSC1	MscS	MscSP	MscK	MscCG	MscMJLR	MscMJ
MSC1	-	12.0	7.1	12.0	8.9	14.1	8.1
MscS	32.2	-	33.3	23.9	12.4	27.7	14.4
MscSP	40.8	70.4	-	23.9	10.1	24.5	25.5
MscK	40.2	61.4	59.1	-	10.1	24.5	22.8
MscCG	33.7	30.9	29.2	31.2	-	8.7	12.4
MscMJLR	51.5	64.5	67.9	58.7	28.2	-	51.6
MscMJ	31.1	34.0	61.8	54.4	33.0	83.9	-

% Similarity

Figure 5.2 Percentage identity and similarity of MscS with homologues studied in this thesis. Top table shows percentage identity (red values read vertically) and percentage similarity (blue values read horizontally) from pair-wise alignments (EMBOSS Needle, Needleman-Wunsch alignment; EMBL-EBI) of full length proteins. Bottom table shows percentage identity and percentage similarity from pair-wise alignments (EMBOSS Needle, Needleman-Wunsch alignment algorithm;EMBL-EBI) of putative cytoplasmic domains subsequent to alignment using ClustalW.

5.3.2 Pore alignment

The first region inspected was the pore-forming helix. An alignment was carried out of the six electrophysiologically characterised MscS-like proteins with the pore lining TM3 helix of MscS which extends from V96 - F127 (Bass *et al.*, 2002). In the main, the TM3 helix of MscS is hydrophobic (Figure 5.3) and is characterised by multiple glycine-alanine repeats (Edwards *et al.*, 2005).

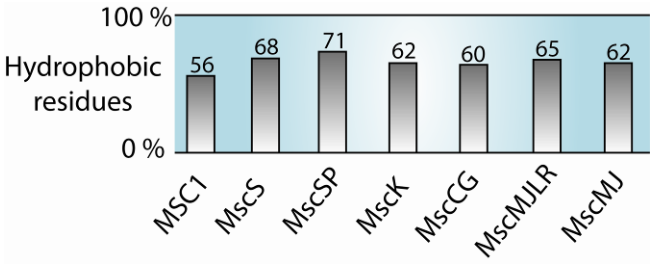

Figure 5.3 Comparison of MscS TM3 helix hydrophobicity with the hydrophobicity of putative pore-forming helices of six homologues. Histogram illustrating the percentage of residues of the putative pore-forming helices that are hydrophobic compared with MscS.

There are no areas which could give insight into the slight anion selectivity exhibited by MscS as previously described (Edwards *et al.*, 2008) (Figure 5.4). In fact even mutations in the pore helix of MscS do not modify selectivity. When you align the other MscS-like proteins there is quite high sequence similarity without the major differences you may expect from the observed selectivity (Figure 5.5). Only two residues are conserved throughout every homologue Q112 and G121. The conserved residue G121 is proposed to be important in both desensitisation to pressure and channel gating (Akitake *et al.,* 2010). It is purported to act as a 'hinge'. From this conservation the suggestion can be made that the gating mechanisms of these channels may,

at least in part, be similar. The role of Q112 is less well documented but this conservation intimates an integral role. In the first crystal structure to be published of MscS by Bass *et al.,* 2002 they make note of the kink formed around G113 and the importance of the glutamine residue preceding it to form the kink. Thus the presence of Q112 may well be a structural feature of this family of channels.

Figure 5.4 Comparison of the putative pore-forming residues of six electrophysiologically characterised MscS homologues. (A) MscS TM3 pore-forming residues aligned with putative pore-forming residues of six electrophysiologically characterised MscS homologues with channels arranged with the most anion selective (MSC1) at the top. (B) Histogram illustrating % conservation of consensus residues at each position, the consensus sequence is contained within the histogram.

Interestingly G113 (important for inactivation) is only conserved in one of the six homologues (MscSP) suggesting that at least within this small cohort of channels inactivation may not be wide spread (discussed later in this chapter).

L109 which forms the hydrophobic lock in MscS is conserved in all homologues apart from MscK where it is replaced by a phenylalanine. The increased volume of phenylalanine may play a role in the reduced

conductance exhibited by MscK. L105 also important for formation of the 'vapour lock' is less well conserved (4 out of the 7 channels).

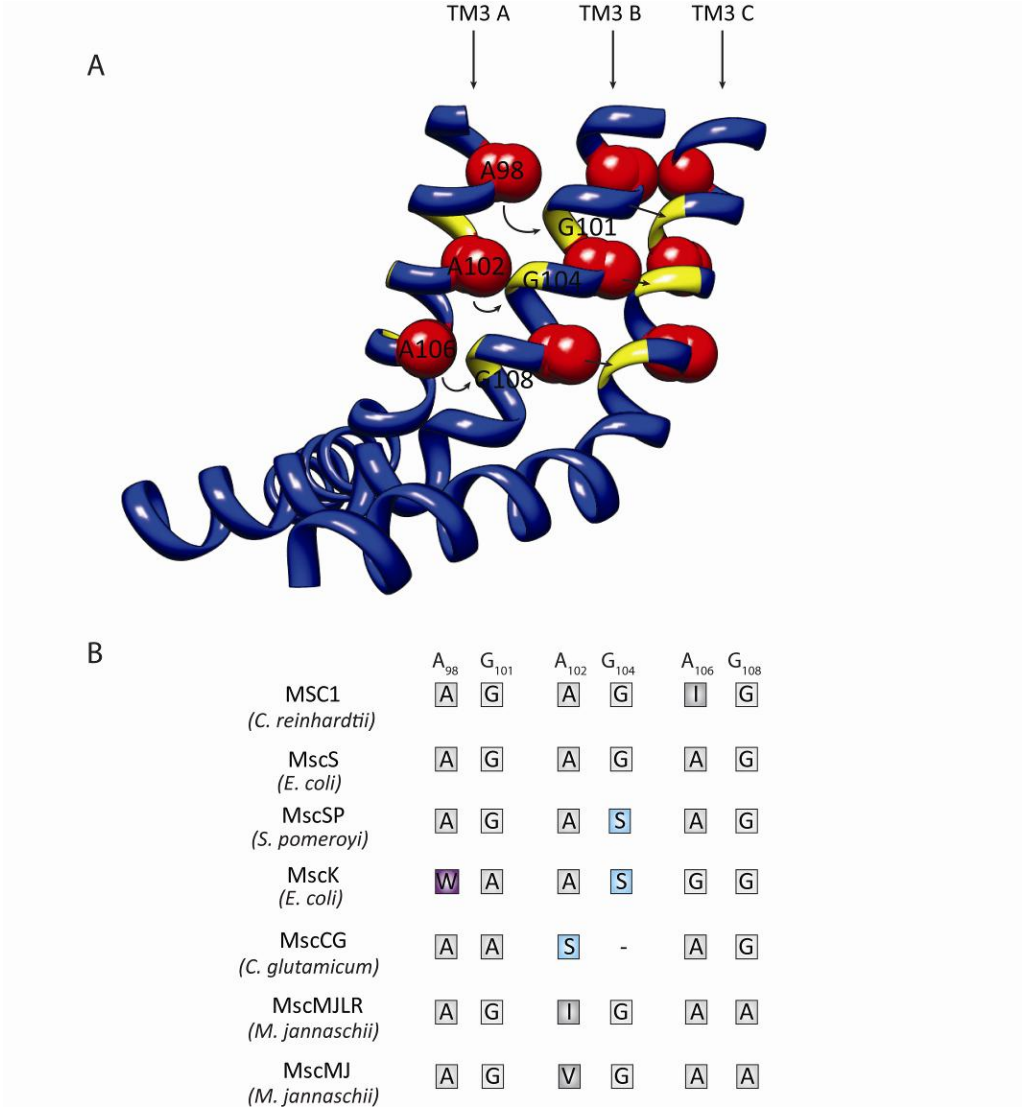

Figure 5.5 Knobs and holes of MscS TM3 helix compared with aligned residues in other homologues. (A) Illustration of alanine glycine packing in MscS (PDB: 2OAU, non-conductive) TM3 with alanines (red) and glycines (yellow) shown from 3 of the 7 monomers. (B) Alignment of alanine-glycine pairs in MscS TM3 with other homologues.

Previously it has been suggested that the tight packing of the TM3 helices seen in MscS (PDB: 2OAU) was enabled through a conserved sequence of glycine-alanine repeats.

Where knobs (alanines) fitted into holes (glycines) to enable tight packing (Edwards *et al.*, 2005). Some of these repeats can be seen in the homologues examined in this chapter, although conservation is moderate, one example being A106 fitting with G108 of a neighbouring helix. Both show moderate conservation throughout these homologues. Another pair showing moderate conservation is A98 and G101 (Figure 5.4 and Figure 5.5). Interestingly MscK possesses a glycine-pair at positions equivalent to A106 and G108 in MscS. Edwards *et al.,* 2005 show that creating glycine pairs lowers activation threshold and MscK has a lower pressure threshold of activation than MscS.

Also not shown in Figure 5.4 but of note, is that a proline at position 129 in MscS is almost completely conserved throughout these homologues, the exception being MscCG where the proline aligns at position 128. Proline residues exhibit a very low helical propensity and it is this residue in MscS that marks the end of the TM3 helix and the start of the cytoplasmic domain (Pace and Scoltz, 1998). This residue was used to mark the beginning of the C-terminal domain when creating pairwise alignments of the channels for sequence identity and similarity of the cytoplasmic domains shown in Figure 5.2.

The sequence similarity between the MscS pore-forming helix and the putative pore forming helices of the 6 MscS homologues is high ranging from 59.4 – 96.9 %. The highest level of similarity (96.9 %) is seen between MscS and MscSP (Figure 5.6). Figure 5.7 shows a homology model of MscSP

(created using the open structure of MscS PDB: 2VV5) compared to the open structure of MscS. Many of the reported residues important for gating and mechanosensing are very similar.

Putative pore-lining helices
% Identity

% Similarity	MSC1	MscS	MscSP	MscK	MscCG	MscMJLR	MscMJ
MSC1	-	41.2	34.4	37.5	21.9	37.5	37.5
MscS	67.6	-	68.8	26.5	18.8	50.0	43.8
MscSP	71.9	96.9	-	21.2	10.1	37.5	37.5
MscK	81.2	76.5	75.8	-	33.8	37.1	30.3
MscCG	68.8	59.4	59.4	75.8	-	31.2	25.0
MscMJLR	81.2	78.1	78.1	71.4	84.4	-	71.9
MscMJ	71.9	81.2	81.2	75.8	75.0	90.6	-

Figure 5.6 Sequence identity and similarity between MscS homologues. This table illustrates percentage identity (blue values read vertically) and percentage similarity (red values read horizontally) from pair-wise alignments (EMBOSS Needle, Needleman-Wunsch alignment; EMBL-EBI) of putative pore-forming residues of all MscS homologues investigated in this chapter.

Interestingly the helices present in the homology models created by SWISS-model (for example of MscSP) closely match those predicted by the transmembrane predictor programme Minnou. Some examples are shown in Figure 5.8 where the helices predicted by Minnou are coloured for comparison.

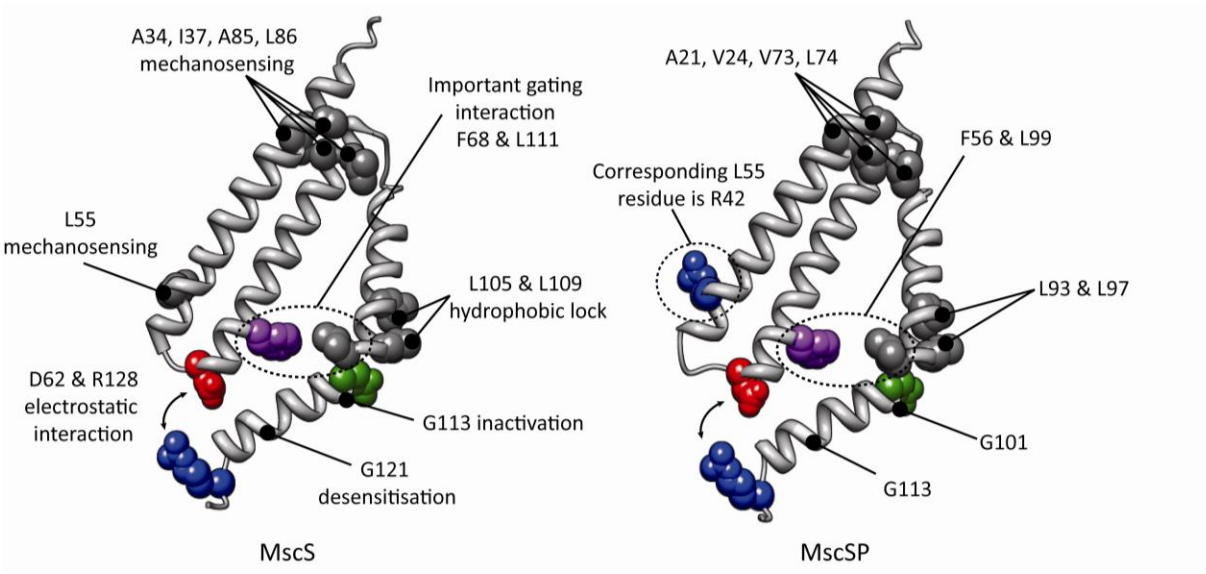

Figure 5.7 Comparison between MscSP and MscS. Left panel shows three TM helices of MscS with important residues for gating, desensitisation, inactivation and mechanosensing shown. Right panel shows a homology model based on MscS crystal structure (PDB: 2VV5) created using SWISS-model software. Putative important residues are illustrated for comparison.

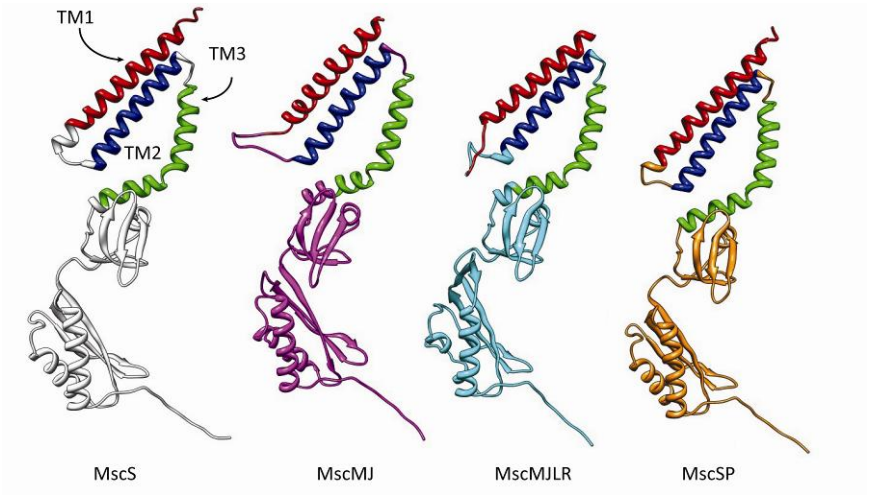

Figure 5.8 Comparison of TM regions. This diagram shows an MscS monomer (PDB: 2VV5) with three homology models of channels investigated in this chapter. The transmembrane regions predicted to be helices by the Minnou programme are coloured red (aligned to TM1 of MscS), blue (Aligned to TM2 of MscS) and green (aligned to TM3 of MscS).

5.3.3 Inactivation

G113 which is purported to be the centre of inactivation (Akitake *et al.*, 2007, Belyy *et al.*, 2010, Kamaraju *et al.*, 2011) is not conserved in 5 of the six MscS-like proteins investigated in this chapter. It is however conserved in MscSP. This is interesting for two reasons. Firstly MSC1 has been reported to display voltage-dependent inactivation but does not have a glycine at the corresponding position (in fact it has a glutamine which has much higher helical propensity)(Nakayama *et al.*, 2007). Secondly MscSP seems not to display any noticeable inactivation despite conservation of the G113 residue (Petrov *et al.,* unpublished). In the other channels MscK, MscMJ, MscCG and MscMJLR the equivalent residue to G113 has much higher helical propensity (glutamate, aspartate, serine, glutamine respectively) and none of these channels exhibit inactivation.

The low helical propensity of G113 allows a kink to form in the TM3 helix and prevents interaction between F68 of TM2 and L111 and L115 of TM3 (Akitake *et al.*, 2007, Belyy *et al.*, 2010, Arkin *et al.*, 1998). This prevents tension being transmitted from TM1-TM2 to the pore. In addition to this an interaction between TM3 and the cytoplasmic domain is also important for inactivation (Koprowski *et al.*, 2011). This interaction is centred around N117 which is highly conserved in MscS homologues. In this chapter it is conserved in 5 of the seven channels (Figure 5.4). This interaction involves hydrogen bonding between N117 and G168 which in turn allows the ‘kink’ to form at G113. Koprowski *et al.,* 2011 showed that an introduction of a positive charge at

either position inhibits inactivation whereas replacement of these residues with opposite charges restores the channels ability to inactivate. A diagrammatic illustration of this is shown in Figure 5.9. G168 is replaced for a serine in MscMJ and MscMJLR which can form hydrogen bonds but may not have sufficient size to bridge the gap between the TM3 helix and β-domain of the cytoplasmic cage.

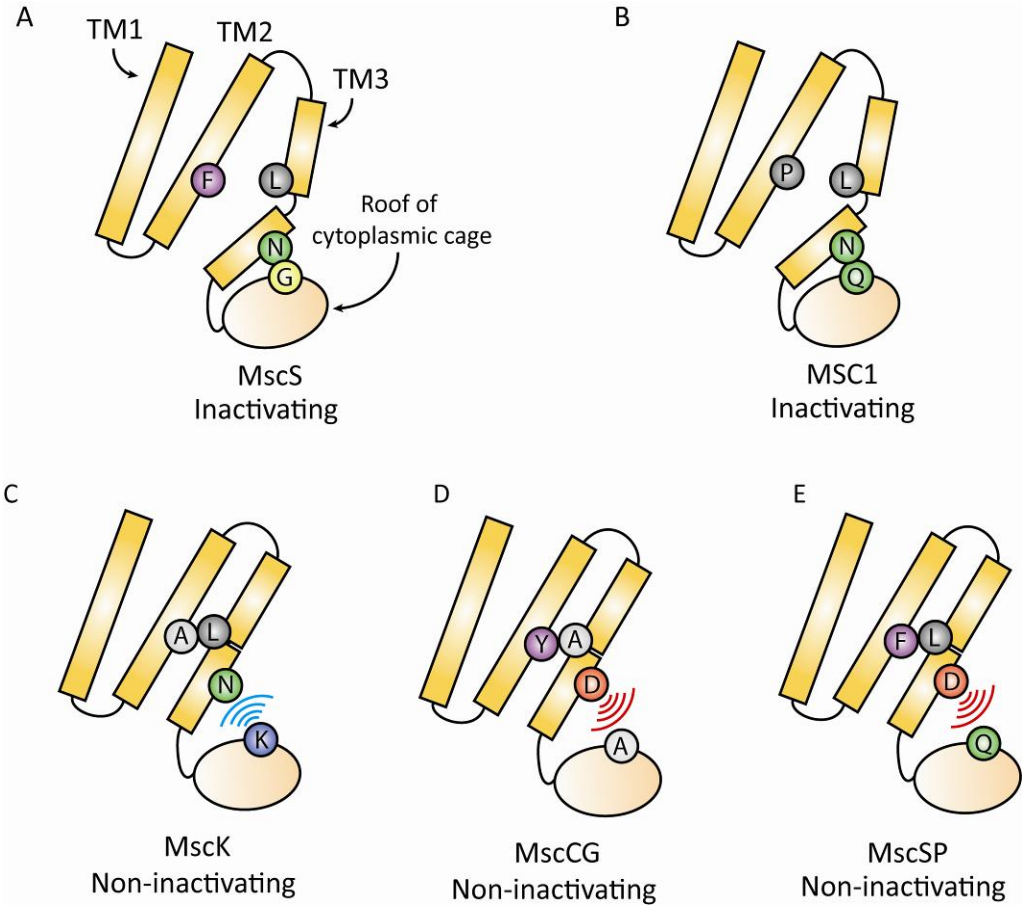

Figure 5.9 Diagrammatic illustration of MscS inactivation. (A) Representation of MscS inactivated state with a kink at G113 in TM3 preventing F68 interacting with L111 and L115 (not shown) thus inhibiting the transmission of tension to the pore. (B) MSC1 which also inactivates and has a conserved interaction between the putative pore-forming helix and the cytoplasmic domain. (C) MscK (D) MscCG and (E) MscSP do not inactivate and they follow what is observed in the mutants reported by Koprowski *et al.,* 2011 i.e. that N117K and G168D do not inactivate and double mutants such as N117K,G168D do exhibit inactivation.

In addition there is no glycine at the equivalent position to 113 in MscMJ and MscMJLR which may explain the lack of inactivation shown by these channels (D and N replacements respectively see Figure 5.4).

From this sequence alignment data the suggestion can be made that while G113 is important for inactivation in MscS and other MscS-like channels, it is not the only structural determinant. Inactivation in MscS and other members of its family also hinges upon interactions between the pore-forming helix and cytoplasmic domain. The fact that MscSP shows such high sequence similarity and a conserved residue at position G113 of MscS but does not exhibit inactivation illustrates how important other mechanisms/residues must be in the inactivation process of this family of channels. As reported by Koprowski *et al.,*the N117/G168 interaction seems to be a big part of the process.

5.3.4 Cytoplasmic domain conservation between MscS-like proteins

As pointed out by numerous previous publications, one area of conservation between different MscS-like proteins is the large cytoplasmic cage. This domain, while possessing lower sequence similarity than the pore lining helices (similarity with MscS ranges from 30.9 to 70.4 %), seems to be present in all MscS-like proteins (Grey shaded area Figure 5.1). In the hydropathy plots in Figure 5.1 the largely negative values in the grey shaded box indicate a hydrophilic region which is water accessible. The fact that the MscS pattern in the hydropathy plot is mirrored in all these six channels indicates a conservation of this region. However in a number of MscS-like proteins such as MscCG there are quite large amino acid sequence insertions (i.e. 43 aa's)

which modify the size of the cytoplasmic domain. The greatest degree of sequence similarity in the cytoplasmic domains, perhaps unsurprisingly, is between MscMJ and MscMJLR (83.9 %) both of which come from *Methanococcus jannaschii*. The degree of sequence similarity between the cytoplasmic regions of MscSP and MscS is also very high at 70.4 % (Figure 5.2).

One similarity between a number of the homologues discussed is the conservation of a potential electrostatic interaction between the loop connecting TM1-TM2 with the top of the cytoplasmic cage (Nomura *et al.,* 2008). In MscS D62 is proposed to interact with R128 and R131 and be involved in not only gating, but also channel inactivation. This conservation is confined to the channels which show the highest sequence similarity with MscS (MscSP: 70.8 %, MscMJ: 51.1 % and MscMJLR: 52.8 %) (Figure 5.2 and Figure 5.6). The fact that D62 and R128/131 come within close proximity in the open structure of MscS (~6 Å; Figure 5.10) and none of the channels where these residues are conserved exhibit inactivation, may hint towards the fact that this electrostatic interaction between the TM linker and the cytoplasmic domain is a conserved part of gating in these MS channels. As shown in Figure 5.10, these residues come within close proximity in the same monomer in the open structure, but in the closed/intermediate state they become close between monomers.

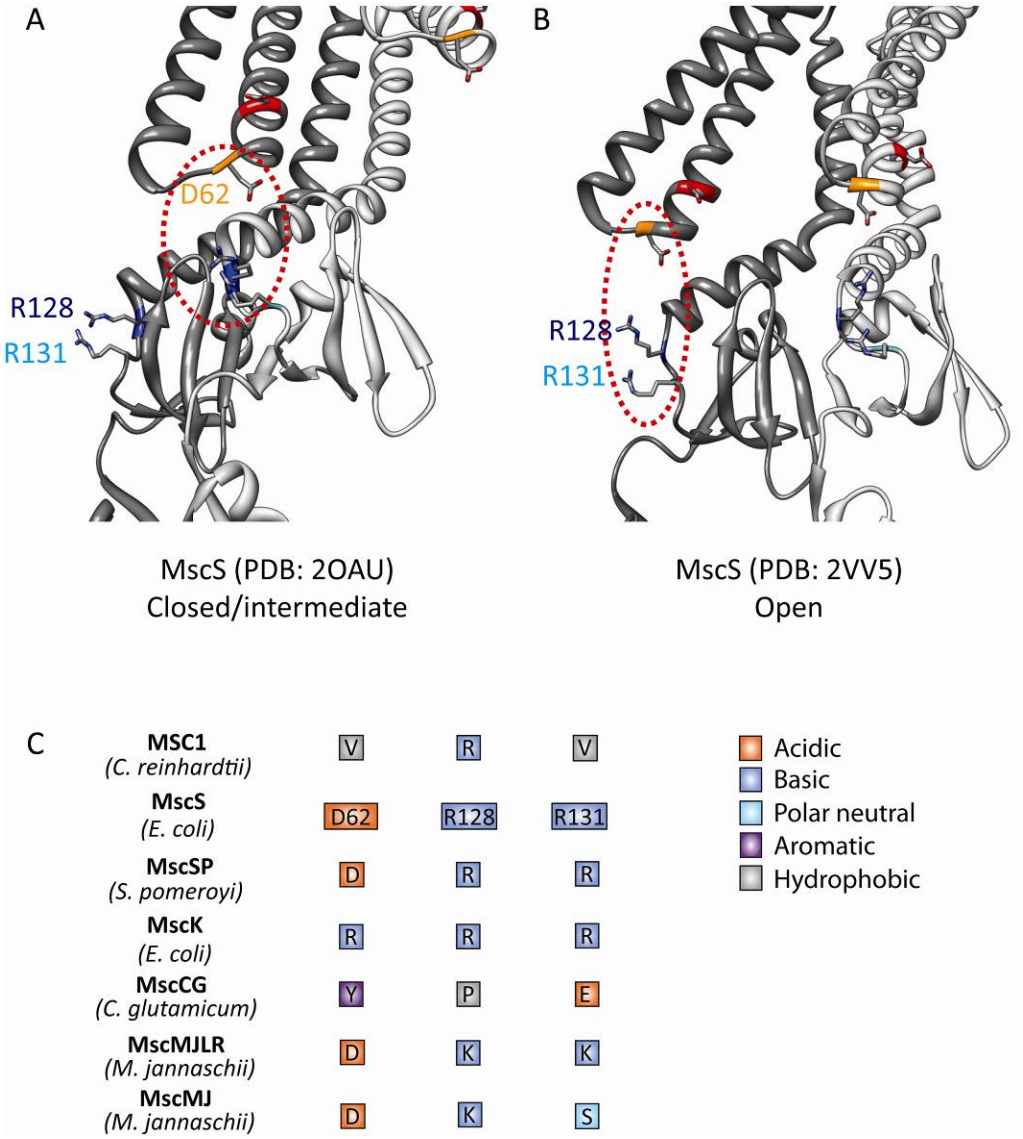

Figure 5.10 Interaction between TM1-TM2 linker and the cytoplasmic domain. (A) MscS in the closed/intermediate state (PDB: 2OAU) shows close proximity of D62 (orange) from one monomer (dark grey) with R128 and R131 of another monomer (light grey). This interaction may stabilise the closed/intermediate sate. (B) In the MscS open state (PDB: 2VV5) D62 of one monomer (dark grey) comes within close proximity of R128 and R131 within the same monomer. This interaction may be necessary for gating as mutations in these areas increase pressure threshold for activation (Nomura *et al.*, 2008). (C) Illustration of the alignment of D62, R128 and R131 of MscS with the six electrophysiologically characterised homologues discussed in this chapter.

This may signify an important interaction firstly in gating where the electrostatic interaction helps coordinate movement between the TM regions and the cytoplasmic domain. It may also mean that the electrostatic interaction also stabilises the closed state (Sotomayor and Schulten, 2004). The former is more likely to be important as reversal of charge at these sites increases the threshold for activation i.e. impairs gating (Nomura *et al.*, 2008). This all fits with other data suggesting that the cytoplasmic domain swells or expands during MscS gating (Machiyama *et al.*, 2009). This assumption does not mean that this interaction is not involved in inactivation, because Nomura *et al.,* 2008 definitively show that mutations in these residues (especially R131) do affect inactivation. It merely serves to suggest that its role in gating is just as important and may well be conserved throughout other closely related MscS homologues.

5.3.5 Vestibular portals of MscS

On initial inspection of the lateral vestibular portals of MscS there are very few distinguishing features. The seven cytoplasmic portals are vaguely hour-glass shaped and are around ~13 Å in diameter. They are surrounded by positively charged (i.e. R184,R185,R238), negatively charged (i.e. E220), polar (i.e. S234) and apolar (i.e. A158, W251) residues. Coulombic charge maps of the region generated using Chimera UCSF v1.6 (standard histidine protonation pH 7.4) illustrate this with few electronegative or positive regions near the portals (Figure 5.11A). However looking from inside the vestibule a strong

area of electronegativity centred on E227 and E187 is clearly visible. While E187 is within close proximity to the portal (6 - 8 Å) E227 is much more distal (> 12Å). The region of electronegativity they produce does represent a potential area in which cations could bind. This would 'screen' off the negative charge in turn giving rise to a mildly more thermodynamically favourable route for anions. This potential binding of cations is indirectly supported by Gamini *et al.,* 2011. The molecular dynamic simulations shown in this paper demonstrate that K^+ ions spend longer inside the vestibule than the negatively charged glutamate ions. In contrast to inactivation about which much has been mentioned in this chapter (Akitake *et al.*, 2007, Belyy *et al.*, 2010, Kamaraju *et al.*, 2011) less is known about MscS selectivity. These regions could represent the basis of MscS selectivity. In addition if cations do bind in to these regions they may also facilitate the occlusion of vestibular portals which in chapter 4 was proposed to be the structural basis of MscS subconducting states.

If this were the mechanism for MscS selectivity then we would expect larger cations to produce higher anion-cation permeability ratios. This is supported by the data presented in chapter 3. Figure 5.12 summarises the data presented in chapter 3 and illustrates how this selectivity mechanism may work. These anion-cation permeability ratios could also be explained by ions wanting to permeate as neutral pairs such as in the glycine receptor something also eluded to in Gamini *et al.,* 2011 (Sugiharto *et al.*, 2008).

A

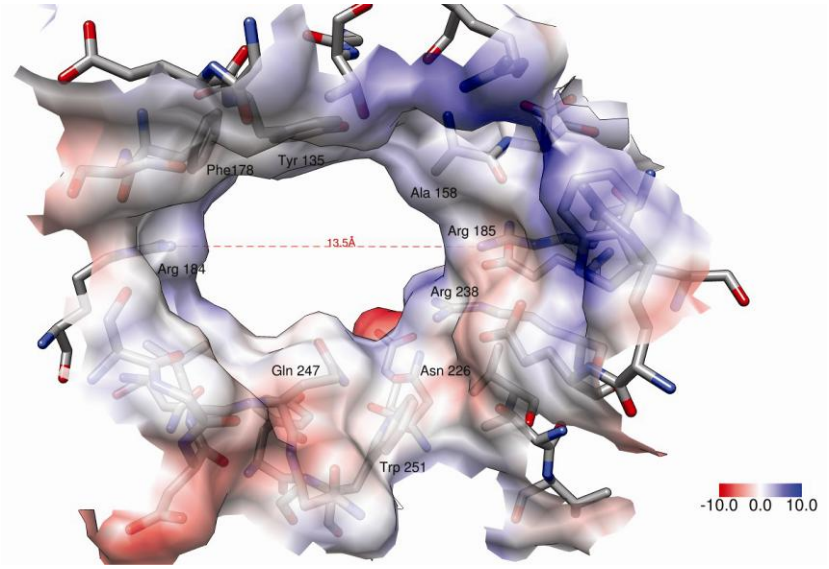

B

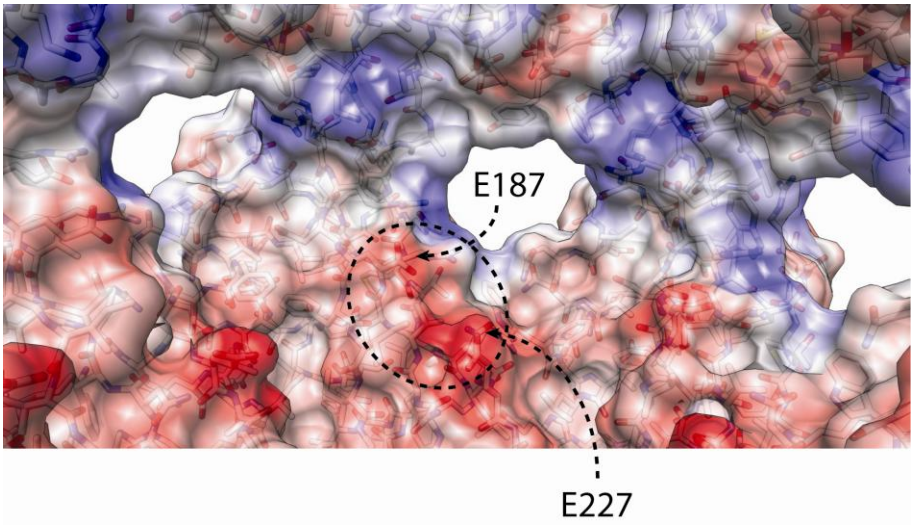

Figure 5.11 Coulombic charge map of MscS vestibular portals. (A) A Coulombic charge map of an MscS vestibular portal as viewed from the cytoplasm. (B) A Coulombic charge map of MscS vestibule as seen from inside showing a highly electronegative region centred around E187 and E227. This may also be influenced by E220. Red colouration signifies electronegativity while blue signifies electropositivity.

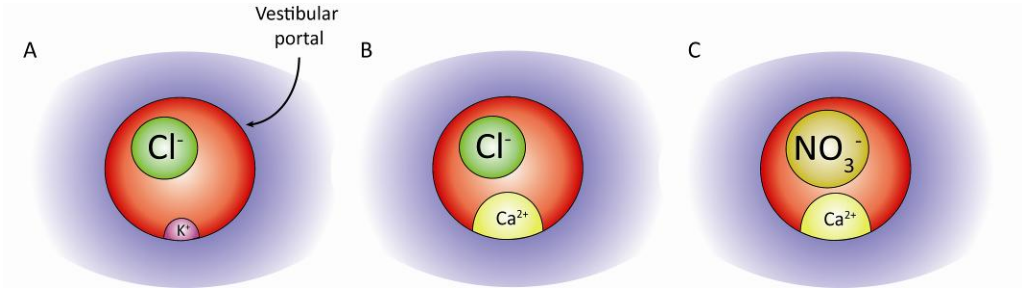

Figure 5.12 Illustration of proposed mechanism of MscS selectivity as viewed from the cytoplasm. (A) K^+ bound near the portal increases the anion selectivity. (B) In the presence of larger cations the anion selectivity increases. (C) In the presence of larger anions the anion-cation permeability increases even further. This scheme is supported by the experimental data set out in chapter 3 ($P_{Cl}/P_K < P_{Cl}/P_{Ca} < P_{NO3}/P_{Ca}$).

In order to further explore the hypothesis that these residues may be involved in processes such as selectivity, or subconducting states alignment of the portal residues was looked at with respect to six other electrophysiologically characterised MscS homologues. There are no detailed reports of subconducting states in these channels but their selectivity is known.

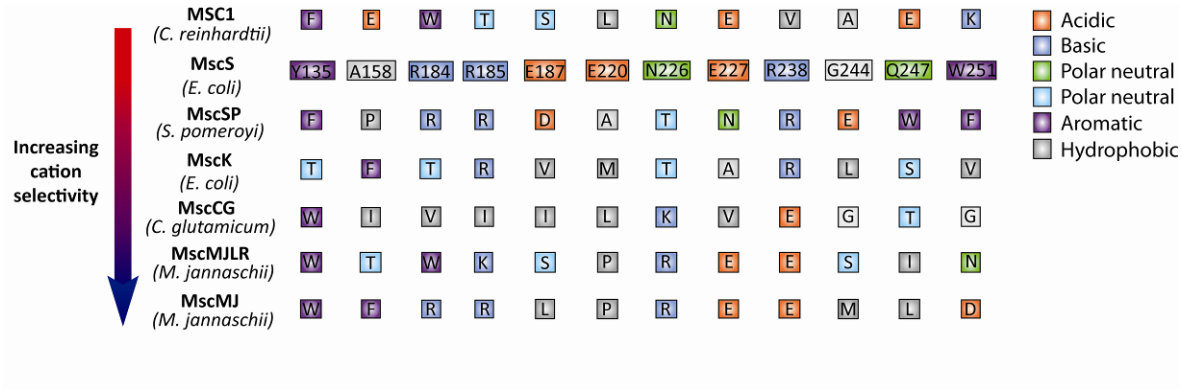

Figure 5.13 Sequence alignment of residues forming MscS vestibular portals with six electrophysiologically characterised homologues. Although E187 and E227 do not form part of the portal they are added for comparison because of the highly electronegative region they create within the vestibule proximal to the portals in MscS.

If we look at the anion selective homologues we can see that in MscSP, which exhibits lower anion selectivity than MscS, there is conservation of an acidic

residue at position 187, but not at position 227. MSC1 which conversely displays much higher anion selectivity does have a conserved glutamic acid residue at an equivalent position to E227 but lacks an acidic residue at 187. MSC1 does however instead have a glutamic acid residue in place of Q247 which in MscS forms part of the lower portion of the vestibular portals (Figure 5.10). Inspection of the most cation selective channels MscMJLR and MscMJ reveals that both have an acidic residue aligned with E227 which seems not to sit well with this hypothesis. They do have an acidic residue at the equivalent position to R238 which faces directly into the portal in MscS. In fact all the cation selective channels shown (MscCG, MscMJLR & MscMJ) have this acidic residue aligned with R238, and all anion selective channels (MscS, MscSP & MscK) with the exception of MSC1 have a positively charged arginine at this position. Obviously whether the six electrophysiologically characterised channels in this chapter display vestibular portals, or how many they possess is not known. However if the homology models described in Figure 5.8 are placed side by side, an example is shown in Figure 5.14A, then lateral vestibular portals begin to appear akin to those seen in MscS. This may well be an artifact introduced by the alignment procedure and the very basic homology model created by the SWISS-model. However the diameter of the portal in MscMJ is similar to that calculated by Kloda *et al.,* 2003 (~9 Å). This diameter is assumed to be the pore diameter but it could be the portal diameter, which acts as the bottle neck for ion permeation, even though there are multiple portals.

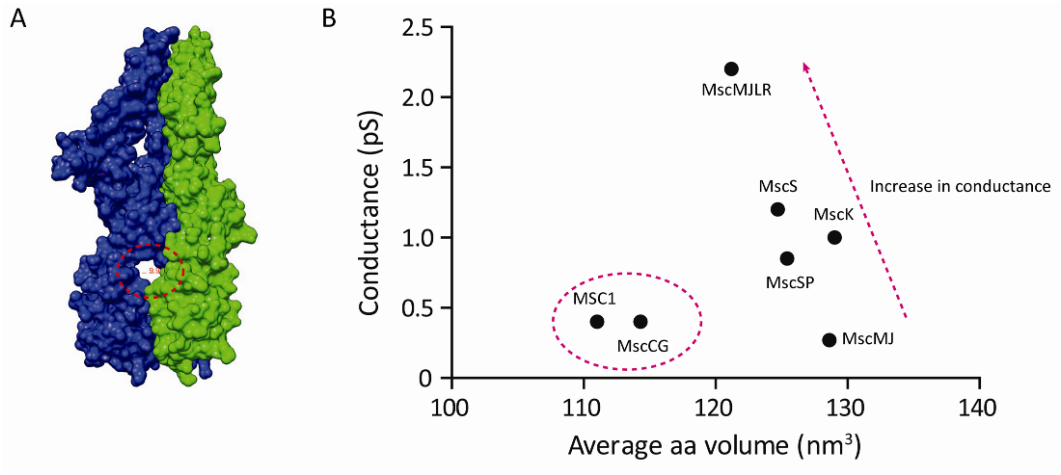

Figure 5.14 Vestibular portals in other MscS-like channels. (A) Space-fill homology model of two MscMJ monomers side by side (based on PDB: 2VV5). The dashed circle illustrates a ~9 Å perforation that looks very reminiscent of the vestibular portals seen in MscS. (B) Plot illustrating how conductance changes with respect to average amino acid volume of 10 residues that form the vestibular portal in MscS. These residues are taken from the alignment shown in Figure 5.12 (not including E187 or E227 as they don't form part of the portal).

This homology model alignment was not carried out for each channel however a test was carried out to see whether the average volume of 10 residues (shown in Figure 5.13) that form the portals in MscS has any correlation with conductance in the MscS homologues, the assumption being that the lower the volume of these residues, the larger the portal, and thus the higher the conductance. The results of this analysis are shown in Figure 5.14. There is a correlation between the most sequence similar homologues (MscS MscK MscSP MscMJ and MscMJLR). For these channels, as the average volume increases, the conductance decreases. The other two channels do not fit this correlation. This may mean that these two less similar homologues do not have vestibular portals similar to that seen in MscS.

5.3.6 Site directed mutagenesis

In order to see if these electronegative regions based around E187 and E227 are involved in selectivity, and also the basis for vestibular portal occlusion, site directed mutagenesis was used. Although E220 is within close proximity to the vestibular portals, there is no conservation of this residue in the other anion selective MscS-like proteins studied. As a result the decision was made to mutate E187 and replace it with oppositely charged arginine, and to mutate E227 and replace it for an alanine, to mimic the alignment seen with the very weakly anion selective MscK. Thus the two mutants created were E187R and E227A. These were created using the primers set out in the methods section of this chapter. The sequencing data from these plasmids are shown in Figure 5.15. After successful sequencing the amount of protein in each sample was calculated using the BCA method as described in chapter 2 materials and methods. Furthermore, to check the monomeric size of the product an SDS-page gel was run of the samples obtained (Figure 5.15). The size of the band is ~29 KDa which is in agreement with previously reported data, despite running slightly lower than the expected 31 KDa (Malcolm *et al.*, 2011, Sukharev, 2002).

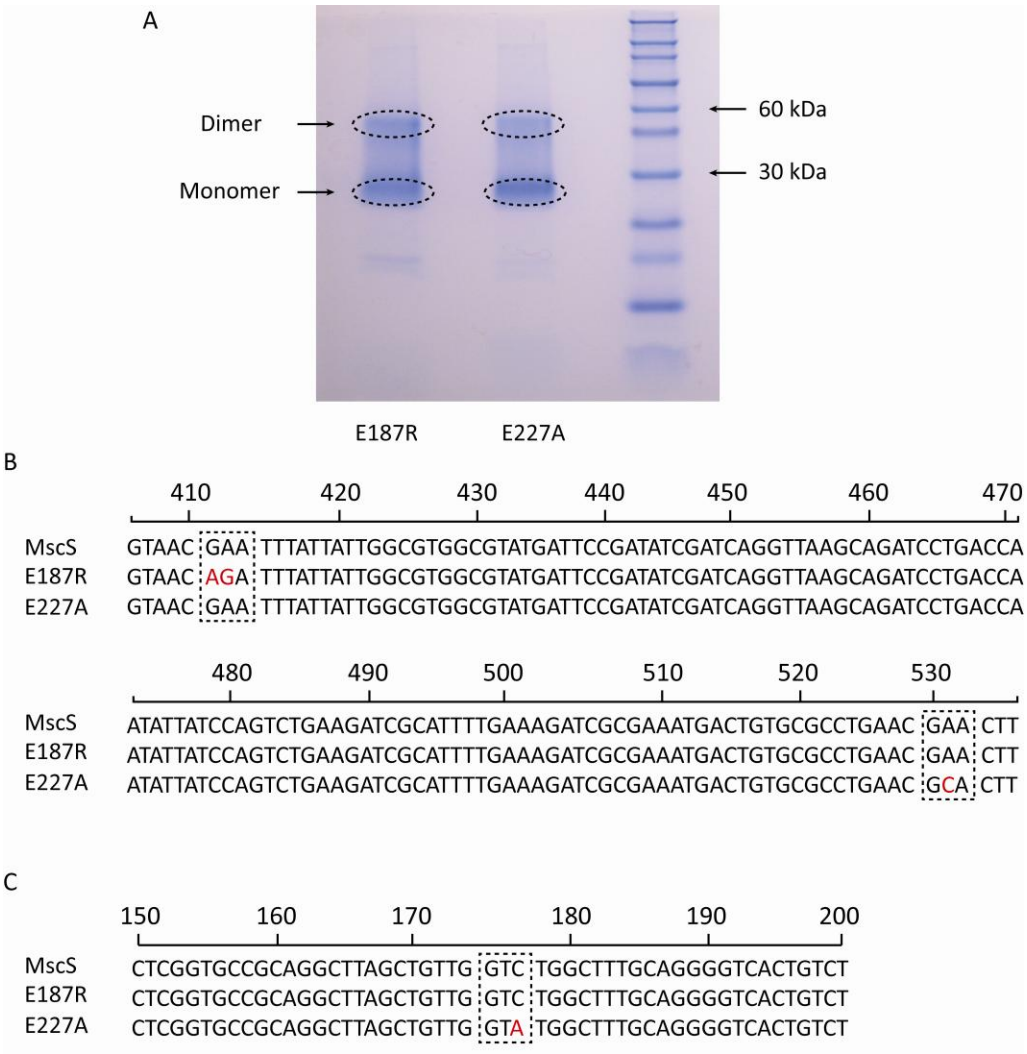

Figure 5.15 Confirming identities of MscS mutants. (A) SDS-page gel of MscS mutants E187R and E227A. Bands are clear at just below 30 kDa and 60 kDa which match the band size for an MscS monomer and dimer. The presence of the dimer is likely explained by excessive sample loading. (B) Sequencing data from plasmids used to express MscS mutants E187R and E227A. The boxed nucleotides match the specific residues being mutated (GAA – Glu, AGA – Arg, GCA – Ala). (C) There is a silent mutation in the E227A mutant plasmid shown in the dashed box (GTC – Val, GTA – Val).

5.3.7 E187R and E227A MscS mutants

The two MscS mutants created did not exhibit any difference in pressure threshold of activation in $BaCl_2$ [WT-MscS: 128.7 ± 20.5 mmHg (n = 4), E187R: 137.9 ± 36.3 mmHg (n = 3) and E227A: 104.7 ± 45.9 mmHg (n = 3)]. These mutants also showed no differences in subconducting behaviour [WT-MscS (n = 4), E187R (n = 3) and E227A (n = 3)]. Multiple long-lived substates were visible at +70 mV pipette potential in symmetrical 100 mM $BaCl_2$ (Figure 5.16).

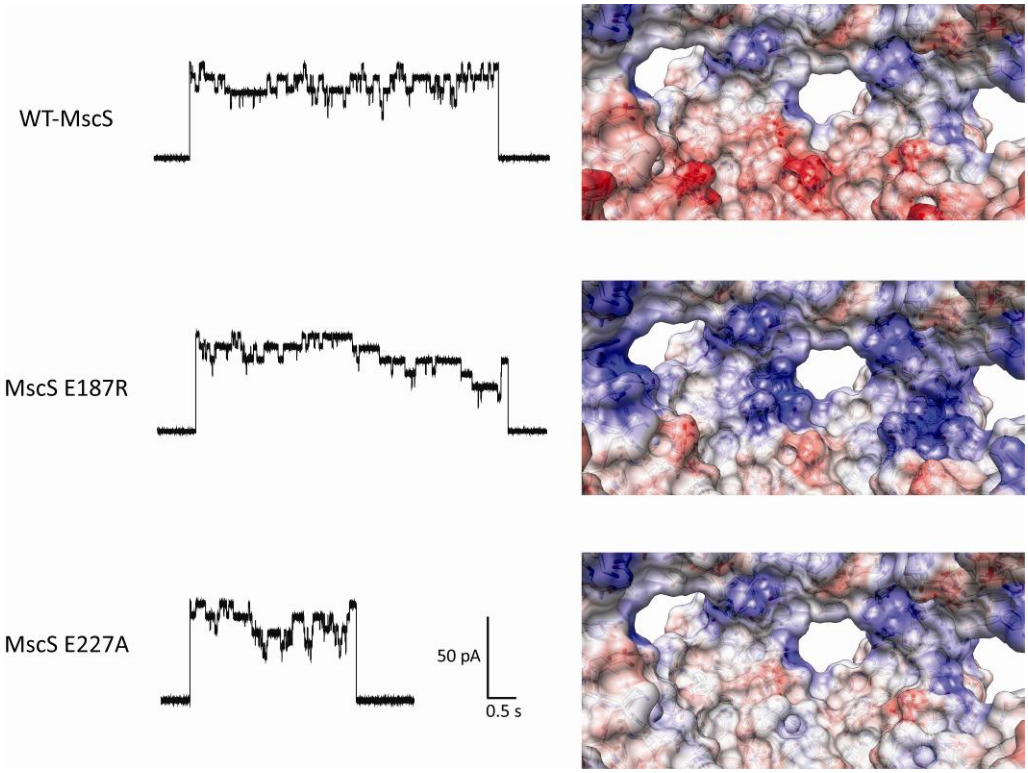

Figure 5.16 Comparison of the activity of wildtype MscS and mutant channels. Left hand panel shows raw records of activity in the presence of symmetrical 100 mM $BaCl_2$, pH 7.4. The right hand panel shows the corresponding Coulombic charge map of the inside of the vestibular portal.

However differences in anion-cation permeability were seen for both mutants (Figure 5.17). Current-voltage relationships for the mutants (E187R and E227A) in asymmetric $BaCl_2$ are not shown due to the large asymmetric $BaCl_2$

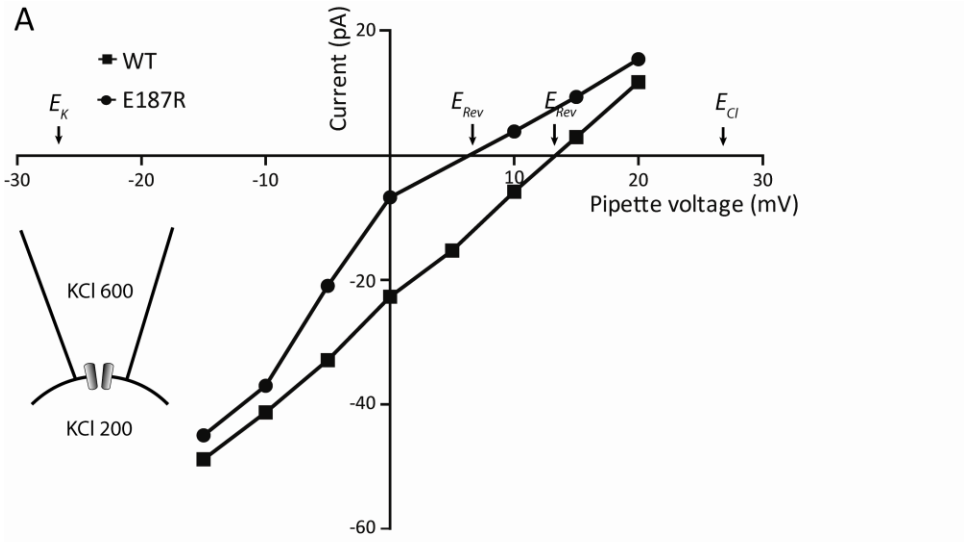

B

	E_{Rev} pipette (mV)	P_{Cl}/P_K	E_{Rev} pipette (mV)	P_{Cl}/P_{Ba}
WT-MscS	+11.82 ±1.07	2.7	+ 16.08 ±0.87	3.9
E187R	+ 5.69 ±0.77	1.5*	+ 5.18 ±0.75	1.3*
E227A	+ 8.5 ±0.34	2.0*	+ 7.97 ±0.57	1.7*

*signifies statistical significance from WT-MscS ($p<0.05$)

Figure 5.17 Selectivity of MscS and two MscS mutants E187R and E227A. (A) Representative current voltage plots of WT-MscS and E187R with ionic composition as shown in the left inset. The equilibrium potentials of K and Cl are marked on the graph as the corresponding pipette potential along with the reversal potential. (B) Anion-cation permeability ratios of WT-MscS, E187R and E227A as determined by the reversal potential in asymmetric KCl (left hand side) (600 mM pipette / 200 mM bath) and asymmetric $BaCl_2$ (right hand side) (200 mM pipette / 50 mM bath). The table illustrates the reversal potential as the corresponding pipette potential.

are not shown due to the large correction for LJP's as discussed in chapter 3. In WT-MscS the reversal potential in $BaCl_2$ moves further towards the reversal potential for Cl^- than in KCl (see also chapter 3). This means that the P_{Cl}/P_{Ba} is

larger than the P_{Cl}/P_K meaning that in WT-MscS more K^+ ions move than Ba^{2+} ions compared to Cl^- ions in the respective experimental conditions. When the reversal potentials for both E187R and E227A were measured in asymmetrical KCl they moved less towards the reversal potential for Cl- (Figure 5.17). Thus these mutant channels exhibit weaker anion selectivity than WT-MscS (Figure 5.17). The P_{Cl}/P_K values are still above one, so there is still some anion selectivity but it is significantly lower. In addition, the P_{Cl}/P_K values are higher for both E187R and E227A than the corresponding P_{Cl}/P_{Ba} values. This pattern is the opposite of that seen for WT-MscS. However due to the SD of the reversal potentials measured, there is no statistical significance between the calculated P_{Cl}/P_K and P_{Cl}/P_{Ba} values for E187R or E227A.

5.4 Discussion

This chapter examined six electrophysiologically characterised homologues of MscS. The sequence alignment data set out in this chapter provides a hint about the structural basis of certain biophysical characteristics such as selectivity. Without the aid of x-ray crystallographic data from all the channels studied it is hard to make any concrete conclusions. However due to the similarity in function and sequence of these homologues, these speculations can give useful insight and are a useful place to start.

As has been previously reported the TM3 pore-lining helix of MscS is mainly hydrophobic, a characteristic shared by the other six homologues investigated. The MscS TM3 helix possesses numerous alanine-glycine pairs which are purported to be involved in gating, aiding the tight packing of the

TM3 helices (Edwards *et al.,* 2005). These pairs are moderately conserved and may well be a universal feature of MscS-like channels.

The leucine at position 109 in MscS which is involved in forming a hydrophobic lock preventing ion permeation is also well conserved. The leucine at position 105 is less well conserved. This suggests that the formation of a 'vapour lock' may well be a characteristic of MscS-like channels. The larger channels such as MscK and also the product of the gene *ybiO* (*E. coli*) have phenylalanines in this position.

Interestingly G113 which has been reported as the centre of inactivation is not well conserved in this cohort of MscS-like channels. Only MscSP shows conservation of this residue. In addition to this MscSP does not exhibit inactivation (Petrov *et al.,* unpublished). From this the suggestion can be made that other interactions are also important for inactivation in these channels not just a 'kink' in the TM3 helix. One of these interactions is between the TM3 helix and the roof of the cytoplasmic domain. In MscS this is mediated via N117 which binds to the peptide backbone around G168. This interaction facilitates kinking at G113 and introduction of charged residues at any of these sites prevents inactivation (Koprowski *et al.,* 2011). In MscSP there is an aspartate residue instead of N117, and it is this potential lack of interaction between the TM3 helix and cytoplasmic domain that may prevent MscSP from inactivating. This TM3-cytoplasmic domain interaction was absent in every channel examined that does not inactivate. In the case of MscMJ and

MscMJLR which also do not inactivate N117 is replaced with a smaller serine residue. From this, and mutagenesis using the crystal structure of MscS the suggestion can be made that this residue is too small to make this necessary interaction even though it is capable of forming hydrogen bonds.

One interaction which is conserved in 4/7 of the channels is an electrostatic interaction between the charged TM linker and the cytoplasmic domain. This reaction is likely to be important in gating. Nomura *et al.,* 2008 show that it is important in determining the kinetics of inactivation in MscS but its presence in other channels that do not inactivate suggests a more integral role in channel gating. Many previous reports suggest that the cytoplasmic domain swells on opening and this electrostatic interaction or 'salt-bridge' could be a conserved mechanism in MscS-like channels that allows cross-talk between the tension sensing TM helices and the cytoplasmic domain. This is only conserved in channels with the most sequence similarity (MscS, MscSP, MscMJ and MscMJLR). Although in MscK and MSC1 there are numerous residues that do not align exactly with D62 and R128/131 which could take on this role. However this interaction doesn't seem to present in MscCG and taking into account its unique structure it would not be a surprise if its gating mechanism were completely different from the other channels mentioned.

Alignment failed to identify any kind of distinguishing feature in the TM3 region which could underpin the selectivity of these channels, which is supported by the fact that mutations in this region do not affect the

selectivity of MscS (Edwards *et al.*, 2008). Thus as has been suggested for MscS previously, the selectivity must lie in the cytoplasmic domain (Sukharev, 2002; Gamini *et al.,* 2011). The large cytoplasmic domain is a feature shared by members of the MscS family and the six electrophysiologically characterised homologues in this chapter are no different. Whether each of the six channels investigated possess seven lateral portals in their cytoplasmic domain is unknown. But due to the sequence similarity and similar function of the channels it seems more than likely that they may possess similar perforations, with the number dependent on their multimeric structure. This chapter has endeavoured to provide some evidence to support this by using crude alignment of an homology model of MscMJ. When two monomers are aligned side by side a perforation of similar characteristics to that in MscS is seen of around 9 Å in diameter. This interestingly matches perfectly the pore diameter which Kloda & Martinac (2001) calculated for this channel. While this is not definitive evidence, and could be coincidental, it does provide some support for this assumption.

A highly electronegative region was identified inside the MscS cytoplasmic domain centred on E187 and E227. The hypothesis was thus formed that cationic interactions with this electronegative area gives rise to the anion selectivity exhibited by MscS. Mutation of these residues gave rise to two mutants (E187R and E227A) with reduced anion selectivity. This means that, at least in part, these residues account for anion selectivity displayed by MscS. Mutation of these residues however did not affect substates. From this the

suggestion can be made that although ion binding may occur here (for selectivity purposes), due to the regions distal nature to the portal, binding is not sufficient to cause portal occlusion. This leads to the assumption that there is another site for binding more proximal to the portals that facilitates ion binding and results in occlusion or that as suggested by Gamini *et al.,* 2011, occlusion is 'unlikely' and thus cannot account for the substates seen.

5.4 Conclusions and future work

In summary the results in this chapter point towards a significant functional role of the cytoplasmic domain not only in MscS but also in other MscS-like channels. This chapter in particular documents the first single residue mutants of MscS that display altered selectivity and puts forward a novel explanation, as opposed to the entropic filtering ability of the cytoplasmic domain (Gamini *et al.,* 2011), for how this selectivity is brought about. The data within this chapter also raise a number of interesting questions;

- E187R and E227A mutants do not display altered substate behaviour. Are there other sites which may bind ions allowing vestibular portal occlusion or are these substates brought about by another mechanism for example as set out in Akitake *et al.,* 2005.
- Is there a role for the electrostatic interaction between the cytoplasmic domain and TM-linker in the gating of other MscS-like channels i.e. MscMJ? This could be investigated using site directed mutagenesis of MscMJ, MscSP and MscMJLR all of which have residues which could mirror this interaction.

- Is the equivalent position of R238 in MscS an important residue for selectivity in MscS-like channels? Due to the correlation between charge at this site and the selectivity of the channels studied in this chapter, this position may represent an interesting target for future investigations.
- Do E187R and/or E227A mutations have any effect on physiological function of the channel? This could be tested using the hypoosmotic shock assay described in the third chapter.
- Are both G113 and a TM3 cytoplasmic domain interaction important for inactivation in MscS-like channels? This could be tested using the very close MscS relative MscSP. If this hypothesis were correct, we would expect to see a mutant of MscSP where we introduce an asparagine at the equivalent position to N117 (which in MscSP is an aspartate residue) in MscS to display inactivation.

Chapter 6: MS channels in defence against lysis subsequent to cell wall attack

6 MS channels in defence against lysis subsequent to cell wall attack

6.1 Introduction

The previous chapters have centred on structural and biophysical questions mainly relating to MscS. In this chapter the focus is more towards the physiological role of MS channels. Bacterial MS channels play an important role in osmoprotection as outlined in the general introduction. However, their diversity in *E. coli* suggests they may in fact possess alternative physiological functions that go beyond osmoprotection. In this chapter the possibility that MS channel expression provides a selective advantage in the presence of agents that weaken the cell wall is explored.

As discussed in the general introduction the mesh work of peptidoglycan in the cell wall maintains cellular morphology and protects the inner membrane from lysis due to the intracellular turgor pressure. Weakening of the cell wall by antibiotics (i.e. β-lactams) or enzymes (i.e. lysozyme) causes an increase in membrane tension in the inner membrane due to internal turgor pressure and can result in cellular lysis. The aim of this chapter is to investigate the hypothesis that MS channels gate in response to this increase in inner membrane tension and work to reduce this pressure by releasing internal osmolytes and thus working to reduce the potential for cellular lysis. If this hypothesis were correct then MS channel expression would provide a selective advantage in situations of cell wall attack or stress. Thus the expectation would be that MS channel knockout strains of bacteria such as *E.*

coli would show increased susceptibility to cell wall inhibiting antibiotics and enzymes such as lysozyme.

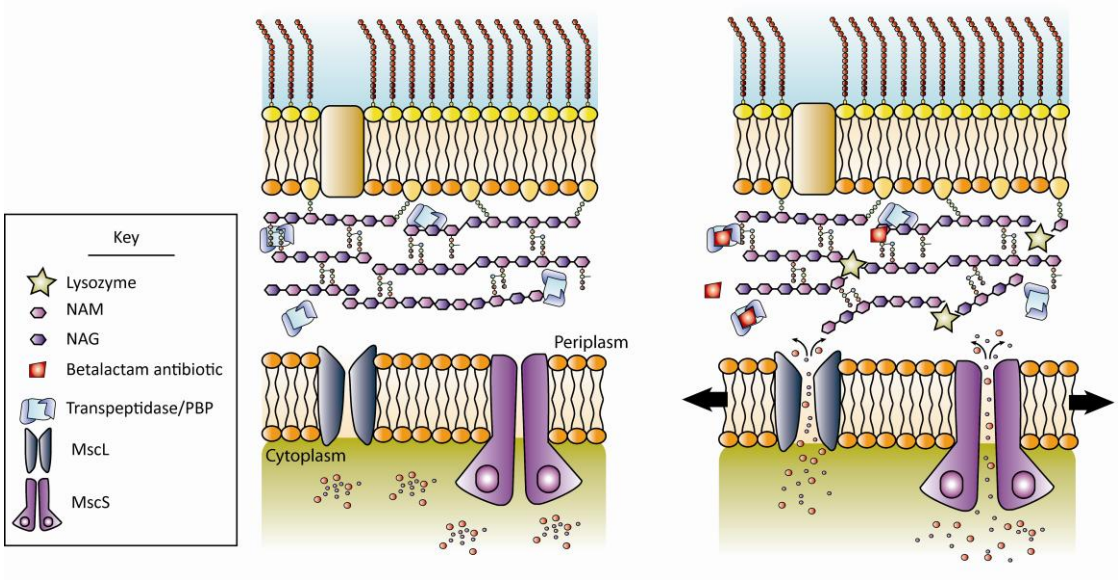

Figure 6.1 Graphic representation of the hypothesis being tested in this chapter. Antibiotics and enzymes can weaken the cell wall of bacteria. This reduction in cell wall integrity can potentially lead to lysis as a result of normal cellular turgor pressure. This chapter aims to look at whether MS channels can work to combat this lysis by relieving pressure through osmolyte efflux.

6.1.2 β-lactam antibiotics

β-lactam antibiotics are widely used clinically to treat numerous infections including tonsillitis, endocarditis and cellulitis. They have a broad spectrum of activity and are safe in pregnancy. The β-lactam antibiotic group is comprised of a large number of structurally related compounds all of which possess a β-lactam ring at the heart of their structure. However, since their advent more than 60 years ago we still do not have an exact idea of their precise mechanism of action. β-lactam antibiotics are known to inhibit cell wall synthesis by impeding peptidoglycan cross-linking in the cell wall. As discussed earlier peptidoglycan is a complex interlocking network of cross-

linked glycan chains composed of alternating NAM and NAG residues (Vollmer *et al.,* 2008). The cross-linking occurs at points on the NAM residues where short peptides are attached usually comprised of three to five amino acids. The cross-linking of glycan chains occurs though transpeptidation catalysed by transpeptidases, also known as PBPs (Macheboeuf *et al.,* 2006).

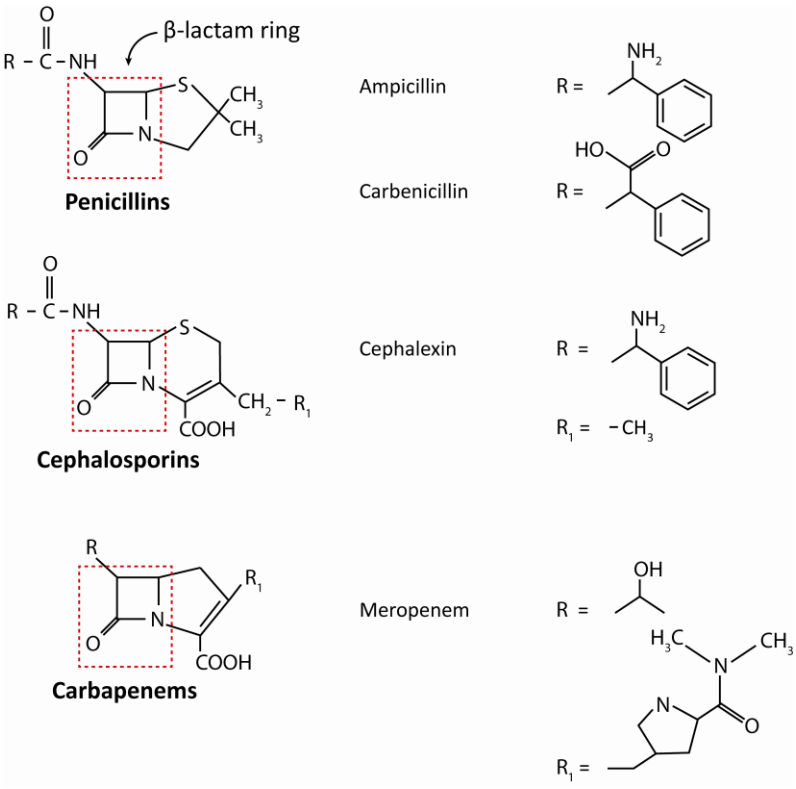

Figure 6.2 Examples of the structures of β-lactam antibiotics. Ampicillin, carbenicillin and cephalexin are used in this chapter to test the hypothesis.

This cross-linking provides the structural rigidity required by the cell wall. β-lactam antibiotics inhibit this transpeptidase activity reducing the structural integrity of the cell wall resulting in cell death. Although the exact events that follow PBP inhibition are less well understood we do however know that PBP

inhibition may result in lytic or non-lytic forms of cell death (Kohanski *et al.,* 2010).

The suggestion that β-lactam antibiotics activate MS channels is supported by the fact that penicillin treatment of *Corynebacterium glutamicum* results in the jettison of osmotically active solutes in particular glutamate. This means that penicillin treatment weakens the cell wall increases the tension in the inner membrane created through normal cellular turgor resulting in MS channel activation. In the case of *Corynebacterium glutamicum* this results in the activation of MscCG (*See chapter 5*)(Nakamaru *et al.,* 2007, Borngen *et al.,* 2010).

6.1.3 Lysozyme

Lysozyme is a glycoside hydrolase which catalyses the breakdown of glycosidic bonds between alternating NAM and NAG residues in peptidoglycan chains resulting in a much weakened cell wall and subsequent cell lysis (Ellison and Giehl, 1991, Davies and Henrissat, 1995, Masschalck and Michiels, 2003). Broadly speaking most Gram-positive bacteria are susceptible to lysozyme whereas Gram-negative bacteria are not. The reason for this is the outer membrane of Gram-negative bacteria such as *E.coli* (Beveridge, 1999, Delcour, 2009, Typas *et al.,* 2010). The negatively charged lipopolysaccharide chains of the outer membrane are cross-linked via divalent cations such as Ca^{2+} and Mg^{2+}. It is this barrier that prevents the movement of compounds such as lysozyme into the periplasmic space. In order to increase

outer membrane permeability making Gram-negative bacteria susceptible to Lysozyme, the Ca^{2+} and Mg^{2+} chelator EDTA is required.

The idea that MS channel opening may represent an advantage in the presence of lysozyme is strengthened by work done at high hydrostatic pressure. At high hydrostatic pressures MS channels favour the closed state (Mcdonald and Martinac, 2005, Petrov *et al.,* 2011). In addition, at high hydrostatic pressures Gram-negative bacteria such as *E. coli* become more susceptible to lysozyme (Masschalck and Michiels, 2003). The fact that at high hydrostatic pressures MS channels are forced into the closed state is not likely to be the only mechanism here but does fit with the central hypothesis of this chapter.

6.1.4 MS channel activators as antimicrobials

While MS channel activation can be beneficial in periods of hypoosmotic downshock or potentially during periods of cell wall stress, MS channel gating comes at a high metabolic price. If we consider the large open pore diameters and the large conductances only small open times are required in order to lose large amounts of important intracellular solutes. As a result, excessive MS channel activation can be toxic as discussed in the general introduction (Section 1.3.9). This chapter aims to see whether MS channel knockout strains show different sensitivity compared with WT strains to two amphipathic compounds, CPZ and benzalkonium chloride (BAC), with antimicrobial activity (Amaral and Lorian, 1991, McDonnell and Russell, 1999, Moen *et al.,* 2012, Sheridan *et al.,* 2012). CPZ is known to activate MS channels (Martinac *et al.,*

1990, Kubalski *et al.,* 1993) probably through changes in bilayer curvature (Dymond *et al.,* 2008). This has also been reported for other channels such as the large conductance Ca^{2+}-activated K channel (BK) channel (Qi *et al.,* 2005) and transient receptor potential channel ankyrin 1 (TRPA1)(Hill and Schaefer, 2007). In comparison to date there is no evidence of any association between BAC and bacterial MS channels. It is conceivable that both of these compounds, at least in part, bring about their antibacterial activity by activation of MS channels *in vivo*. So in addition to testing whether MS channel activation is protective in periods of cell wall stress this chapter aims to test whether excessive activation induced by BAC and or CPZ account for their toxic bacterial effects.

6.1.5 Chapter aims

This main aim of this chapter is to investigate whether knocking out MS channels results in altered *E .coli* susceptibility to widely used antibacterial agents that target the bacterial cell wall. This will involve monitoring growth of MS channel knockout strains in the presence of β-lactam type antibiotics (carbenicillin, ampicillin and cephalexin) and lysozyme and the determination of the minimum inhibitory concentration (MIC) of betalactam antibiotics against MS channel knockout strains (MJF465) and wild type (FRAG-1) *E. coli* strains. In addition, this chapter aims to investigate whether the antibacterial effects of two amphipathic compounds, CPZ and BAC, are affected by MS channel expression.

The specific aims of this chapter are as follows:

(i) investigate the rate of growth of MS channel knockouts in comparison WT *E. coli.*

(ii) investigate whether MS channel knockout strains have different sensitivity to penicillins (ampicillin, carbenicillin) than WT strains.

(iii) investigate whether MS channel knockout strains have different sensitivity to cephalosporins (cephalexin) than WT strains.

(iv) investigate whether MS channel knockout strains have different sensitivity to lysozyme than WT strains.

(v) investigate whether MS channel knockout strains have different sensitivity to benzalkonium chloride and chlorpromazine.

6.2 Methods

6.2.1 Bacterial strains

In any growth experiments using single knockouts of *E. coli* from the Keio collection the WT parent strain BW25113 was used as the control. In any growth experiment using multiple knockouts of MS channels, i.e. MJF465 (MscL, MscS and MscK) and MJF453 (MscL and MscK), the WT *E. coli* parent strain FRAG-1 was used as the control. For full genotypic details *see chapter 2 materials and methods*.

6.2.2 Bacterial growth

E. coli strains were grown in M9 minimal media (in $g.L^{-1}$: 2 Na_2HPO_4, 1 KH_2PO_4, 1 NH_4Cl, 0.2 NaCl) supplemented with 0.1 % glucose pH 7.2 at 37 °C. Bacterial growth was monitored using a microtitre plate reader as set out in chapter 2 materials and methods. Growth was monitored over periods from 4 – 10 hours with absorbance readings at 590 nm being taken every 15 minutes.

6.2.3 MIC evaluation

The MIC of ampicillin (0.15 – 256 $\mu g.ml^{-1}$) was determined against WT FRAG-1 *E. coli* and MJF465 ($MscL^-$, $MscS^-$ & $MscK^-$) strains using MIC evaluator strips (Oxoid). The Oxoid MIC evaluator strips were used as set out in the manufacturers protocol. Firstly single *E. coli* colonies were inoculated into 10 ml of LB media and grown at 200 rpm and 37 °C overnight. Subsequently 1 ml of overnight culture was added to 10 ml of fresh LB media and each strain was grown to an OD of exactly 0.3. 5 µl of this culture was diluted with 195 µl of LB media then spread over an LB agar plate. An Oxoid MIC evaluator test

strip was then placed onto the agar plate with the weakest antibiotic containing end of the strip placed down first. The bacteria were then grown for 16 hours and the MIC measured against values on the strip.

6.2.4 Electrophysiology

The electrophysiology set up was as described in chapter 2 materials and methods. The effect of BAC was tested on azolectin liposomes containing MscS alone and co-reconstituted MscS and MscL at protein lipid ratios of 1:10000. MscL and MscS full-length sequences housed in pQE60-LacI vectors with 6x-His tags were expressed and purified as set out in chapter 2. The electrophysiological recordings were carried out in symmetrical solutions containing in mM: 200 KCl, 40 $MgCl_2$ 5 HEPES, pH 7.4; KOH. Microelectrodes had typical resistances of between 3 – 5 MΩ in these recording solutions and all experiments were carried out at +30 mV pipette potential.

6.2.5 Statistical analysis

Statistical analysis was carried out using Graphpad prism 5. One-way ANOVA was used to determine statistical significance between growth of *E. coli* strains at individual points in time. Depending on the number of groups either Bonferonis or Tukeys post hoc tests were used to determine significant differences between specific strains. Statistical significance was assumed at p-values < 0.05.

6.3 Results

6.3.1 WT *E. coli* BW25113 in the presence of ampicillin

Growth of *E. coli* in the presence of ampicillin only became affected from concentrations of ampicillin at and above 1 μg.ml^{-1}. At concentrations of 10 μg.ml^{-1} and 100 μg.ml^{-1} there was no growth after six hours (Figure 6.3). As a result concentrations of 1 μg.ml^{-1} and 3 μg.ml^{-1} were used to compare growth of WT and single MS channel knockout Keio clones (Figure 6.3).

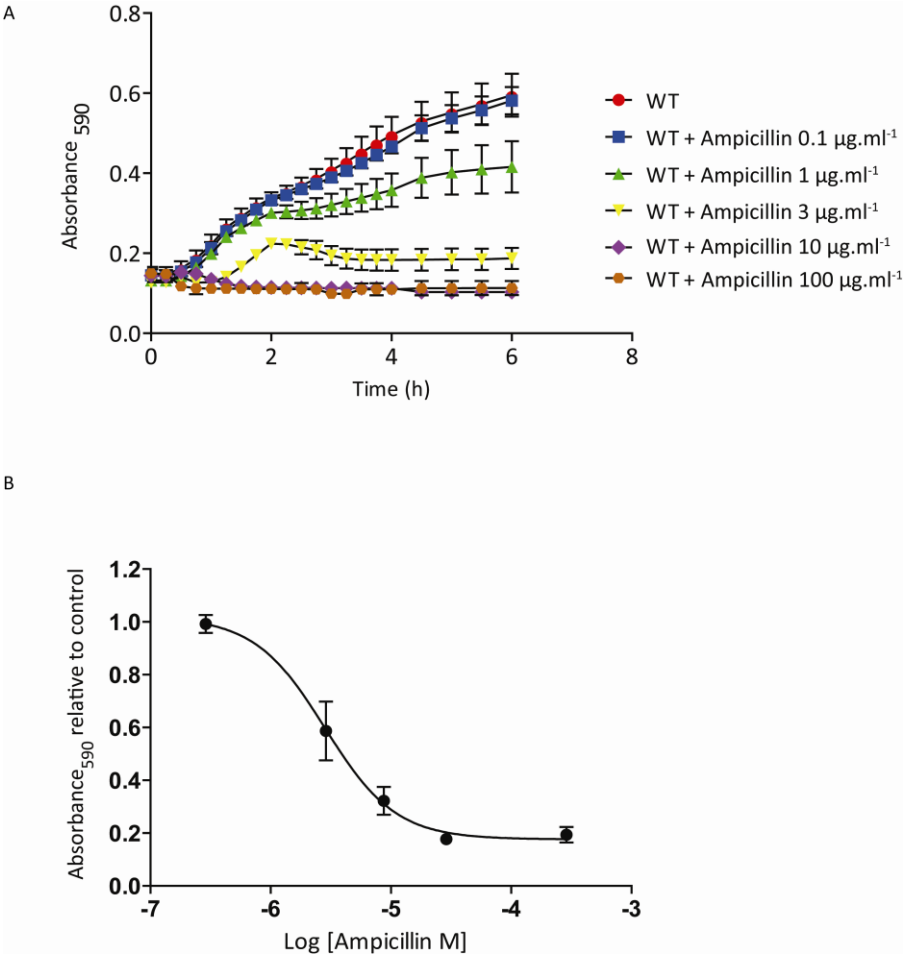

Figure 6.3 Effect of ampicillin on WT *E. coli*. (A) Absorbance of *E. coli* samples grown in the presence of ampicillin at concentrations from 0.1 – 100 μg.ml^{-1}. (n = 3) (B) Dose response curve of ampicillin on WT BW25113 *E. coli* growth. The response is plotted as the absorbance relative to control at the 6 hour point. Error bars represent ± SEM n =3.

6.3.2 Growth of single MS channel knockouts

The growth of three Keio clones containing single MS channel knockouts ($MscL^-$, $MscS^-$ and $MscK^-$) were compared to the wild type BW25113 strain. There was very little difference seen between growth rates in single MS channel knockouts as illustrated in Figure 6.4. The generation times were calculated for each mutant and ranged between 117 and 125 minutes which is in agreement with previously calculated *E. coli* generation times in minimal media (Bernstein *et al.,* 2002). On slowing of growth and entry into stationary phase at around 6 hours after initial growth there was a trend towards MscS mutants growing slower although this difference was not statistically significant.

6.3.3 Growth of single MS channel knockouts in ampicillin

In the presence of 1 and 3 $\mu g.ml^{-1}$ a single knockout of MscS showed reduced absorbance at 4 hours. This reduction in absorbance was statistically significant. In the presence of 1 $\mu g.ml^{-1}$ absorbance at 4 hours for the WT strain was 0.253 ± 0.003 (n = 3) whereas the single MscS knockout strain absorbance was 0.190 ± 0.006 (n = 3). The same effect was seen in the presence of 3 $\mu g.ml^{-1}$ of ampicillin where WT absorbance was 0.092 ± 0.003 (n = 3) and the single MscS knockout strain absorbance was 0.038 ± 0.002 (n = 3)(Figure 6.5).

A

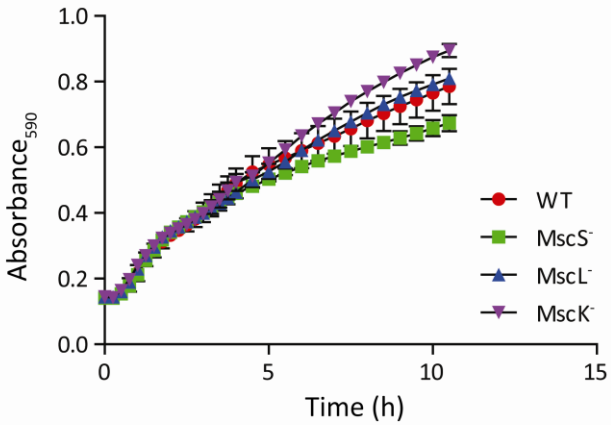

B

Strain	Generation time (m)
WT BW25113	117 ± 13 (n = 3)
MscL-	112 ± 10 (n = 3)
MscS-	118 ± 13 (n = 3)
MscK-	125 ± 16 (n = 3)

Figure 6.4 Growth of single MS channel knockouts (MscL$^-$, MscS$^-$ and MscK$^-$) in comparison to WT BW25113 strain. (A) Growth of WT *E. coli* BW25113 in comparison to single MS channel knockouts. There is a trend towards MscS to grow slower than WT. Error bars represent ± SD n =3. (B) The generation time of each strain was calculated using the equations set out in *chapter 2 materials and methods*. The generation time is represented in minutes ± SD.

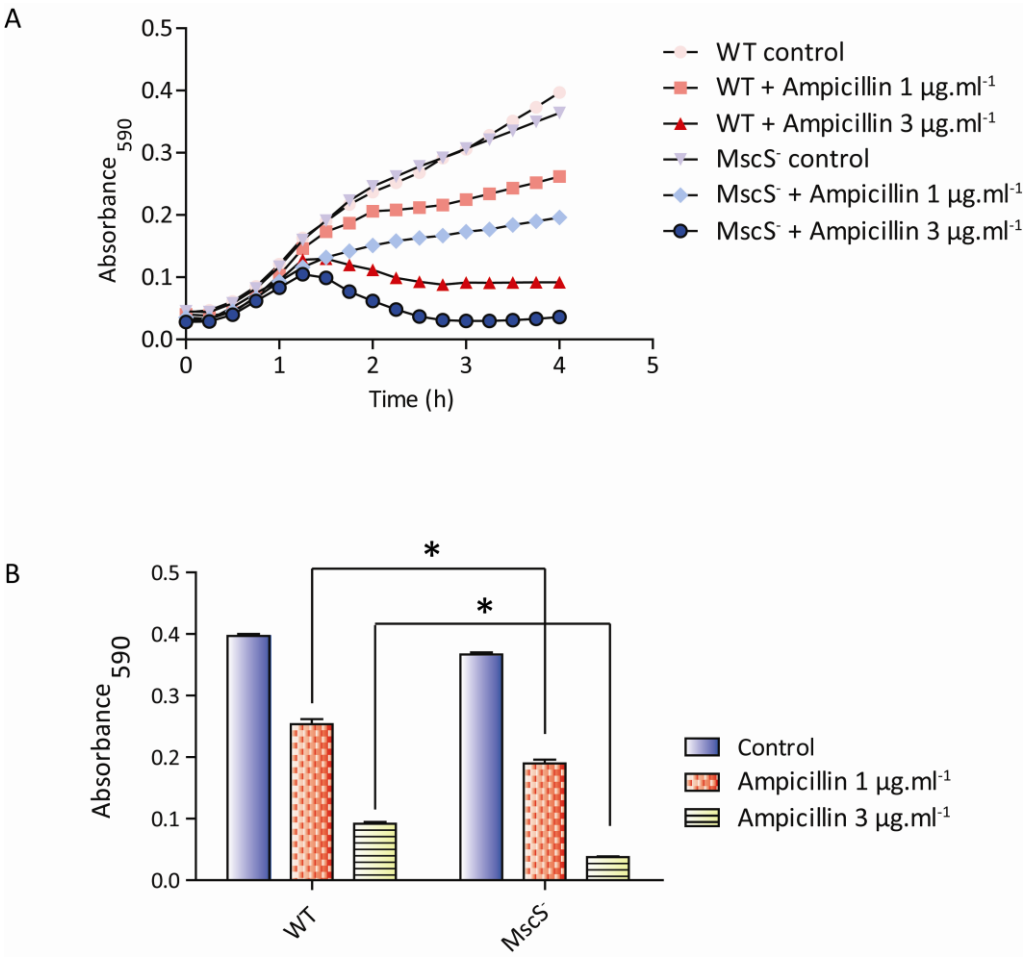

Figure 6.5 The effect of ampicillin on WT BW25113 *E. coli* and a single MscS knockout strain. (A) Growth over a six hour period of WT and knockout strain ($MscS^-$) in the absence and presence of ampicillin 1 and 3 $\mu g.ml^{-1}$ (n = 3). (B) Comparison of absorbance after four hours (n = 3). *represents statistical significance p-value < 0.05 as determined by one-way ANOVA and Tukey's post hoc test. Error bars represent ± SEM.

Interestingly the difference in absorbance between the single MscS knockout and the WT BW25113 *E. coli* strain was not mirrored in the single MscL or MscK knockouts. In these single knockouts the absorbance after 4 hours was not statistically different from that of the WT (Figure 6.6).

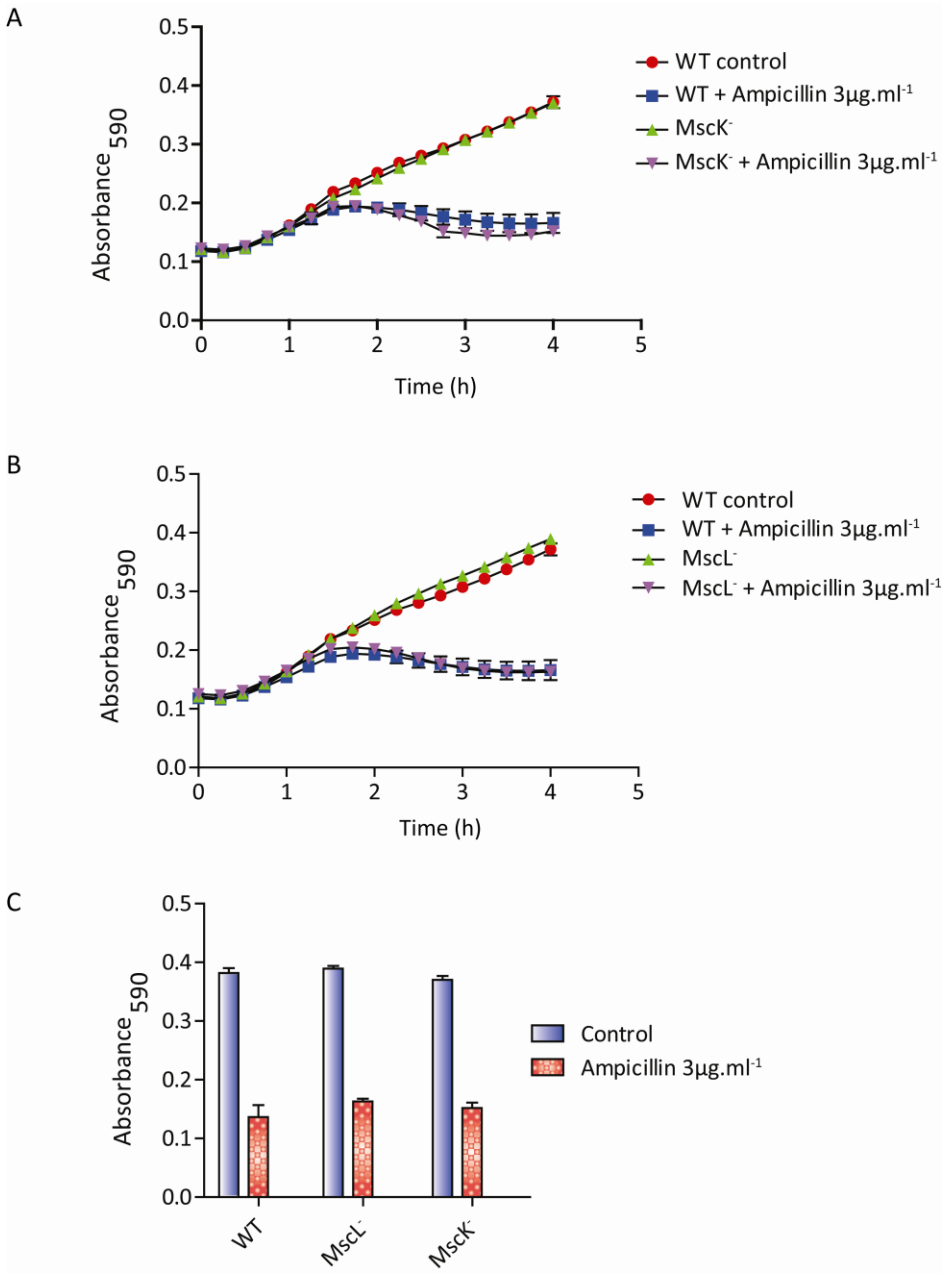

Figure 6.6 The effect of ampicillin on WT *E. coli* and single MscL and MscK knockout strains. (A) Growth of WT *E. coli* BW25113 compared with a single MscK knockout over four hours in the absence and presence of ampicillin 3 µg.ml^{-1}. (B) Growth of WT *E. coli* compared with a single MscL knockout over four hours in the absence and presence of ampicillin 3 µg.ml^{-1}. (C) Comparison of absorbance after four hours of WT *E. coli* compared with a single MscK and MscL knockout over four hours. All data in Figure 6.6 is from the same experiment (n = 6). Error bars represent ± SEM (n = 3).

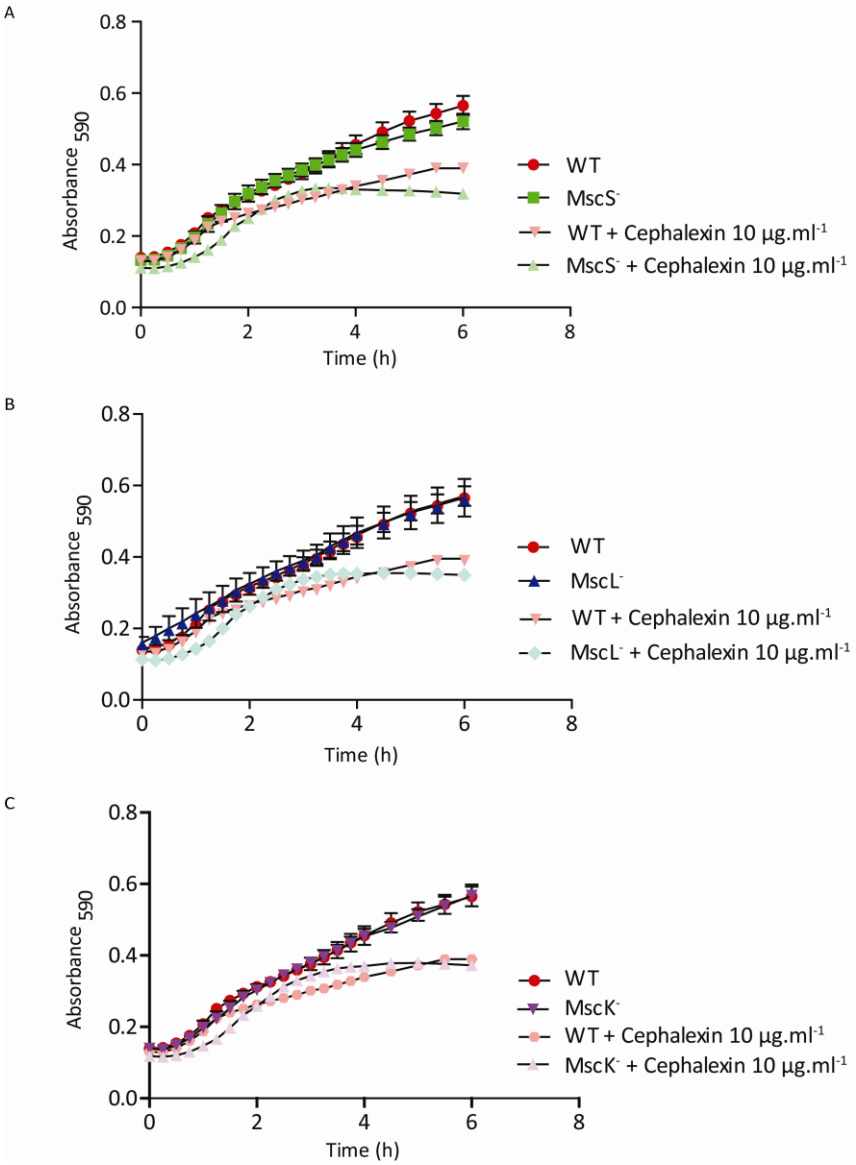

Figure 6.7 The effect of cephalexin on WT *E. coli* and single MscL, MscS and MscK knockout strains. (A) Growth of WT *E. coli* BW25113 compared with a single MscS knockout over six hours in the absence and presence of cephalexin 10 µg.ml^{-1}(n = 6). (B) Growth of WT *E. coli* compared with a single MscL knockout over six hours in the absence and presence of cephalexin 10 µg.ml^{-1}(n = 6). (C) Growth of WT *E. coli* compared with a single MscK knockout over six hours in the absence and presence of cephalexin 10 µg.ml^{-1}(n = 6). Error bars represent ± SEM.

6.3.4 Growth of single MS channel knockouts in cephalexin

In addition to ampicillin the same effect is seen with cephalexin (10 μg.ml^{-1})(Figure 6.7). In the presence of cephalexin the single MscS channel knockout has a lower absorbance after six hours of treatment. This difference at the six hour point is only statistically significant for the MscS knockout and not the MscL or MscK knockout [WT: 0.401 ± 0.008 (n = 3), MscS KO: 0.318 ± 0.005 (n = 3)].

6.3.5 Growth of multiple MS channel knockouts in carbenicillin

In order to further probe this effect of MscS expression on the sensitivity of β-lactam antibiotics the double knockout strain MJF453 (MscL^{-}, MscK^{-}) and triple knockout strain MJF465 (MscL^{-}, MscS^{-} and MscK^{-}) were used. Firstly an interesting point to note is that FRAG-1 strains seemed to grow faster than BW25113 strains in exactly the same growth media with the generation time of WT FRAG-1 being 92 ± 7 minutes as compared to 117 ± 17 minutes for the WT BW251123 strain. The absorbance of MJF465 at the six hour point was significantly lower than that of WT FRAG-1 *E. coli* cells in the presence of another β-lactam antibiotic carbenicillin (6 μg.ml^{-1}). The MJF453 strain (not devoid of MscS) shows similar susceptibility to carbenicillin compared with WT FRAG-1. In addition to this the calculated generation times suggest that while there is little to no difference in the generation times of these three strains (WT FRAG-1, MJF465 and MJF453) the addition of carbenicillin slows the generation by around ~10 minutes. Again the effects of carbenicillin like

cephalexin and ampicillin seem to coincide with the entry of these cells into stationary phase after 2-3 hours growth.

A

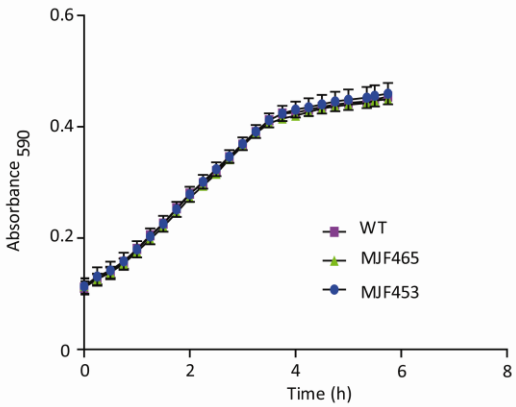

B

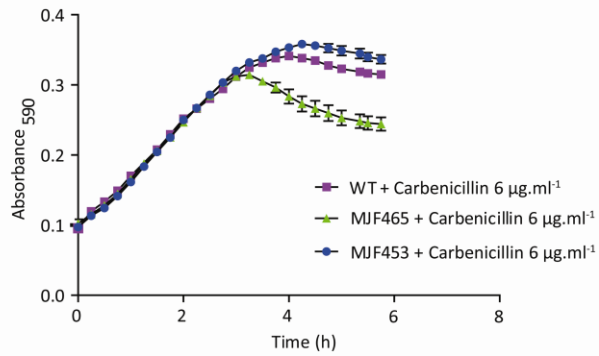

C

Strain	Generation time (min)	
	Control	Carbenicillin 6 µg.ml^{-1}
WT FRAG-1	92 ± 7 (n = 4)	107 ± 19 (n = 3)
MJF453	88 ± 9 (n = 4)	101 ± 13 (n = 3)
MJF465	90 ± 3 (n = 4)	106 ± 14 (n = 3)

Figure 6.8 The effect of carbenicillin on WT FRAG-1, MJF465 and MJF453 *E. coli* strains. (A) Comparison of growth of WT FRAG-1 *E. coli* cells and a double and triple MS channel knockout. (B) Comparison of growth of WT FRAG-1 *E. coli* cells and a double and triple MS channel knockout in the presence of carbenicillin 6 µg.ml^{-1} (C) Shows the generation time of these strains in M9 minimal media. Note that the generation times are quicker than the BW25113 strain. Error bars represent ± SEM (n =3).

In order to further determine whether these effects reported in this chapter are physiologically relevant the MIC concentration of ampicillin against WT FRAG-1 and MJF465 strains was investigated. Using the MIC evaluator strip method the MIC of ampicillin on WT FRAG-1 *E.coli* cells was determined as 8 $\mu g.ml^{-1}$ (Figure 6.9). The MIC for ampicillin against the MJF465 strain was lower on all plates (4 $\mu g.ml^{-1}$).

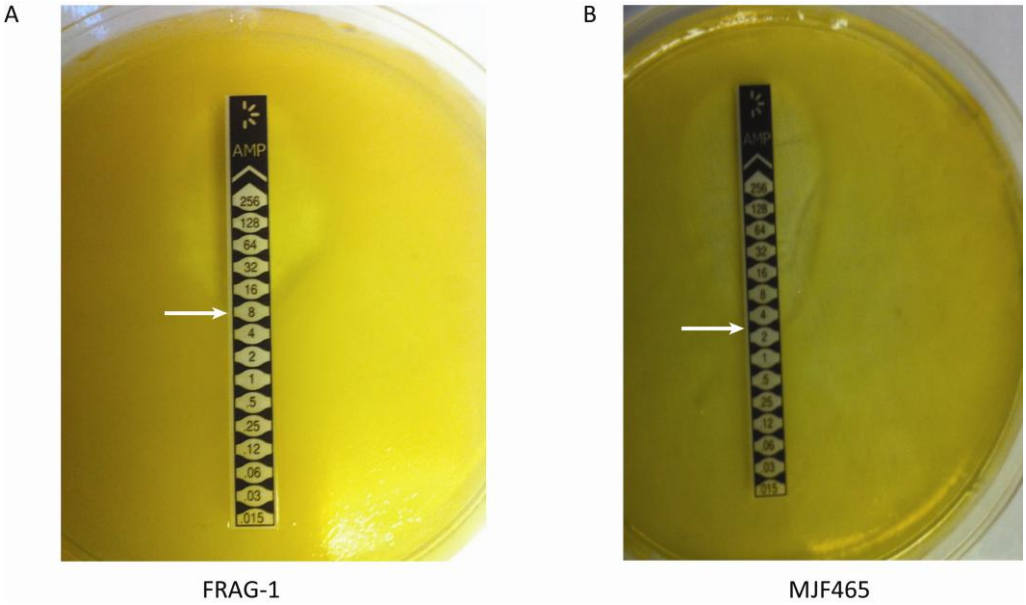

Figure 6.9 Determination of the minimum inhibitory concentration of ampicillin using an MIC evaluator strip (0.015 – 256 $\mu g.ml^{-1}$). This was calculated for FRAG-1 (8 $\mu g.ml^{-1}$;n = 3)(left hand panel shows representative plate) and MJF465 (4 $\mu g.ml^{-1}$;n = 2)(right hand panel shows representative plate).

6.3.6 Growth of multiple MS channel knockouts in lysozyme

In addition to β-lactam antibiotics as mentioned in the introduction, lysozyme can also affect the integrity of the bacterial cell wall. This concentration of Lysozyme (1.5 $mg.ml^{-1}$) was used as it has been previously estimated to be present in tears (Aine and Morsky, 1984). Although there is a mild antimicrobial effect of lysozyme and EDTA together on *E. coli* there is no

difference after six hours growth between the WT and triple knockout strain (Figure 6.10). In addition to this combination effect there does seem to be an effect of EDTA 1 mM alone. Both the WT strain and the single MscS knockout have a lower absorbance at the six hour point in the presence of EDTA compared with control [WT: 0.437 ± 0.010 (n = 4), WT + EDTA: 0.390 ± 0.002 (n = 4), MJF465: 0.432 ± 0.009 (n = 4), MJF465 + EDTA: 0.379 ± 0.011 (n = 4)]. One strange finding was an initial dip in absorbance in the lysozyme treated groups at around 35 minutes. This initial dip in absorbance is difficult to explain but happened reproducibly over three experiments

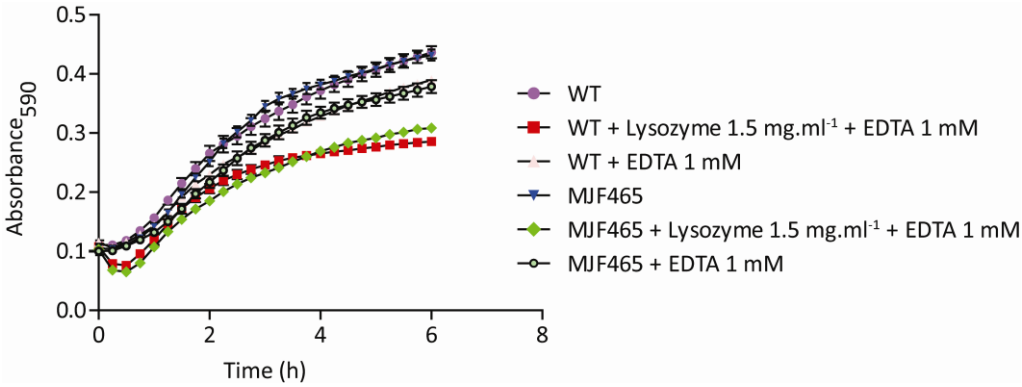

Figure 6.10 The effect of Lysozyme on WT *E. coli* and a triple knockout strain in the presence of EDTA. This graph shows the effect on WT FRAG-1 *E. coli* growth in the presence of Lysozyme 1.5 mg.ml^{-1} and EDTA 1 mM. Without EDTA Lysozyme has no effect on *E. coli* because it is a Gram-negative bacterium. Error bars represent ± SEM (n =3).

6.3.7 Growth of WT E. coli in the presence of carbenicillin and $GdCl_3$

In an attempt to gain further evidence for the involvement of MS channels in this increase in susceptibility, the effect of a known MS channel blocker Gd^{3+} was investigated in the presence of the β-lactam antibiotic carbenicillin. The question being does the addition of the MS channel blocker Gd^{3+} show similar effects to that of MS channel gene ablation? The addition of 300 µM $GdCl_3$ did

not affect the growth of WT FRAG-1 neither did it affect this strains susceptibility to carbenicillin (Figure 6.11).

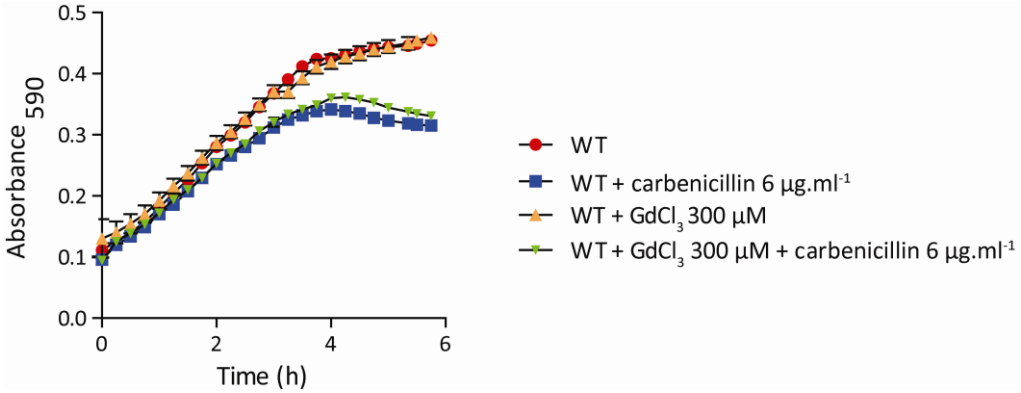

Figure 6.11 The effect of carbenicillin on WT *E. coli* FRAG-1 in the presence of the known bacterial MS channel blocker $GdCl_3$. The growth of FRAG-1 over six hours was compared in the presence of carbenicillin 6 $\mu g.ml^{-1}$ with and without 300 µM $GdCl_3$. Error bars represent means ± SEM (n =3).

Up to this point it has been shown that MscS channel knockouts fair slightly worse than their WT counterparts in the presence of a β-lactam antibiotic. This is not mirrored in the presence of the cell wall degrading enzyme lysozyme and can't be mimicked using the MS channel blocker Gd^{3+}. In the last section of this chapter the investigation switches to two amphipathic compounds, BAC and CPZ (Amaral and Lorian 1991).

6.3.8 Do CPZ and BAC target bacterial MS channels?

Both CPZ and BAC were tested on WT FRAG-1 *E. coli* and MJF465 knockout strains to determine whether these strains display differential sensitivity to these compounds. The hypothesis being that expression of MS channels in this case could be a disadvantage as these channels would open in response to the presence of BAC and CPZ (Martinac *et al.,* 1990, Dymond *et al.,* 2008)

which would result in an amelioration of growth. Firtsly the effect of CPZ was determined. Concentrations of 150 and 300 µM reduced bacterial growth whereas 50 µM had no effect on growth. No differences were identified between the WT FRAG-1 *E. coli* and MJF465 triple knockout at 50 µM and 150 µM CPZ. The growth of *E. coli* at these two concentrations was almost identical with values of absorbance at six hours which are not statistically significant. However at 300 µM CPZ there is a difference in growth of between the WT FRAG-1 strain and the MJF465 strain. This concentration seems to inhibit growth in both strains completely up until between 6 and 7 hours when the MJF465 strain began growing again. In all experiments the WT strain had not started growing by the end of the 10 hour period (Figure 6.12)[WT FRAG-1: 0.097 ± 0.009 (n = 3), MJF465: 0.165 ± 0.007 (n = 3)].

A similar effect was seen with the quaternary ammonium compound BAC. In the presence of both 10 and 15 $\mu g.ml^{-1}$ of BAC the MJF465 triple knockout strain had significantly higher absorbance at the 10 hour point in every experiment when compared to WT FRAG-1 *E. coli* cells (Figure 6.13C & D). In addition a similar effect to that seen with CPZ 300 µM was seen with BAC 15 $\mu g.ml^{-1}$. Up until between 7 and 8 hours neither strain grew at all then at this

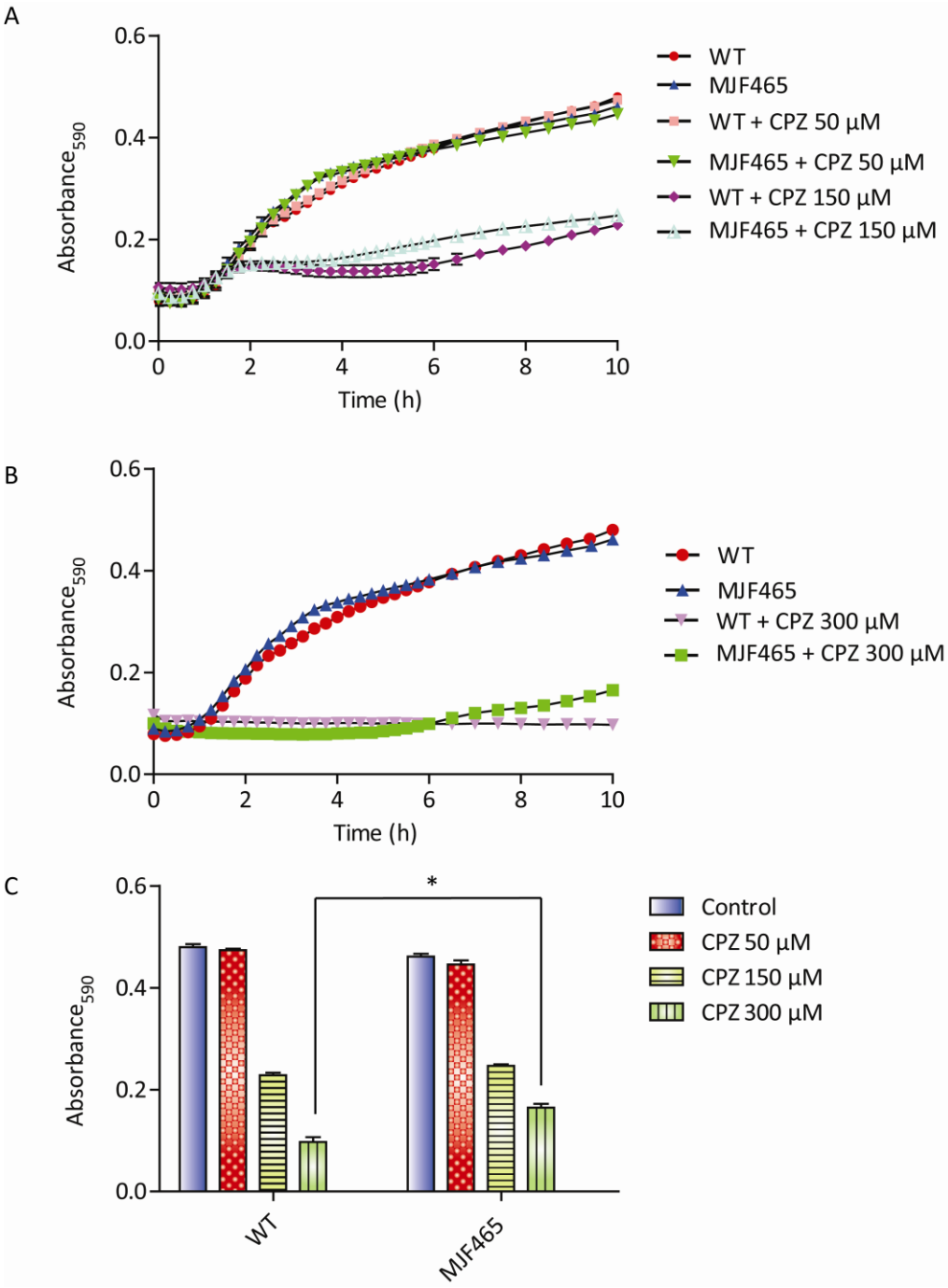

Figure 6.12 The effect of CPZ on the growth of WT FRAG-1 and MJF465 *E. coli* strains. (A) The effect of CPZ (50 and 150 µM) on the growth of WT FRAG-1 and MJF465 *E. coli* strains. (B) The effect of CPZ 300 µM (C) Histogram summarising the data shown in (A) and (B). Error bars represent ± SEM (n = 3). *denotes statistical significance as determined by one-way ANOVA with Tukey's post-hoc test ($p < 0.05$).

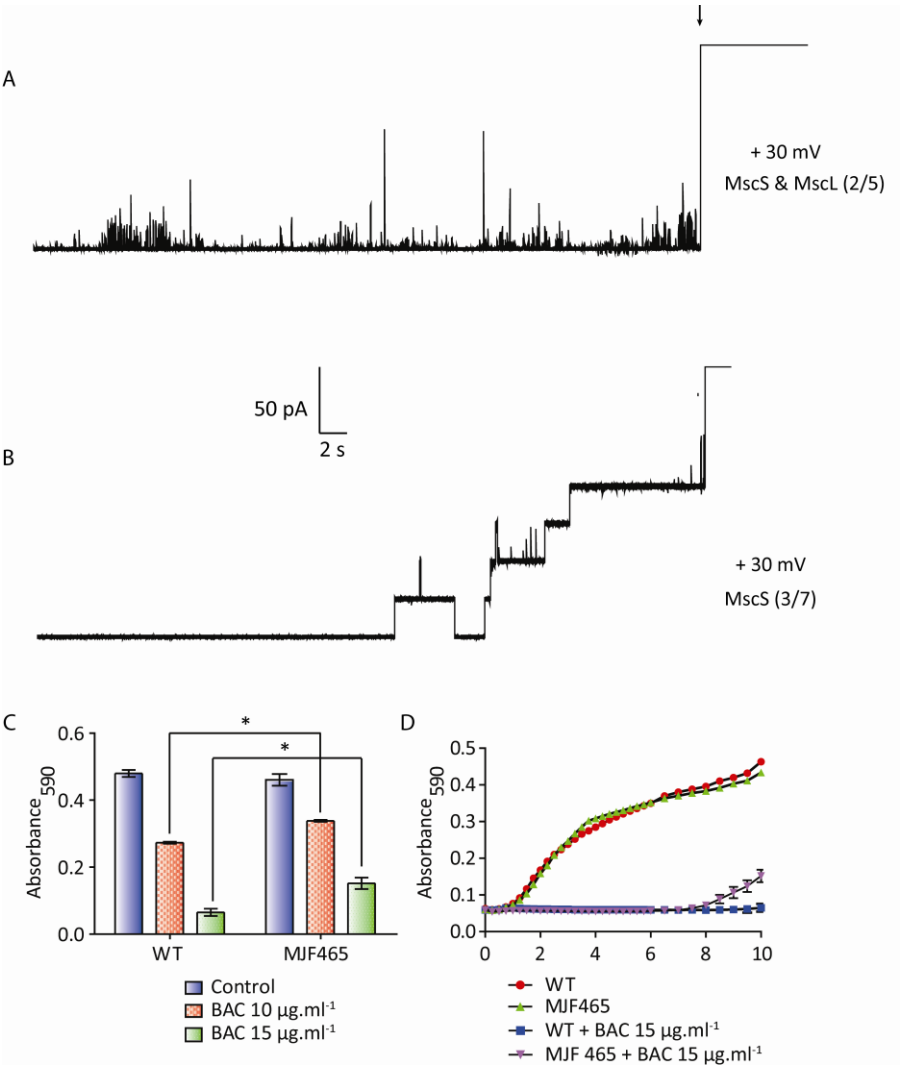

Figure 6.13 The effect of BAC on reconstituted MS channels and *E. coli* growth. (A) A raw record of an excised inside-out patch at + 30 mV pipette potential of an azolectin liposome containing co-reconstituted MscS and MscL at a protein:lipid ratio of 1:10000 6 minutes after addition of BAC 20 µg.ml^{-1}. This flickery behaviour prior to patch rupture (identified by the downward arrow) was identified in 2/5 patches. (B) is the same as (A) with liposomes only containing MscS. This record shows characteristic behaviour of MscS prior to patch rupture. Both records (A) and (B) are recorded in the absence of pressure application. (C) Histogram illustrating the absorbance after 10 hours of both WT FRAG-1 *E. coli* and MJF465 strains in the absence and presence of BAC (10 and 15 µg.ml^{-1}). (D) Illustration of a growth experiment following the growth of FRAG-1 and MJF465 strains in the presence of BAC 15 µg.ml^{-1}. No growth is seen up until 8 hours in the MJF465 strain when growth starts. By the 10 hour point there is still no measurable growth of the FRAG-1 strain.

point the MJF465 strain began to grow and at 10 hours the WT strain still had not grown at all. Furthermore experiments using liposomes containing MscS alone and co-reconstituted MscS and MscL show that BAC 20 $\mu g.ml^{-1}$ can, at least to a degree activate MS channels. In MscS liposomes alone activity similar to that seen in Figure 3.13B was identified in 3/7 patches prior to rupture. At this concentration of BAC rupture occurred in all seven patches and took between 6 and 13 minutes to occur. This is in contrast to control patches where without mechanical stimuli patches could be maintained for 30 – 40 minutes very easily. In MscS patches the activity seen was characteristic of MscS i.e. 30 pA amplitude openings at 30 mV pipette potential. These openings were only identified immediately prior to patch rupture (patch rupture point is indicate on Figure 6.13 by a downward arrow). In contrast no such characteristic openings were observed in liposome patches where MscL and MscS were re-constituted together. In 2/5 of these patches activity such as that shown in Figure 6.13A was identified. This flickery behaviour may be rapid openings of MscL and or MscS or just patch degradation. Unfortunately no 'empty' liposomes were patched in the presence of BAC for comparison.

6.4 Discussion

The principal physiological role of bacterial MS channels is in osmoprotection however this chapter endeavoured to investigate a potentially novel physiological role for this family of channels (Levina *et al.,* 1999). Growth experiments using single MS channel knockouts of MscL, MscS and MscK of *E. coli* grown in M9 minimal media showed no significant differences with generation times fitting with previously reported data (Bernstein *et al.,* 2002). Despite there being no difference in generation times there was a trend for the MscS knockout to have a lower absorbance after 10 hour growth periods. This affect seemed to coincide with entry into stationary phase after around 5 to 6 hours. This is interesting as this is the point at which MS channel expression will begin to rise in conjunction with RpoS levels (Stokes *et al.,* 2003).

This chapter demonstrates that single MscS channel knockouts show increased susceptibility to carbenicillin ampicillin and cephalexin. In addition, the MIC of ampicillin against the MJF465 strain (4 $\mu g.ml^{-1}$) was lower than that of the WT FRAG-1 strain. This MIC fits well with the growth experiments where 3 $\mu g.ml^{-1}$ causes almost total prevention of growth in the MJF465 strain. Furthermore neither single MscL or MscK knockouts showed any altered sensitivity to any of the β-lactam antibiotics. To further implicate MscS the growth of the MJF465 strain (triple KO) was investigated in carbenicillin compared with WT and a double knockout strain of MscL and MscK. The double knockout MJF453 strain showed almost identical sensitivity

to the WT FRAG-1 strain whereas the MJF465 strain had consistently lower absorbance after 6 hours of growth.

The difference in sensitivity of *E. coli* MscS knockouts to carbenicillin, ampicillin and cephalexin is only slight. However, this slight difference would be magnified under selection pressures such as the presence of low levels of cell wall inhibiting antibiotics. Thus the suggestion is that MscS expression provides a selective advantage to *E. coli* in the presence of cell wall inhibiting antibiotics.

The question then becomes why does MscS expression represent a selective advantage but not MscL or MscK? This may be due to relative abundance. There are numerous (>100) copies estimated per cell for MscS but very few are estimated for MscK (Stokes *et al.,* 2003). So while MscK may have a low enough pressure threshold to activate and prevent lysis, the prevalence of this channel is not high enough to change sensitivity to β-lactam antibiotics. MscL on the other hand is supposed to gate just below the lytic limit of the membrane (Sukharev *et al.,* 1999) and has high relative density (Bialecka-Fornal *et al.,* 2012). By the time it gates the cell wall may be so damaged that it cannot prevent lysis. So MscS may have the right pressure threshold and relative abundance to fulfil this role.

Despite these differences in antibiotic sensitivity, there was no difference in the sensitivity to lysozyme between WT FRAG-1 *E. coli* and MJF465 strains. The use of EDTA to make the outer membrane permeable and increase the

sensitivity to lysozyme was necessary in this experiment but caused a small retardation in growth itself. This is interesting as in chapter 3 of this thesis EGTA at a concentration of 5 mM caused no noticeable effect on growth. There was also no impact on the effect of carbenicillin by the MS channel blocker Gd^{3+} (Ermakov *et al.,* 2010). While the concentration of Gd^{3+} used in this chapter has been shown to block bacterial MS channels (100 -300 μM) *in vitro* (Hase *et al.,* 1995, Ermakov *et al.,* 2010) the concentration required to functionally block, MscL for example, *in vivo* is much higher (1 mM) (Ewis and Lu, 2005). It would be useful therefore to increase the concentration of Gd^{3+} and investigate whether this leads to an increase in susceptibility of *E. coli* to β-lactam antibiotics.

In addition to assessing the positive role MS channels can play in bacterial physiology this chapter also endeavoured to look at the negative roles they can play. This was attempted using the amphipathic antimicrobials BAC and CPZ. The effect of both compounds was investigated on bacterial growth and the effect of BAC was also looked at on MS channels reconstituted in azolectin liposomes.

Electrophysiological analysis suggests that BAC may in fact cause bacterial MS channel activation in liposome patches. The differences in MS channel response to BAC addition in liposomes containing MscS alone and co-reconstituted MscS and MscL is very interesting. Initially it seems odd that in 3/7 patches MscS openings were recorded in the presence of no pressure

application after BAC addition, but not in co-reconstituted liposomes. However recent evidence suggests that co-reconstituting these channels changes pushes up the pressure threshold of activation for MscS (Nomura *et al.,* 2012). This may explain why no 'clean' channel activity was identified in co-reconstituted liposomes. To unequivocally prove these openings are due to BAC mediated activation of MscS further control experiments are required using 'blank' liposomes to ensure that the activity identified is not solely due to the affects of BAC on the liposomal membrane.

In conjunction with this electrophysiological data the growth data set out in this chapter also point towards MS channels being targeted by BAC as well as CPZ. In both cases growth of the WT was significantly lower at 10 hour time points. In addition at the highest concentration of BAC (15 $\mu g.l^{-1}$) and CPZ (300 µM) used there seemed to be no growth at all of the WT strain after 10 hours whereas the MJF465 triple knockout strain started growing after between 6-8 hours. This regrowth after such a prolonged period is puzzling. This could imply that both CPZ and BAC are broken down overtime. Whether this breakdown is an active process, or whether it is a passive process induced by heat or pH is unknown. If this start in regrowth many hours after initiation of the growth experiments is related to breakdown of CPZ and or BAC we may expect growth in the WT FRAG-1 strain to begin at some point in time, with these experiments being too short to identify this. This idea may also infer that both CPZ and BAC at these concentrations are bacteriostatic and not bacteriocidal. As bacteriocidal activity would cause death of bacterial cells

resulting in no cells being available to regrow. An alternative argument would be that these concentrations are bacteriocidal and we are selecting for a specific subpopulation of cells that are inherently less sensitive to these agents but because this population's size is initially very small it takes a long time for them to grow. While there is a long literature on the reversal of drug resistance by CPZ (Kristiansen *et al.,* 2003, Coutinho *et al.,* 2009 Kristiansen *et al.,* 2010), there is little information about mechanisms that reduce the sensitivity of bacteria to CPZ. With respect to resistance to BAC more information is available (Moen *et al.,* 2012). One interesting point is that a BAC resistant isolate identified by Moen *et al.*, 2012 shows up regulation of RpoS. Up-regulation of RpoS would likely result in MS channel up-regulation (Stokes *et al.,* 2003) which doesn't fit with the hypothesis that BAC, as part of its mechanism of action, may target bacterial MS channels.

Taking in to account the growth data and the electorphysiological data presented in this chapter it does seem that, at least in part, MS channel activation accounts for the antibacterial activity in *E. coli* cells of CPZ and BAC.

6.5 Conclusions and future work

In summary this chapter illustrates the good and the bad side to bacterial MS channels. Firstly the benefit of MS expression was demonstrated by the fact that the growth of *E. coli* in the presence of ampicillin, carbenicillin and cephalexin was reduced in a single MscS knockout and in the MJF465 strain ($MscL^-$,$MscS^-$ and $MscK^-$) in comparison to WT. No differences in growth were seen in single MscL MscK or a double knockout of MscL and MscK. Thus

expression of MscS seems to modify the susceptibility of *E. coli* to three β-lactam antibiotics. The relatively small effects observed lead to the observation that MscS expression is a selective advantage to *E. coli* during periods of cell wall stress. In addition, the differences observed seem to coincide with entry into stationary phase where MS channel expression has been reported to be at its highest (Stokes *et al.,* 2003). Finally excessive activation of MS channels can be toxic and this chapter has demonstrated that the sensitivity of *E. coli* is modified to the antimicrobial amphitpaths CPZ and BAC suggesting that, at least in part, these compounds work by activating MS channels. These results therefore raise a number of interesting questions:

- Is the trend towards lower growth in all MscS channel knockout strains a physiologically relevant observation? If so what role does MscS have to play in cellular survival and proliferation in *E. coli*?
- Is the MIC of β-lactam antibiotics different in any of the single MS channel knockouts? Do the MICs of any other widely used antibiotics such as macrolides change?
- Why is it that only MscS alters susceptibility to the antibiotics tested?
- How much is susceptibility changed if all seven MS channel genes (*mscL*, *yggB*, *kefA*, *ybdG*, ybiO, *yjeP* and *ynaI*) are knocked out? As this strain now exists the same experiments, as completed in this chapter, could be carried out using this *Δ7* strain (Edwards *et al.,* 2012). This includes experiments looking at β-lactam antibiotic sensitivity but also looking at sensitivity to BAC and CPZ.

- Does the Lysozyme susceptibility of Gram-positive bacteria, such as *S. aureus*, change if their cohort of MS channels are knocked out.
- Is the MIC of β-lactam antibiotics different in any of the single MS channel knockouts? Do other cell wall targeted antibiotics show differences in activity against the WT and MS channel knockout strains? Examples to look at would be carbapenems such as meropenem and antibiotics such as vancomycin and teicoplanin although this would have to be carried out in Gram-positive bacteria as these two antibiotics are not active against Gram-negative microbes. Do the MICs of any other widely used antibiotics such as macrolides change on ablation of MS channel genes?
- Does MS channel expression affect bacterial susceptibility to attack by the complement component of the immune system? This could be tested using human serum and MS knockout *E. coli* strains.
- Does the antimicrobial spider venom toxin, GsMTx-4 a known MS channel blocker, demonstrate antibacterial synergy with (Hurst *et al.,* 2009, Kamaraju *et al.,* 2010). If knocking out MscS makes E. coli more sensitive to β-lactam antibiotics then the application of GsMTX-4 and subsequent MscS blockade should result in a synergistic antibacterial effect.
- Does BAC activate MS channels? This could be pursued by testing the effect of BAC on MS reconstituted in membranes of different lipid composition. If activation is mediated in the same way that it is

thought to happen with CPZ i.e. bilayer insertion and membrane curvature (Martinac *et al.,* 1990, Drymond *et al.,* 2008), we may expect channels inserted in liposomes containing a high percentage of negatively charged phospholipids to be more sensitive to BAC. This effect could also be looked at in native *E. coli* membrane using spheroplasts.

Chapter 7: General discussion and conclusions

7 General discussion and conclusions

7.1 Discussion

This year marks the 25th anniversary of the discovery of bacterial MS channels (Martinac *et al.,* 1987). Since that first documentation of pressure sensitive channel activity, bacterial MS channels have become arguably one of the best characterised channel families (Reviewed in Booth *et al.,* 2007). Much like their K^+ selective bacterial counterparts (i.e. KscA)(Doyle *et al.,* 1998) bacterial MS channels have been widely used to gain insight into the most intimate of questions relating to channel structure and function. The bacterial MS channels represent the most primitive and simplistic models for the study of mechanosensation (Hamill and Martinac 2001, Sukharev and Anishkin, 2004) gating solely in response to membrane tension, and as a result there is an abundance of both structural and functional data (Reviewed in Perozo, 2006, Haswell *et al.,* 2011) relating to these channels (Chang *et al.,* 1998, Levina *et al.,* 1999, Bass *et al.,* 2002, Perozo *et al.,* 2002, Steinbacher *et al.,* 2007, Wang *et al.,* 2008, Belyy *et al.,* 2010, Schumann *et al.,* 2010). In comparison to other bacterial channels their main physiological role, in osmoprotection, is well explored and documented (Levina *et al.,* 1999, Nakamaru *et al.,* 1999, Schumann *et al.,* 2010, Bucarey *et al.,* 2012). Homologues of these channels have been found littered throughout all three domains of life (Martinac *et al.,* 1987, Szabo *et al.,* 1992, Le Dain *et al.,* 1998, Kloda and Martinac *et al.,* 2001, Haswell and Meyerowitz *et al.,* 2006, Nakayama *et al.,* 2007, Peyronnet *et al.,* 2008, Borngen *et al.,* 2010). Despite the raft of information available there are

still numerous questions regarding these channels that remain unanswered. For example at least 7 MS channel family members are present in *E. coli*, *with* only two being required for osmoprotection (Levina *et al.,* 1999). This large degree of genetic redundancy hints at roles not yet identified for this most widely studied of channel families. One possible role in protection against lysis subsequent to cell wall attack is explored in this thesis. In addition, the large open pore diameters (Perozo *et al.,* 2002, Wang *et al.,* 2008) of these channels means that their gating is of large metabolic consideration to bacterial cells. These vast pore sizes and large electrochemical gradients for certain ions such as Ca^{2+} (Jones *et al.,* 2002) means that on gating these channels may become conduits for ion entry and not just a gateway for osmolyte efflux. In all likelihood the selectivity of MscS is important in reducing the metabolic cost of gating this channel by balancing charged osmolyte efflux (Gamini *et al.,* 2011). This in turn ameliorates any large change in membrane potential which is the major driver for ATP synthesis in *E. coli* (Dimroth *et al.,* 2000, Bot and Prodan, 2010). In order for this process to occur the selectivity of MscS, despite its relative weak nature in comparison to other channels (Martinac *et al.,* 1987, Sukharev, 2002, Sotomayor *et al.,* 2007), is imperative. However this most integral feature of MscS is not well understood.

This thesis has addressed numerous structural and functional questions relating to bacterial MS channels. The aim was to definitively show divalent cation permeation *in vitro* and *in vivo*. Furthermore an attempt was made to

investigate a novel hypothesis regarding the physiological role of MS channels, alluded to in the previous section.

Firstly it was established that MscS channel openings can be detected in native spheroplast membranes in the presence 100 mM symmetrical $CaCl_2$. During this experimentation a channel of ~90 pS was also identified which did not display MS channel activity and required substantial depolarising steps (≥ 65 mV) to gate. Similar channel activities were also seen in $MgSO_4$ and $MgCl_2$. Due to the instability of spheroplast membranes at these high voltages it was difficult to gain sufficient records to characterise this 'novel' activity. The channel may represent a polyhydroxybutyrate/polyphosphate channel as described by Das *et al.,* 1997. However this ~100 pS channel has never been recorded in native *E. coli* spheroplast membranes and this conductance was measured in symmetrical 200 mM $CaCl_2$ rather than 100 mM $CaCl_2$ in this thesis. The recent study of Edwards *et al.,* 2012 characterises an extra 3 MS channels present in *E. coli* membranes (Edwards *et al.,* 2012). These channels are the gene products of *ybiO* (~1 nS), *ynaI* (~100 pS) and *yjeP* (~300 pS). It is a possibility that one of these three channels, or YbdG, may give rise to this channel activity which could explain its low prevalence. However all show characteristic pressure sensitivity which was not detected in the recordings of this ~90 pS channel. If this channel could be characterised it represents a really exciting research avenue as to date no Ca^{2+} permeable channel has ever been recorded in native *E. coli* spheroplast membranes.

The MscS openings identified in symmetrical 100 mM $CaCl_2$ exhibited characteristic pressure sensitivity similar to that previously reported (Martinac *et al.,* 1987, Sukharev, 2002, Nomura *et al.,* 2006, Maksaev and Haswell, 2011). The conductance calculated at positive potentials in symmetrical $CaCl_2$ and $BaCl_2$ was less than that in symmetrical 200 mM KCl. This difference in conductance is likely explained by a combination of the reduced bulk conductivity of 100 mM $CaCl_2$ and $BaCl_2$ recording solutions in comparison to 200 mM KCl containing recording solutions, and the lower level of anion-divalent cation permeability when compared with anion-monovalent cation permeability (P_{Cl}/P_K = 2.7: P_{Cl}/P_{Ca} = 3.7 & P_{Cl}/P_{Ba} = 3.9). In addition to this, MscS also exhibited stronger rectification in symmetrical Ca^{2+} and Ba^{2+} than when monovalent ions were the major permeant cation. In fact, the rectification at negative pipette potentials seems to be related to the hydrated ionic radii of the major permeant cation following the order: Ca^{2+} ~ Ba^{2+} > Li^+ ~ Na^+ > K^+ > Rb^+ > Cs^+.

Both CPZ (100 µM) (Martinac *et al.,* 1990, Kubalski *et al.,* 1993) and a reduction in external osmolarity (~350 mOsm)(Levina *et al.,* 1999) caused rises in $[Ca^{2+}]_i$ in WT FRAG-1 *E. coli*. This rise was transient in the case of the hypoosmotic shock (~100 s) and more prolonged in the case of CPZ. The peak of the Ca^{2+} transient induced by the hypoosmotic shock was reduced by half in a triple knockout mutant ($MscL^-$, $MscS^-$ and $MscK^-$). In addition, the CPZ induced $[Ca^{2+}]_i$ rise was blunted by approximately ~35 % in the triple knockout. From this the suggestion can be made that Ca^{2+} does enter

bacterial cells via one or all of these three MS channels (MscL, MscS and MscK) when they gate *in vivo*. The residual transient could be due to Ca^{2+} movement via other MS channels (YbiO, YbdG, YjeP and YnaI) or lysis of 'weak' bacterial cells and the resulting liberation of aequorin (Schumann *et al.,* 2010, Edwards *et al.,* 2012). However it is important to note that a hypoosmotic shock of this size, while causing marked MS channel activation should *NOT* be of sufficient magnitude to induce lysis in *E. coli* even in the triple knockout strain (Levina *et al.,* 1999, Schumann *et al.,* 2010). Investigation of which channel is mediating this rise could be easily carried out using a combination of single MS channel knockout strains and multiple MS channel knockout strains. This Ca^{2+} influx could represent a physiological signal as numerous bacterial proteins and more than 100 bacterial genes are sensitive to calcium (Norris *et al.,* 1996, Dominguez, 2004, Naseem *et al.,* 2009).

In addition to the movement of Ca^{2+} via MS channels this thesis also identified that in the presence of symmetrical 100 mM Ca^{2+} or Ba^{2+} MscS exhibits numerous long lived subconducting states. Experimentation to a maximum pipette voltage of + 140 mV identified no more than 8 conducting states. These conducting states were equally spaced (10-14 % of unitary conductance) and increased in number from + 50 (1 to 3 conducting states depending on major permeant cation) to + 80 mV (maximum 8 conducting states) pipette potential. As the voltage increased MscS spent less time in the fully open state and more time in the lower subconducting states. Above + 90

mV pipette potential in most cases the channel continued to fluctuate in the lowest subconducting states for minutes after pressure was removed. MscS subconducting states have been documented before, with the propensity for MscS to reside in substates increased at negative pipette voltages (Shapovalov and Lester, 2004, Akitake *et al.,* 2005, Sotomayor *et al.,* 2007). This thesis is the first in depth report of MscS substates at high positive pipette voltages. The current paradigm regarding the structural basis of MscS subconducting states put forward by Akitake *et al.,* 2005 involves the asynchronous recruitment/inactivation of MscS monomers which gives rise to differences in open pore diameter and thus unitary conductance. Due to the fact the current paradigm is not able to easily account for this number of MscS subconducting states this thesis speculates on another possible structural mechanism. This mechanism is based on intermittent occlusion of the lateral vestibular portals of MscS. In an attempt to gain evidence for this hypothesis estimation of the pore diameter of the smallest subconducting state was carried out. If this hypothesis were correct then the lowest subconducting state should be a result of ion permeation solely via the pore aligned coaxially with the transmembrane pore. The estimation using Hille's equation is in agreement with this hypothesis with the pore diameter estimated as ~9 Å in $CaCl_2$ and $BaCl_2$ whereas the pore diameter in the open crystal structure is ~8 Å. Obviously the length used to carry out this calculation is critical to the final pore value. In this thesis 35 Å was used to estimate the thickness of the bilayer. The argument could be made that the

actual path length, if we imagine while in the lowest subconducting state that MscS is a simple cylinder, should be somewhere near 80 Å (i.e. the full length of the channel). If this calculation is carried out then the value is somewhere close to ~5 Å which is slightly lower than that shown in the crystal structure (Wang *et al.,* 2008). In order to further test this hypothesis the crystallographic structure of MscS was interrogated to see whether there were any sites that may participate in ionic interactions with permeating cations that could bring about vestibular portal occlusion. To aid this search for ionic interaction sites this thesis compared the structure of MscS with that of six other electrophysiologically characterised homologues. In doing this the opportunity was taken to compare the sequences of these channels and look for structural determinants of biophysical behaviour.

Sequence alignment of the pore-lining helix of MscS with the other six homologues failed to identify any structural differences that could account for the vastly different selectivity profiles of these channels (Li et al., 2002, Kloda and Martinac, 2001, Nakayame *et al.,* 2007, Borngen *et al.,* 2010, Petrov *et al.,* unpublished). In addition sequence alignment suggested explanations for the lack of inactivation seen in the majority of these homologues (Akitake *et al.,* 2007, Koprowski *et al.,* 2011). Furthermore conserved glycine-alanine pairs were identified in putative pore-lining helices of these homologues likely important for gating (Edwards, *et al.,* 2005) as well as potential electrostatic interactions between putative TM linkers and the cytoplasmic domains (Nomuta *et al.,* 2008). An homology model of the recently characterised

MscSP was also created and putative important residues for mechanosensitive channel function were identified.

Sequence alignment of the large water-filled cytoplasmic domain conserved in all MscS homologues was investigated. While structural similarity in the cytoplasmic domain was low for MscCG, MscMJ and MSC1 (~30%) it was much higher for MscK, MscMJLR and MscSP (~60 – 70 %). Alignment pointed towards a number of conserved cytoplasmic residues. In particular it was noted that a large region of electronegativity was present in the MscS cytoplasmic domain proximal to the lateral vestibular portals. This was centred round 3 acidic residues E187, E227 and E220. The first two residues E187 and E227 showed moderate conservation in the anion selective MscS homologues but were more distal to the pore than E220. In order to test whether these residues were important in binding and thus vestibular portal occlusion site directed mutagenesis was employed. The E227 was mutated for an alanine, this residue aligned with E227 in the MscK sequence (cytoplasmic domain similarity >70 %). And the E187 residue was mutated to an arginine as *in silico* mutations showed this replacement had the largest impact on this electronegative region. Neither of these mutants displayed modified conducting states but they did however exhibit modified anion selectivity. The mechanism for this, put forward in this thesis, is that the electronegative area binds cations for relatively short periods of time creating a more thermodynamically favourable route for anions but still nabbing high ionc throughput. This is supported by Gamini *et al.,* 2011 in which molecular

dynamic simulations show a marked increase in the dwell time of K^+ in the cytoplasmic vestibule in comparison to glutamate. This may mean that the entropic filter function suggested by Gamini *et al.,* 2011 directly involves these charged cytoplasmic residues.

These subconducting states identified in this thesis, at potentials likely to occur *in vivo*, add another layer to the regulation of MscS. Its pressure sensitivity, inactivation and relatively weak selectivity reflect the highly adapted nature of MscS. This highly tuned channel activity has been honed over many evolutionary years to perfectly fit its physiological role. This thesis speculates on a potential structural mechanism that brings about these subconducting states but fails to provide any strong evidence supporting this hypothesis. Never-the-less this mechanism still represents a simple and attractive explanation even if, at this present time, it is only speculative.

In addition to looking at these structural questions relating to the biophysical characteristics of MscS this thesis also attempted to test a hypothesis regarding a novel physiological role for MS channels. This involved MS channels working to prevent cellular lysis in the face of cell wall stress for example in response to antibiotics or enzymes. Data in this thesis shows that single MscS channel knockouts show increased sensitivity to β-lactam antibiotics (cephalexin, ampicillin and carbenicillin). This effect is not shared by MscL or MscK and is likely down to the relative abundance of MscS and its pressure threshold for activation. This was further supported by the use of multiple MS channel knockouts showing that a triple knockout ($MscL^-$, $MscS^-$

and MscK$^-$) but not a double knockout (MscL$^-$ and MscK$^-$) had increased susceptibility to both carbenicillin and ampicillin. The sensitivity of strains is only slightly changed (~ 20 %) hence the suggestion that MscS expression is a selective advantage in the presence of cell wall attack mediated by β-lactam antibiotics (Kohanski *et al.,* 2010). This is not any form of resistance mechanism. In addition to this positive effect of MS channels it was also found that the amphipathic compounds BAC (McDonnell and Russell, 1999) and CPZ (Kristiansen *et al.,* 2003) had reduced efficacy against MS channel knockout strains. From this data we can suggest that both CPZ and BAC target MS channels in *E. coli* and that this, at least in part, brings about their toxic effects (Martinac *et al.,* 1990, Kubalski *et al.,* 1993, Dymond *et al.,* 2008). This is not their sole mechanism of action, quite obviously, as strains lacking MscS, MscK and MscL are still susceptible to damage by these compounds. To further support this notion the addition of BAC caused spontaneous MscS channel activity in reconstituted liposomes. So while MS channels are protectors of cell membrane integrity in the face of hypoosmotic shocks or cell wall targeting antibiotics they also unfortunately for bacterial cells can be targeted by antimicrobial agents.

7.2 Recommendations for further work

This thesis raises many interesting questions and suggests many interesting research avenues for the future. A number of the main areas for focus are discussed in the following paragraphs.

7.2.1 MscS selectivity

First and foremost is the investigation of MscS selectivity. This thesis points towards a role for charged residues in the cytoplasmic domain in MscS selectivity. This is of great interest as unlike K^+, Na^+ and Ca^{2+} channels the residues implicated are not present in the pore region. The data supporting this is gained from only two vestibular mutants. Further more extensive mutagenesis of this area could aim at irrefutably illustrating that the selectivity of MscS is determined by the cytoplasmic domain. An example of future experimental strategies would be to mutate multiple vestibular portal residues to a specific amino acid such as alanine. Interesting residues identified in this thesis include E220 and R238. Furthermore during this thesis two other vestibular mutants were created but time constraints prevented their characterisation. These mutated residues (R185 and R184) line the sides of the vestibular portals with the mutants produced being R185E and R184E.

7.2.2 A 'novel' Ca^{2+} channel

Characterisation of a novel divalent channel in *E. coli* membranes is also an attractive option. As mentioned previously Ca^{2+} plays a key role in bacterial physiology (Norris *et al.,* 1996, Holland et al., 1999, Dominguez, 2004) but to date no specific Ca^{2+} influx or efflux mechanisms have been identified in *E.*

coli. This channel proved difficult to characterise however, if it were a novel channel it would warrant the technical challenges.

7.2.3 MS channels as antimicrobial targets

Further characterisation of novel MS channel activators such as BAC would also be interesting. This would involve investigation of compounds that are already used for their antimicrobial activity but may affect mechanosensitive channels. This includes antibiotics such as daptomycin (Lopes Baratella da Cunha Camargo *et al.,* 2008). For example it would be interesting to see whether the Δ7 strain documented in Edwards *et al.,* 2012 shows differential sensitivity to compounds such as BAC.

An exciting prospect coming out of this thesis is the possibility that the Ca^{2+} assay using aequorin could be turned into a high-throughput screen for the identification of novel MS channel activators. As discussed in this thesis MS channels represent an attractive antibiotic target for various reasons however no specific modulators are currently available as a starting point for drug development. Measuring Ca^{2+} influx using a 96 well plate set up would allow testing of large numbers of compounds in short spaces of time. The premise being that if a compound causes a Ca^{2+} rise in the WT strain but it is blunted in the KO strain this compound potentially activates MS channels. This approach has the added bonus of being *in vivo* meaning that the process would automatically select for compounds that can permeate through the Gram-negative outer membrane which is a major stumbling block for antibiotics.

Taking into account the large pore diameter (Perozo et al., 2002, van den Bogaart *et al.,* 2007) of MscL these identified compounds may not only have inherent antimicrobial activity but also present a novel delivery mechanism for other antibiotics that find it difficult to access the bacterial cytoplasm.

7.2.4 Probing the structural basis of MscS subconducting states

The structural basis of MscS subconducting states could also be further explored in a similar manner to that of the selectivity mechanism. Mutants could be created to see whether changing the vestibular portals, for example by creating stable ion binding sites affects the subconducting behaviour.

7.3 Conclusions and summary of major findings

The findings documented in this thesis show multiple effects of divalent cations on the biophysical behaviour of MscS. In addition, from data within this thesis the suggestion can be made that Ca^{2+} influx via MS channels occurs *in vivo*. Further work is required to identify whether this Ca^{2+} flux is of physiological relevance. The main results of this thesis can be described as follows:

- Ca^{2+} moves *in vivo* via MS channels in response to a hypoosmotic shock (~350 mOsm) and application of the phenothiazine antipsychotic CPZ (100 µM). Which channel (MscL, MscS or MscK) is carrying this current is currently unknown.
- The presence of Ca^{2+} and Ba^{2+} causes MscS to exhibit multiple long lived subconducting states at positive pipette potentials. The maximum number identified in this thesis was 8 up to a maximum pipette voltage of + 140 mV.
- Charged residues in the cytoplasmic vestibule of MscS are important for its anion selectivity. In particular E187 and E227 which form a region of electronegativity near each of the seven lateral vestibular portals. The likely mechanism relates to cation binding. Although more mutational experiments are required to unequivocally confirm this conclusion.

- MscS *E. coli* knockout strains exhibit differential sensitivity to three β-lactam type antibiotics. This selective advantage is not conveyed by MscL or MscK only MscS. This represents a new important physiological function for this channel.
- The amphipathic quaternary ammonium compound benzalkonium chloride activates MS channels *in vitro*. In addition *E. coli* strains devoid of MS channels show a reduced sensitivity to this antimicrobial agent.

References

Aine, E. & Morsky, P. (1984) Lysozyme concentration in tears - assessment of reference values in normal subjects. *Acta Opthalmol,* 62**:** 932-938.

Akashi, K., Miyata, H., Itoh, H. & Kinosita Jr, K. (1996) Preparation of giant liposomes in physiological conditions and their characterization under an optical microscope. *Biophys J,* 71**:** 3242-3250.

Akitake, B., Anishkin, A., Liu, N. & Sukharev, S. (2007) Straightening and sequential buckling of the pore-lining helices define the gating cycle of MscS. *Nat Struct Mol Biol,* 14**:** 1141-1149.

Akitake, B., Anishkin, A. & Sukharev, S. (2005) The "Dashpot" Mechanism of stretch-dependent gating in MscS. *J General Physiol,* 125**:** 143-154.

Amaral, L., Kristiansen, J. E., Thomsen, V. F. & Markovich, B. (2000) The effects of chlorpromazine on the outer cell wall of *Salmonella typhimurium* in ensuring resistance to the drug. *Int J Antimicrob Agents,* 14**:** 225-229.

Amaral, L. & Lorian, V. (1991) Effects of chlorpromazine on the cell envelope proteins of *Escherichia coli*. *Antimicrob Agents Chemother,* 35**:** 1923-1924.

Amaral, L., Viveiros, M. & Molnar, J. (2004) Antimicrobial activity of phenothiazines. *In Vivo,* 18**:** 725-731.

Anishkin, A., Gendel, V., Sharifi, N. A., Chiang, C. S., Shirinian, L., Guy, H. R. & Sukharev, S. (2003) On the conformation of the COOH-terminal domain of the large mechanosensitive channel MscL. *Journal of General Physiology,* 121**:** 227-244.

Arkin, I. T., Sukharev, S. I., Blount, P., Kung, C. & Brunger, A. T. (1998) Helicity, membrane incorporation, orientation and thermal stability of the large conductance mechanosensitive ion channel from *E. coli*. *Biochim Biophys Acta,* 1369**:** 131-140.

Arnold, K., Bordoli, L., Kopp, J. & Schwede, T. (2006) The SWISS-model workspace: A web-based environment for protein structure homology modelling. *Bioinformatics,* 22.

Ashcroft, F. M. (2000) *Ion channels in health and disease,* Florida, Academic Press.

Ashcroft, F. M. (2006) Katp channels and insulin secretion: A key role in health and disease. *Biochem Soc Trans,* 34.

Badminton, M. N., Campbell, A. K. & Rembold, C. M. (1996) Differential regulation of nuclear and cytosolic Ca^{2+} in Hela cells. *J Biol Chem,* 271**:** 31210-31214.

Barry, P. H. (1994) Jpcalc, a software package for calculating liquid junction potential corrections in patch-clamp, intracellular, epithelial and bilayer measurements and for correcting junction potential measurements. *J Neurosci Methods,* 51**:** 107-116.

Basle, A., Iyer, R. & Delcour, A. H. (2004) Subconductance states in OmpF gating. *Biochim Biophys Acta,* 1664**:** 100-107.

Basle, A., Rummel, G., Storici, P., Rosenbusch, J. P. & Schirmer, T. (2006) Crystal structure of osmoproin OmpC from *E. coli* at 2 Å. *J Mol Biol,* 362**:** 933-942.

Bass, R., Strop, P., Barclay, M. T. & Rees, D. C. (2002) Crystal structure of *Escherichia coli*, MscS, a voltage-modulated and mechanosensitive channel. *Science,* 298**:** 1582-1587.

Bechinger, B. (1997) Structure and functions of channel-forming peptides: Magainins, cecropins, melittin and alamethicin. *J Membr Biol,* 156**:** 197-211.

Belyy, V., Anishkin, A., Kamaraju, K., Liu, N. & Sukharev, S. (2010) The tension-transmitting 'clutch' in the mechanosensitive channel MscS. *Nat Struc Mol Biol,* 17**:** 451-459.

Bernstein, J. A., Khodursky, A. B., Lin, P.-H., Lin-Chao, S. & Cohen, S. N. (2002) Global analysis of mRNA decay and abundance in *Escherichia coli* at single-gene resolution using two-color fluorescent DNA microarrays. *Proc Natl Acad Sci USA,* 99**:** 9697-9702.

Betanzos, M., Chiang, C. S., Guy, H. R. & Sukharev, S. (2002) A large iris-like expansion of a mechanosensitive channel protein induced by membrane tension. *Nat Struct Biol,* 9**:** 704-710.

Bialecka-Fornal, M., Lee, H. J., Deberg, H. A., Gandhi, C. S. & Phillips, R. (2012) Single-cell census of mechanosensitive channels in living bacteria. *Plos One,* 7**:** Epub ahead of print.

Birkner, J. P., Poolman, B. & Kocer, A. (2012) Hydrophobic gating of mechanosensitive channel of large conductance evidenced by single-subunit resolution. *Proc Natl Acad Sci U S A,* 109**:** 12944-12949

Boer, M., Anishkin, A. & Sukharev, S. (2011) Adaptive MscS gating in the osmotic permeability response in *E. coli*: The question of time. *Biochem,* 50**:** 4087-4096.

Booth, I. R., Edwards, M. D., Black, S., Schumann, U. & Miller, S. (2007) Mechanosensitive channels in bacteria: Signs of closure? *Nat Rev Microbiol,* 5**:** 431-440.

Borngen, K., Battle, A. R., Moker, N., Morbach, S., Marin, K., Martinac, B. & Kramer, R. (2010) The properties and contribution of the corynebacterium glutamicum mscs variant to fine-tuning of osmotic adaptation. *Biochim Biophys Acta,* 1798**:** 2141-2149.

Bot, C. T. & Prodan, C. (2010) Quantifying the membrane potential during *E. coli* growth stages. *Biophysical Chemistry,* 146**:** 133-137.

Bucarey, S. A., Penn, K., Paul, L., Fenical, W. & Jensen, P. (2012) Genetic complementation of the obligate marine *Actinobacterium Salinispora tropica* with the large mechanosensitive channel gene MscL rescues cells from osmotic downshock. *Appl Environ Microbiol,* 78**:** 4175-4182.

Campbell, A. K. (1983) *Intracellular calcium, its universal role as regulator,* Chichester, John Wiley and Sons.

Campbell, A. K. (1988) *Chemiluminescence: Principles and applications in biology and medicine* Chichester and Wienhiem, Horwood.

Campbell, A. K., Kricka, L. J. & Stanley, P. E. (Eds.) (1994) *Bioluminescence and chemiluminescence: Fundamental and applied aspects*, Wiley, Chichester.

Cao, B., Porollo, A., Adamczak, R., Jarrell, M. & Meller, J. (2006) Enhanced recognition of protein transmembrane domains with prediction-based strcutural profiles. *Bioinformatics,* 22**:** 303-309.

Chang, G., Spencer, R. H., Lee, A. T., Barclay, M. T. & Rees, D. C. (1998) Structure of the MscL homolog from *mycobacterium tuberculosis*: A gated mechanosensitive ion channel. *Science,* 282**:** 2220-2226.

Corry, B., Hurst, A. C., Pal, P., Nomura, T., Rigby, P. & Martinac, B. (2010) An improved open-channel structure of MscL determined from FRET confocal microscopy and simulation. *J Gen Physiol,* 136**:** 483-494.

Coutinho, H. D. M., Costa, J. G. M., Lima, E. O., Falcao-Silva, V. S. & Siqueira-Junior, J. P. (2009) Potentiating effect of *Mentha arvensis* and chlorpromazine in the resistance to aminoglycosides of methicillin - resistant *Staphylococcus aureus*. *In Vivo,* 23**:** 287-289.

Cruickshank, C. C., Minchin, R. F., Le Dain, A. C. & Martinac, B. (1997) Estimation of the pore size of the large-conductance mechanosensitive ion channel of *Escherichia coli*. *Biophys J,* 73**:** 1925-1931.

Darszon, A., Labarca, P., Nishigaki, T. & Espinosa, F. (1999) Ion channels in sperm physiology. *Physiol Rev,* 79**:** 481-510.

Das, S., Lengweiler, U. D., Seebach, D. & Reusch, R. N. (1997) Proof for a nonproteinaceous calcium-selective channel in *Escherichia coli* by total synthesis from (r)-3-hydroxybutanoic acid and inorganic polyphosphate. *Proc Natl Acad Sci USA,* 94**:** 9075-9079.

Delcour, A. H. (2009) Outer membrane permeability and antibiotic resistance. *Biochim Biophys Acta,* 1749**:** 808-816.

Dimroth, P., Kaim, G. & Matthey, U. (2000) Crucial role of the membrane potential for ATP synthesis by F_1F_o ATP-synthases. *J Exp Biol,* 203**:** 51-59.

Dominguez, D. (2004) Calcium signalling in bacteria. *Mol Microbiol,* 54**,** 291.

Dorwart, M. R., Wray, R., Brautigam, C. A., Jiang, Y. & Blount, P. (2010) *S. aureus* MscL is a pentamer *in vivo* but of variable stoichiometries in vitro: Implications for detergent-solubilized membrane proteins. *Plos Biol,* 8**:** e1000555.

Dowhan, W. (1997) Molecular basis for membrane phospholipid diversity: Why are there so many lipids? *Ann Rev Biochem,* 66**,** 199-232.

Edwards, M. D., Bartlett, W. & Booth, I. R. (2008) Pore mutations of the *Escherichia coli* MscS channel affect desensitization but not ionic preference. *Biophys J,* 94**:** 3003-3013.

Edwards, M. D., Black, S., Rasmussen, T., Rasmussen, A., Stokes, N. R., Stephen, T., Miller, S. & Booth, I. R. (2012) Characterization of three novel mechanosensitive channel activities in *Escherichia coli*. *Channels,* 6**:** Epub ahead of print.

Edwards, M. D. & Booth, I. R. (2011) Analysis of novel mechanosensitive channel activities in *Escherichia coli*. *Biophys J,* 100**:** 280a-281a.

Edwards, M. D., Li, Y. Z., Kim, S., Miller, S., Bartlett, W., Black, S., Dennison, S., Iscla, I., Blount, P., Bowie, J. U. & Booth, I. R. (2005) Pivotal role of the glycine-rich TM3 helix in gating the MscS mechanosensitive channel. *Nat Struct Mol Biol,* 12**:** 113-119.

Ellison, R. T. & Giehl, T. J. (1991) Killing of Gram-negative bacteria by lactoferrin and lysozyme. *J Clin Invest,* 88**:** 1080-1091.

Ermakov, Y. A., Kamaraju, K., Krishnendu, S. & Sukharev, S. (2010) Gadolinium ions block mechanosensitive channels by altering the packing and lateral pressure of anionic lipids. *Biophys J,* 98**:** 1018-1027.

Folgering, J. H., Wolters, J. C. & Poolman, B. (2005) Engineering covalent oligomers of the mechanosensitive channel of large conductance from escherichia coli with native conductance and gating characteristics. *Protein Sci,* 14**:** 2947-2954.

Fox, J. A. (1987) Ion channel subconductance states. *J Membr Biol,* 97**:** 1-8.

Gamini, R., Sotomayor, M., Chipot, C. & Schulten, K. (2011) Cytoplasmic domain filter function in the mechanosensitive channel of small conductance. *Biophys J,* 101**:** 80-89.

Gangola, P. & Rosen, B. P. (1987) Maintenance of intracellular calcium in *Escherichia coli*. *J Biol Chem,* 262**:** 12570-12574.

Gensen, G. S. & Haswell, E. S. (2012) Functional analysis of conserved motifs in the mechanosensitive channel homolog mscs-like2 from arabidopsis thaliana. *Plos One,* 7**:** Epub ahead of print.

Grajkowski, W., Kubalski, A. & Koprowski, P. (2005) Surface changes of the mechanosensitive channel MscS upon its activation, inactivation, and closing. *Biophys J,* 88**:** 3050-3059.

Grage, S. L., Keleshian, A. M., Turdzeladze, T., Battle, A. R., Tay, W. C., May, R. P., Holt, S. A., Contera, S. A., Haertlein, M., Moulin, M., Pal, P., Rohde, P. R., Forsyth, V. T., Watts, A., Huang, K. C., Ulrich, A. S. & Martinac, B. (2011) Bilayer-mediated clustering and functional interaction of mscl channels. *Biophysical Journal,* 100**,** 1252-1260

Hase, C. C., Le Dain, A. C. & Martinac, B. (1995) Purification and functional reconstitution of the recombinant large mechanosensitive ion channel (MscL) of *Escherichia coli*. *J Biol Chem,* 270**:** 18329-34.

Hase, C. C., Minchin, R. F., Kloda, A. & Martinac, B. (1997) Cross-linking studies and membrane localization and assembly of radiolabelled large mechanosensitive ion channel (MscL) of *Escherichia coli*. *Biochem Biophys Res Comm,* 232**:** 777-782.

Haswell, E. S. & Meyerowitz, E. M. (2006) Mscs-like proteins control plastid size and shape in *Arabidopsis thaliana*. *Current Biology,* 16**:** 1-11.

Haswell, E. S., Peyronnet, R., Barbier-Brygoo, H., Meyerowitz, E. M. & Frachisse, J.-M. (2008) Two MscS homologs provide mechanosensitive channel activities in the *Arabidopsis* root. *Curr Biol,* 18**:** 730-734.

Haswell, E. S., Phillips, R. & Rees, D. C. (2011) Mechanosensitive channels: What can they do and how do they do it? *Structure,* 19**:** 1356-1369.

Hill, K. & Schaefer, M. (2007) TRPA1 is differentially modulated by the amphipathic molecules trinitrophenol and chlorpromazine. *J Biol Chem,* 282**:** 7145-7153.

Icho, T. & Raetz, C. R. H. (1983) Multiple genes for membrane-bound phosphatases in escherichia-coli and their action on phospholipid precursors. *J Bacteriol,* 153**:** 722-730.

Iscla, I., Levin, G., Wray, R., Reynolds, R. & Blount, P. (2004) Defining the physical gate of a mechanosensitive channel, MscL, by engineering metal-binding sites. *Biophys J,* 87**:** 3172-3180.

Jentsch, T. J., Hübner, C. A. & Fuhrmann, J. C. (2004) Ion channels: Function unravelled by dysfunction. *Nat Cell Biol,* 6**:** 1039-1047.

Jones, H. E., Holland, I. B. & Campbell, A. K. (2002) Direct measurement of free Ca^{2+} shows different regulation of Ca^{2+} between the periplasm and the cytosol of *Escherichia coli*. *Cell Calcium,* 32**:** 183-192.

Kamaraju, K., Belyy, V., Rowe, I., Anishkin, A. & Sukharev, S. (2011) The pathway and spatial scale for MscS inactivation. *J Gen Physiol,* 138**,** 49-57.

Kloda, A. & Martinac, B. (2001) Molecular identification of a mechanosensitive channel in archaea. *Biophysical Journal,* 80**:** 229-240.

Kocer, A., Walko, M., Bulten, E., Halza, E., Feringa, B. L. & Meijberg, W. (2006) Rationally designed chemical modulators convert a bacterial channel protein into a ph-sensory valve. *Angew Chem Int Ed Engl,* 45**:** 3126-3130.

Kocer, A., Walko, M., Meijberg, W. & Feringa, B. L. (2005) A light-actuated nanovalve derived from a channel protein. *Science,* 309**,** 755-758.

Kohanski, M. A., Dwyer, D. J. & Collins, J. (2010) How antibiotics kill bacteria: From targets to networks. *Nat Rev Microbiol,* 8**:** 423-435.

Koprowski, P., Grajkowski, W., Isacoff, E. Y. & Kubalski, A. (2011) Genetic screen for potassium leaky small mechanosensitive channels (MscS) in *Escherichia coli* recognition of cytoplasmic beta domain as a new gating element. *J Biol Chem,* 286**:** 877-888.

Koprowski, P. & Kubalski, A. (2003) C termini of the *Escherichia coli* mechanosensitive ion channel (MscS) move apart upon the channel opening *J Biol Chem,* 88**:** 3050-3059.

Kristiansen, M. M., Leandro, C., Ordway, D., Martins, M., Viveiros, M., Pacheco, T., Kristiansen, J. E. & Amaral, L. (2003) Phenothiazines alter resistance of methicillin-resistant strains of *Staphylococcus aureus* (MRSA) to oxacillin *in vitro*. *Int J Antimicrob Agents,* 22**:** 250-253.

Kubalski, A., Martinac, B., Ling, K. Y., Adler, J. & Kung, C. (1993) Activities of a mechanosensitive ion channel in an *Escherichia coli* mutant lacking the major lipoprotein. *J Membr Biol,* 131**:** 151-160.

Laver, D. R. & Gage, P. W. (1997) Interpretation of substates in ion channels: Unipores or multipores? *Prog Biophys Mol Biol,* 67**:** 99-140.

Le Dain, A. C., Saint, N., Kloda, A., Ghazi, A. & Martinac, B. (1998) Mechanosensitive ion channels of the archaeon *Haloferax volcanii*. *J Biol Chem,* 273**:** 12116-12119.

Lehen'kyi, V., Shapovalov, G., Skryma, R. & Prevarskaya, N. (2011) Ion channels in control of cancer and cell apoptosis. *Am J Physiol Cell Physiol*.

Levina, N., Totemeyer, S., Stokes, N. R., Louis, P., Jones, M. A. & Booth, I. R. (1999) Protection of *Escherichia coli* cells against extreme turgor by activation of MscS and MscL mechanosensitive channels: Identification of genes required for MscS activity. *EMBO J,* 18**:** 1730-1737.

Li, Y. Z., Moe, P. C., Chandrasekaran, S., Booth, I. R. & Blount, P. (2002) Ionic regulation of MscK, a mechanosensitive channel from *Escherichia coli*. *EMBO J,* 21**:** 5323-5330.

Lopes Baratella Da Cunha Camargo, I., Neoh, H. M., Cui, L. & K, H. (2008) Serial daptomycin selection generates daptomycin-nonsusceptible *Staphylococcus aureus* strains with a heterogeneous vancomycin-intermediate phenotype. *Antimicrob Agents Chemother,* 52**:** 4289–4299.

Macdonald, A. G. & Martinac, B. (2005) Effect of high hydrostatic pressure on the bacterial mechanosensitive channel MscS. *Eur Biophys J,* 34**:** 434-441.

Macheboeuf, P., Contreras-Martel, C., Job, V., Dideberg, O. & Dessen, A. (2006) Penicillin binding proteins: Key players in bacterial cell cycle and drug resistance processes. *FEMS Microbiol Rev,* 30**:** 673-691.

Machiyama, H., Tatsumi, H. & Sokabe, M. (2009) Structural changes in the cytoplasmic domain of the mechanosensitive channel MscS during opening. *Biophys J,* 97**:** 1048-1057.

Maksaev, G. & Haswell, E. S. (2012) Expression and characterisation of the bacterial mechanosensitive channel MscS in *Xenopus laevis* oocytes. *J Gen Physiol* 138**:** 641-649.

Malcolm, H. R., Heo, Y.-Y., Elmore, D. E. & Maurer, J. A. (2011) Defining the role of the tension sensor in the mechanosensitive channel of small conductance. *Biophys J,* 101**:** 345-352.

Martinac, B., Adler, J. & Kung, C. (1990) Mechanosensitive ion channels of *Escherichia coli* activated by amphipaths. *Nature,* 348**:** 261-263.

Martinac, B., Buechner, M., Delcour, A. H., Adler, J. & Kung, C. (1987) Pressure-sensitive ion channel in *Escherichia coli*. *Proc Natl Acad Sci USA,* 84**:** 2297-2301.

Masschalck, B. & Michiels, C. W. (2003) Antimicrobial properties of lysozyme in relation to foodborne vegetative bacteria. *Crit Rev Microbiol,* 29**:** 191-214.

Mcdonnell, G. & Russell, D. A. (1999) Antiseptics and disinfectants: Activity, action, and resistance. *Clin Microbial Rev,* 12**:** 147-149.

Mclaggan, D., Jones, M. A., Gouesbet, G., Levina, N., Lindey, S., Epstein, W. & Booth, I. R. (2002) Analysis of the kefa2 mutation suggests that KefA is a cation-specific channel involved in osmotic adaptation in *Escherichia coli*. *Mol Microbiol,* 43**:** 521-536.

Miller, S., Bartlett, W., Chandrasekaran, S., Simpson, S., Edwards, M. D. & Booth, I. R. (2003a) Domain organisation of the MscS mechanosensitive channel channel of *E. coli*. *EMBO J,* 22**:** 36-46.

Miller, S., Edwards, M. D., Ozdemir, C. & Booth, I. R. (2003b) The closed structure of the mscs mechanosensitive channel. Cross-linking of single cysteine mutants. *J Biol Chem,* 278**:** 32246-32250.

Miyazaki, C., Kuroda, M., Ohta, A. & Shibuya, I. (1985) Genetic manipulation of membrane phospholipid-composition in *Escherichia coli* - pgsa mutants defective in phosphatidylglycerol synthesis. *Proc Natl Acad Sci USA,* 82**:** 7530-7534.

Nakamaru, J., Hirano, S., Ito, M. & Wachi, M. (2007) Mutations of the *corynebacterium glutamicum* ncgl1221 gene, encoding a mechanosensitive channel homolog, induce L-glutamic acid production. *Appl Environ Microbiol***,** 4491-4498.

Nakamaru, Y., Takahashi, Y., Unemoto, T. & Nakamura, T. (1999) Mechanosensitive channel functions to alleviate the cell lysis of marine bacterium, *Vibrio alginolyticus*, by osmotic downshock. *FEBS Letters,* 444**:** 170-172.

Nakayama, Y., Fujiu, K., Sokabe, M. & Yoshimura, K. (2007) Molecular and electrophysiological characterization of a mechanosensitive channel expressed in the chloroplasts of *Chlamydomonas*. *Proc Natl Acad Sci USA,* 104**:** 5883-5888.

Naseem, R., Davies, S. R., Jones, H., Wann, K. T., Holland, I. B. & Campbell, A. K. (2007) Cytosolic Ca^{2+} regulates protein expression in *E. coli* through release from inclusion bodies. *Biochem Biophys Res Comm,* 360**:** 33-39.

Naseem, R., Holland, I. B., Jacq, A., Wann, K. T. & Campbell, A. K. (2008) pH and monovalent cations regulate cytosolic free Ca^{2+} in *E. coli*. *Biochim Biophys Acta,* 1778**:** 1415-1422.

Naseem, R., Wann, K. T., Holland, I. B. & Campbell, A. K. (2009) ATP regulates calcium efflux and growth in *E. coli*. *J Mol Biol,* 391**:** 42-56.

Nguyen, T., Clare, B., Guo, W. & Martinac, B. (2005) The effects of parabens on the mechanosensitive channels of *E. coli*. *Eur Biophys J,* 34**:** 389-395.